Correlation of Site Variability from SASW and CPT Measurements

A Thesis
presented to
the Faculty of the Graduate School
at the University of Missouri

In Partial Fulfillment
of the Requirements of the Degree
Master of Science

By
JESSE F. MOYLES
Dr. Brent L. Rosenblad, P. E., Thesis Supervisor
MAY 2018

The undersigned, appointed by the dean of the Graduate School, have examined the thesis entitled

CORRELATION OF SITE VARIABILITY FROM SASW AND CPT MEASUREMENTS

Presented by Jesse F. Moyles

A candidate for the degree of Master of Science

And hereby certify that in their opinion it is worthy of acceptance

---

Dr. Brent L. Rosenblad, P.E., Chair

Dr. John J. Bowders, P.E.

Dr. Allen L. Thompson, P.E.

ACKNOWLEDGEMENTS

There are several people, and a few institutions, to whom I owe a great debt of gratitude. I'll start by thanking the entire University of Missouri Geotechnical Engineering faculty and staff for facilitating a fantastic graduate program at MU. I am especially thankful to my faculty advisors, Dr. Brent Rosenblad and Dr. John Bowders, who were involved with this project from start to finish and are the source of much professional guidance and personal inspiration. I very much appreciate that they let me take this thesis my own direction, though they well knew it was the wrong one at times. I would also like to thank Dr. J. Erik Loehr and Dr. Ahmed Abu El-Ela for taking the time to examine, discuss, and make meaningful suggestions regarding this project along the way. Additionally, I must thank my fellow students, Mohammed Khan, Nathaniel Dummerth, Hashim Al-Sumaiday, Ghaith Al-Sharify, and Nimer (*The Hammer*) Alselami who not only helped me with this project, but with all of my studies at MU.

None of this research would have been possible without the generosity of Ameren Missouri and Reitz & Jens, Inc. I am especially thankful to Mike Wagstaff, of Ameren Missouri, and Jeff Fouse, of Reitz & Jens, Inc., for coordinating access to the UWL site and associated CPT data. I must also thank my boss, Captain Kevin King (USN), for granting me the flexibility to complete this thesis while working full time.

On a more personal note, I am incredibly grateful for the support of my wonderful wife, Lauren, without whom I could never have completed this project. Her time and energy spent facilitating my work greatly outweighs what is reflected in the text. Finally, and most importantly, I would like to thank God for bringing together all things that made this work possible.

TABLE OF CONTENTS

ABSTRACT

Geotechnical site characterization programs are designed to reduce uncertainty and maximize the efficiency of geotechnical design. Ironically, however, many site characterization programs are inefficient themselves as they call for extensive intrusive testing conducted at regular intervals. This thesis attempts to improve the efficiency of such programs by drawing a correlation between variability in CPT and SASW measurements across a geotechnical site. With such a correlation, the practicing engineer could potentially modify the extent (and cost) of intrusive testing based on observed variability in surface wave dispersion. To examine this correlation, CPT and SASW data from the Labadie Utility Waste Landfill (UWL) near Labadie, Missouri were analyzed. Variability was quantified through coefficients of variation (COV) calculated amongst CPT measurements (q_t and f_s) for a particular depth (z) and SASW phase velocity (V_{ph}) for a particular wavelength (λ) at five locations within the UWL. Positive correlations were achieved utilizing a method developed in this thesis wherein q_t was converted to an equivalent corrected tip resistance (q_{teq}) by weighting q_t in the same manner that Rayleigh wave energy is weighted with depth. Utilizing this method, a linear regression between the mean COV of V_{ph} and q_{teq} yields a slope of 0.18, an intercept of 0.02, a coefficient of determination (R^2) of 0.751, and a p-value of 0.057. Removing outliers and COVs calculated in the highly variable upper 5 ft of soil yields a slope of 0.19, an intercept of 0.02, a R^2 of 0.961, and a p-value of 0.003. Finally, a relationship between q_{teq} and V_{ph} was developed that facilitates the estimation of dispersion curves from q_t alone. Utilizing this relationship, dispersion curves estimated from q_t were, on average, within 10% of those measured.

1 Introduction

1.1 Background

At its core, site characterization is about reducing uncertainty in order to enhance geotechnical design. Most commonly, sites are characterized based on existing information (geologic maps, soil surveys, past engineering records, local knowledge, etc.) and a finite number of borings, standard penetration tests (SPT), cone penetration tests (CPT) or other intrusive geotechnical tests. Perhaps counterintuitively, however, the primary objective of many site characterization measures is not only to obtain the engineering properties of the subsurface, but to more generally determine the site's subsurface stratigraphy. Once the general composition of the subsurface is known, a few additional tests to determine engineering properties are often all that is needed for geotechnical design.

Site characterization state-of-practice generally recommends intrusive testing be conducted at regular intervals depending on the site and the type of project (FHWA ED-88-053 2003). However, because geologic materials are typically deposited over large expanses relative to geotechnical sites, it is often the case that for a given site, relatively little variation is seen in the soil profile and the engineering properties thereof. Therefore, instead of providing information that leads to substantial changes in geotechnical design, excessive intrusive testing more often serves as a mere validation of subsurface consistency.

This research aims to improve the efficiency of site characterization programs by utilizing a surface wave method (SWM), in this case the Spectral Analysis of Surface Waves (SASW) method, to quantify subsurface variability. Though SWMs only determine the dispersive nature of surface waves, they can provide valuable insight into the spatial

variability of the subsurface. This is especially true when the inversion process is omitted and phase velocity dispersion curves are considered alone. As stated by Stokoe et al. (1994) "dispersion curves alone can be valuable in quickly evaluating spatial variability at a given site".

1.2 Objective and Scope of Study

As intuitive as Stokoe's stated principle is, to date, no specific procedure or research has verified or quantified its utility as a geotechnical site characterization tool. This thesis will evaluate Stokoe's statement by examining variability in SASW dispersion curves relative to variability in CPT measurements. In doing so, this thesis will determine whether SASW dispersion curves, in conjunction with traditional site characterization methods, may improve the efficiency of site characterization practice by reducing the number of intrusive tests needed to sufficiently characterize a site.

Specifically, this thesis sets out to test the following hypothesis: *variability in SASW dispersion curves is correlated to variability in CPT measurements*. In order to achieve this goal, the following tasks were identified:

- Determine a suitable geotechnical site with extensive CPT data
- Develop an appropriate method to compare variability in SASW dispersion curves and CPT measurements
- Conduct SASW testing
- Quantify variability in SASW and CPT measurements
- Accept or reject the hypothesis
- Provide recommendations for engineering application and further research

1.3 Thesis Organization

Chapter 2 provides a literature review of the state-of-practice for SASW and CPT testing as well as their current role in site characterization. A brief description of the Labadie UWL site including the geologic history, generalized soil profiles, and geotechnical testing history is provided in Chapter 3. Chapter 4 outlines the methods utilized during CPT and SASW testing as well as those applied to data reduction and variability analyses. Results of CPT, SASW, and variability analyses are presented in Chapter 5. Chapter 6 includes discussion of the methodology, results, and limitations of the study. Finally, a summary of this research project and the conclusions drawn from it are presented in Chapter 7.

2 Literature Review

2.1 Overview

Literature regarding a direct correlation between variability in SASW dispersion curves and CPT measurements is not currently available. However, much work has been done that considers SASW and CPT independently with respect to site characterization. Section 2.2 provides an overview of SASW as well as its limitations, advancements, and current use in site characterization. Section 2.3 is a brief overview of the current state of practice of CPT. Finally, Section 2.4 summarizes state-of-practice site exploration guidelines for intrusive testing.

2.2 Spectral Analysis of Surface Waves (SASW)

Spectral Analysis of Surface Waves (SASW) was pioneered in the early 1980s following the advent of field-portable digital data acquisition and signal-processing equipment. The principal utility of SASW is that shear wave velocities are directly proportional to the stiffness of the material through which they propagate. Thus, from them intrinsic properties of engineering significance may be obtained. In the 1980's and 90's the most common method for analyzing shear waves in geo-materials was cross-hole and down-hole methods. However, both of these techniques are intrusive, costly, and time consuming. Because SASW measures the propagation of Rayleigh waves at the surface, it is significantly more cost effective (Stokoe et al. 1994).

Before SASW, the steady-state Rayleigh wave method was the primary surface method used to obtain a shear wave velocity profile. For this method, vibrations are emitted at constant frequency and sensors are moved further and further away from each other until

they are in phase. When two receivers are in phase, shear wave velocities are obtained by simply multiplying the frequency by the receiver spacing. After repeating this process for several frequencies, velocities are plotted against their respective frequency or wavelength and a dispersion curve takes form (Stokoe et a. 1994).

As is outlined in Stokoe et al. (1994), by 1994 advances in data analysis and on-site computing made it possible to use impulse, swept-sinusoidal, or random noise as inputs. Utilizing two receivers and a data analyzer, a Fast Fourier Transform (FFT) is performed on-site and the input signal from each receiver is separated into individual frequencies with varying phases. The phase difference (φ) for each frequency (f) between the two receivers is then calculated and travel time (t) between receivers for each frequency can be determined (Eq. 2.1). It then follows that the Rayleigh wave velocity (V_R) for a given frequency is the receiver spacing (S) (assuming the distance from the first receiver to the source is the same) divided by the travel time (Eq. 2.2). Finally, the wavelength (λ_R) for each frequency is obtained by dividing V_R by the frequency (Eq. 2.3). This process is carried out for the available range of frequencies and a dispersion curve is produced.

$$t(f) = \frac{\varphi(f)}{2\pi f} \tag{2.1}$$

$$V_R = \frac{S}{t(f)} \tag{2.2}$$

$$\lambda_R = \frac{V_R}{f} \tag{2.3}$$

In SASW, shear wave velocity (V_s) profiles are achieved by forward modeling potential velocity profiles to fit the measured dispersion curve. The V_s profile is therefore not a unique solution, but one of several possible solutions. Further, because Rayleigh waves must propagate through shallow layers on their way to deeper layers, resolution of

shear wave velocities decreases with depth. As a rule of thumb, SASW is only able to discern soil/rock layers with thicknesses greater than about 20% of the depth (Stokoe et al. 1994). That is, at 10 ft below the surface, one cannot expect to discern layers thinner than 2 ft. Finally, it is important to note that SASW is not a point measurement. Rather it provides the globally averaged V_s for given depths as measured from the source to the furthest receiver.

2.2.1 SASW & Site Characterization

The SASW method outlined by Stokoe et al. (1994) was one of the most widely used surface methods in geotechnical site characterization. However, during the late 90's researchers made a number of improvements to surface wave methods (SWM) which eventually led to the development of Multichannel Analysis of Surface Waves (MASW). These improvements included advances in spatial array processing, using low-frequency passive energy, utilizing multiple modes of wave propagation, and data smoothing (Rix et al. 2001). Though only one of these methods (smoothing) was implemented while using SASW for this thesis, all have enhanced the potential of surface waves for site characterization.

Today, the most common application of SWM in site characterization is seismic site response analysis. However, until recently doubt has existed in the geotechnical community as to the suitability of surface methods for such analyses. The chief complaint is that lack of resolution and non-uniqueness in V_s profiles can yield unconservative site response spectra. Foti et al. (2009) disproved this notion showing that while subsurface profiles, as determined by SWM, are non-unique and sensitive to initial model inputs, they

still provide an accurate global account of seismic site response. The underlying principle is that sites with similar global surface wave propagation are likely to be similar with respect to seismic response. That is to say, sites with similar dispersion curves will behave similarly during seismic events.

In order to test their hypothesis, the authors utilized robust Monte Carlo analyses of a synthetic site as well as two actual sites. The analyses were performed by creating several random models that fit a given dispersion curve. Figure 2.1 shows six shear wave velocity profiles that were randomly generated to fit a given dispersion curve. Each of these profiles were then analyzed in Shake91 for seismic site response. Figure 2.2 shows that the difference in seismic site response for all six profiles is negligible. From all of the analyses performed, it was determined that response spectra and amplification factors for all randomly generated sites fall within 5-10% of the exact solution. Similar Monte Carlo simulations were created for two actual sites, Torre Pellice and La Salle, Italy which both yielded the same results as the synthetic case.

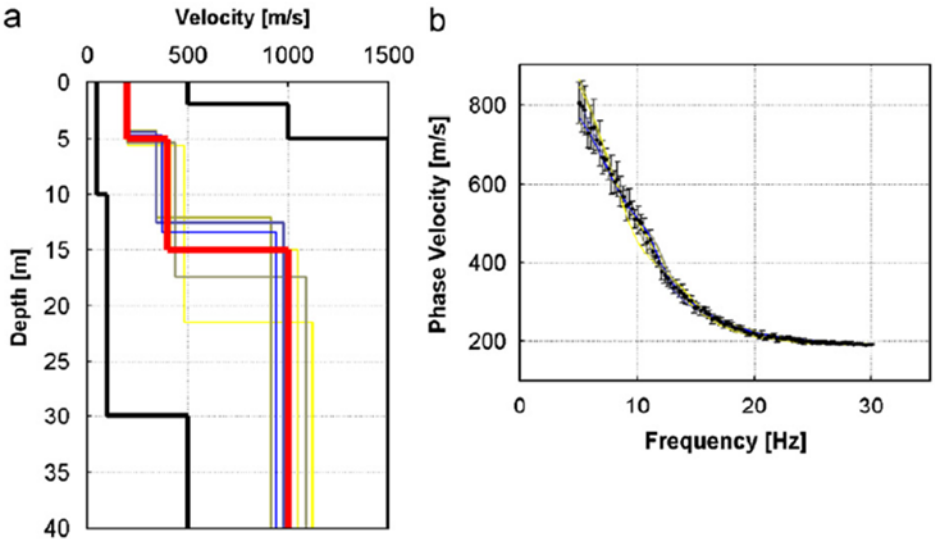

Figure 2.1 – a.) Six randomly generated velocity profiles b.) Corresponding dispersion curves (Foti et al. 2009).

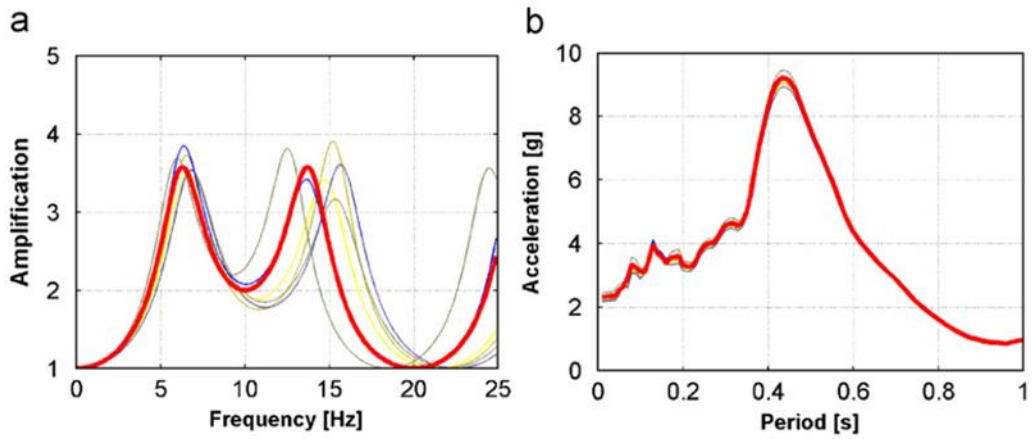

Figure 2.2 – a.) Amplification functions b.) Response spectra (Foti et al. 2009).

In conducting their study, Foti et al. (2009) countered the most widespread criticism of SWM for seismic site response. While it is certain that stiffness and velocity profiles achieved via SWM are not unique solutions, their non-uniqueness bears little significance with respect to seismic performance. That is to say, if sites are equivalent with respect to Rayleigh wave dispersion, they too are equivalent with respect to seismic site response. Furthermore, SWM are well-suited for such investigations.

2.2.2 SASW Summary

For nearly 60 years, surface waves have been used to characterize geotechnical sites. Advances in data analysis and computing eventually facilitated on-site FFT analyses and SASW supplanted the steady-state Rayleigh wave method. State-of-the-art SWM now incorporates MASW utilizing both active and passive energy. With respect to site characterization, SWM are typically used to supplement data obtained from conventional (SPT, CPT, borings, etc.) analyses or serve as a baseline for choosing the type and quantity of conventional site investigation methods. They are particularly effective in terms of

seismic site response and recent research has discredited claims that solution non-uniqueness may yield unconservative site response spectra.

2.3 Cone Penetration Test

The cone penetration test (CPT) is a widely-used, efficient, and reliable method for geotechnical site characterization. Today, most CPT systems are outfitted with pore-water pressure transducers and are referred to as a piezocone penetration tests (CPTU) (Figure 2.3). Another common CPT variation is the seismic piezocone penetration test (SCPTU) which includes at least one geophone and is capable of measuring shear wave velocities with depth. Less common are CPT systems capable of measuring resistivity (RCPTU) or taking photographs or video of the soil at depth.

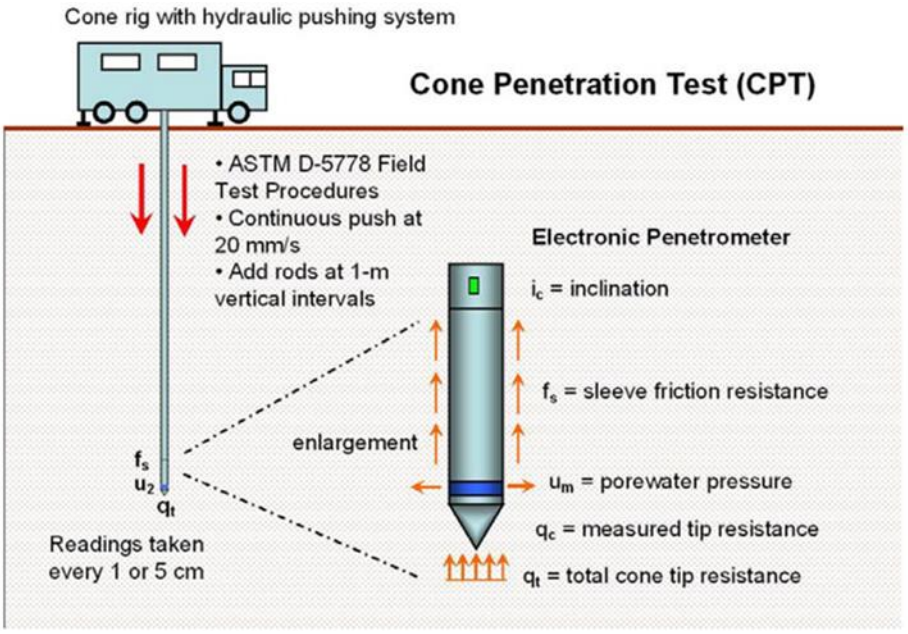

Figure 2.3 – Cone penetration test (Mayne 2007).

From the three primary CPTU measurements (q_c, f_s, u_m) a wide range of correlations for geotechnical parameters (soil type, unit weight, stress history, shear wave velocity, undrained shear strength, friction angle etc.) have been well-established. Economically the CPT is quite efficient with costs ranging from $6 to $13.5 per foot depending on test size, location, material specific requirements, and post-grouting etc. (Mayne 2007). This compares to $12 to $33 per foot for traditional borings, depending on similar factors, making the CPT about half the cost of a traditional boring (Mayne 2007).

Several correlations have also been developed for estimating V_s from CPT measurements. While many are available for all soils, most have been developed for a specific soil type and are functions of various combinations of q_c, q_t, f_s, confining stress (σ_v), effective confining stress (σ'_v), and depth (Table 2.1). Overall, the range of equations and their coefficients of determination vary widely and are ultimately a function of the applied methods and input data. The theoretical relationship between V_s and CPT measurements resides in the fact that many of the factors that affect small-strain (G_{max}) and large-strain stiffness are the same. Hardin and Drnevich (1972) describe G_{max} as a function of void ratio (e), mean principal effective stress (σ'_o), and overconsolidation ratio (OCR), all of which affect large-strain stiffness in the same manner. That is, both small-strain and large-strain moduli increase with decreasing e and increasing σ'_o and OCR. Other soil properties that have proportional effects on large and small-strain moduli include soil type, geologic age, and cementation (Wair, DeJong, & Shantz 2012).

Table 2.1 – CPT-V_s correlations (from Wair et al. 2012).

Soil Type	Study	Geologic Age	Number of Data Pairs	r^2	V_S (m/s)	(Eq #)
All Soils	Hegazy & Mayne (1995)	Quaternary	323	0.70	$(10.1 \log(q_c) - 11.4)^{1.67} (100\ f_s/q_c)^{0.3}$	(5.6)
	Mayne (2006)	Quaternary	161	0.82	$118.8 \log(f_s) + 18.5$	(5.7)
	Piratheepan (2002)	Holocene	60	0.73	$32.3\ q_c^{0.089}\ f_s^{0.121}\ D^{0.215}$	(5.8)
	Andrus et al. (2007)	Holocene & Pleistocene	185	(H) 0.71 (P) 0.43	$2.62\ q_t^{0.395}\ I_C^{0.912}\ D^{0.124}\ SF^a$	(5.9)
	Robertson (2009)	Quaternary	1,035	----	$[(10^{(0.55I_c+1.68)})\ (q_t - \sigma_v) / p_a\ ]^{0.5}$	(5.10)
Sand	Sykora & Stokoe (1983)	----	256	0.61	$134.1 + 0.0052\ q_c$	(5.11)
	Baldi et al. (1989)	Holocene	----	----	$17.48\ q_c^{0.13}\ \sigma'^{0.27}_v$	(5.12)
	Hegazy & Mayne (1995)	Quaternary	133	0.68	$13.18\ q_c^{0.192}\ \sigma'^{0.179}_v$	(5.13)
	Hegazy & Mayne (1995)	Quaternary	92	0.57	$12.02\ q_c^{0.319}\ f_s^{-0.0466}$	(5.14)
	Piratheepan (2002)	Holocene	25	0.74	$25.3\ q_c^{0.163}\ f_s^{0.029}\ D^{0.155}$	(5.15)
Clay	Hegazy & Mayne (1995)	Quaternary	406	0.89	$14.13\ q_c^{0.359}\ e_0^{-0.473}$	(5.16)
	Hegazy & Mayne (1995)	Quaternary	229	0.78	$3.18\ q_c^{0.549}\ f_s^{0.025}$	(5.17)
	Mayne & Rix (1995)	Quaternary	339	0.83	$9.44\ q_c^{0.435} e_0^{-0.532}$	(5.18)
	Mayne & Rix (1995)	Quaternary	481	0.74	$1.75\ q_c^{0.627}$	(5.19)
	Piratheepan (2002)	Holocene	20	0.91	$11.9\ q_c^{0.269}\ f_s^{0.108}\ D^{0.127}$	(5.20)

Units: q_c, q_t, f_s, σ_v, and σ'_v are measured in kilopascals (kPa), and depth (D) is measured in meters (m). p_a = 100 kPa.
[a]SF = 0.92 for Holocene and 1.12 for Pleistocene

2.4 Boring and Sampling in Site Characterization Practice

Of particular interest to this study is the manner in which inherent uncertainties are dealt with in practice. In cases where deterministic design is applied, inherent uncertainties are generally handled by incorporating factors of safety and conducting boring and sampling on a regular interval. Less commonly, reliability-based design methods simultaneously account for inherent and measurement uncertainties based on statistical

models of soil parameters and, even less commonly, soil stratigraphy. These methods also require boring and sampling on a regular, and often smaller interval.

The Federal Highway Administration (FHWA) outlines minimum standards for boring and sampling in FHWA ED-88-053 (2003) (Table 2.2). The FHWA publication also specifies that rigid rules cannot be established and the guidelines contained therein are considered the reasonable minimum; ultimately leaving the problem to engineering judgement. Table 2.2 shows that borings are generally recommended every hundred to few hundred feet depending on the type of project. The FHWA publication goes on to recommend types of borings depending on the specific geomaterial. For sands, SPTs are recommended with samples taken every 5 ft or at major changes in soil strata. For clays, SPT and thin wall tube samples should also be taken every 5 ft and field vane tests are recommended to obtain in-situ shear strengths. For rock, continuous cores should be taken. Finally, for borrow sites any equipment that allows direct observation of the material is recommended.

Table 2.2 – FHWA minimum guidelines for boring and sampling (FHWA ED-88-053 2003).

Geotechnical Feature	Minimum Number of Borings	Minimum Depth of Borings
Structure Foundation	1 per substructure unit under 30 m (100 ft) in width 2 per substructure unit over 30 m (100 ft) in width Additional borings in areas of erratic subsurface conditions	Spread footings: 2B where L< 2B, 4B where L > 2B and interpolate for L between 2B and 4B Deep foundations: 6m (20ft) below tip elevation or two times maximum pile group dimension, whichever is greater If bedrock is encountered: for piles core 3 m (10 ft) below tip elevation; for shafts core 3D or 2 times maximum shaft group dimension below tip elevation, whichever is greater.
Retaining Structures	Borings spaced every 30 to 60 m (100 to 200 ft). Some borings should be at the front of and some in back of the wall face.	Extend borings to depth of 0.75 to 1.5 times wall height When stratum indicates potential deep stability or settlement problem, extend borings to hard stratum
Bridge Approach Embankments over Soft Ground	When approach embankments are to be placed over soft ground, at least one boring should be made at each embankment to determine the problems associated with stability and settlement of the embankment. Typically, test borings taken for the approach embankments are located at the proposed abutment locations to serve a dual function.	Extend borings into competent material and to a depth where added stresses due to embankment load is less than 10% of existing effective overburden stress or 3 m (10 ft) into bedrock if encountered at a shallower depth Additional shallow explorations (hand auger holes) taken at approach embankment locations to determine depth and extent of unsuitable surface soils or topsoil.
Centerline Cuts and Embankments	Borings typically spaced every 60 m (200 ft) (erratic conditions) to 120 m (400 ft) (uniform conditions) with at least one boring taken in each separate landform. For high cuts and fills, should have a minimum of 3 borings along a line perpendicular to centerline or planned slope face to establish geologic cross-section for analysis.	Cuts: (1) in stable materials extend borings minimum 5 m (15 ft) below depth of cut at the ditch line and, (2) in weak soils extend borings below grade to firm materials or to twice the depth of cut whichever occurs first. Embankments: Extend borings to a hard stratum or to a depth of twice the embankment height.
Landslides	Minimum 3 borings along a line perpendicular to centerline or planned slope face to establish geologic cross-section for analysis. Number of sections depends on extent of stability problem. For active slide, place at least on boring each above and below sliding area	Extend borings to an elevation below active or potential failure surface and into hard stratum, or to a depth for which failure is unlikely because of geometry of cross-section. Slope inclinometers used to locate the depth of an active slide must extend below base of slide.
Ground Improvement Techniques	Varies widely depending in the ground improvement technique(s) being employed. For more information see "Ground Improvement Technical Summaries" FHWA SA-98-086R.	
Material Sites (Borrow sources, Quarries)	Borings spaced every 30 to 60 m (100 to 200 ft).	Extend exploration to base of deposit or to depth required to provide needed quantity.

2.5 Summary

In order to best compare variability in SASW dispersion curves and CPT measurements, it is important to examine the state-of-practice of each. Since the 1980's, SWM have been a cheap and reliable method for non-intrusive subsurface investigation. Recent developments in SWM such as spatial array processing, data smoothing, and utilization of low-frequency passive energy and multiple modes of wave propagation have significantly enhanced SWM capabilities (Rix et al. 2001). Furthermore, work by Foti et al. (2009) shows that inverted shear wave velocity profiles are less significant to seismic site response than the dispersive nature of the soil.

Similar to SWM, CPT technology continues to improve and now incorporates continuous and precise sampling of upwards of ten independent measurements (Mayne 2007). Combined with advancements in data processing, CPT now provides what is arguably the most cost-effective and reliable site exploration tool in the geotechnical inventory. The efficiency with which CPT (and SWM) are used for site characterization, however, has seen little change. Advanced methods for geotechnical site characterization such as the Bayesian approach and random field theory have been developed, but are seldom used in practice. Ultimately, state-of-practice site characterization continues to handle inherent uncertainty through broad recommendations and engineering judgement.

3 Site Description

3.1 Introduction

Several factors were considered while identifying potential geotechnical sites for this study. First, in order to perform enough testing to make a statistically significant correlation, a large site (at least 100 acres) with several CPT soundings taken at regular intervals was preferred. The site should also have relatively flat topography in order to make comparison of spatial variability more simplistic. Consistent groundwater conditions were also desirable so that the fairest comparison may be made between recent SASW measurements and older CPT soundings. Finally, the site should be relatively free from excessive vegetation, standing water, be accessible for foot and vehicular traffic, and have otherwise favorable surface conditions for SASW testing.

3.2 Labadie Utility Waste Landfill (UWL) Site

Fortunately for this study, the Labadie Power Plant utility waste landfill (UWL) meets virtually all of the desirable site criteria. The plant is located on the Missouri River floodplain approximately 2.5 miles northeast of Labadie, Missouri. It is owned and operated by Ameren Missouri, an electric and gas utility company, headquartered in St. Louis, Missouri. In May of 2009, a detailed site investigation (DSI) plan was approved by the Missouri Department of Natural Resources (MDNR) for a UWL adjacent to the plant for the disposal of coal combustion residuals (CCR). The plan was prepared by Reitz & Jens, Inc. of St. Louis, Missouri and GREDELL Engineering Resources, Inc. of Jefferson City, Missouri. The field investigation began in September 2009 and was completed in January 2010 and the DSI report was submitted in February 2011. Today,

the site remains largely unused with only the westernmost 40 acres of the site being used for the UWL. The remainder of the site is currently being leased for agricultural purposes.

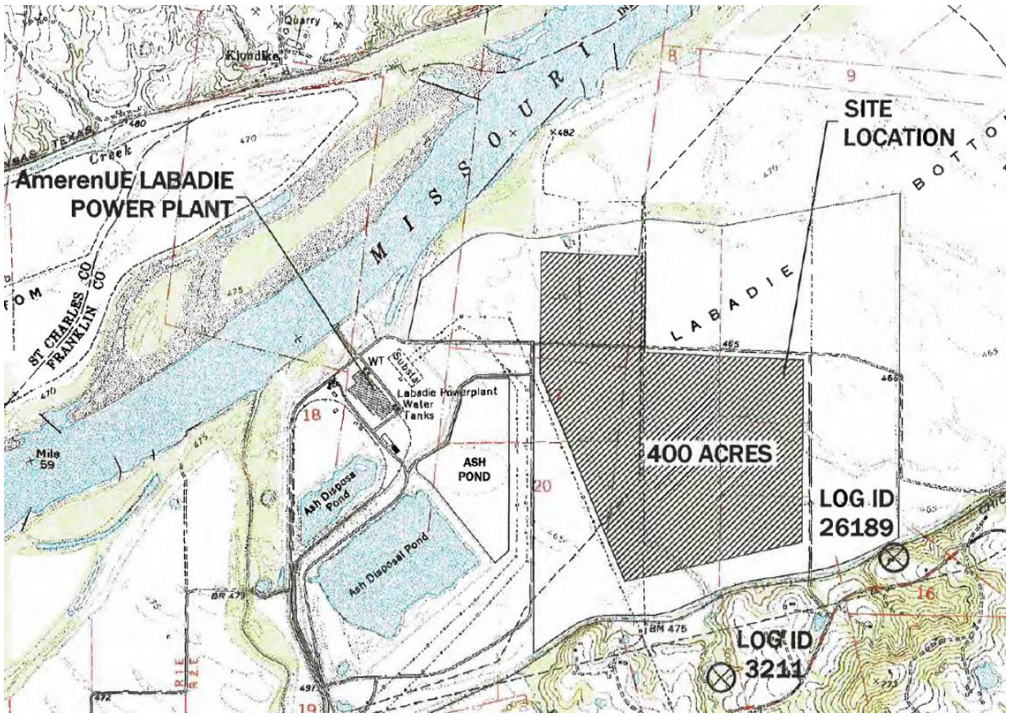

Figure 3.1 – Labadie UWL site (GREDELL Engineering Resources, Inc. and Reitz & Jens, Inc. 2011).

As described in the 2011 DSI report by GREDELL Engineering Resources, Inc. and Reitz & Jens, Inc., the UWL site is approximately 400 acres of Holocene Missouri River alluvial deposits. The site is remarkably flat with total topographic relief less than 10 ft. The site is bounded to the north by a flood levee and Labadie Bottom Road, to the east by Davis Road, to the west by Labadie Bottom Road, and to the south by Becker Creek (Figure 3.1). As is typical of Missouri River alluvial deposits, the upper 15 ft generally consist of fine sands, silts and clays. From 15 to 50 ft, fairly homogenous course grained

sands are prevalent. From 50 to 100 ft, sandy gravels, gravel, and even cobbles are present as particle size generally increases with depth. Middle Ordovician sedimentary deposits consisting of dolomites with occasional beds of limestone and sandstone are encountered at approximately 100 ft across the site. Finally, 2007 boring records have the groundwater table at 10 to 20 ft below the ground surface. More recent piezometer readings from June 2016 have the groundwater table ranging from about 5 to 9 ft, and those from December 2016 have it at 9 to 18 ft.

The field investigation was initiated in the summer of 2009 and completed in January of 2010 under the supervision of senior geologist Mikel Carlson, R. G., of GREDELL Engineering Resources, Inc. and senior project manager Jeffrey Fouse, P. E., of Reitz & Jens, Inc. In total, it consisted of 24 borings, 76 CPT soundings, and the instillation of 100 piezometers, all of which were done in accordance with applicable ASTM standards and spaced on a grid pattern across the 400-acre site (Figure 3.2). All borings and CPT soundings were taken to a minimum depth of 35 ft which is approximately 20 ft below the proposed depth of the UWL. Three borings were extended to auger refusal which occurred at approximately 100 ft (Appendix D). For cases where cone refusal occurred at less than 35 ft, a second sounding was taken in an attempt to increase penetration.

Finally, a few randomly selected CPT soundings were verified by performing an additional sounding or boring at approximately the same location. All samples were logged in accordance with applicable ASTMs and moisture content tests were performed on all fine-grained samples. Additional testing such as unconsolidated-undrained and consolidated-undrained triaxial tests, one-dimensional consolidation tests, and flexible-wall hydraulic conductivity tests were conducted at the discretion of the senior project

manager in accordance with stated site characterization goals (GREDELL Engineering Resources, Inc. and Reitz & Jens, Inc. 2011).

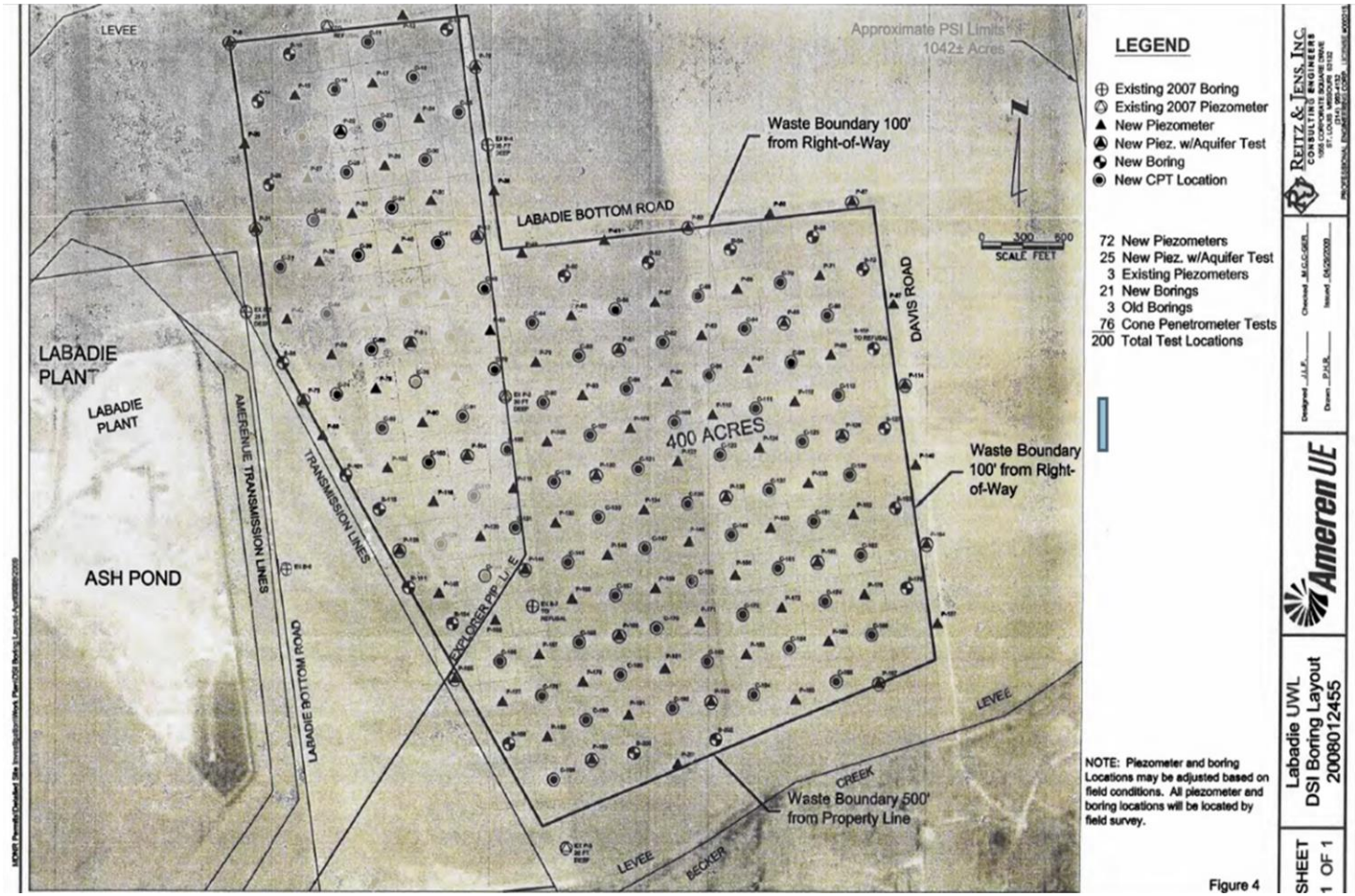

Figure 3.2 – Labadie UWL boring diagram (GREDELL Engineering Resources, Inc. and Reitz & Jens, Inc. 2011).

3.3 Subdivision of the UWL

Correlation of variability in SASW dispersion curves and CPT tip resistance is best examining utilizing several geotechnical sites. However, field testing at several geotechnical sites was impractical due to this study's limited budget. The UWL site was therefore broken into several smaller "sites" which will be referred to as "groups" from this point forward. In total, six, eight-acre groups consisting of at least five points where CPT soundings were performed were created (Figure 3.3). Groups were chosen based on size, availability of CPT soundings, and the need to have enough groups to determine a statistically significant variability correlation. All points within the groups are numbered consistent with the 2011 DSI report and groups are numbered based on their center point. Because there are points where more than one CPT sounding was taken, some groups contain more than 5 points. For example, Group 80 consists of Points 64, 66, 66A, 80, 92, and 94, however tests 66 and 66A were done at approximately the same location.

The northernmost group, and the only group north of Labadie Bottom Road, is Group 23 and consists of Points 16, 18, 23, 28, and 30. Group 80 is the northwesternmost group south of Labadie Bottom Road, and as previously mentioned consists of Points 64, 66, 66A, 80, 92, and 94. Group 84 is the northeasternmost group and consists of Points 68, 70, 84, 96, and 98. Group 135 is the center group south of Labadie Bottom Road and includes Points 121, 123, 135, 135A, 147, 147A, and 149. The southwesternmost group is Group 180 and consists of Points 168, 168A, 170, 180, 190, and 192. Finally, the southeasternmost group is Group 184 and includes Points 172, 174, 184, 194, and 196. A more detailed diagram with exact locations for each point is also provided in Chapter 4.

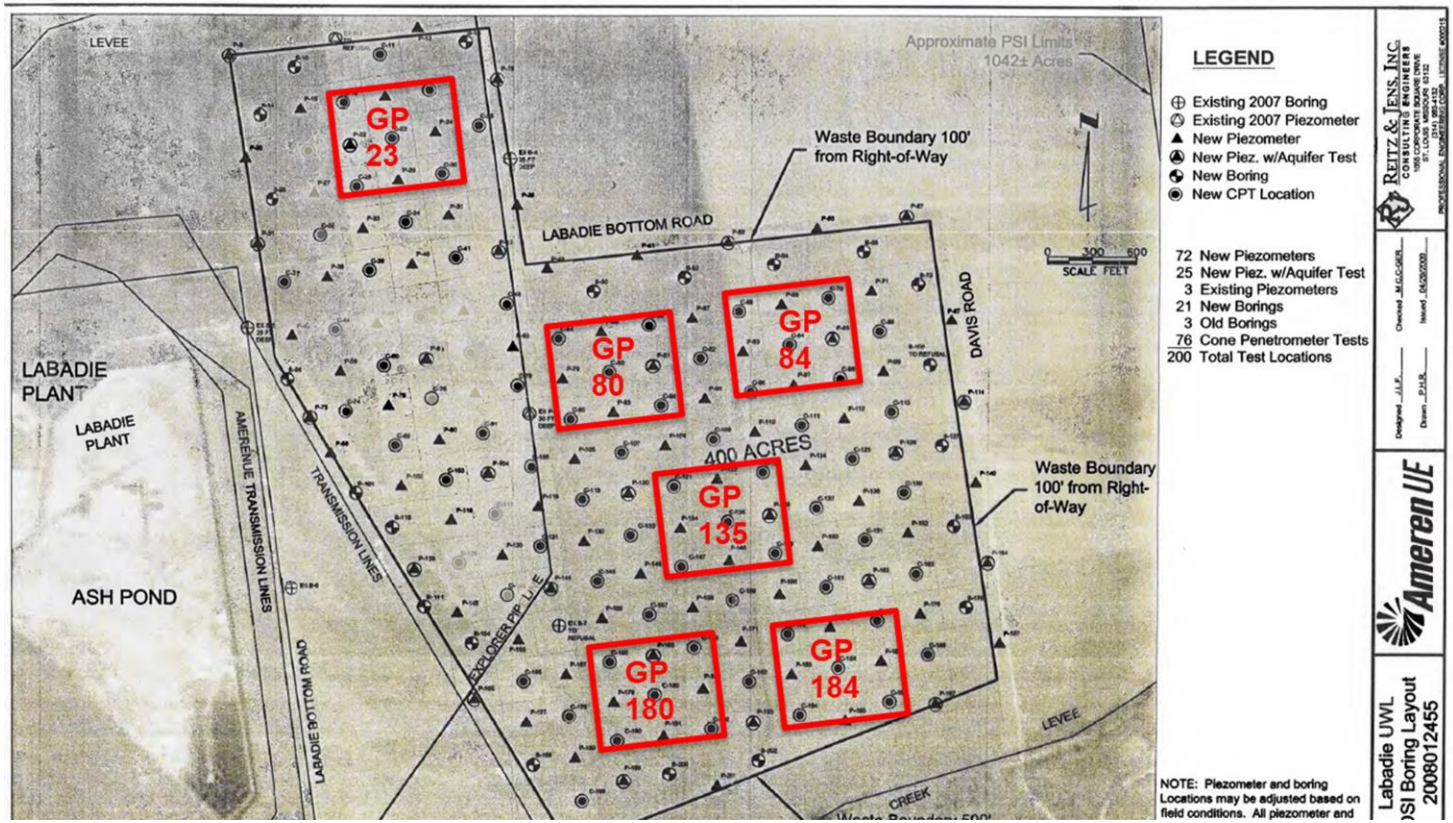

Figure 3.3 – Labadie UWL boring diagram from GREDELL Engineering Resources, Inc. and Reitz & Jens, Inc. 2011, with group overlay.

4 Methods

4.1 Overview

This chapter provides a detailed account of the methods utilized to determine a correlation between variability in SASW dispersion curves and CPT measurements. CPT procedures used by Reitz & Jens, Inc. are briefly outlined in Section 4.2. SASW field testing procedures, data reduction and dispersion curve fitting are provided in Sections 4.3 and 4.4. The preliminary method utilized for quantifying variability in SASW dispersion curves and CPT data is explained in Section 4.5. Finally, an explanation of the equivalent wavelength method (EWM) and an example variability quantification are provided in Section 4.6.

4.2 Cone Penetration Testing

As is detailed in the 2011 DSI report, cone penetration testing was conducted in October, November, and December of 2009 by Reitz & Jens, Inc. All tests were conducted in accordance with ASTM D5778 “Electronic Friction Cone and Piezocone Penetration Testing of Soils” utilizing an AMS-probe rig with 1.5-in cone. The CPT rig was operated by Terra Drill, Inc. of Dupo, Illinois under the supervision of Reitz & Jens geotechnical engineer Christopher Cook, P. E. For this thesis, the processed CPT measurements provided in the 2011 DSI report were utilized. Prior to their utilization, processed measurements were selectively verified from raw data and found to be correct in all cases.

4.3 SASW Testing

A total of 29 SASW tests were conducted at the Labadie UWL site on the 19th, 21st, and 22nd of November 2016. Figure 4.1 shows the location, general surface conditions, and outcome of each planned test. Testing began in the northwestern corner of the site and progressively moved south and east. Weather was fairly consistent each day with highs around 45° and lows around 30° with no precipitation. On the 19th, wind was approximately 10 mph out of the northwest, while winds on the 21st and 22nd were calm. Originally, 34 tests were planned but heavy overgrowth in the northeastern section made SASW testing impractical (Figure 4.1). Of the 29 tests, 26 resulted in usable dispersion curves. Dispersion curves for Points 123 and 147 could not be identified due to scatter in phase diagrams, and incorrect test procedures resulted in inverted data for Point 92.

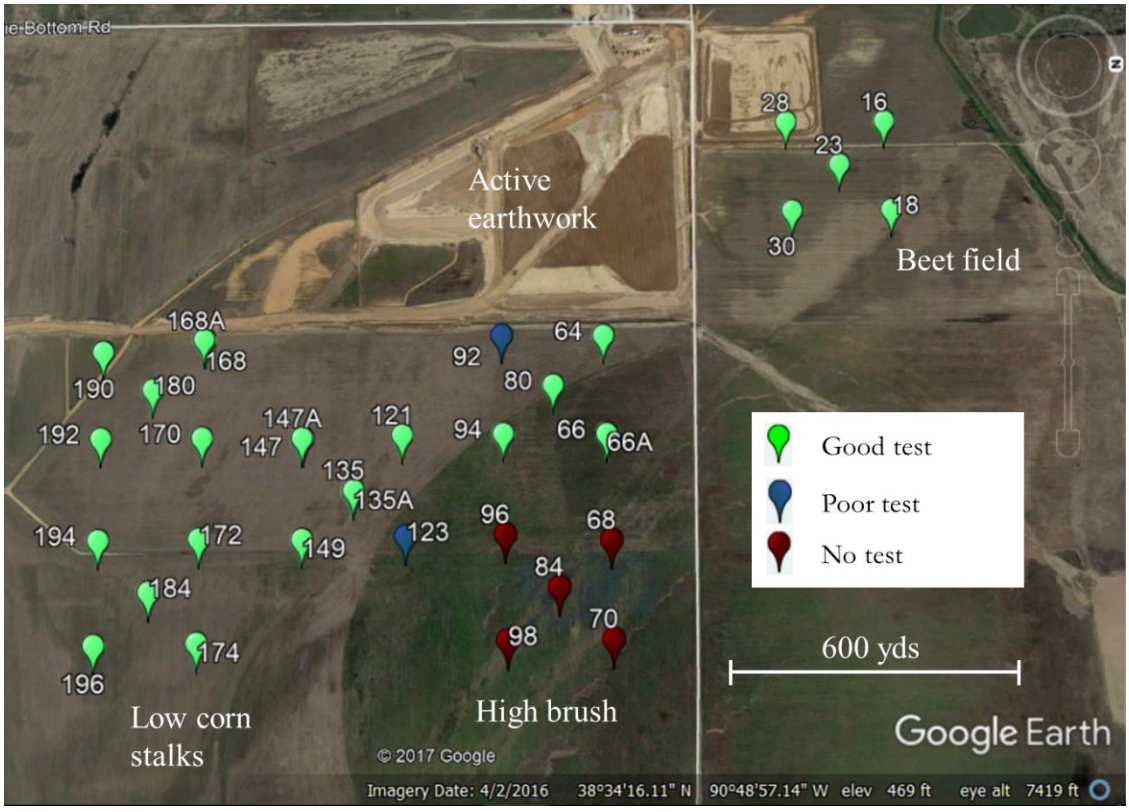

Figure 4.1 – Labadie UWL SASW testing overview.

4.3.1 Equipment

SASW testing was completed utilizing a SignalCalc ACEII dynamic signal analyzer version 4.8.309 and Geospace GS-11D 4.5 Hz rotating coil geophones. Geophones were housed in waterproof hard cases with 3-in spikes and connected with 300 ft of two-conductor, twisted, shielded pair wire (Figure 4.2). A 100-ft tape was used to mark source and receiver locations and a 10-lb sledge hammer and 50-lb drill bit were used to generate surface waves. Prior to field testing, all geophones were checked for phase consistency.

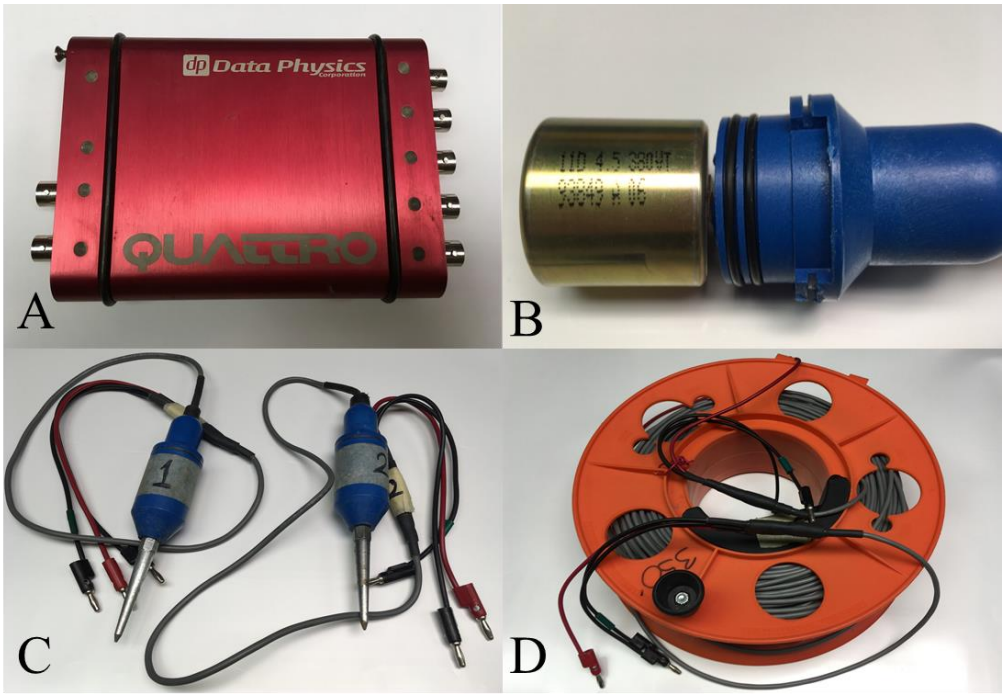

Figure 4.2 – SASW testing equipment A.) Data Physics signal analyzer B.) Geospace 4.5 Hz geophone C.) Geophones in waterproof casing with seating spikes D.) 300 ft of two-conductor, twisted, shielded pair wire.

4.3.2 Procedures

SASW tests were carried out at 29 points following the procedure outlined by Stokoe et al. (1994). Each center point for SASW testing corresponds to the location of a CPT sounding taken during the UWL site investigation. Exact locations were determined utilizing a Garmin Fortrex 401 global positioning system accurate (95%) from 15 to 30 ft. After determining a center point, pre-marked tape was laid with markings for each receiver spacing and source location (Figure 4.3). To mitigate the effects of background noise from UWL earthwork, receivers were oriented in-line with the direction of the background source. For points north of Labadie Bottom Road, testing was arrayed south to north and for points south of Labadie Bottom Road, west to east.

Figure 4.3 – SASW testing at Labadie UWL site, November 2016.

A target depth of 40 ft was chosen to coincide with CPT soundings typically taken to 36 ft. Receiver spacings of 5, 10, 20, and 40 ft were utilized for all tests with the only exceptions being Points 66, 66A, and 64. At Points 66 and 64, soft topsoil coupled with high background noise (bulldozers working approximately 350 yards west) limited receiver spacing to 30 ft. At Point 66A, tests were done with receiver spacings of both 30 and 40 ft to coincide with testing at Point 66.

Impulses were generated by impacting the 10-lb sledge hammer or 50-lb drop weight into blocks of wood seated firmly on the ground (Figure 4.3). For receiver spacings of 5 and 10 ft, the 10-lb sledge hammer generally produced sufficient energy when applied directly to the ground. Most tests at 20-ft receiver spacings required the wood block to effectively transfer energy from the hammer to the soil. At 40-ft receiver spacings, nearly all tests required the 50-lb drop weight be dropped from 5 to 7 ft onto the block of wood. Each site required careful selection of impulse trigger settings and responded differently to applied energy. While no specific observations were made regarding applied energy, it was generally noted that sites north of Labadie Bottom Road with firm silty topsoil required less energy, and those immediately south with mushy loam and tall vegetation required the most energy.

A minimum of three impulse signals were stacked for every test. For each receiver spacing, tests were deemed of sufficient quality when smooth wrapped phase diagrams were achieved across the first two full cycles of phase. If large jumps, significant skew, or low signal-to-noise ratios were observed, tests were restarted or additional impulses were stacked. Roughly half of the tests were completed with the minimum number of impulses and half required re-testing or additional stacking.

4.4 SASW Data Reduction and Dispersion Curve Fitting

Data were reduced and dispersion curves fitted utilizing WinSASW Version 2.2. Text (.txt) files were exported from SignalCalc for each test point and receiver spacing combination and subsequently loaded into WinSASW. Interactive masking was performed for each test and the first 180° of phase were generally disregarded (to avoid near field effects) while the three subsequent cycles of phase were used (180° to 900° unwrapped). Exceptions to these generalities were taken and more cycles of phase were used if phase diagrams displayed exceptionally low scatter. Similarly, phase diagrams were truncated within the targeted area if they exhibited unusual jumps or significant scatter.

Figure 4.4 shows selective masking of phase diagrams from Point 30. Shaded areas were discarded while unshaded areas were utilized to calculate the dispersion curve. At this location, for receiver spacings of 10 and 20 ft, the first three full cycles of phase were utilized and the rest discarded. For the 5-ft receiver spacing, an abnormality is present in the third cycle of phase resulting in a truncated target area. Similarly, the 40-ft receiver spacing exhibits a large jump in the second cycle of phase causing subsequent cycles of phase to be discarded.

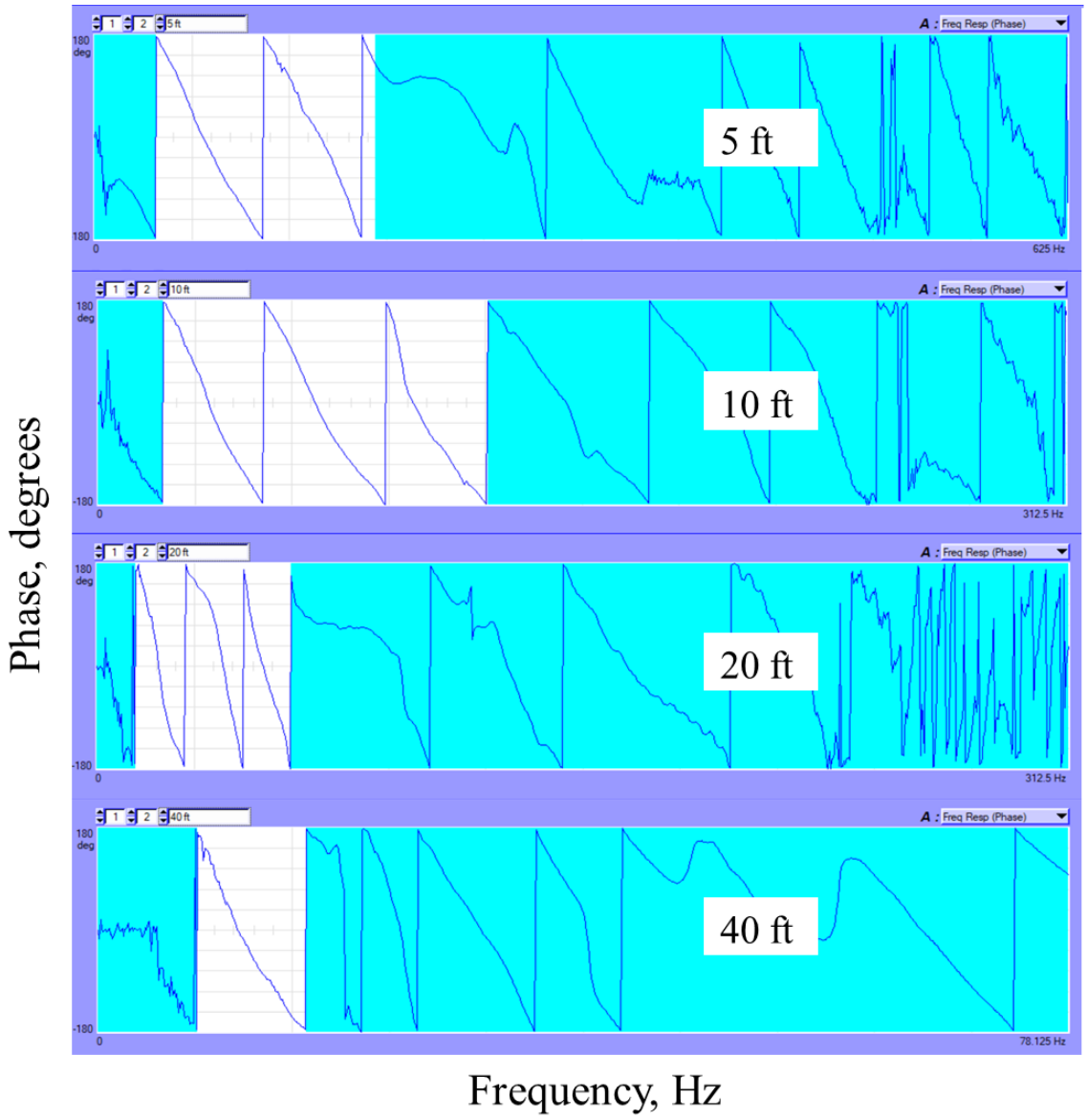

Figure 4.4 – WinSASW selective masking for Point 30. Vertical axis in degrees of phase (-180 to 180), horizontal axis in Hz.

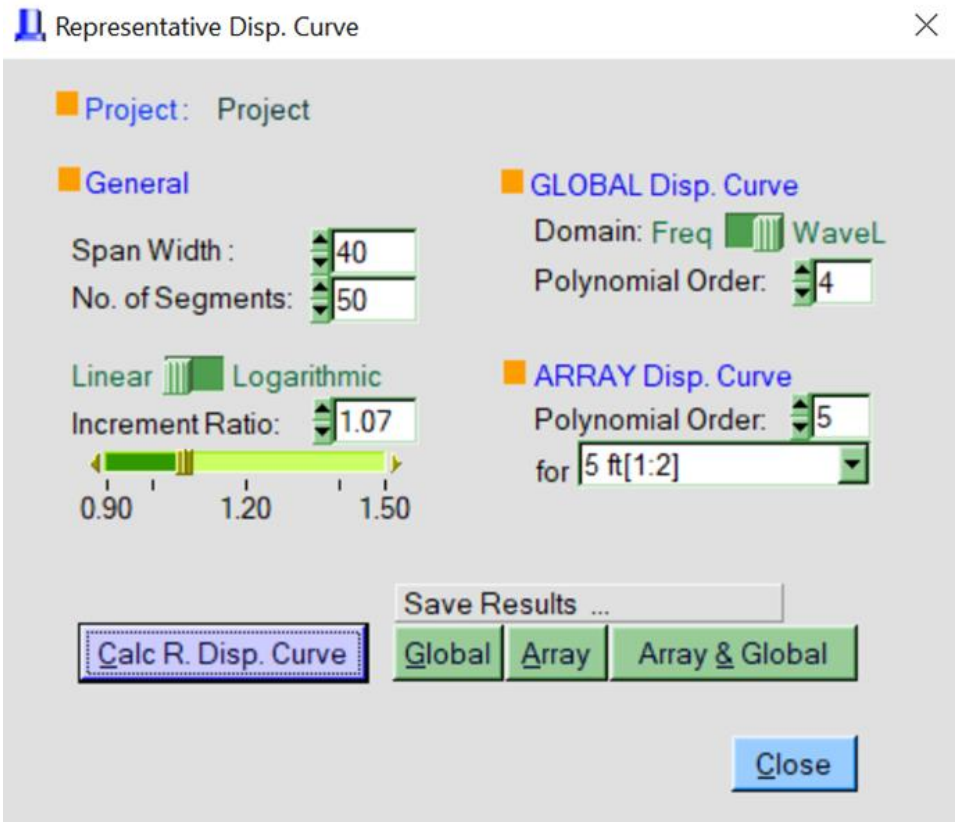

Figure 4.5 – WinSASW 2.2 representative dispersion curve settings.

Global dispersion curves were fitted according to wavelength and phase velocity utilizing default settings in WinSASW. The only exception to default settings is that dispersion curves were calculated in the wavelength domain (Figure 4.5). Figure 4.6 shows the composite measured dispersion curve for Point 30 consisting of individual dispersion curves for each receiver spacing (5 ft, 10 ft, 20 ft, 40 ft). The global dispersion curve for Point 30 is shown in Figure 4.7.

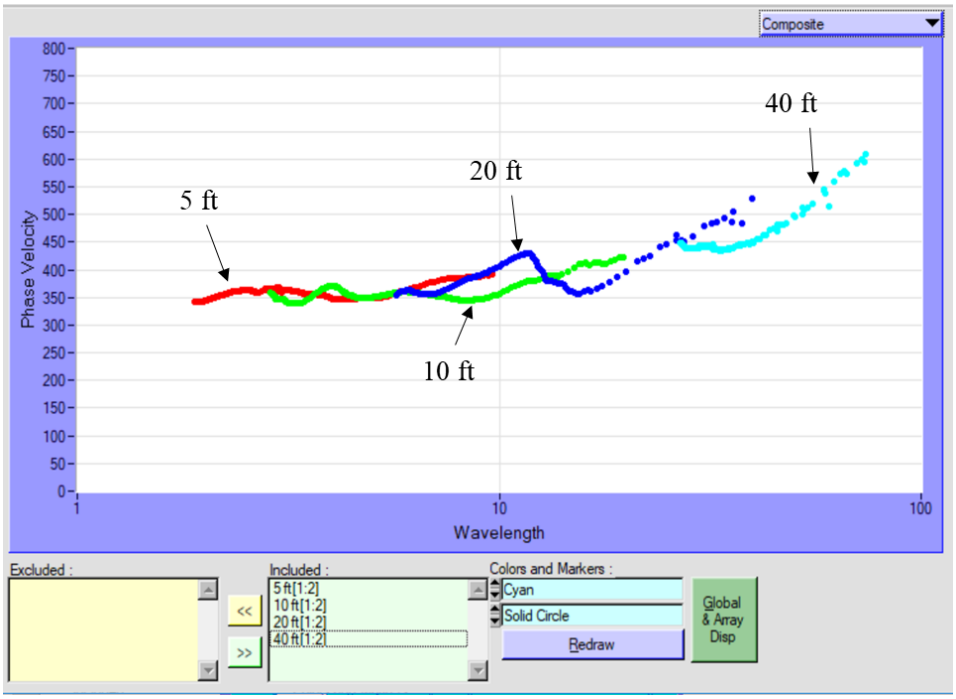

Figure 4.6 – Point 30 composite dispersion curve with associated receiver spacings.

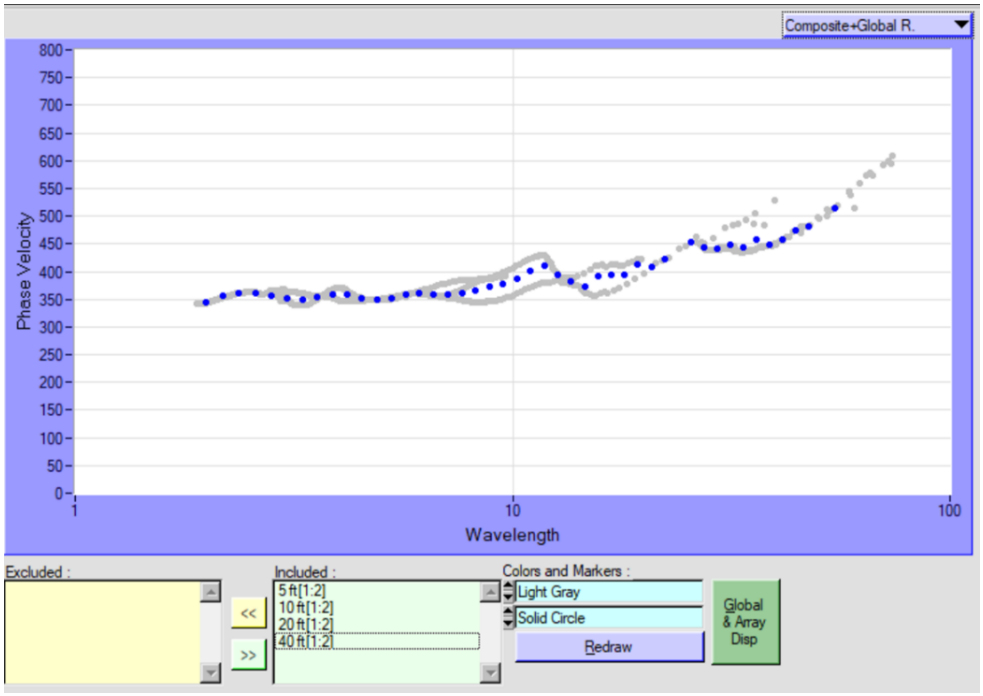

Figure 4.7 – Point 30 global dispersion curve (blue dots).

Finally, global dispersion curves were occasionally calculated with missing receiver spacings. This was only possible if the remaining segments sufficiently overlapped (Figure 4.8). All global dispersion curves were exported from WinSASW as text files containing phase velocity (V_{ph}), wavelength (λ), and frequency (f) for further processing in Microsoft Excel.

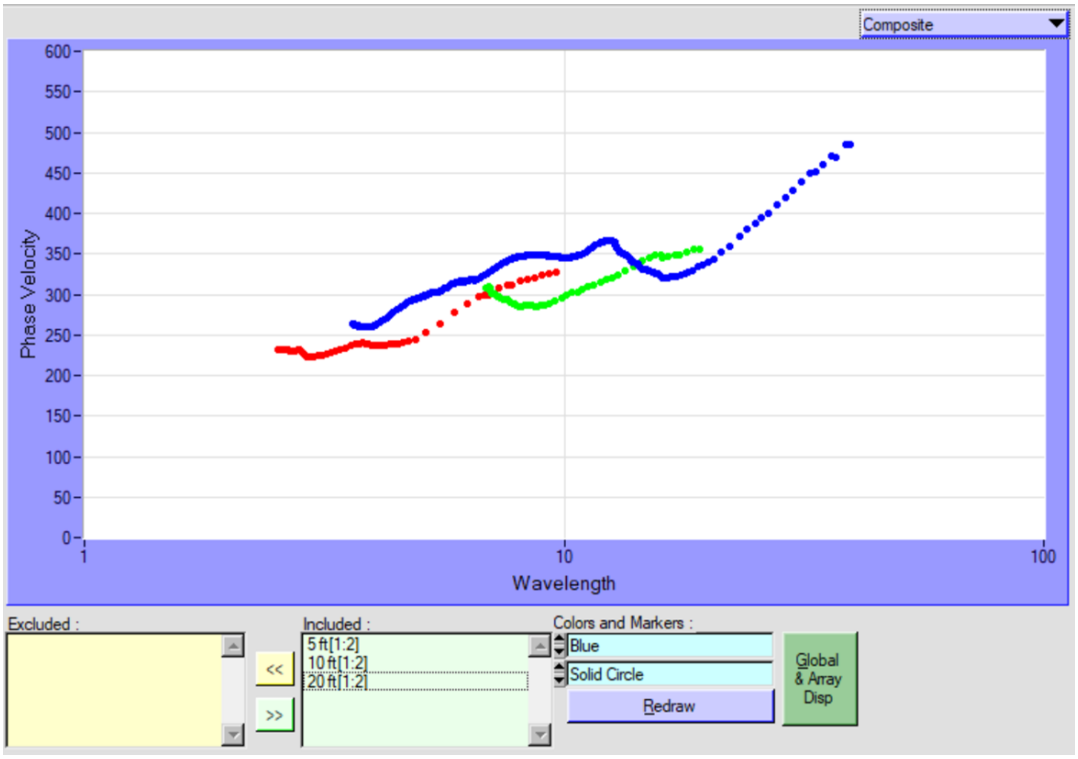

Figure 4.8 – Point 28 composite dispersion curve (no 40-ft receiver spacing).

4.5 Quantifying variability

Two approaches were utilized to quantify and compare variability in CPT and SASW data. The first method will be referred to as the "preliminary method" and the second the "equivalent wavelength method" (EWM). The preliminary method is a straightforward approach that was intended as a starting point for the development of a more refined

method. The EWM was developed only after the limitations of the preliminary method were realized through data analysis. In essence, the EWM incorporates the same framework as the preliminary method but improves it by weighting CPT data as a function of Rayleigh wave energy with depth. In doing so, the EWM ensures that an equitable comparison is made between measurements taken across approximately the same depths.

4.5.1 Preliminary Method

The preliminary method quantifies variability by calculating and averaging COVs of SASW and CPT data. Recall from Section 4.4 that measured SASW dispersion curves consist of phase velocity (V_{ph}) and their corresponding wavelength (λ). Put simply, the preliminary method quantifies variability of dispersion curves by calculating COVs amongst V_{ph} for the same λ measured at several test points within a group. A challenge in utilizing this method is that in WinSASW, dispersion curves are not calculated at constant λ. In order to compare V_{ph} at the same λ for each dispersion curve, V_{ph} must therefore be interpolated for desired values of λ. For the preliminary method, V_{ph} was interpolated every 0.5 ft for λ less than 10 ft, every 1 ft for λ between 10 and 20 ft, and every 5 ft thereafter (Figure 4.9, Table 4.2).

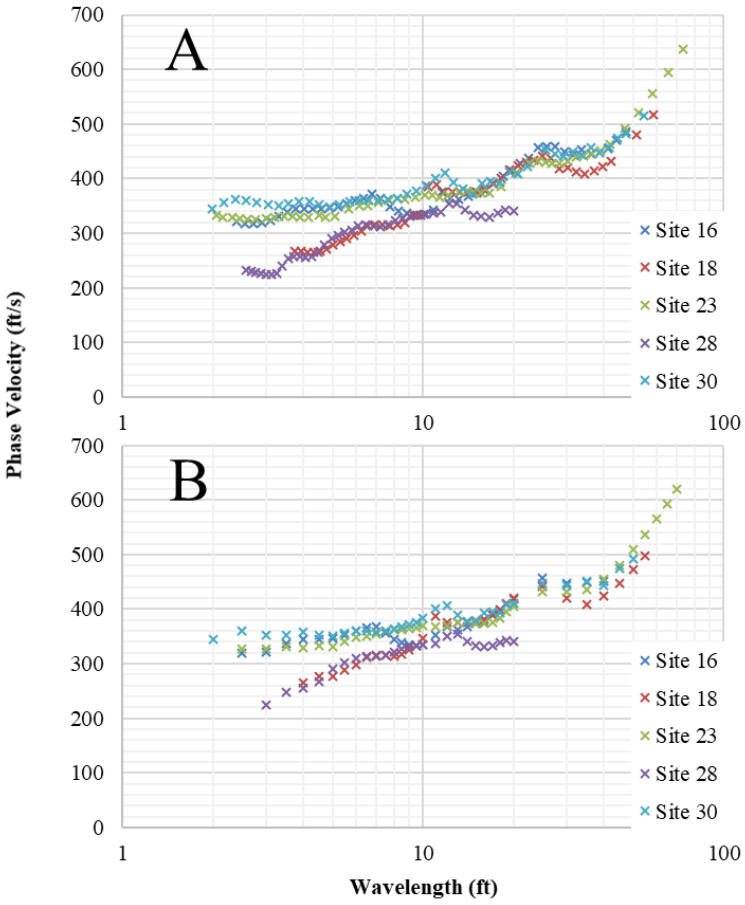

Figure 4.9 – Group 23 global dispersion curves A.) Direct from WinSASW B.) Interpolated for same wavelengths.

Once all V_{ph} values have been interpolated for every test point within a group, COVs are calculated for each λ (Table 4.2). However, because not all dispersion curves yield V_{ph} over the same range of λ, cases exist where V_{ph} for a particular λ are not available at every test point within a group. In such cases, COVs are calculated if three or more V_{ph} are available for any particular λ. This concept is illustrated in Table 4.2 where COVs are calculated when three or more V_{ph} values are available (λ ranging from 2.5 to 50 ft). Finally, COVs for each λ are averaged to provide the overall mean COV for the group (Table 4.2).

Table 4.2 – Group 23 dispersion curve variability calculation.

λ (ft)	Point 16 V_{ph} (ft/s)	Point 18 V_{ph} (ft/s)	Point 23 V_{ph} (ft/s)	Point 28 V_{ph} (ft/s)	Point 30 V_{ph} (ft/s)	COV V_{ph}
2.0					345	
2.5	320		327		361	0.065
3.0	321		328	224	353	0.184
3.5	337		330	248	353	0.149
4.0	345	266	329	256	358	0.151
4.5	345	278	332	267	353	0.126
5.0	348	278	330	291	350	0.104
5.5	353	288	341	302	355	0.094
6.0	360	299	349	310	360	0.086
6.5	367	312	351	314	360	0.076
7.0	368	316	355	313	359	0.075
7.5	356	315	359	315	361	0.071
8.0	344	314	363	322	363	0.066
8.5	339	317	363	328	368	0.064
9.0	336	325	364	331	373	0.061
9.5	332	332	367	333	376	0.062
10.0	334	347	370	335	383	0.062
11.0	353	388	368	338	402	0.070
12.0	369	376	369	350	406	0.055
13.0	363	376	375	354	389	0.036
14.0	368	376	377	340	378	0.043
15.0	373	375	374	333	379	0.053
16.0	376	382	373	331	392	0.063
17.0	388	390	377	332	394	0.068
18.0	400	399	384	339	393	0.066
19.0	409	411	394	343	408	0.073
20.0	418	419	405	340	411	0.083
25.0	458	442	431		447	0.025
30.0	447	420	432		444	0.029
35.0	449	409	435		451	0.044
40.0	452	424	455		443	0.032
45.0		447	481		475	0.039
50.0		473	509		493	0.036
55.0		498	537			
60.0			565			
65.0			592			
70.0			619			
Avg	-	-	-	-	-	**0.072**

The preliminary method compares CPT data in the same manner as SASW dispersion curves, with depth (z) replacing λ, and q_t or f_s replacing V_{ph} (Table 4.3). For each group of CPT soundings, a COV is calculated from q_t or f_s at a given depth. For depths where less than three measurements are available, no COV is calculated. Coefficients of variation are then averaged across the range of available depths to provide the overall mean COV of q_t or f_s for the group. The mean COV of CPT data may then be compared to the mean COV of V_{ph} from dispersion curves measured at the same physical locations.

Table 4.3 – Group 23 CPT q_t variability calculations.

Group 23 (16,18,23,28,30)						
Depth (ft)	Point 16 q_t (psi)	Point 18 q_t (psi)	Point 23 q_t (psi)	Point 28 q_t (psi)	Point 30 q_t (psi)	COV q_t
1.25	266	148	150	265	136	0.34
3.75	207	194	215	174	177	0.09
6.25	281	179	367	155	299	0.34
8.75	384	610	314	333	943	0.51
11.25	368	571	770	394	1513	0.65
13.75	762	1191	1279	169	2495	0.73
16.25	1007	1189	1201	972	693	0.20
18.75	1272	826	552	1208	1321	0.32
21.25	1768	776	1567	1242	1441	0.28
23.75	2664	1404	2454	1803	1617	0.27
26.25	1865	2413	2387	1835	2550	0.15
28.75	2898	3011	1518	1838	2323	0.28
31.25	2463	1603	2953	1591	2085	0.27
33.75	4296	2457	2775	2679	1270	0.40
36.25	4684	1948	4116	1496	2568	0.47
Avg	-	-	-	-	-	**0.35**

4.5.2 Equivalent Wavelength Method (EWM)

The second method utilized to compare CPT and SASW data was developed based on the shortcomings of the preliminary method. An in-depth discussion of those shortcomings and the need to enhance the preliminary method is provided in Chapter 6. The equivalent wavelength method (EWM) utilizes much of the same procedure as the preliminary method, with the following improvements:

1. CPT data (q_t, f_s) are weighted proportionally to Rayleigh wave energy distribution as a function of depth.
2. The same number of CPT and SASW measurements, taken across the same depths, are compared.

The principle behind the first improvement lies in the way Rayleigh wave energy dissipates exponentially with depth (Figure 4.10). This phenomenon causes the stiffness of upper soil layers to have a larger effect on Rayleigh wave propagation than stiffness of lower layers. For example, in a Rayleigh wave with λ_R = 10 ft, the overwhelming majority of wave energy (more than 70%) propagates through the upper 5 ft of soil. A simple approximation for quantifying the weight or percent of Rayleigh wave energy bounded between any two depths for a given λ is given below from Leong and Aung (2012).

$$W_i = \frac{\int_{Z_{i-1}}^{Z_i} f\left(\frac{z}{\lambda}\right) dz}{\int_0^{\lambda} f\left(\frac{z}{\lambda}\right) dz} \tag{4.1}$$

$$f\left(\frac{z}{\lambda}\right) = 1 - (z/\lambda)^{3/2} \tag{4.2}$$

Where Z_{i-1} is the depth at the top of layer i, and Z_i is the depth at the bottom of layer i for a particular λ. For example, the weight W_i (or percent) of Rayleigh wave energy transmitted between 2.5 and 5 ft below the surface for λ_R = 10 ft is calculated as follows:

$$W_i = \frac{\int_{Z_{i-1}}^{Z_i} f\left(\frac{Z}{\lambda}\right) dz}{\int_0^{\lambda} f\left(\frac{Z}{\lambda}\right) dz} = \frac{\int_{Z_{i-1}}^{Z_i} \left[1 - \left(\frac{Z}{\lambda}\right)^{\frac{3}{2}}\right] dz}{\int_0^{\lambda} \left[1 - \left(\frac{Z}{\lambda}\right)^{\frac{3}{2}}\right] dz}$$

$$= \frac{\left[Z_i - (2/5)Z_i\left(\frac{Z_i}{\lambda}\right)^{3/2}\right] - \left[Z_{i-1} - (2/5)Z_{i-1}\left(\frac{Z_{i-1}}{\lambda}\right)^{3/2}\right]}{\lambda - \frac{2}{5}\lambda} =$$

$$\frac{\left[5 - (2/5)5\left(\frac{5}{10}\right)^{3/2}\right] - \left[2.5 - \left(\frac{2}{5}\right)2.5\left(\frac{2.5}{10}\right)^{3/2}\right]}{10 - \frac{2}{5}10} = 0.32 \; or \; 32\%$$

This simple energy approximation can be used to weight CPT data with depth in approximately the same manner that Rayleigh wave energy is distributed. To achieve such an approximation, several "equivalent wavelengths" (λ_{eq}) and corresponding CPT measurements (CPT_{eq}) consisting of the equivalent corrected tip resistance (q_{teq}) or the equivalent skin friction (f_{seq}) are calculated for each site. CPT_{eq} is calculated by summing the product of each CPT measurement (q_t or f_s) for a given depth and its corresponding weight (W_i) (Eq. 4.3). Thus, each CPT sounding is converted into several CPT_{eq} measurements (q_{teq}, f_{seq}) each corresponding to a particular λ_{eq}. Finally, variability in q_{teq} or f_{seq} for each λ_{eq} may be compared in the same manner that variability in V_{ph} is compared for a specific λ in the preliminary method.

$$CPT_{eq(\lambda_{eq})} = \sum\left(CPT_i \cdot W_{i(\lambda_{eq})}\right) \tag{4.3}$$

Table 4.3 shows the values of W_i applied to CPT_i in calculating CPT_{eq} for a particular λ_{eq}. For example, CPT_{eq} for λ_{eq} = 2.5 ft is calculated by multiplying the CPT measurement taken at 1.25 ft (center of interval from 0 to 2.5 ft) by 1.0. Similarly, CPT_{eq} for λ_{eq} = 5 ft, is calculated by summing the CPT measurement at 1.25 ft multiplied by 0.715, and the CPT measurement at 3.75 ft multiplied by 0.285. This process is repeated and CPT_{eq} is calculated for as many as 15 λ_{eq} depending on the depth of the CPT sounding.

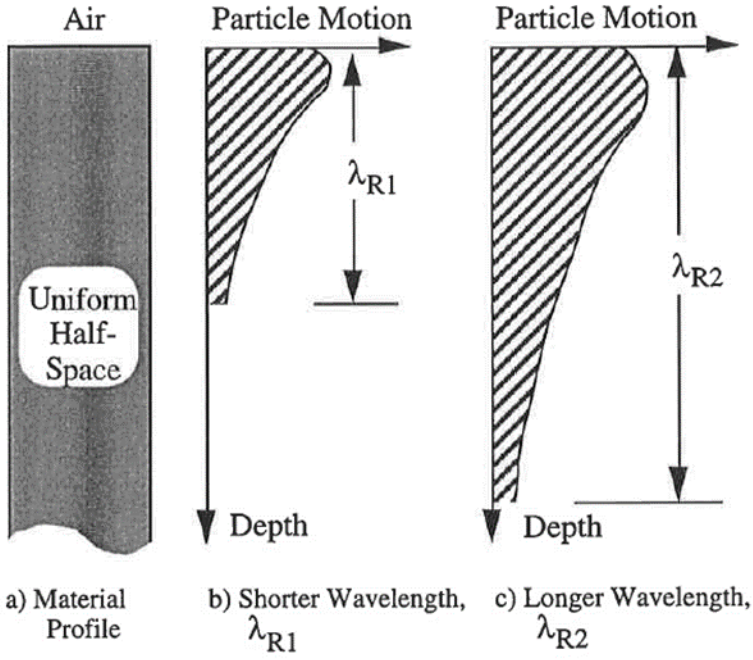

Figure 4.10 – Approximate distribution of vertical particle motion with depth for different length Rayleigh waves (from Stokoe et al. 1994).

Table 4.3 – Equivalent wavelength CPT weighting. Chart values are weights (W_i) applied to CPT measurements taken at the specified depth (z) for a particular λ_{eq}.

λ_{eq} (ft) / z (ft)	2.5	5	7.5	10	12.5	15	17.5	20	22.5	25	27.5	30	32.5	35	37.5
1.25	1.000	0.715	0.513	0.396	0.321	0.270	0.233	0.205	0.182	0.165	0.150	0.138	0.127	0.118	0.110
3.75		0.285	0.356	0.320	0.278	0.243	0.214	0.191	0.172	0.157	0.144	0.133	0.123	0.115	0.108
6.25			0.131	0.210	0.215	0.203	0.187	0.172	0.158	0.146	0.135	0.126	0.117	0.110	0.104
8.75				0.075	0.138	0.154	0.154	0.148	0.140	0.132	0.124	0.117	0.110	0.104	0.099
11.25					0.048	0.097	0.115	0.120	0.120	0.116	0.112	0.107	0.102	0.097	0.093
13.75						0.034	0.072	0.089	0.097	0.099	0.098	0.096	0.093	0.090	0.086
16.25							0.025	0.056	0.071	0.079	0.083	0.083	0.083	0.081	0.079
18.75								0.019	0.044	0.058	0.066	0.070	0.072	0.072	0.072
21.25									0.015	0.036	0.049	0.056	0.060	0.063	0.064
23.75										0.012	0.030	0.041	0.048	0.052	0.055
26.25											0.010	0.025	0.035	0.042	0.046
28.75												0.009	0.022	0.030	0.037
31.25													0.007	0.019	0.027
33.75														0.006	0.016
36.25															0.005

Finally, the second improvement to the preliminary method is implemented in the EWM by comparing variability in CPT_{eq} to variability in V_{ph} across the same λ or λ_{eq}. That is, for every calculated CPT_{eq} at a specific location, V_{ph} for the same λ is interpolated from SASW data. For situations where either CPT_{eq} or V_{ph} for the same λ are unavailable due to a lack of CPT or SASW data, no comparison is made.

4.5.3 EWM Example Calculation

Recall that Group 23 consists of Points 16, 18, 23, 28, and 30, and that each point represents a specific surface location where a CPT sounding and SASW test have been conducted. First, after ensuring that CPT and SASW data are available for all points in Group 23, q_{teq} is calculated for λ_{eq} ranging from 2.5 to 37.5 ft on a 2.5-ft interval. Table 4.4 shows q_{teq} calculations for Point 16 and Table 4.5 shows q_{teq} calculations for all points in Group 23. Once all q_{teq} values are calculated, a COV for each λ_{eq} may be determined. In the case of Group 23, the COV of q_{teq} is calculated for all 15 λ_{eq} because q_{teq} is available for three or more points for all λ_{eq}. However, final COVs and the overall mean COV for the group cannot be calculated until the availability of V_{ph} from SASW testing is known.

Table 4.4 – EWM calculation of q_{teq} for Point 16.

Depth z (ft)	Measured CPT data			EWM		
	q_t (psi)	f_s (psi)	u (psi)	λ_{eq} (ft)	q_{teq} (psi)	f_{seq} (psi)
1.25	266	2.9	-0.8	2.5	266	2.9
3.75	207	4.6	-1.3	5.0	249	3.4
6.25	281	3.8	-2.0	7.5	247	3.6
8.75	384	2.8	-2.7	10.0	259	3.6
11.25	368	2.9	-3.5	12.5	274	3.6
13.75	762	3.9	-0.4	15.0	299	3.5
16.25	1007	6.8	1.3	17.5	340	3.6
18.75	1272	5.9	3.5	20.0	392	3.7
21.25	1768	9.9	3.4	22.5	455	3.9
23.75	2664	10.0	5.0	25.0	536	4.2
26.25	1865	5.5	6.5	27.5	623	4.5
28.75	2898	10.0	7.3	30.0	710	4.7
31.25	2463	5.8	8.7	32.5	799	4.9
33.75	4296	12.6	9.3	35.0	894	5.1
36.25	4684	17.0	10.0	37.5	1002	5.3

Table 4.5 – EWM calculation of q_{teq} for Group 23.

λ_{eq} (ft)	Point 16 q_{teq} (psi)	Point 18 q_{teq} (psi)	Point 23 q_{teq} (psi)	Point 28 q_{teq} (psi)	Point 30 q_{teq} (psi)	COV q_{teq}
2.5	266	148	150	265	136	0.39
5.0	249	161	168	239	148	0.25
7.5	247	168	201	218	172	0.16
10.0	259	204	228	218	244	0.09
12.5	274	252	267	232	360	0.18
15.0	299	313	333	240	516	0.31
17.5	340	385	409	261	642	0.35
20.0	392	446	466	303	722	0.34
22.5	455	491	516	355	787	0.31
25.0	536	533	583	414	844	0.24
27.5	623	588	663	481	906	0.21
30.0	710	660	737	548	973	0.18
32.5	799	733	811	611	1036	0.16
35.0	894	802	888	674	1089	0.13
37.5	1002	866	972	736	1137	0.11
Avg	--	--	--	--	--	**0.23**

Next, V_{ph} values are interpolated from SASW dispersion curves for the same λ utilized in calculating q_{teq} (Table 4.6). Once V_{ph} values have been interpolated for all points, they are compared to available q_{teq} from CPT testing. Table 4.7 shows that in the case of Group 23, V_{ph} values are missing at λ of 2.5 ft for Point 18, as well as λ of 2.5 ft and 22.5 to 37.5 ft for Point 28. Therefore, mean COV calculations for both q_{teq} and V_{ph} will exclude COVs for λ of 2.5 ft at Point 18, and λ of 2.5 ft and 22.5 to 37.5 ft at Point 28 (Table 4.8).

Table 4.6 – Interpolation of target V_{ph} values for Point 16.

Raw Dispersion Data			Interpolation		Raw Dispersion Data			Interpolation	
V_{ph} (ft/s)	f (Hz)	λ (ft)	λ target (ft)	V_{ph} (λ target) (ft/s)	V_{ph} (ft/s)	f (Hz)	λ (ft)	λ target (ft)	V_{ph} (λ target) (ft/s)
322	134.0	2.4			343	31.8	10.8		
318	124.4	2.6	2.5	320	376	32.6	11.5		
317	116.4	2.7			363	29.5	12.3		
319	109.8	2.9			363	27.5	13.2	12.5	363
323	104.3	3.1			368	26.1	14.1		
330	99.9	3.3			374	24.8	15.1	15.0	373
338	95.9	3.5			377	23.4	16.1		
344	91.5	3.8			392	22.7	17.2		
345	86.1	4.0			404	21.9	18.4	17.5	394
345	80.6	4.3			415	21.1	19.7		
345	75.6	4.6			427	20.3	21.1	20.0	418
347	71.1	4.9			437	19.4	22.5	22.5	437
349	67.0	5.2	5.0	348	456	18.9	24.1		
354	63.6	5.6			459	17.8	25.8	25.0	458
360	60.5	5.9			459	16.6	27.6	27.5	459
365	57.4	6.3			449	15.2	29.5		
371	54.7	6.8			443	14.0	31.5	30.0	447
365	50.3	7.2			453	13.4	33.7	32.5	447
349	45.0	7.7	7.5	356	445	12.3	36.1	35.0	449
340	41.1	8.3			454	11.0	41.3	37.5	447
337	38.1	8.8			470	10.6	44.2		
332	35.2	9.4			485	10.3	47.3		
335	33.2	10.1	10.0	334	--	--	--	--	--

Table 4.7 – Variability of V_{ph} at selected λ for Group 23.

λ (ft)	Point 16 V_{ph} (ft/s)	Point 18 V_{ph} (ft/s)	Point 23 V_{ph} (ft/s)	Point 28 V_{ph} (ft/s)	Point 30 V_{ph} (ft/s)	COV V_{ph}
2.5	320		327		361	0.065
5.0	348	278	330	291	350	0.104
7.5	356	315	359	315	361	0.071
10.0	334	347	370	335	383	0.062
12.5	363	376	372	355	395	0.041
15.0	373	375	374	333	379	0.053
17.5	394	394	379	337	394	0.066
20.0	418	419	405	340	411	0.083
22.5	437	431	427		425	0.013
25.0	458	442	431		447	0.025
27.5	459	429	428		444	0.033
30.0	447	420	432		444	0.029
32.5	447	412	439		446	0.038
35.0	449	409	435		451	0.044
37.5	447	416	448		452	0.038
Avg	--	--	--	--	--	**0.051**

Finally, after COV calculations are made for available λ where three or more values are present in each case, the overall mean COV of q_{teq} and V_{ph} is calculated for the group. For Group 23, the mean COV of V_{ph} is 0.051 (Table 4.7) and the mean COV of q_{teq} for the same λ is 0.23 (Table 4.8). As previously stated, this example excludes some q_{teq} measurements because no corresponding V_{ph} is available. It should be noted, however, that cases also exist where V_{ph} values are not utilized because no corresponding q_{teq} is available.

Table 4.8 – Variability of q_{teq} at selected λ_{eq} for Group 23. Struck through values not included in COV q_{teq} calculation.

λ_{eq} (ft)	Point 16 q_{teq} (psi)	Point 18 q_{teq} (psi)	Point 23 q_{teq} (psi)	Point 28 q_{teq} (psi)	Point 30 q_{teq} (psi)	COV q_{teq}
2.5	266	~~148~~	150	~~265~~	136	0.39
5.0	249	161	168	239	148	0.25
7.5	247	168	201	218	172	0.16
10.0	259	204	228	218	244	0.09
12.5	274	252	267	232	360	0.18
15.0	299	313	333	240	516	0.31
17.5	340	385	409	261	642	0.35
20.0	392	446	466	303	722	0.34
22.5	455	491	516	~~355~~	787	0.31
25.0	536	533	583	~~414~~	844	0.24
27.5	623	588	663	~~481~~	906	0.21
30.0	710	660	737	~~548~~	973	0.18
32.5	799	733	811	~~611~~	1036	0.16
35.0	894	802	888	~~674~~	1089	0.13
37.5	1002	866	972	~~736~~	1137	0.11
Avg	--	--	--	--	--	**0.23**

5 Results

5.1 Overview

This chapter provides the results of all CPT and SASW tests as well as the results of all variability and additional analyses. Section 5.2 contains plots of q_t vs z for all CPT soundings as well as an initial variability analysis. Detailed CPT results for all points including all associated measurements and correlations can be found in the 2011 DSI report. Section 5.3 provides the results of SASW testing in the form of phase velocity dispersion curves for all points and all groups. Variability correlations between dispersion curves and CPT data utilizing the preliminary method are provided in Section 5.4. Finally, variability correlations, general results, and additional correlations utilizing the EWM are presented in Section 5.5.

5.2 CPT Measurements and Initial Comparison

After establishing the UWL as a viable site and obtaining CPT measurements from Reitz & Jens, Inc., a preliminary examination of the raw and processed data was conducted. Processed data were selectively verified from raw data and found to be accurate in all cases. For each point, processed CPT data incudes q_t, f_s, u_m, and several other correlated values given at 2.5-ft intervals starting at a depth of 1.25 ft and extending to a depth of 36.25 ft or cone refusal. For each depth, given measurements are not point measurements, but averages across the 2.5-ft interval. For example, measurements (q_t, f_s, u_m) provided for a depth of 1.25 ft are average measurements across the interval from 0 to 2.5 ft just as measurements provided for 21.25 ft are average measurements across the interval from 20

to 22.5 ft. Plots of q_t vs z for all points are included in Appendix A. Additionally, CPT measurements and all associated plots can be found in the 2011 DSI report.

Generally, CPT soundings across the UWL show low q_t (0-300 psi) for depths from 0 to 15 ft and then progressively increase to around 3000 psi at a depth of 35 ft. Plots of q_t vs z for Group 23, the northwesternmost group, are provided in Figure 5.1. Most points initially show q_t of around 300 psi or less for the first 10 to 15 ft. After reaching 10 to 15 ft in depth, stiffness gradually increases to around 2600 psi at 35 ft with Points 16 and 23 having q_t as great as 4400 psi. One exception to the general trend is Point 30 which becomes stiff at around 10 ft, then rapidly drops to around 700 psi (Appendix A, Figure A.18). Finally of all q_t vs z plots in Group 23, the most scatter is observed in Points 18 and 30 (Appendix A, Figures A.6 & A.18) with q_t varying in excess of 1500 psi over only 2.5 ft in each case.

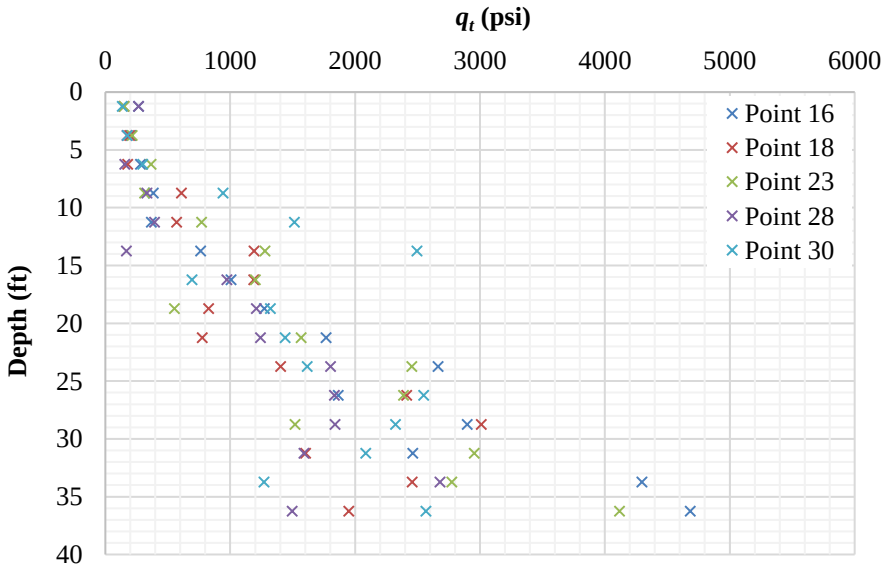

Figure 5.1 – Group 23 tip resistance (q_t) vs depth (z).

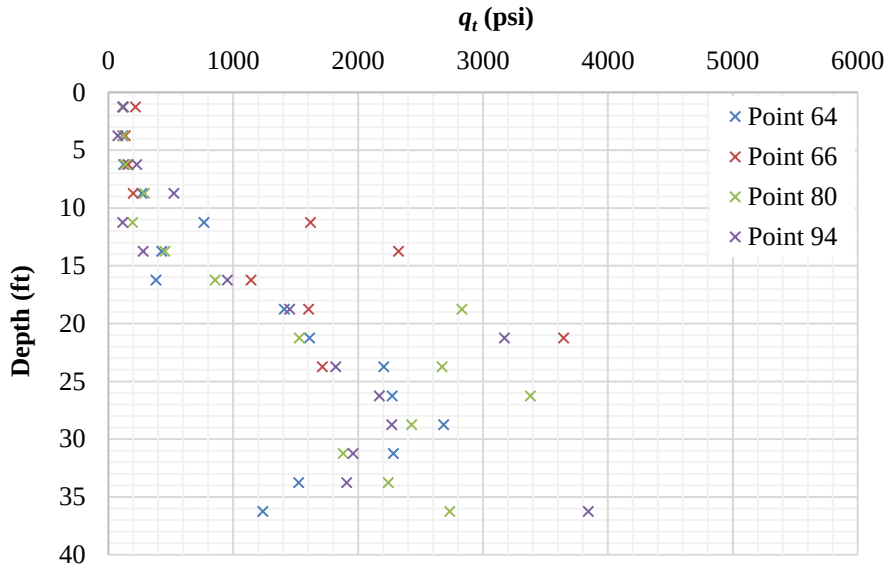

Figure 5.2 – Group 80 tip resistance (q_t) vs depth (z).

CPT soundings for the northwesternmost group south of Labadie Bottom Rd., Group 80, are also quite soft in the upper 12 to 15 ft with most q_t measurements less than 400 psi (Figure 5.2). Corrected tip resistance then progressively increases to approximately 2400 psi at 35 ft. Two of the four points in Group 80 show significant scatter with more than 1500 psi variation in q_t across less than 2.5 ft in depth. The most atypical sounding in Group 80 is Point 64 (Appendix A, Figure A.22), which shows a typical increase in q_t until about 30 ft at which point q_t gradually decreases to about 1200 psi at 35 ft of depth.

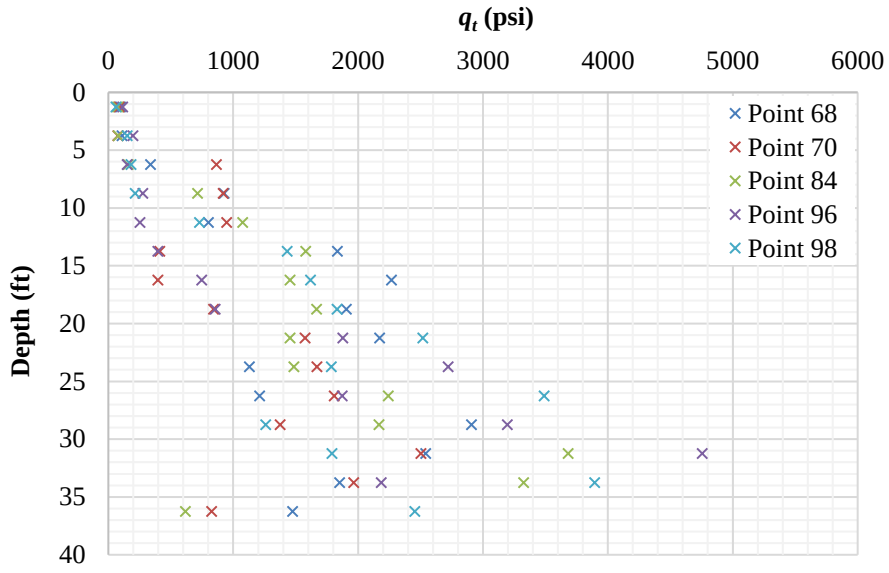

Figure 5.3 – Group 84 tip resistance (q_t) vs depth (z).

Group 84 is the northeasternmost group south of Labadie Bottom Rd. For this group, q_t vs z displays significant scatter with four of the five points having variation in q_t greater than 1500 psi over less than 2.5 ft of depth (Figure 5.3). Atypical soundings include Points 70 and 84 which both have soft material with q_t of approximately 700 psi at 35 ft (Appendix A, Figure A.38 & A.39). Also, Points 84 and 96 have stiff layers with q_t in excess of 3800 psi at a depth of approximately 32 ft (Appendix A, Figures A.39 & A.40). Finally, the most atypical sounding is Point 98 where variation in excess of 2000 psi is repeatedly encountered from 20 to 35 ft (Appendix A, Figure A.41).

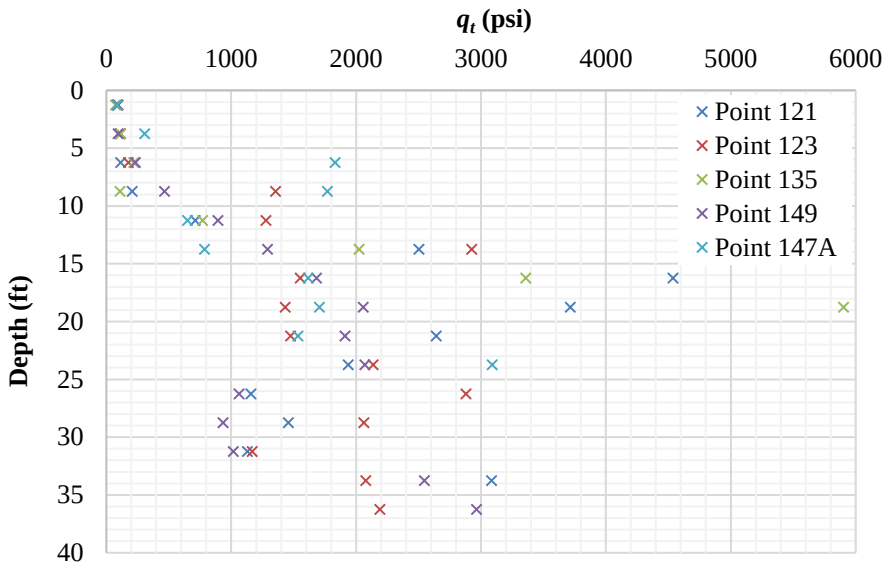

Figure 5.4 – Group 135 tip resistance (q_t) vs depth (z).

Group 135, the center group south of Labadie Bottom Rd., shows the most variability of all group q_t vs z plots (Figure 5.4). Two of the five soundings were refused at less than 35 ft with Point 135 having refusal at 16 ft and Point 147A having refusal at 25 ft (Appendix A, Figures A.51 & A55). Point 147A is also unusually stiff from 6 to 9 ft with q_t of around 1800 psi. Point 121 shows q_t rapidly increase from 200 psi at 9 ft to 4500 psi at 15 ft followed by a decline to only 1200 psi at 30 ft (Appendix A, Figure A.43). Point 149 also exhibits unusual behavior with a soft section (1000 psi) from about 25 to 32 ft (Appendix A, Figure A.47). Of the five soundings in Group 135, four show changes in q_t in excess of 1500 psi over approximately 2.5 ft in depth.

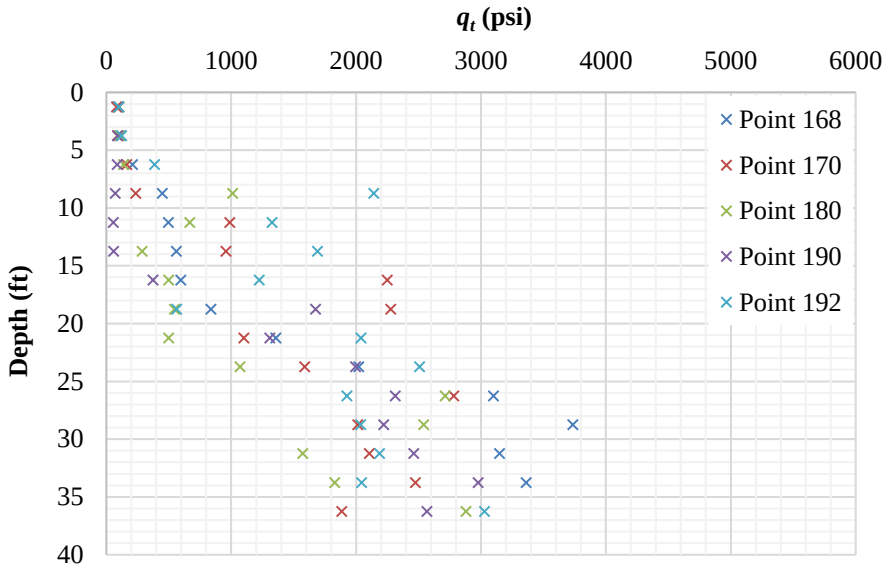

Figure 5.5 – Group 180 tip resistance (q_t) vs depth (z).

The southwesternmost group, Group 180, shows more consistency in the general trend of q_t vs z while individual soundings display some scatter (Figure 5.5). The most atypical sounding is Point 190 where q_t is less than 100 psi from the surface to 15 ft, then sharply increases to 1700 psi at 20 ft (Appendix A, Figure A.75). Of the five soundings in Group 180, two have changes in q_t greater than 1500 psi across less than 2.5 ft of depth.

Finally, the southeasternmost group, Group 184, is typical until about 25 ft at which point soundings show more variability (Figure 5.6). Of the five soundings in Group 180, three have greater than 1500 psi variability in q_t across less than 2.5 ft of depth. Point 184 has an extremely stiff inclusion at 25 ft with q_t near 5500 psi followed by below average stiffness of only about 1500 psi at 35 ft (Appendix A, Figure A.91). Point 196 is also atypical with a sharp decrease in q_t from 2300 psi at 29 ft to only 400 psi at 34 ft (Appendix A, Figure A.99).

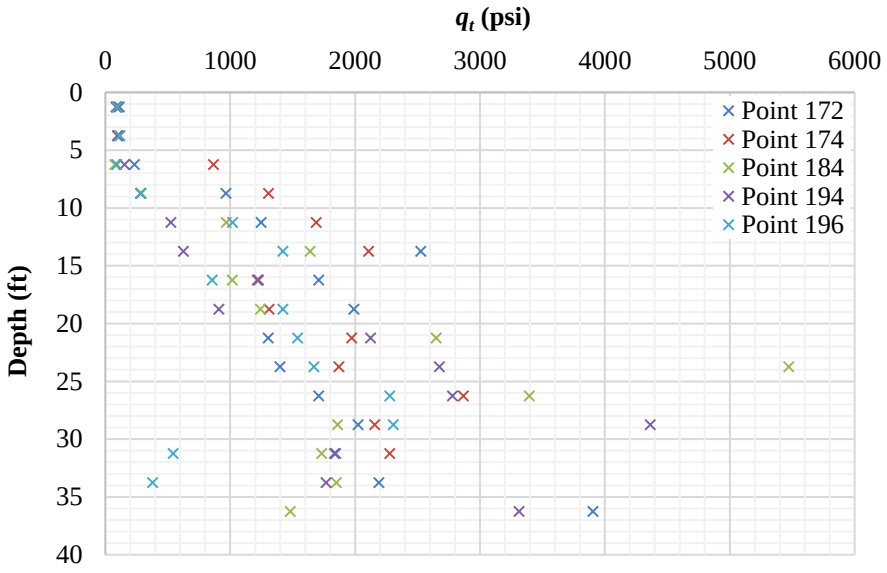

Figure 5.6 – Group 184 tip resistance (q_t) vs depth (z).

5.2.1 Verification of Selected CPT Soundings

The 2011 DSI report includes several CPT soundings taken at approximately the same physical locations (within 15 ft). In many cases, the additional test was conducted to verify shallow tip refusal, but there are also cases where additional tests were performed to verify the precision of the measurements. Figures 5.7, 5.8, and 5.9 show side-by-side CPT measurements. The average difference in CPT measurements taken at the same depth for Points 66, 135, and 168 is approximately 30%. This 30% difference, however, is largely due to differences in q_t at depths greater than 25 ft for Point 168. When those specific measurements are not considered, the average difference is reduced to approximately 18%. For all nine locations where a redundant CPT sounding was taken, the mean difference in q_t is approximately 22%.

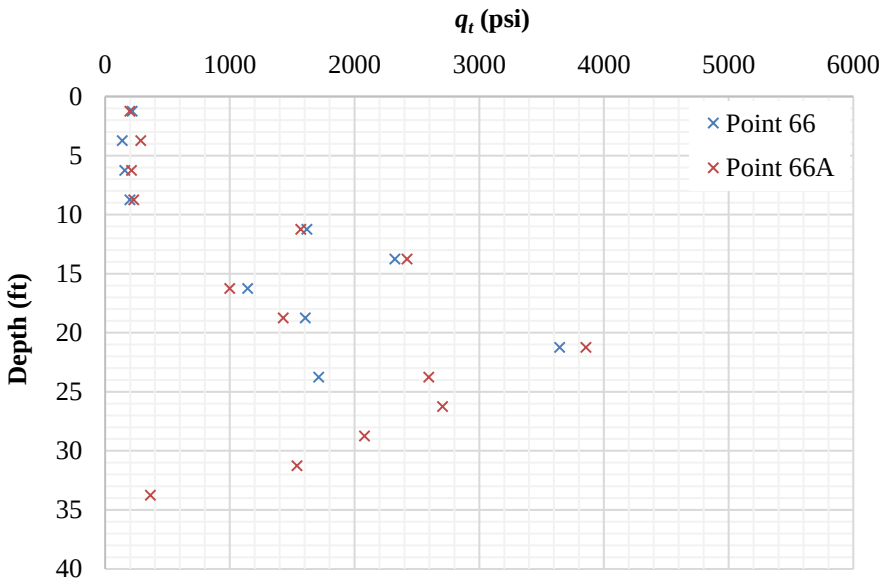

Figure 5.7 – Point 66 and 66A tip resistance (q_t) vs depth (z).

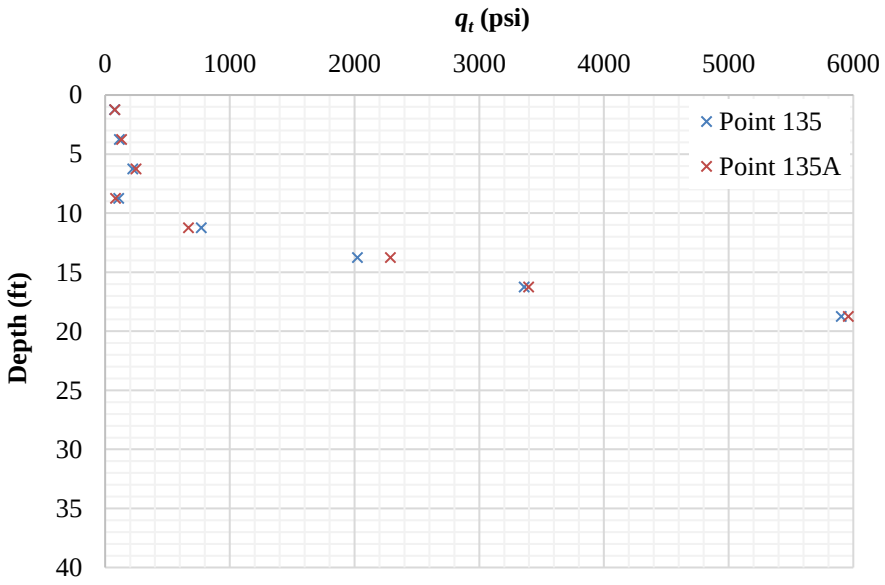

Figure 5.8 – Point 135 and 135A tip resistance (q_t) vs depth (z).

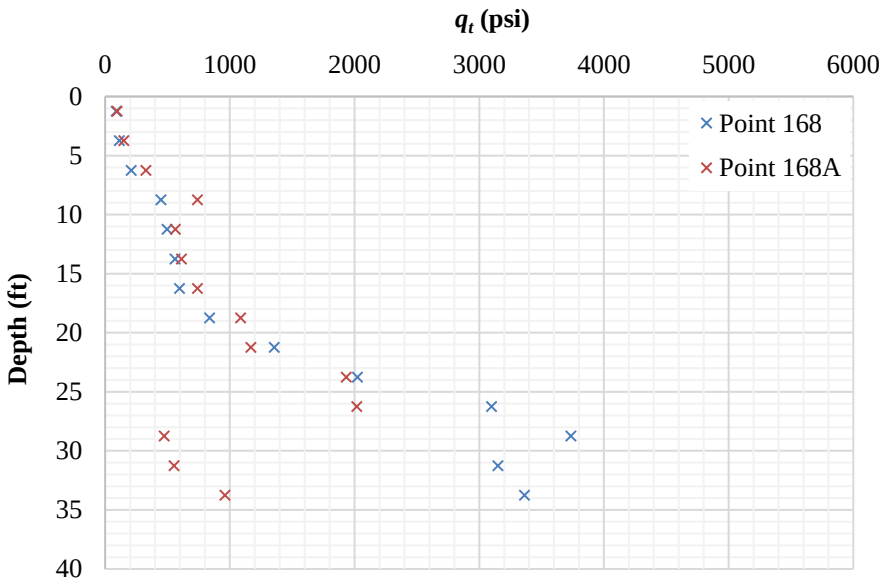

Figure 5.9 – Point 168 and 168A tip resistance (q_t) vs depth (z).

5.2.2 Preliminary Variability Analysis of CPT Data

Prior to any SASW testing, a brief variability analysis of CPT data was conducted to examine the suitability of the UWL site and the preliminary method. Specifically, the analysis was intended to determine whether a sufficient range in variability existed amongst groups of CPT measurements. This variability analysis was carried out as described in Section 4.5.1 and considered variability in q_t and f_s. Figure 5.10 shows that among the six groups analyzed, the average COV in q_t for each group ranges from about 0.35 to 0.56. Similarly, the average COV in f_s ranges from 0.35 to 0.54. It also shows that utilizing this method, variability in q_t is related to variability in f_s at an approximate 1:1 ratio. Based on these results, the range in variability at the UWL site was deemed sufficient to proceed with SASW testing. Further, the approximate 1:1 correlation between mean COVs for q_t and f_s served as an initial validation of the preliminary method.

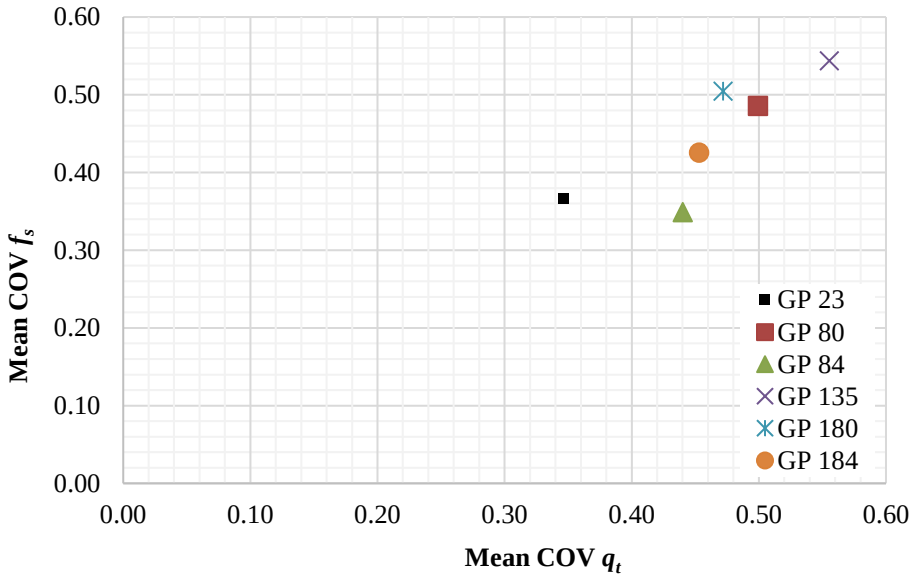

Figure 5.10 – Preliminary variability analysis of UWL CPT data.

5.3 SASW Dispersion Curves

Phase velocity dispersion curves were obtained from SASW testing as described in Section 4.3 and are provided for each point in Appendix A. Generally, the UWL site yields V_{ph} between 150 and 350 ft/s for the smallest λ (1-5 ft) and gradually increases to 490 to 730 ft/s for the largest wavelengths (50-75 ft). When calculated utilizing the preliminary method, however, dispersion curves show much less variability than CPT data with mean COVs ranging from approximately 0.07 to 0.1.

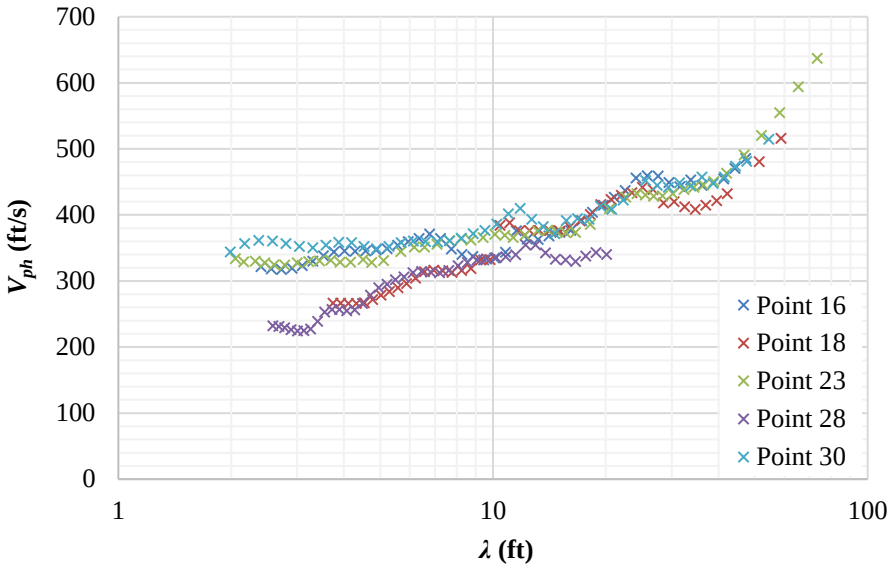

Figure 5.11 – Group 23 dispersion curves.

The northwesternmost group, Group 23, has two distinct trends in dispersion curves for λ less than 20 ft (Figure 5.11). The first trend is exhibited in Points 16, 23, and 30 with V_{ph} starting at around 350 ft/s and increasing at a rate of about 4 ft/s/ft to around 450 ft/s at λ of 25 ft. From λ of 25 to 35 ft, V_{ph} decreases slightly and at λ greater than 35 ft, V_{ph} increases at a rate of about 4.3 ft/s/ft. The second trend is seen in Points 18 and 28 which have V_{ph} that are 15 to 25% lower than the rest of the group. However, for Point 28, V_{ph}, for λ longer than approximately 10 ft is not available due to poor data quality. The COV in V_{ph} for Group 23 as calculated utilizing the preliminary method is 0.072.

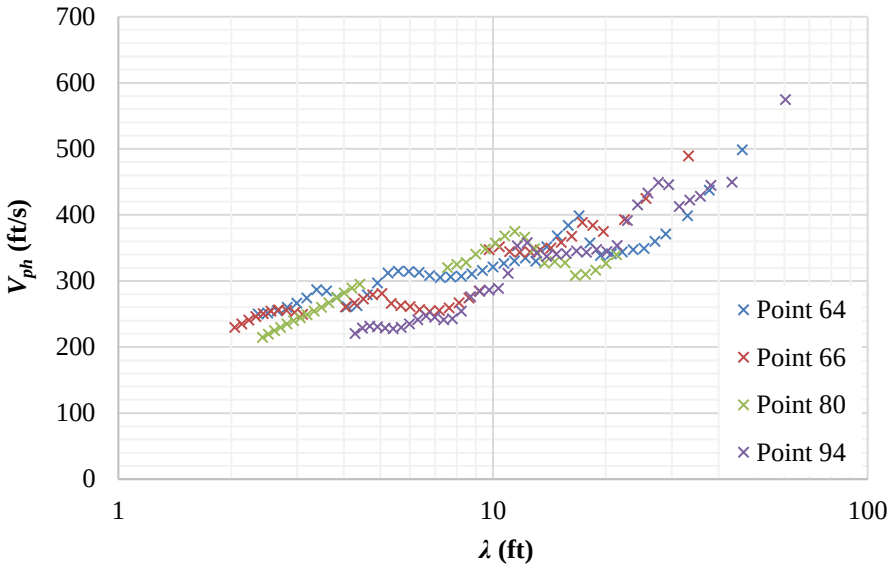

Figure 5.12 – Group 80 dispersion curves.

Group 80, the northwesternmost group south of Labadie Bottom Rd., shows an increase in V_{ph} from about 250 ft/s at small λ to around 375 ft/s at λ of 15 ft (Figure 5.12). From λ of 15 to 25 ft, V_{ph} remains fairly constant but increase at a rate of approximately 4 ft/s/ft for longer wavelengths. Point 94 is notably different from the rest of the group in that V_{ph} is around 50 ft/s slower from λ of 4 to 8 ft. Utilizing the preliminary method, the COV of V_{ph} for Group 80 is 0.085.

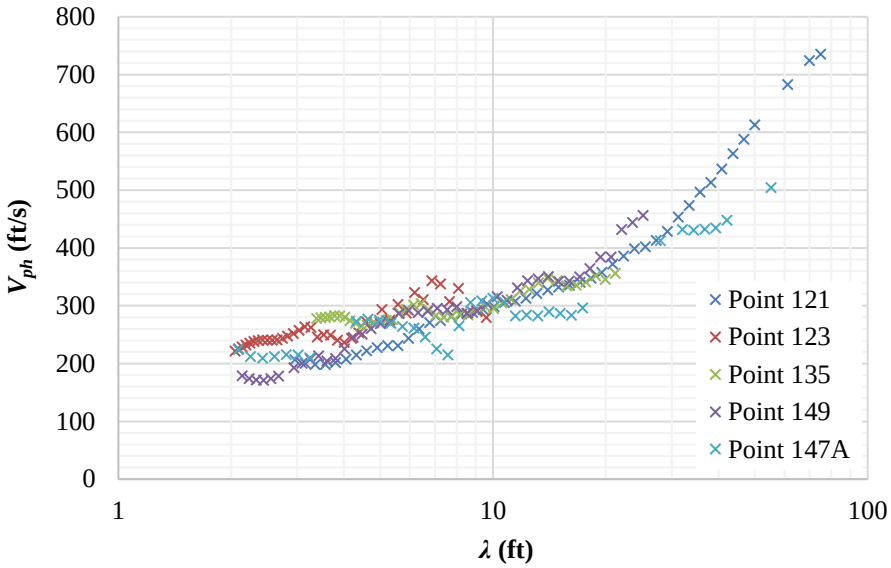

Figure 5.13 – Group 135 dispersion curves.

Dispersion curves in Group 135, the center group south of Labadie Bottom Rd., have V_{ph} of around 200 ft/s at small λ and increase to around 350 ft/s over the first 15 ft of λ (Figure 5.13). Of the five SASW tests in Group 135, only two (121 & 147A) yielded results beyond λ of 30 ft. At these wavelengths, Point 147A has V_{ph} approximately 10% lower than Point 121. Point 121 also yields the highest V_{ph} of all UWL tests at 735 ft/s for λ of 75 ft. Using the preliminary method, the COV of V_{ph} for Group 135 is 0.079.

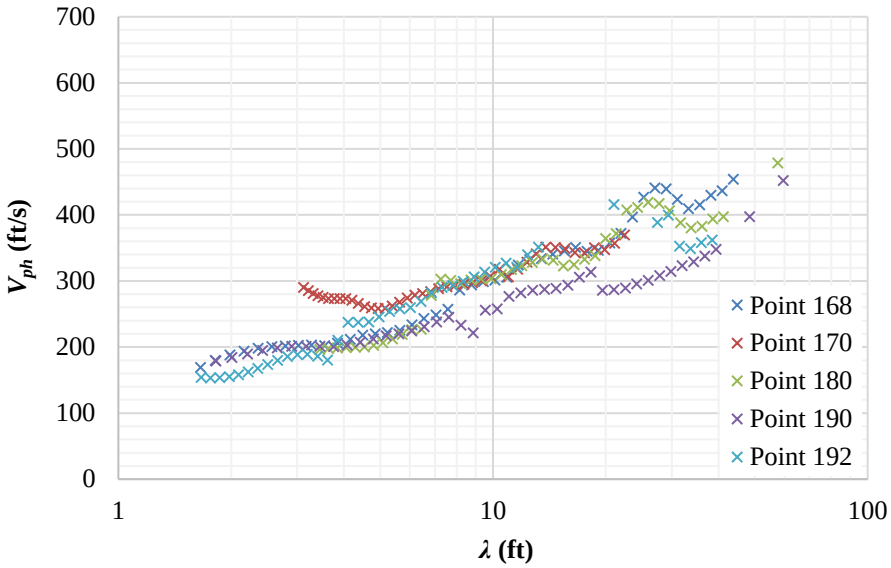

Figure 5.14 – Group 180 dispersion curves.

Group 180 is marked by significant variation in V_{ph} for λ less than 5 ft and greater than 20 ft. V_{ph} for λ less than 5 ft varies from 275 ft/s for Point 170 to 153 ft/s for Point 192 (Figure 5.14). V_{ph} for all points except 190 then converge at 300 ft/s for λ of 8 ft. At this λ, V_{ph} for Point 190 is approximately 10% lower at 260 ft/s. Beyond λ of 20 ft, V_{ph} varies by as much as 130 ft/s between points, but in all cases, increases at a rate of approximately 2.5 ft/s/ft. Group 180 V_{ph} has a COV of 0.099 as calculated with the preliminary method.

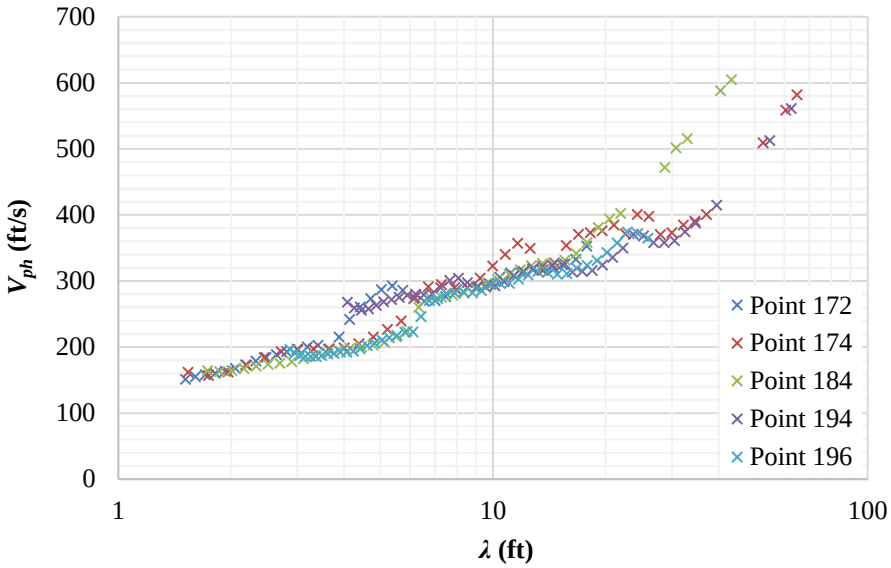

Figure 5.15 – Group 184 dispersion curves.

Finally, Group 184 dispersion curves present the least amount of variability with a COV of 0.071. In all cases, V_{ph} at small λ is around 160 ft/s and increases at a rate of 12 ft/s/ft to around 200 ft/s at λ of 4 ft (Figure 5.15). All points then exhibit a marked increase in V_{ph} to approximately 275 V_{ph} at λ of 7 ft. V_{ph} then increases at a rate of approximately 5 ft/s/ft to 313 ft/s at λ of 15 ft. At λ of 15 ft, Group 184 increases at a rate of 12 ft/s/ft to around 375 ft/s at λ of 20 ft where V_{ph} decreases slightly until λ of 30 ft. Beyond λ of 30 ft, Point 184 yields V_{ph} about 40% higher than Points 194 and 174, however, V_{ph} increases at approximately the same rate in all three cases.

5.3.1 Verification of Selected SASW Tests

For points where side-by-side CPT soundings were taken, side-by-side SASW tests were also conducted. Additional SASW tests were generally taken by moving the SASW array approximately 5 to 10 ft perpendicular to the long axis of the array. Figures 5.16 to

5.18 show the results of side-by-side SASW testing. The figures indicate that a close association exists in all cases with only a couple of exceptions. Figure 5.17 shows that for Point 135A, V_{ph} varies significantly for λ up to 6 ft. However, dispersion curves of Points 135 and 135A are essentially the same for λ greater than 6 ft. This deviation is most likely due to the stiffness of the upper two to three feet of topsoil. Also, Figure 5.18 shows that for Point 168, there is about a 50 ft/s difference in V_{ph} for λ of approximately 10 ft. This difference could be the result of variability in the subsurface or poor test data in the 10-ft receiver spacing.

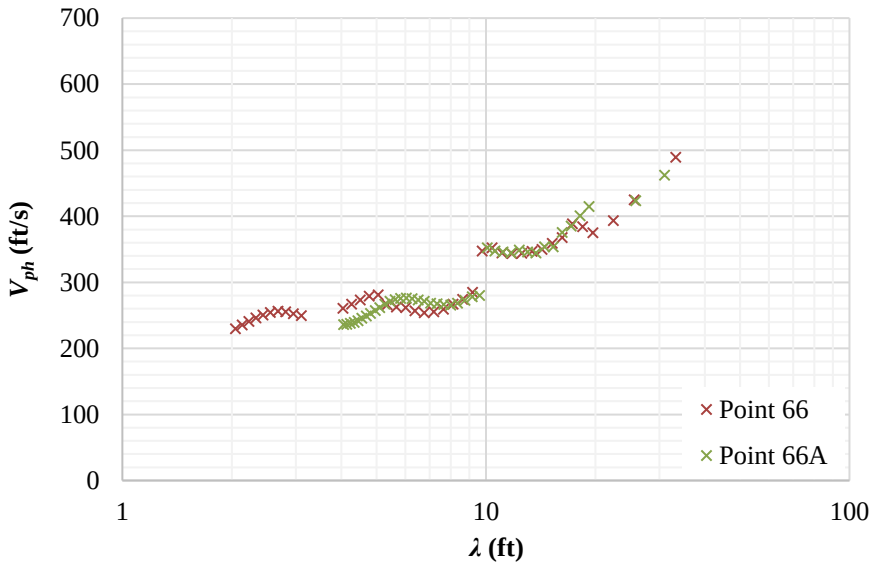

Figure 5.16 – Point 66 SASW verification.

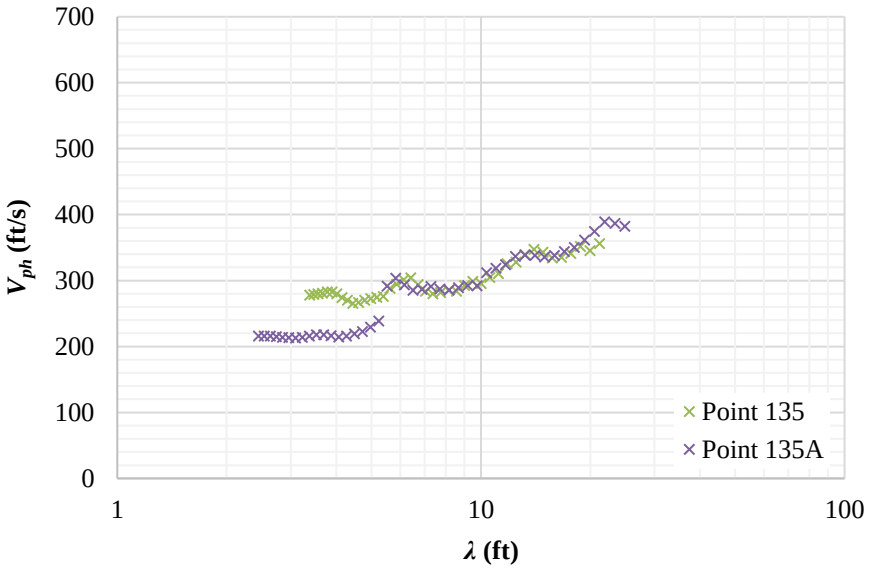

Figure 5.17 – Point 135 SASW verification.

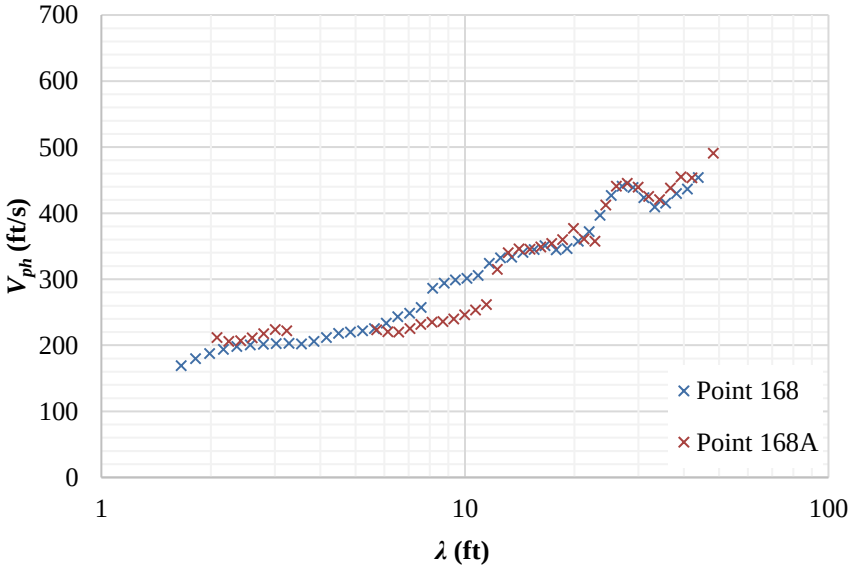

Figure 5.18 – Point 168 SASW verification.

5.4 Preliminary Variability Correlation

After achieving COVs for CPT and SASW data for each group utilizing the preliminary method, COVs were plotted to determine whether a correlation exists and/or what improvements could be made. For this analysis, the COV of q_t and the COV of f_s for each group were plotted against the COV of V_{ph} for the same. In both cases, following two observations are made:

1. The COV of CPT data is much larger than the COV of V_{ph}.
2. A statistically significant correlation does not exist.

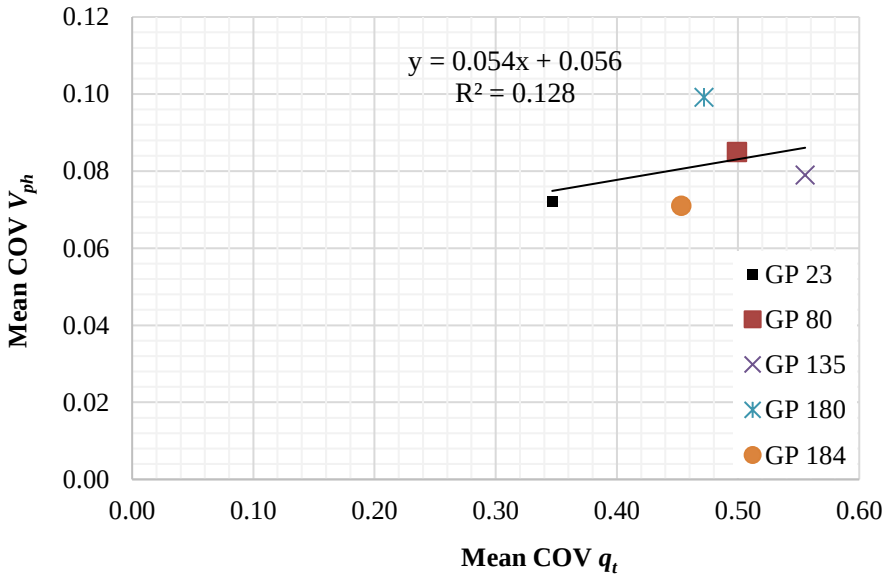

Figure 5.19 – Mean COV V_{ph} vs Mean COV q_t.

A plot of the mean COV q_t vs the mean COV V_{ph} is shown in Figure 5.19. A regression analysis yields an R^2 of 0.128 with a slope of 0.054, an intercept of 0.056, and a probability value (p-value) of 0.55. The mean COV of f_s vs the mean COV of V_{ph} is shown in Figure

5.20. In this case, the regression analysis is only slightly better with an R^2 of 0.36, a slope of 0.099, an intercept of 0.035, and a p-value of 0.29.

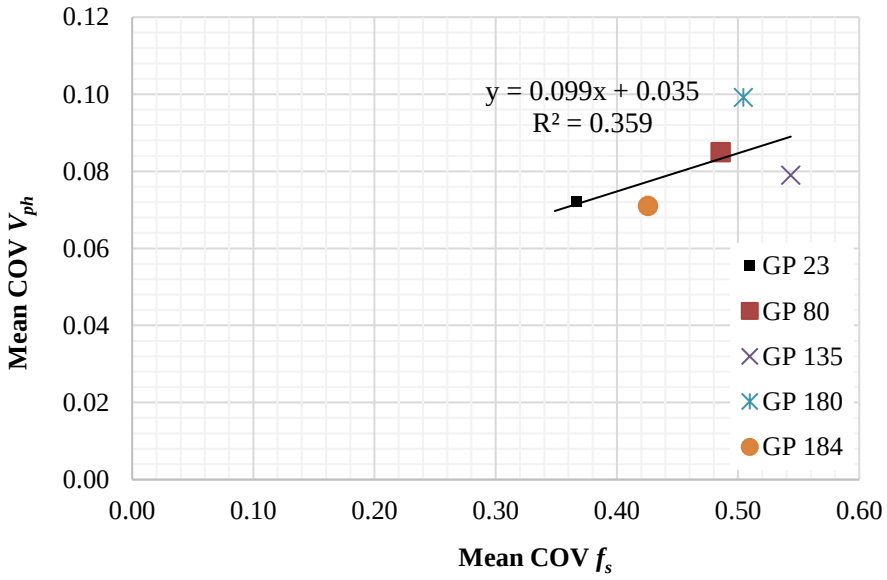

Figure 5.20 – Mean COV V_{ph} vs Mean COV f_s.

5.5 Equivalent Wavelength Method

The methodology for the equivalent wavelength method (EWM) is described in detail in Section 4.5.2. The first step in application of the EWM is calculation of the equivalent corrected tip resistance (q_{teq}) for desired λ. For this study, q_{teq} and V_{ph} were calculated at each test point for wavelengths of 2.5 to 37.5 ft on a 2.5-ft interval. Individual plots of q_{teq} vs λ are available in Appendix A and group plots of q_{teq} vs λ are available in Appendix B.

Figures 5.21 and 5.22 are plots of q_t vs z and q_{teq} vs λ, respectively, for Point 30. Of note is the significant reduction in scatter in q_{teq} vs λ as well as the prominent increase in q_{teq} at a wavelength of approximately 15 ft. Both of these phenomena are the result of weighted averaging of q_t in accordance with Rayleigh wave energy distribution. In this

case, a significant portion of energy for λ greater than 15 ft is propagated through the stiff soil layer encountered from 9 to 14 ft.

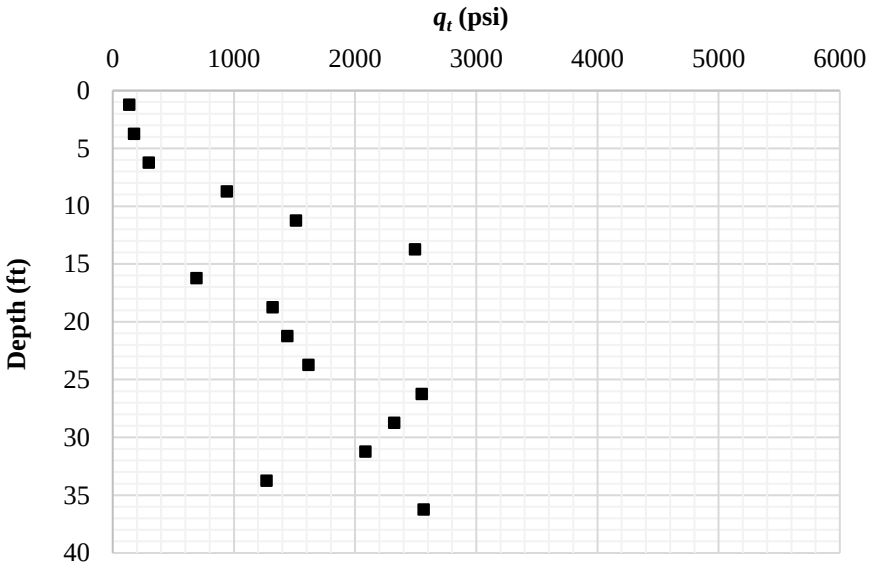

Figure 5.21 – Point 30 q_t vs z.

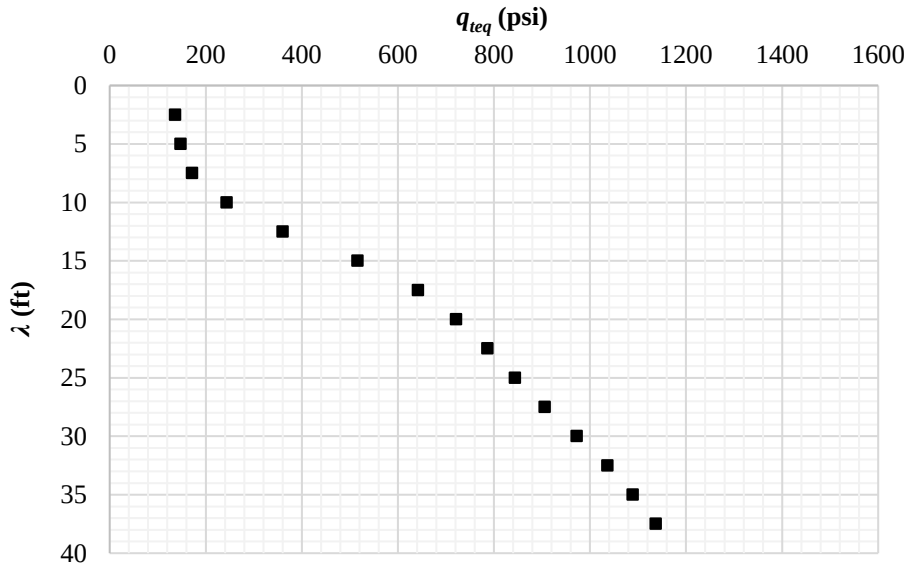

Figure 5.22 – Point 30 q_{teq} vs λ.

Applied to Group 23, the EWM transforms a scattered q_t vs z plot (Appendix B, Figure B.3) into a much more manageable q_{teq} vs λ plot as shown in Figure 5.23. The figure also shows, however, that for λ less than 5 ft, there is significant variation in q_{teq}. This trend is also observed in Group 80 (Appendix B, Figure B.7) and is caused by significant variability in the stiffness of the upper 5 ft of soil. At the UWL, variability in the upper 5 ft is the result of several factors including time elapsed since last plowing, depth of plowing, root penetration, surface water and seepage conditions, and depth to the groundwater table. Beyond wavelengths of 10 ft, these factors are still incorporated in the calculation of q_{teq}, but their effect is less pronounced.

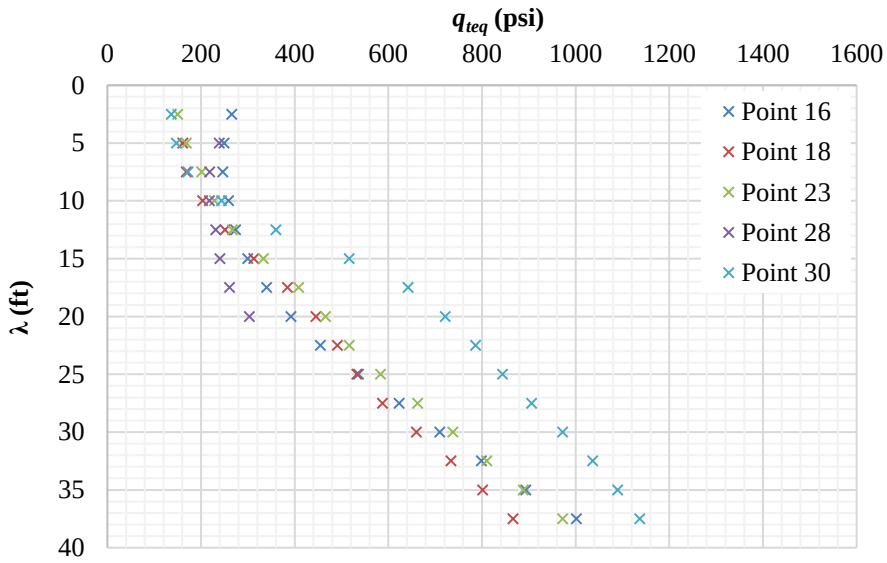

Figure 5.23 – Group 23 equivalent tip resistance (q_{teq}) vs wavelength (λ).

Another trend observed in the Group 23 q_{teq} vs λ plot (Figure 5.23) is that significant spikes in q_t at depths between 7 and 15 ft result in a marked increase in q_{teq} for longer λ. This is especially noticeable for Points 30, 147A, and 192 of Groups 23, 135, and 180

respectively (Appendix B). In each case, however, the increase in q_{teq} does not correspond to a noticeable increase in V_{ph}. This indicates that the CPT probe is passing through a relatively small, stiff inclusion or layer, that is not prevalent enough across the span of the site to cause an appreciable increase in V_{ph}.

5.5.1 EWM Variability Correlation

Utilizing the EWM, variability in V_{ph} was compared to variability in q_{teq} and f_{seq}. Figure 5.24 shows that in the case of f_{seq}, no discernable trend exists. The lowest mean COV in f_{seq} is approximately 0.182 for Group 80 and the highest is 0.262 for Group 23. Groups 135 and 180 have similar COVs in f_{seq} at 0.257 and 0.251, respectively, and Group 184 has a COV of 0.208. None of these values, however, are correlated to the mean COV of V_{ph} in any meaningful way. Based on this finding and those of the preliminary method, no further evaluation of variability in f_s or f_{seq} relative to V_{ph} will be presented.

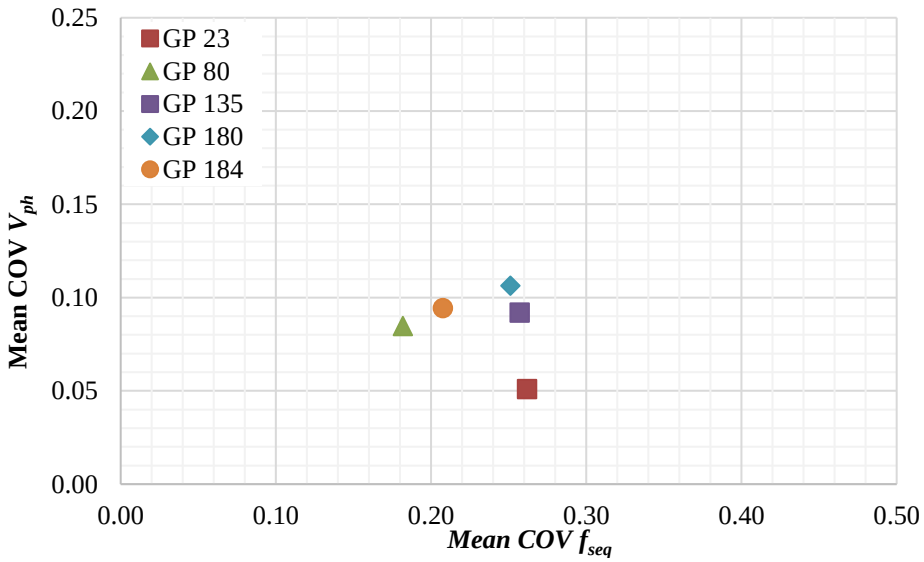

Figure 5.24 – Mean COV V_{ph} vs Mean COV f_{seq}.

Unlike f_{seq}, variability in q_{teq} shows a much stronger correlation to variability in V_{ph}. Figure 5.25 shows the mean COV for V_{ph} vs the mean COV of q_{teq} for each group. The lowest COVs for q_{teq} and V_{ph} are from Group 23 at 0.22 and 0.05 respectively. The highest mean COV for q_{teq} is from Group 135 at 0.48, however, this high COV is due almost exclusively to the high q_{teq} values of Point 147A (Appendix B, Figure B.12). The highest mean COV in V_{ph} is from Group 180 where dispersion curves show consistent variation across the range of measured wavelengths. A regression analysis through the data presented in Figure 5.25 yields an R^2 of 0.751 with a slope of 0.177, an intercept of 0.019, and a p-value of 0.057. In this case, a regression through the origin yields a slightly larger slope of 0.23.

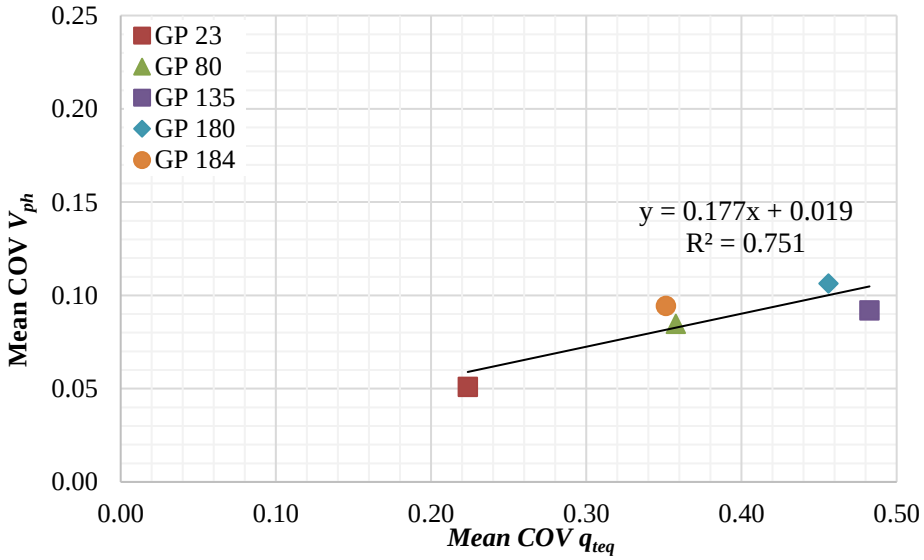

Figure 5.25 – Mean COV V_{ph} vs Mean COV q_{teq}.

Several modifications to the data were made in an attempt to improve the EWM regression analysis. These modifications include removal of outlier data such as that of Points 30, 147A, and 192 as well as exclusion of COVs for λ of 2.5 through 7.5 ft. Of all attempted modifications, the only case yielding a p-value less than 0.05 occurs when all of Point 147A as well as COVs for λ of 2.5 and 5 ft for all points are excluded (Figure 5.26). In this case, a regression analysis yields a R^2 of 0.961, a slope of 0.192, an intercept of 0.013, and a p-value of 0.003.

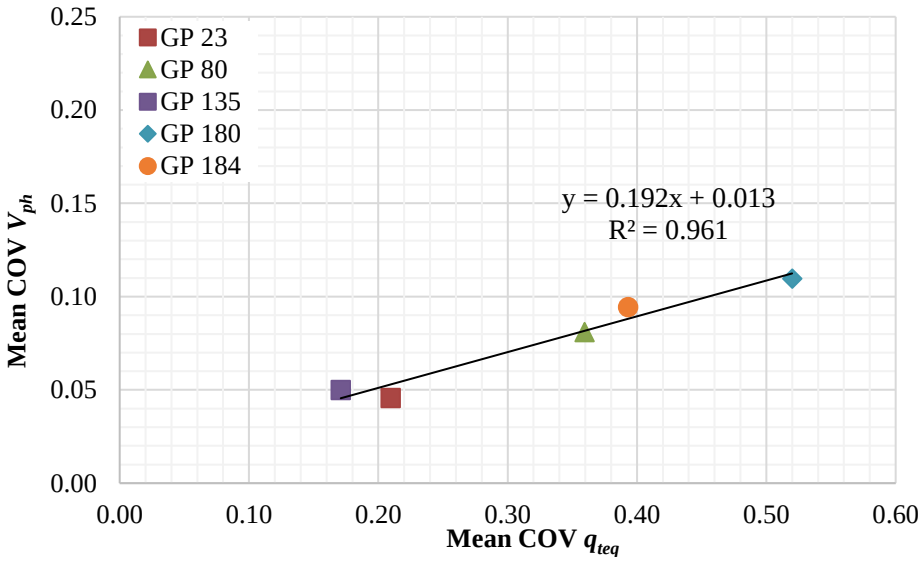

Figure 5.26 – Mean COV V_{ph} vs Mean COV q_{teq}, Point 147A and COVs of $\lambda \leq 5$ ft excluded.

Table 5.1 – Summary of variability correlation results.

Group	Preliminary Analysis		EWM Analysis		EWM, Point 147 & all $\lambda \leq 5$ ft excluded	
	Mean COV V_{ph}	Mean COV q_t	Mean COV V_{ph}	Mean COV q_{teq}	Mean COV V_{ph}	Mean COV q_{teq}
23	0.07	0.35	0.05	0.22	0.05	0.21
80	0.09	0.50	0.08	0.36	0.08	0.36
84	--	0.44	--	--	--	--
135	0.08	0.56	0.09	0.48	0.05	0.17
180	0.10	0.47	0.11	0.46	0.11	0.52
184	0.07	0.45	0.09	0.35	0.10	0.38
p-value	0.554		0.057		0.003	

5.5.2 Relationship between V_{ph} and q_{teq}

Utilizing the EWM to examine variability in phase velocity dispersion curves and CPT tip resistance involves the calculation of V_{ph} and q_{teq} for several λ at each test point. Plots of V_{ph} vs λ and q_{teq} vs λ for each point are provided in Appendix A. When V_{ph} and q_{teq} for the same λ are plotted, a positive and statistically significant relationship exists. This relationship is shown, in the V_{ph}-q_{teq} plane, for Point 174 in Figure 5.27. The plot shows that V_{ph} increases sharply relative to q_{teq} across the lowest λ (2.5-7.5 ft), but for $\lambda > 7.5$ ft (third point from left to right), V_{ph} increases consistently at a rate of about 0.1 ft/s/psi. V_{ph} vs q_{teq} plots for all individual test points are provided in Appendix A and group plots of V_{ph} vs q_{teq} are provided in Appendix B.

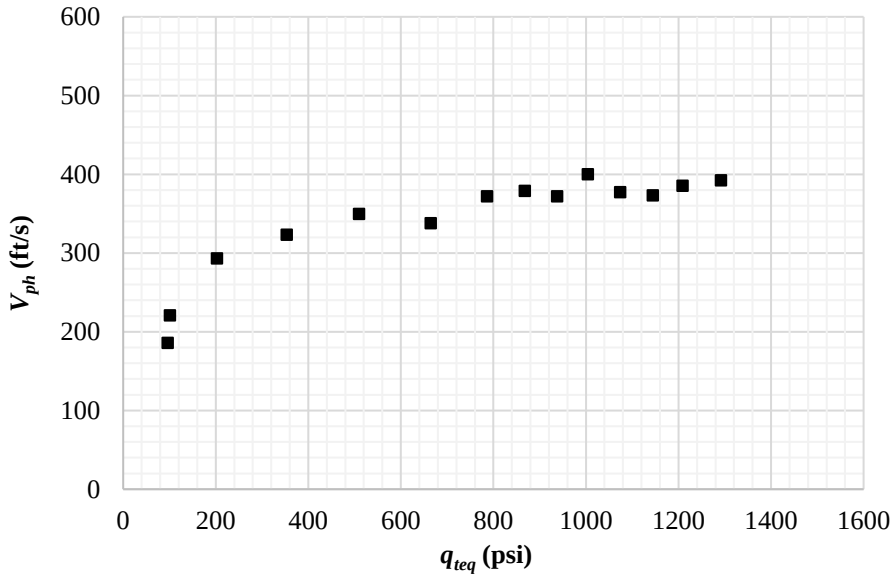

Figure 5.27 – V_{ph} vs q_{teq} for Point 174.

Figure 5.28 shows that when V_{ph} vs q_{teq} (for the same λ) are plotted for all available UWL points, their relationship becomes more obvious. Inconsistency in topsoil conditions causes variability in the lowest measured V_{ph} across the site, however, points tend to merge as V_{ph} approaches 300 ft/s with a corresponding q_{teq} of approximately 175 psi. Figure 5.28 also shows that the gradual increase in V_{ph} relative to q_{teq} for $\lambda > 7.5$ ft is also consistent across the UWL. When all available data are fitted with a power function, the resulting R^2 is approximately 0.618 (Figure 5.28). Finally, Figures 5.29 and 5.30 show that R^2 is improved when Point 147A and $\lambda \leq 5$ ft are removed from the dataset.

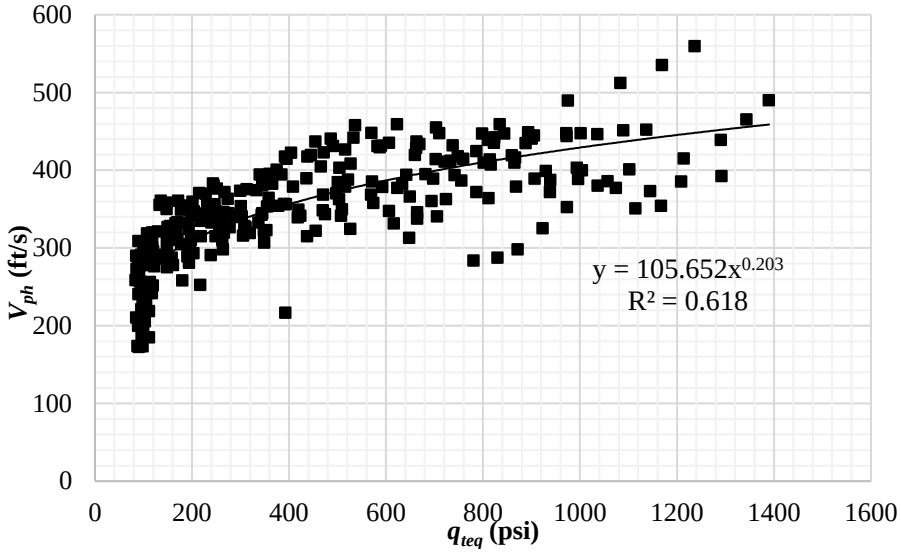

Figure 5.28 – V_{ph} vs q_{teq}, all available UWL points.

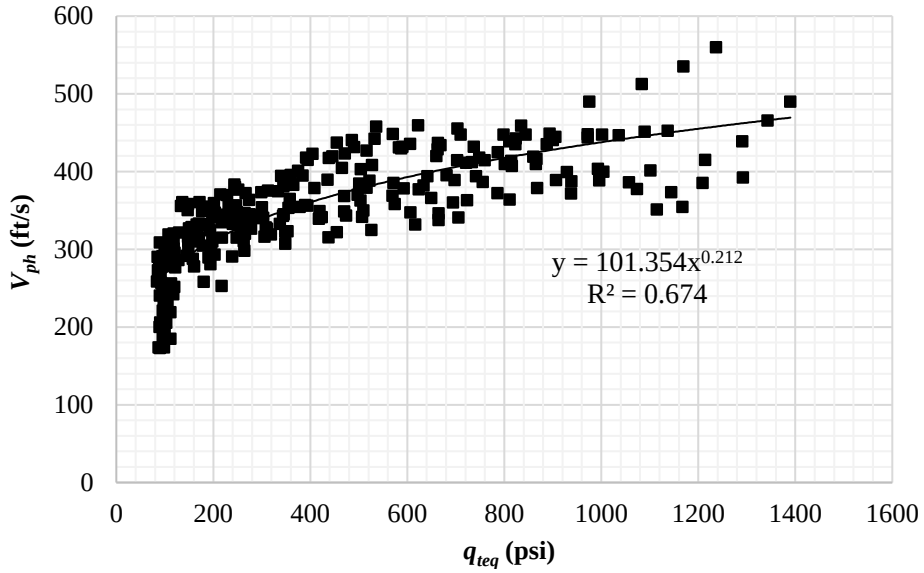

Figure 5.29 – V_{ph} vs q_{teq}, Point 147A removed.

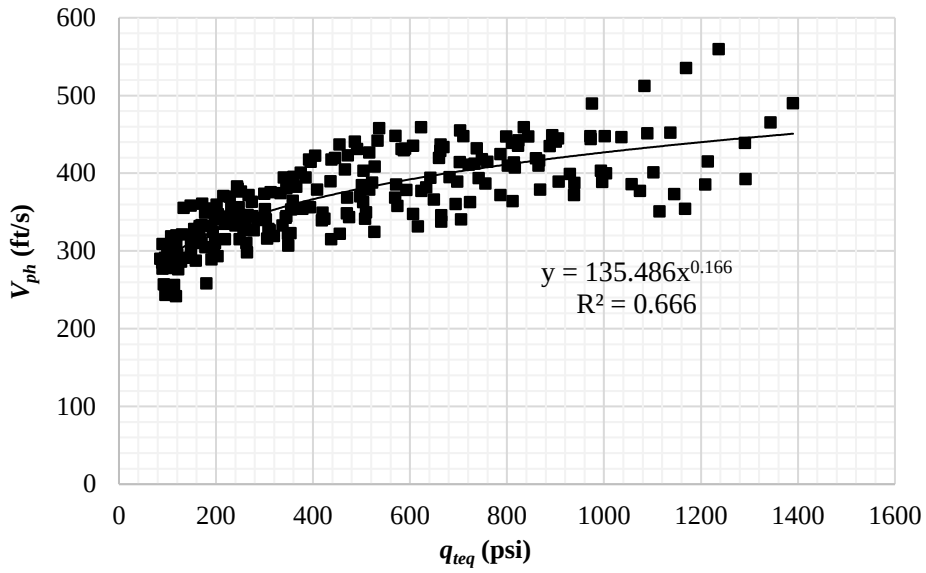

Figure 5.30 – V_{ph} vs q_{teq}, Point 147A and $\lambda \leq 5$ ft removed.

Utilizing the power functions presented in Figures 5.28, 5.29, and 5.30, it becomes possible to approximate dispersion curves from raw CPT measurements. The first step in this approximation is utilizing the EWM to transform q_t into q_{teq} for desired λ. For each desired λ, the calculated q_{teq} and power function are then used to approximate V_{ph}. When the power function from Figure 5.29 is utilized to back-calculate V_{ph} for all UWL test points, the mean difference between the back-calculated and measured V_{ph} is less than 10%. Figure 5.31 shows back-calculated and measured V_{ph} for Point 194. In this case, the mean difference in measured and back-calculated V_{ph} is approximately 6.5%. Plots of all measured UWL dispersion curves and those back-calculated from raw CPT data utilizing this method are provided in Appendix C.

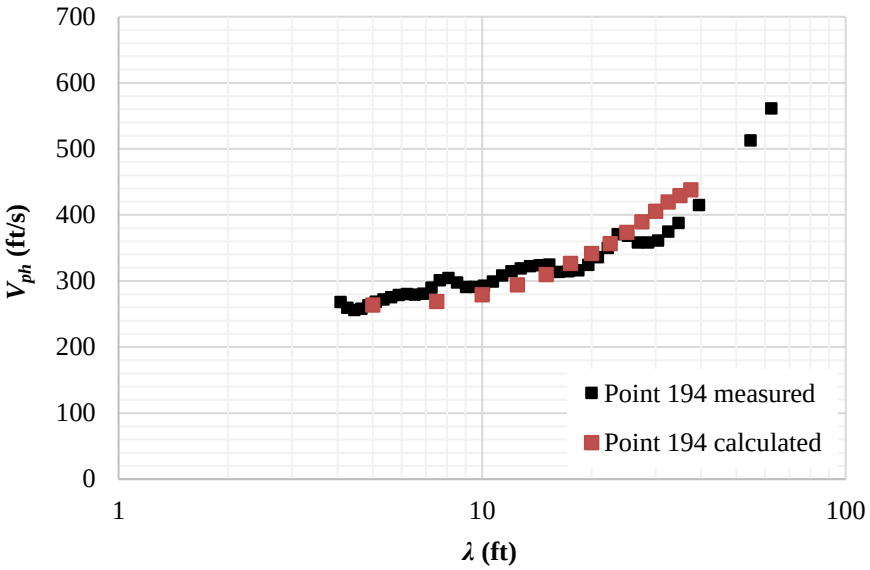

Figure 5.31 – Measured and back-calculated V_{ph} for Point 194.

6 Discussion

6.1 Overview

While many aspects of this study warrant further discussion, this chapter covers only those most directly related to the acceptance or rejection of the hypothesis. Section 6.2 discusses the most difficult aspect of this study: finding an appropriate method to compare variability in SASW and CPT data. The failure of the preliminary method is discussed in Section 6.3 and the success of the equivalent wavelength method (EWM) is discussed in Section 6.4. Section 6.5 covers the nature and utility of the correlation between V_{ph} and q_{teq} that makes possible the estimation of SASW dispersion curves from CPT data alone. Finally, the practical and statistical limitations of this study are discussed in Section 6.7.

6.2 Challenges in Comparing Variability of SASW and CPT Data

Quantifying variability in CPT data relative to SASW data is difficult for a number of reasons. First, CPT measurements are generally taken every couple of centimeters in depth at a relatively well-defined point in lateral space. Across the range of measurements with depth, it is reasonable to assume that any individual measurement, say q_t at a depth of 5 ft, is only affected by the properties of the soil within a small area surrounding the measurement. This contrasts greatly to SASW where V_{ph} for a particular λ is affected by the stiffness of the entire soil column over significant lateral expanses. As is shown in Table 4.3, the depth of penetration for a particular λ is at least equal to λ itself. Further, in the case of this study, global dispersion curves are the compilation of up to four smaller dispersion curves taken across lateral expanses ranging from 10 to 80 ft.

Another non-trivial task is determining which CPT measurement(s) should be compared to phase velocity dispersion curves. Tip resistance (q_c) is the most intuitive choice as it responds in the same manner as V_{ph} to many of the same conditions. As mentioned in Section 2.3, both V_{ph} and q_t generally increase with confining pressure, geologic age, cementation, and overconsolidation ratio, and decrease with increasing void ratio. In practice, most correlations between V_s and CPT measurements use a combination of q_c and f_s that are dependent on soil type and site-specific conditions (Table 2.1). Of the 15 equations presented in Table 2.1, only two weight f_s more heavily than q_c or q_t and only one relationship (Mayne 2006) relates V_s to f_s alone. Given the wide range of relationships between V_s, q_c, and f_s, comparing variability in V_s and some combination of q_c and f_s would be dependent on the chosen q_c-f_s combination. This study therefore only considers variability in V_s as compared to variability in q_t or f_s individually. Finally, with respect to using q_t or q_c, Wair et al. (2012) recommend that when pore pressure measurements are available, q_t should be used in lieu of q_c.

6.3 Failure of the Preliminary Method

The preliminary method was the first attempt at overcoming the limitations and the fundamental differences between CPT and SASW measurements. Based on the results presented in Section 5.4, it is clear the preliminary method yields no discernable correlation between variability in CPT and SASW data. In this case, only the slightest indication of a potential correlation exists between V_{ph} and f_s while virtually no indicators of a correlation exist between V_{ph} and q_t. Though it is interesting that a slightly more positive correlation occurs in comparing f_s to V_{ph}, neither relationship is statistically significant and the

disparity is most likely caused by one of the following: randomness of the data or less fluctuation in f_s (relative to q_t) about the trend with depth.

While several mechanisms contribute to the failure of the preliminary method, the root cause is that relatively large fluctuations in CPT measurements are not reflected in SASW dispersion curves. This disparity is reflected in the data as roughly half of the CPT q_t vs z soundings have variability of more than 1500 psi over only a couple of feet in depth (Appendix A). This contrasts greatly to SASW dispersion curves which increase and decrease much more consistently. The difference is predominantly due to the fact that CPT soundings are very susceptible to variations in stiffness that occur over very small areas in space. Such variations in stiffness cause tremendous fluctuations in CPT data, but cannot be detected globally with SASW dispersion curves.

In order to improve the preliminary analysis, variability about the trend with depth for CPT measurements must be more comparable to those of V_{ph} with respect to λ. The EWM accomplishes this by transforming CPT measurements into those that are weighted in approximately the same proportions as Rayleigh wave energy with respect to depth (CPT_{eq}). Though the EWM is still incapable of accounting for the global nature of SASW measurements (laterally), it significantly reduces variability in CPT data. Table 5.1 shows that the mean COV of q_t ranges from 0.35 to 0.56 with the preliminary method while those of q_{teq} (EWM) range from 0.22 to 0.46. Further, like SASW dispersion curves, fluctuations in CPT_{eq} are much more gradual than those of raw CPT data.

The second major improvement of the EWM is that it uses the same number of measurements in the calculation of mean COVs. In the preliminary method, COVs are taken for all available depths (CPT) and wavelengths (SASW) where three or more values

are available. Therefore, mean COVs of SASW incorporate around 35 data points whereas those of CPT are taken from only 10 to 15. In converting CPT measurements to CPT_{eq} for the same λ from SASW testing, each mean COV is based on the same number of data points and a more equitable comparison is achieved.

Another problem with the preliminary method is that there is no way to ensure that CPT and SASW measurements (q_t, f_s, V_{ph}) are influenced by the properties of soil at the same (or similar) depths. For example, for which λ should the COV of V_{ph} be compared to the COV of q_t taken at a depth of 6.25 ft? Based on the relative weighting of CPT data shown in Table 4.3, it is reasonable to say that the COV of q_t taken at 6.25 ft should be compared to the COV of V_{ph} for λ of 12.5 ft. This is because the highest concentration of wave energy is propagated through the depth interval from 5 to 7.5 ft. However, the table also shows that only around 20% of the total energy stored in a 12.5-ft wave propagates through the same. The EWM accounts for this problem by only comparing V_{ph} and q_{teq} for the same λ or λ_{eq}.

Comparing V_{ph} and q_{teq} for the same λ is critical to achieving a fair comparison. This is especially true for V_{ph} as small fluctuations in mean COVs may produce significant changes in variability correlations (Figures 5.19, 5.25, 5.26). The extent to which the mean COV for a particular group changes as a function of selected λ is exemplified by the changes in the mean COV of V_{ph} between the preliminary method and the EWM. Table 5.1 shows that while the range in mean COV of V_{ph} is essentially the same in both cases, the mean COV of V_{ph} for individual groups fluctuates by as little as 10% and as much as 28%. Furthermore, the mean COV of Groups 23 and 80 increases while the mean COV of Groups 135, 180, and 184 decreases. The relative order of group variability, therefore, changes

from 184, 23, 135, 80, 180 in the preliminary method, to 23, 184, 80, 180, 135 in the EWM. Such significant changes in the mean COV of V_{ph}, merely as a result of selected λ, underscores the importance of a consistent and equitable method of selection.

6.4 Variability Correlation with the EWM

Utilizing the EWM and including all available data, the correlation between the mean COV of V_{ph} and the mean COV of q_{teq} yields an R^2 of 0.757 and a p-value of 0.057 (Figure 5.25). While the null hypothesis cannot be rejected in this case, achieving a p-value of 0.057 without removing any outliers or otherwise modifying the dataset is highly indicative of a correlation. Figure 5.25 shows that the mean COV of V_{ph} increases at a rate of about 0.18 relative to the mean COV of q_{teq} and the intercept is approximately 0.02. Furthermore, the 95% confidence interval (CI) on the intercept ranges from -0.05 to 0.09 and includes the theoretical intercept of zero.

When the dataset is improved by removal of Point 147A as well as V_{ph} and q_{teq} from λ of 2.5 and 5 ft for each test, the regression is markedly improved. In this case, the null hypothesis can be rejected and a statistically significant correlation between the variability in V_{ph} and q_{teq} for the same λ does exist. The regression analysis shown in Figure 5.26 yields a p-value of 0.003, an R^2 of 0.961, and a slope of 0.19. In this case the 95% CI on the intercept also includes the origin and ranges from -0.012 to 0.037.

6.4.1 Exclusion of Point 147A and $\lambda \leq 5$ ft

An examination of Figure 6.1 shows that CPT soundings at Points 147 and 147A measure a very stiff inclusion (q_t of approximately 1800 psi) between 5 and 10 ft below the

ground surface. While there are other cases with similarly high q_t at shallow depths (Points 30, 123, 180, 192), what makes Point 147A particularly unusual is that the stiff inclusion is not reflected in SASW data. In fact, Figure B.10 shows that for λ of 7 to 17 ft, V_{ph} for Point 147A is actually quite low relative to the rest of Group 135. The combination of a such a high q_t coupled with a low V_{ph} make Point 147A an obvious outlier when q_{teq} vs V_{ph} is plotted for the same λ (Figure B.12). The most plausible explanation for this anomaly is that the stiff inclusion is localized and not prevalent across the span of SASW testing.

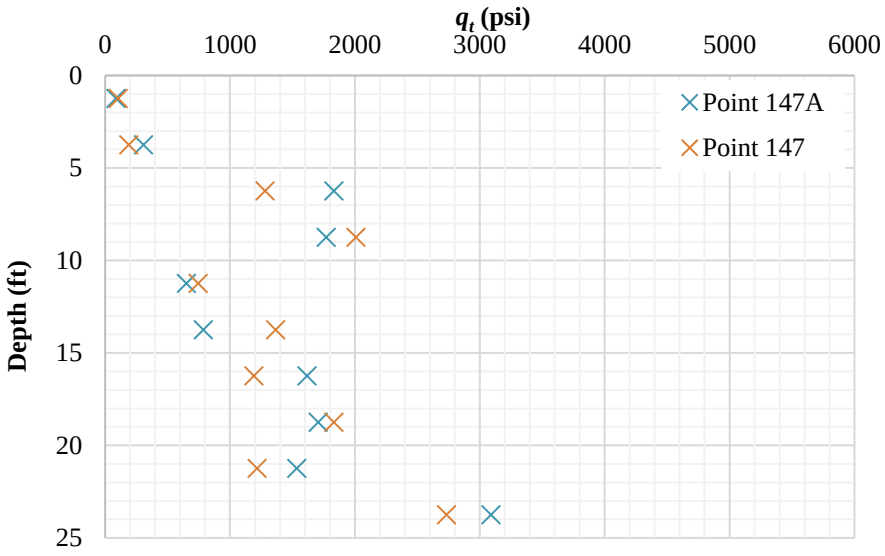

Figure 6.1 – Points 147 and 147A tip resistance (q_t) vs depth (z).

Regarding the exclusion of COVs taken at λ of 2.5 and 5 ft, it is important to note that the exclusion of these COVs does not completely exclude individual measurements taken at λ of 2.5 and 5 ft. Corrected tip resistance (q_t) taken at depths from 0 to 6.25 ft still influence q_{teq} for λ of 7.5 ft or greater. The same concept applies to Rayleigh waves and V_{ph} as stiffness in upper soil layers still influence λ of 7.5 ft or longer. The exclusion of V_{ph}

and q_{teq} for λ of 2.5 and 5 ft, in this case, serves as hedge against variability associated with fluctuating topsoil conditions at the UWL site.

6.5 Correlation of V_{ph} and q_{teq} for the same λ

An additional result of this study is the development of a correlation between V_{ph} and q_{teq} for the same λ. For the UWL site, this correlation facilitated the estimation of phase velocity dispersion curves from q_t within 10% of those measured (Section 5.5.2). This relationship is valuable because existing correlations only relate q_t to V_s (Table 2.1) and are particularly sensitive to local fluctuations in q_t. This can be problematic in the cases where cobbles, clasts, lenses, or other local inclusions cause significant changes in q_t but are generally insignificant with respect to overall seismic site response. The EWM mitigates the effect of such fluctuations by weighting q_t proportionally to Rayleigh wave energy with depth and thereby decreases the relative value of any single q_t measurement.

Of the three equations presented in Figures 5.28, 5.29, and 5.30, the most useful for back-calculation of V_{ph} from q_{teq} is that of Figure 5.29 (presented below as Equation 6.1). For this correlation, Point 147A is removed from the dataset as well as COVs calculated for λ of 2.5 and 5 ft. The power function describing this relationship yields an R^2 of 0.674 and is the best overall representation of the entire dataset. When Equation 6.1 is utilized to back-calculated dispersion curves for all associated points, the mean difference between measured and calculated dispersion curves is 9.3%. A simplified version of the equation is presented as Equation 6.2. Utilizing this relationship, the mean difference between measured and back-calculated dispersion curves is 11.5%.

$$V_{ph}(ft/s) = 101\left(q_{teq}(psi)\right)^{0.212} \quad (6.1)$$

$$V_{ph}(ft/s) = 100\left(q_{teq}(psi)\right)^{0.2} \quad (6.2)$$

A potential area of vulnerability for this relationship is what happens at longer λ and stiffer material. This study only considers V_{ph} and q_{teq} for λ up to 37.5 ft. Figures 5.28, 5.29, and 5.30 show that at long λ and high V_{ph}, there are two cases where V_{ph} increases sharply relative to q_{teq}. The test points associated with these measurements are 121 and 184 and an examination of their dispersion curves (Figure A.42 & A.90) show that both are fairly typical. In both cases V_{ph} is in excess of 450 ft/s at λ of 30 ft and increasing at a rate of approximately 10 ft/s/ft. What is unusual, however, is that both q_t vs z plots (Figures A.43 & A.91) have distinct stiff inclusions. Point 121 is stiff from depths of 12 to 20 ft and Point 184 is stiff from 20 to 25 ft. These stiff inclusions, underlain by softer material, cause an increase in V_{ph} that is not well-accounted for in q_{teq}. However, if q_t measurements were continued to deeper depths, q_{teq} would also increase as more energy is propagated through the stiff inclusions.

6.6 Limitations

The results presented in this thesis are limited in a number of ways. One of the largest limitations associated with any study is the precision and accuracy of the source measurements. The accuracy of CPT and SASW measurements are related to nature of the tests and the diligence with which they are carried out. In the case of this study, there are

no obvious indications that any significant equipment or procedural errors were made and the results are therefore assumed to be reasonably accurate. Precision, on the other hand, can be examined in the side-by-side test results presented in Sections 5.2.1 and 5.3.1. Comparison of side-by-side CPT measurements show that differences in measured q_t for the same depth are on average within about 20% of each other. A similar comparison of side-by-side SASW data found that V_{ph} values were, on average, within about 7.6% for the same λ. Given the nature of the UWL site, which contains interbedded lenses of stiff and soft material and large particles or even cobbles, the level of precision achieved in both cases is commensurate with the nature of the measurement and material measured.

A key limitation of the variability correlations presented in this thesis are their statistical applicability. For this study, the Labadie UWL was divided into six groups and COVs for V_{ph} and q_{teq} are calculated with a sample size (n) of 5. Assuming lognormal distribution of V_{ph} and q_{teq}, the 95% CI (of the COV) of V_{ph} data with a COV of 0.1 ranges from approximately 0.06 to 0.3 (Verrill). Further, the 95% CI of q_{teq} data with COV of 0.3 is approximately 0.17 to 0.95 (Verrill). Therefore, COVs calculated for V_{ph} and q_{teq} (for a specific λ) may or may not be an accurate representation of the COV across the entire area of the group.

Granted, however, that COVs amongst V_{ph} and q_{teq} for a particular λ are not a precise representation of the variability of the entire site, they are still a valid measure of variability amongst the five points measured. Furthermore, the mean COV of each group (for all λ) is a reasonable approximation of the collective variability between the 5 points. Finally, it should be noted that all tests were spaced in accordance with FHWA minimum guidelines for boring and sampling. Therefore, in order to increase n for each calculated COV, either

the number of tests must increase over the same area, or the area of each group must encompass more tests. The latter, of course, yields fewer data points (for the same site) in the mean COV q_{teq} vs mean COV V_{ph} regression.

7 Conclusions

7.1 Summary

The main goal of any geotechnical site characterization program is to reduce uncertainty in order to enhance the efficiency of geotechnical design. Ironically, however, many site characterization programs are inefficient themselves as they are often based on intrusive geotechnical testing at regular intervals. The goal of this thesis was to investigate a potential method for improving the efficiency of geotechnical site characterization programs by developing a correlation between variability in CPT and SASW measurements. Specifically, this thesis set out to test the following hypothesis: *variability in SASW dispersion curves is correlated to variability in CPT measurements.*

The Labadie UWL site was chosen to test the hypothesis based on its accessibility, relatively flat topography, and extensive existing CPT data. Two methods were employed to analyze CPT data obtained from Reitz & Jens, Inc. and SASW data obtained through field testing. The first method, referred to as the preliminary method, ultimately failed to produce any meaningful relationship between variability in CPT and SASW data. Though many mechanisms were responsible for its failure, the most significant issue was that relatively large fluctuations in CPT data were not reflected in SASW dispersion curves. The second method, referred to as the EWM, overcame this shortcoming by weighting CPT measurements with respect to depth in the same manner that Rayleigh wave energy is weighted. In doing so, a measurement called the equivalent corrected tip resistances (q_{teq}) was developed and calculated over the same λ for which V_{ph} measurements are available from SASW dispersion curves.

A statistically significant correlation was achieved in comparing variability in q_{teq} to variability in V_{ph} for the same λ. The first comparison, shown in Figure 5.25, yields an R^2 of 0.757 and a p-value of 0.057. Though the null hypothesis could not be rejected in this case, it warranted further investigation and a few modifications to the dataset were made. After removing Point 147A as an obvious outlier, as well as V_{ph} and q_{teq} from λ of 2.5 and 5 ft for all tests due to fluctuations in topsoil conditions, the correlation was significantly improved. The regression analysis shown in Figure 5.26 yields a p-value of 0.003, an R^2 of 0.961, and a slope of 0.19. Furthermore, the 95% CI on the intercept ranges from -0.012 to 0.037 and encompasses the theoretical intercept of zero.

In addition to variability correlations, an equation relating q_{teq} to V_{ph} (Eq. 6.1) was developed that facilitates the estimation of dispersion curves from q_t alone. After converting raw q_t values to q_{teq} utilizing Table 4.3, Equations 6.1 and 6.2 facilitate the transformation of q_{teq} for a particular λ into an estimated V_{ph} for the same. Utilizing Equation 6.1 to back-calculate dispersion curves at the UWL site resulted in a mean difference of only 9.3% from those that were measured. It is therefore possible to estimate the dispersive nature of the site with reasonable confidence based solely on q_t vs z data. However, until further research confirms or rejects the findings of this study, all correlations developed herein should be used with caution and limited to the Labadie UWL site or similar Holocene Missouri River deposits.

7.2 Recommendations for Future Research

There are many ways the research presented in this thesis can be expanded or improved. An attempt to reproduce the results of this study at a different geotechnical site

is the first step in validating the findings. Future research should focus on improving the EWM by increasing the number of tests for a particular site or increasing the level of resolution for each set of tests (CPT and SWM). Test resolution may be improved by including V_{ph} and q_{teq} for more λ or by utilizing an enhanced SWM such as MASW. More work is also needed to validate, or invalidate, the correlation equations developed between V_{ph} and q_{teq}, specifically Equations 6.1 and 6.2. While these correlations are best tested though extensive testing at several sites, a comparison can be made (at a similar geotechnical site) with as little as one dispersion curve and one CPT sounding. Finally, while these equations make possible the estimation of dispersion curves from q_t alone, a more valuable use would be to develop a method wherein q_t may be estimated from dispersion curves alone. Some exploratory research was done to this end but ultimately failed due to low resolution in V_{ph} as a function of q_{teq}. The combination of enhanced SWM and/or a different geotechnical site may increase the plausibility of such a correlation.

References

Cai, G., Puppala, A. J., & Liu, S. (2014). Characterization on the correlation between shear wave velocity and piezocone tip resistance of Jiangsu clays. *Engineering Geology,171*, 96-103. doi:10.1016/j.enggeo.2013.12.012

Cao, Z., Wang, Y., & Li, D. (2016). Quantification of prior knowledge in geotechnical site characterization. *Engineering Geology,203*, 107-116.

United States, Department of Transportation, Federal Highway Administration. (2003). Checklist and Guidelines for Review of Geotechnical Reports and Preliminary Plans and Specifications (Vol. FHWA ED-88-053). Washington, DC: National Highway Institute.

Foti, S., Comina, C., Boiero, D., & Socco, L. (2009). Non-uniqueness in surface-wave inversion and consequences on seismic site response analyses. *Soil Dynamics and Earthquake Engineering,29*(6), 982-993. doi:10.1016/j.soildyn.2008.11.004

Michigan Department of Transportation, Construction & Technology Support Area Geotechnical Services Unit. (2004). *Geotechnical Investigation and Analysis Requirements for Structures*. MI.

GREDELL Engineering Resources, Inc. and Reitz & Jens, Inc. (2011). Detailed Site Investigation, Proposed Utility Waste Disposal Area, Ameren Labadie Power Plant (Rep.). Jefferson City, MO.

Hardin, B. O., & Drnevich, V. P. (1972). Shear Modulus and Damping in Soils: Design Equations and Curves. Journal of the Soil Mechanics Foundation Division, ASCE, SM7, 667-692.

Hussien, M. N., & Karray, M. (2016). Shear wave velocity as a geotechnical parameter: an overview. *Canadian Geotechnical Journal*,*53*(2), 252-272. doi:10.1139/cgj-2014-0524

Lai, C. G., Rix, G. J., Foti, S., & Roma, V. (2002). Simultaneous measurement and inversion of surface wave dispersion and attenuation curves. *Soil Dynamics and Earthquake Engineering*,*22*, 923-930.

Leong, E., & Aung, A. (2012). Weighted average velocity forward modelling of Rayleigh surface waves. *Soil Dynamics and Earthquake Engineering*,*43*, 218-228. doi:10.1016/j.soildyn.2012.07.030

Leong, E. C., & Aung, A. M. (2013). Global Inversion of Surface Wave Dispersion Curves Based on Improved Weighted Average Velocity Method. *Journal of Geotechnical and Geoenvironmental Engineering, 139*(12), 2156-2169. doi:10.1061/(asce)gt.1943-5606.0000939

Lew, M., Ii, K. H., Davis, C. A., Ponnaboyina, H., Hudson, M. B., & Perry, D. L. (2012). A Comparison of SASW Survey Results with In Situ Field Investigation Methods. *GeoCongress 2012*. doi:10.1061/9780784412121.279

Mayne, P. W., Christopher, B. R., & DeJong, J. (2002). *Subsurface investigations-geotechnical site characterization: reference manual* (United States, Department of Transportation, Federal Highway Administration, National Highway Institute). Washington, DC.

Mayne, P. W. (2007). *Cone Penetration Testing State-of-Practice* (Rep. No. NCHRP Project 20-05). Washington, DC: Transportation Research Board Synthesis Study.

Park, C. B., Miller, R. D., & Xia, J. (1999). Multichannel analysis of surface waves. *Geophysics,64*(3), 800-808.

Park, C. B., Miller, R. D., Xia, J., & Ivanov, J. (2007). Multichannel analysis of surface waves (MASW)—active and passive methods. *The Leading Edge,26*(1), 60-64. doi:10.1190/1.2431832

Phoon, K., & Kulhawy, F. (1999). Characterization of geotechnical variability. *Canadian Geotechnical Journal,36*, 612-624.

Phoon, K., & Kulhawy, F. (1999). Evaluation of geotechnical property variability. *Canadian Geotechnical Journal,36*, 625-639.

Rix, G. J., Lai, C. G., Orozco, M. C., Hebeler, G. L., & Roma, V. (2001). Recent Advances in Surface Wave Methods for Geotechnical Site Characterization. In *XV International Conference on Soil Mechanics and Geotechnical Engineering, 2001*. Istanbul.

Robertson, P. K., Sasitharan, S., Cunning, J. C., & Sego, D. C. (1996). Shear-wave velocity to evaluate in-situ state of Ottawa sand. International Journal of Rock Mechanics and Mining Sciences & Geomechanics Abstracts,33(2). doi:10.1016/0148-9062(96)83957-x

Robertson, P. K., & Cabal, K. L. (2015). *Guide to Cone Penetration Testing for Geotechnical Engineering* (6th ed., Rep.). Signal Hill, CA: Gregg Drilling & Testing, Inc.

Stokoe, K. H., II, Wright, S. G., Bay, J. A., & Roesset, J. M. (1994). *Characterization of Geotechnical Sites by SASW Method*. New Delhi, India: 13th International Conference on Soil Mechanics and Foundation Engineering.

Thompson, E. M., Baise, L. G., & Kayen, R. E. (2006). Spatial Correlation of Shear-Wave Velocity within San Francisco Bay Sediments. *GeoCongress 2006*. doi:10.1061/40803(187)134

Tokimatsu, K. (1995). *Geotechnical Site Characterization Using Surface Waves* (Rep.). Tokyo, Japan: Tokyo Institute of Technology.

Tran, K. T., & Hiltunen, D. R. (2012). Two-Dimensional Inversion of Full Waveforms Using Simulated Annealing. *Journal of Geotechnical and Geoenvironmental Engineering*,*138*(9), 1075-1090. doi:10.1061/(asce)gt.1943-5606.0000685

Verrill, S. (2003). *Confidence Bounds for Normal and Lognormal Distribution Coefficients of Variation* (Rep. No. FPL-RP-609). Madison: Department of Agriculture.

Wair, B. R., DeJong, J. T., & Shantz, T. (2012). *Guidelines for Estimation of Shear Wave Velocity Profiles* (Rep. No. PEER 2012/08). CA: Pacific Earthquake Engineering Research Center Headquarters.

Zhang, J., Huang, H., Juang, C., & Su, W. (2014). Geotechnical reliability analysis with limited data: Consideration of model selection uncertainty. *Engineering Geology*,*181*, 27-37. doi:10.1016/j.enggeo.2014.08.002

Appendices

Appendix A: Point plots

Group 23

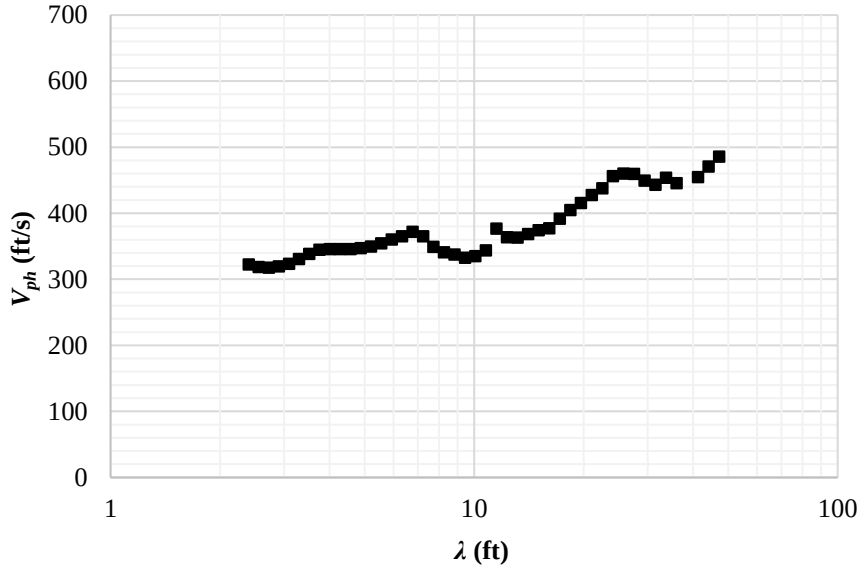

Figure A.1 – Point 16 dispersion curve.

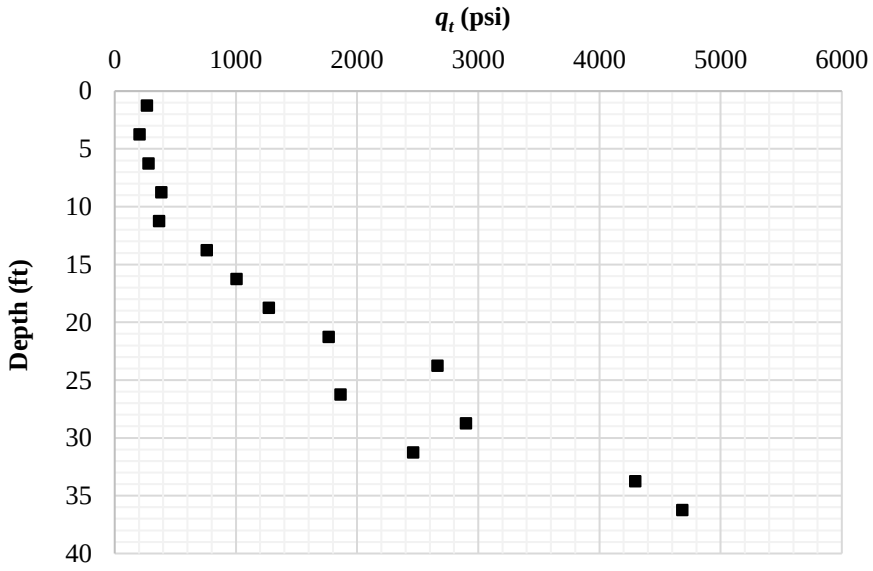

Figure A.2 – Point 16 tip resistance (q_t) vs depth (z).

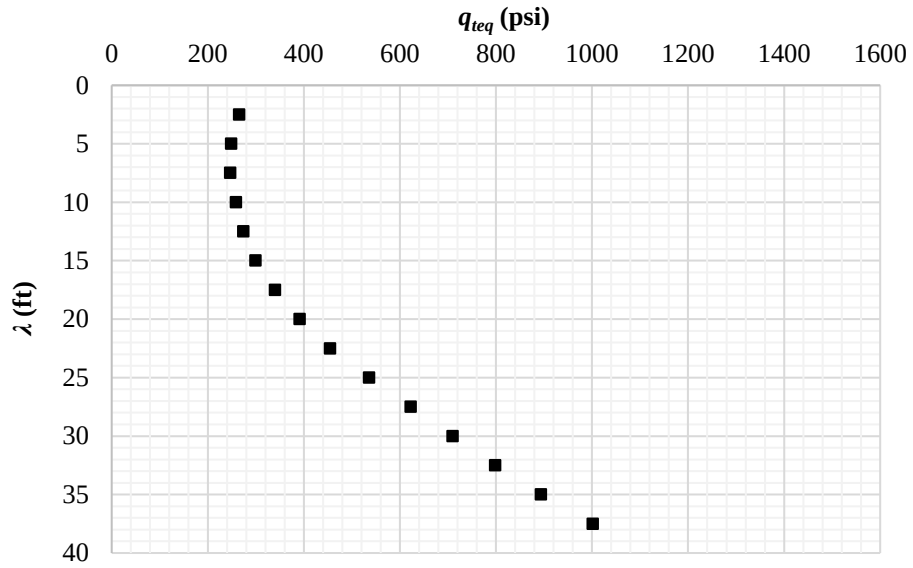

Figure A.3 – Point 16 equivalent tip resistance (q_{teq}) vs wavelength (λ).

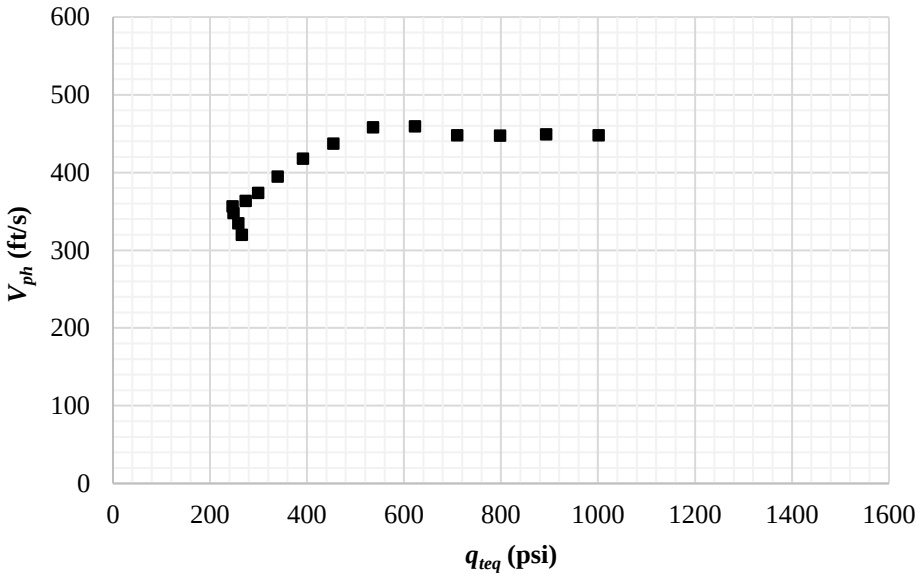

Figure A.4 – Pont 16 equivalent tip resistance (q_{teq}) vs phase velocity (V_{ph}) for the same λ.

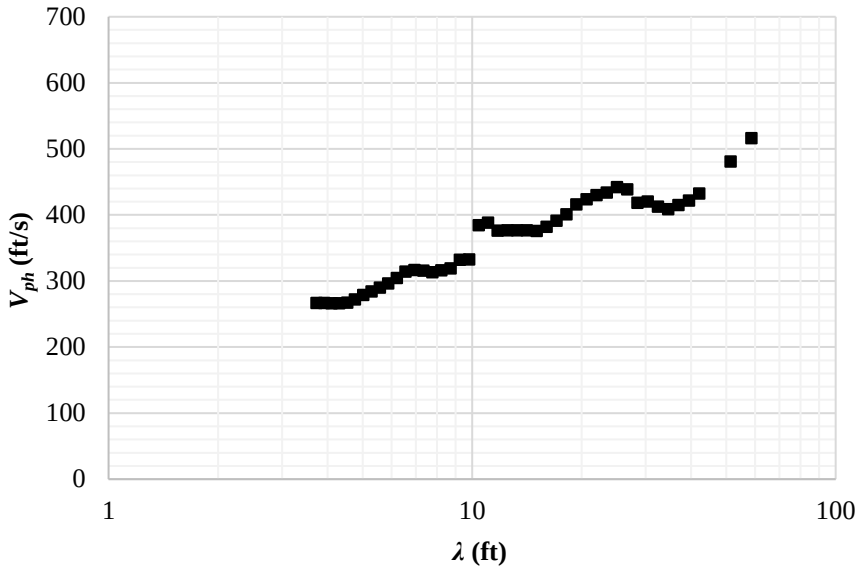

Figure A.5 – Point 18 dispersion curve.

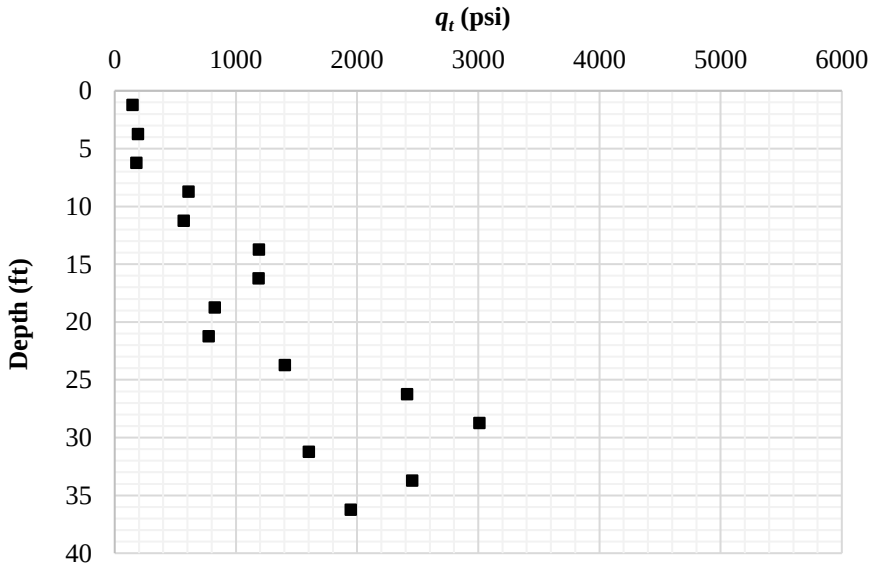

Figure A.6 – Point 18 tip resistance (q_t) vs depth (z).

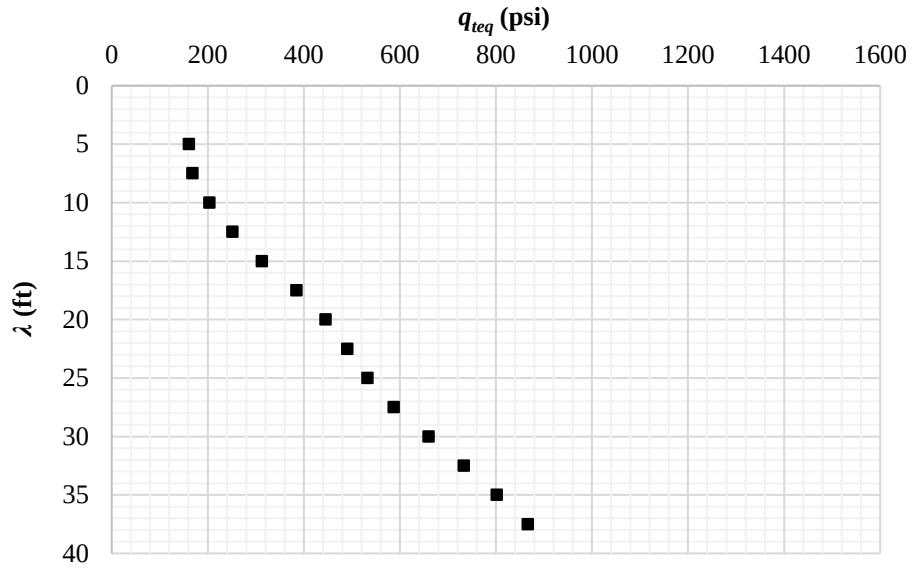

Figure A.7 – Point 18 equivalent tip resistance (q_{teq}) vs wavelength (λ).

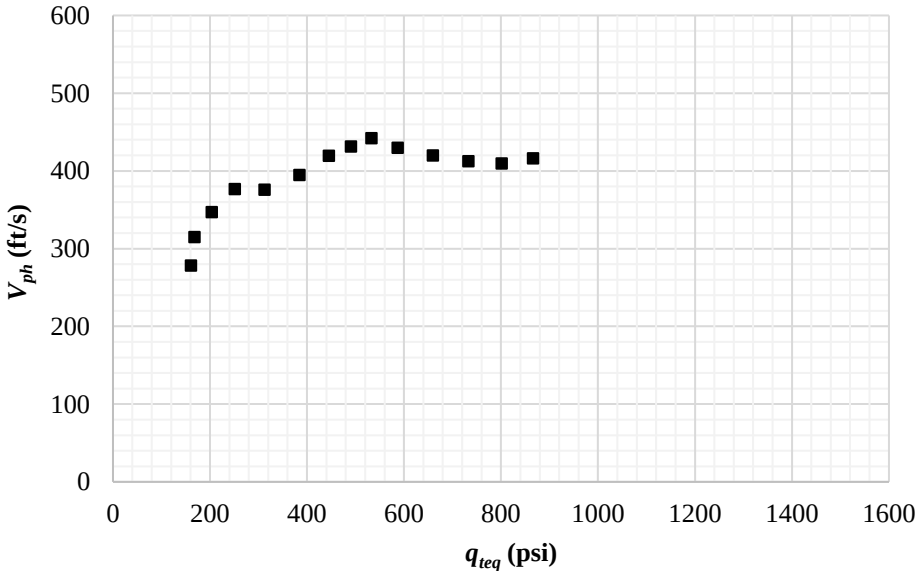

Figure A.8 – Pont 18 equivalent tip resistance (q_{teq}) vs phase velocity (V_{ph}) for the same λ.

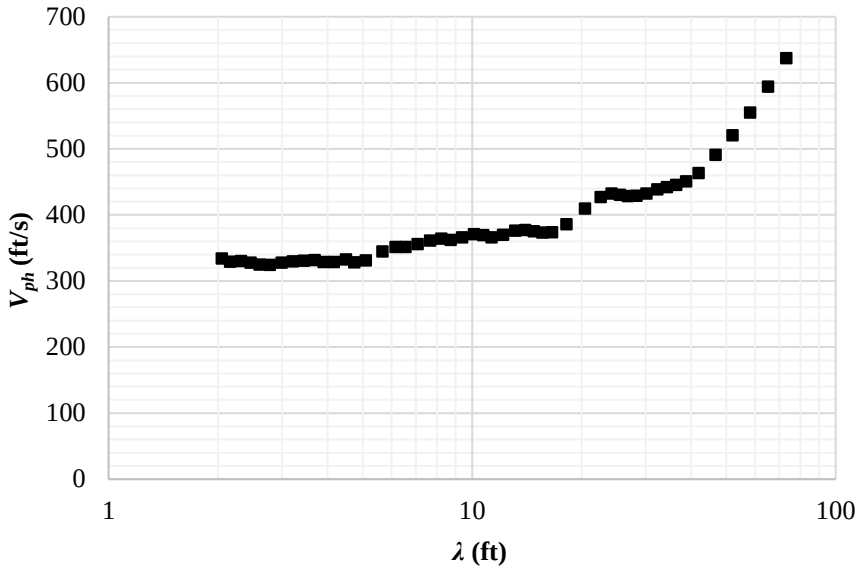

Figure A.9 – Point 23 dispersion curve.

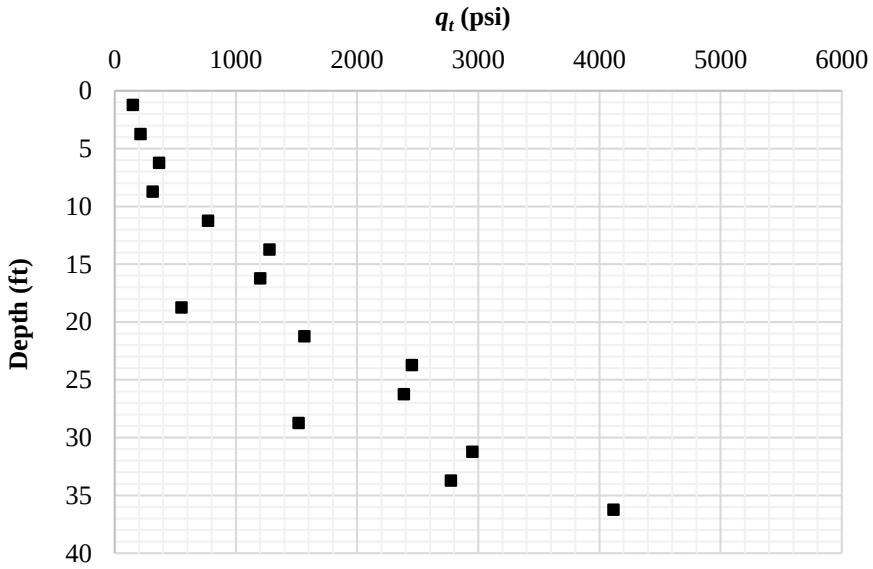

Figure A.10 – Point 23 tip resistance (q_t) vs depth (z).

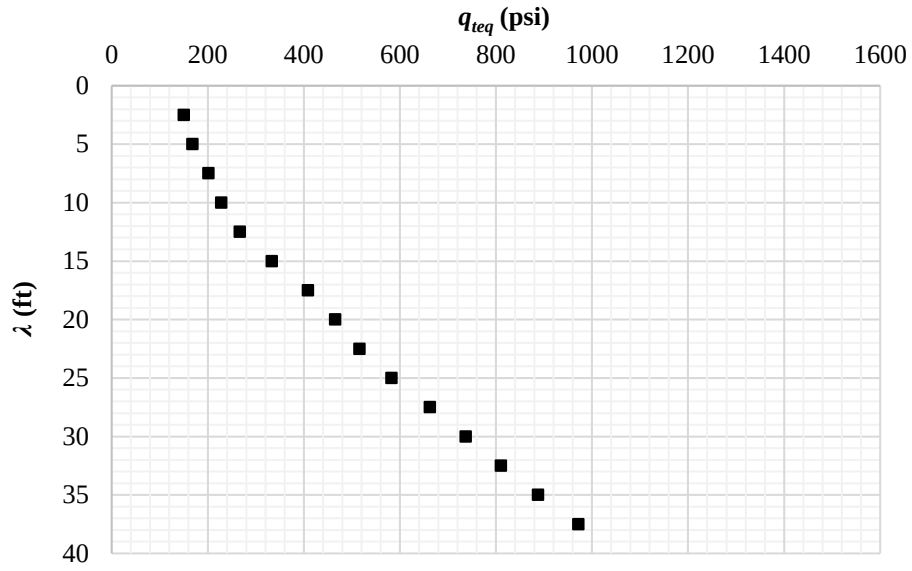

Figure A.11 – Point 23 equivalent tip resistance (q_{teq}) vs wavelength (λ).

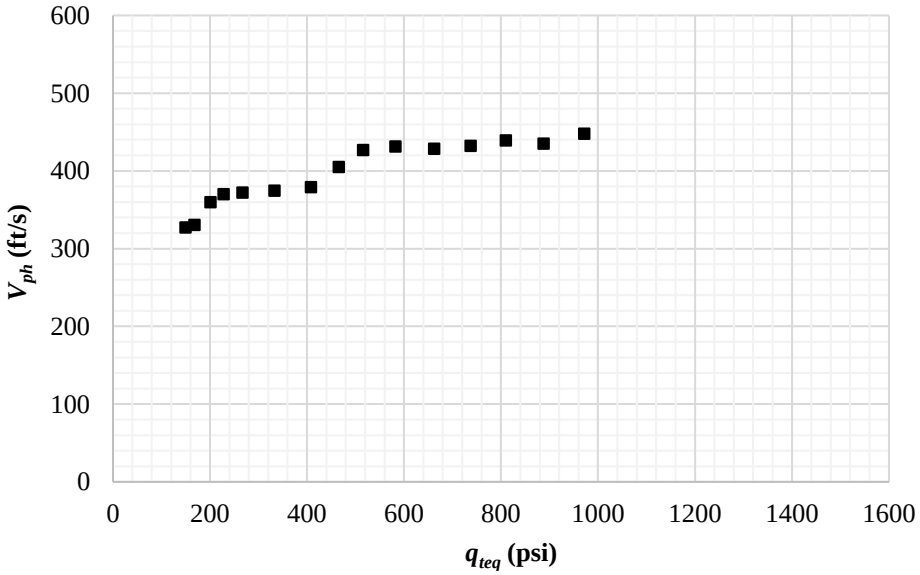

Figure A.12 – Pont 23 equivalent tip resistance (q_{teq}) vs phase velocity (V_{ph}) for the same λ.

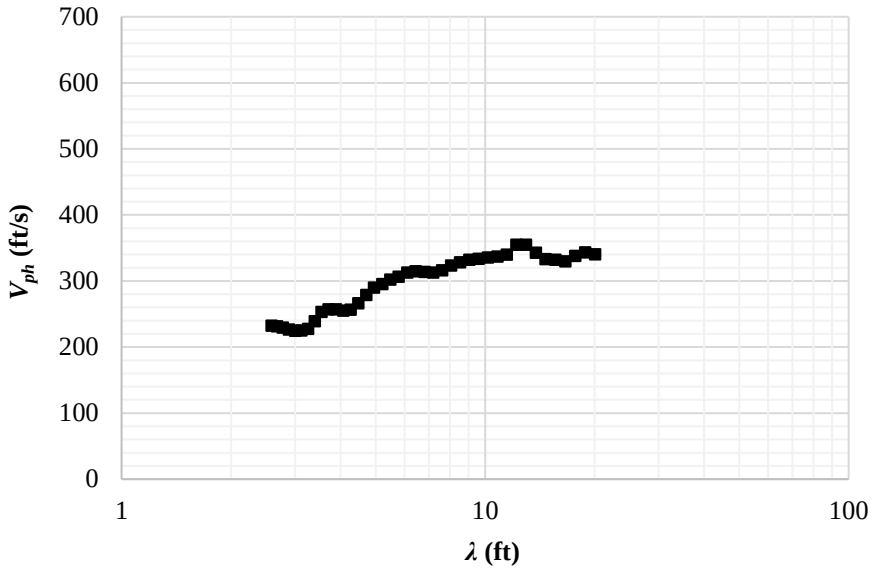

Figure A.13 – Point 28 dispersion curve.

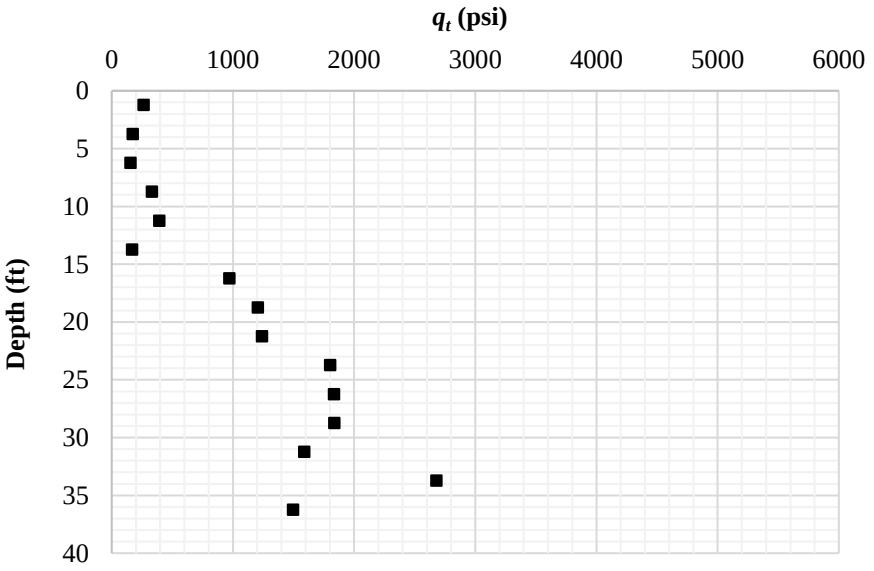

Figure A.14 – Point 28 tip resistance (q_t) vs depth (z).

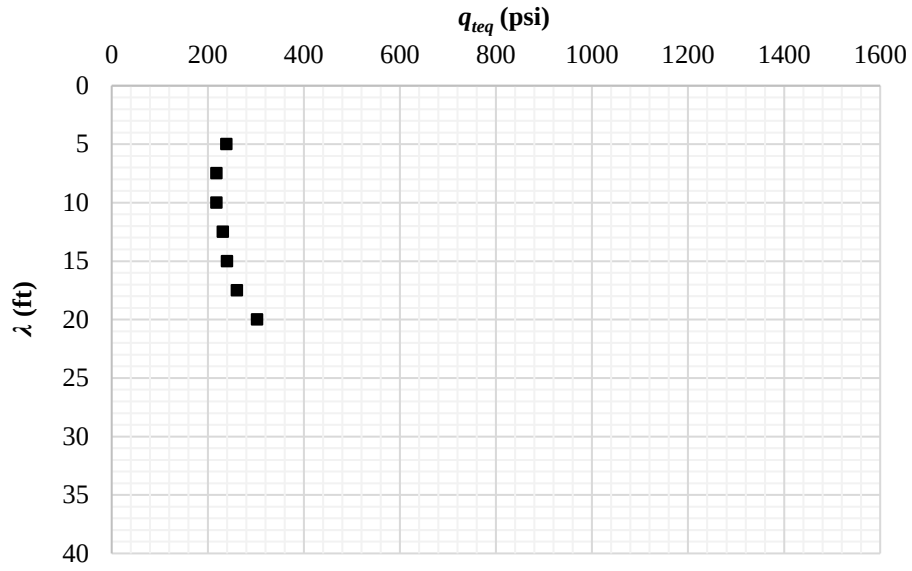

Figure A.15 – Point 28 equivalent tip resistance (q_{teq}) vs wavelength (λ).

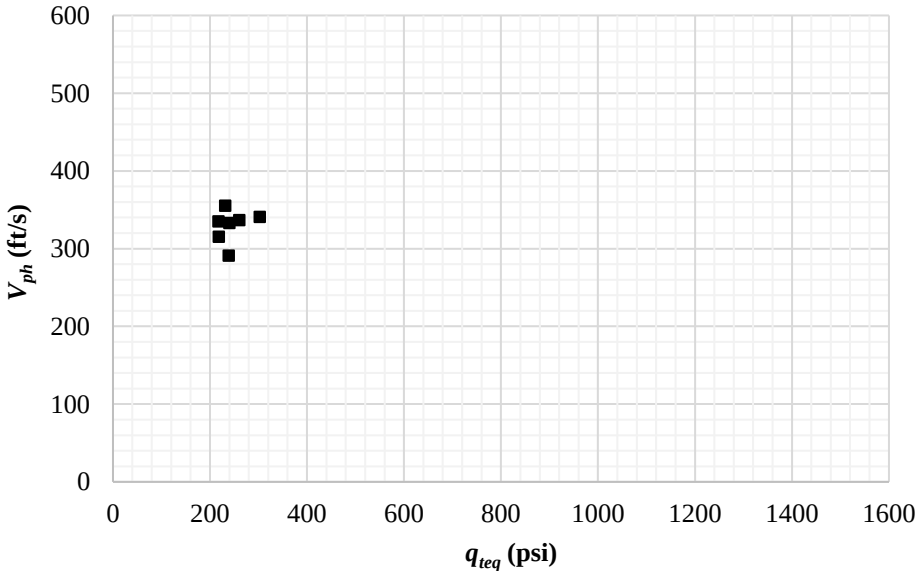

Figure A.16 – Pont 28 equivalent tip resistance (q_{teq}) vs phase velocity (V_{ph}) for the same λ.

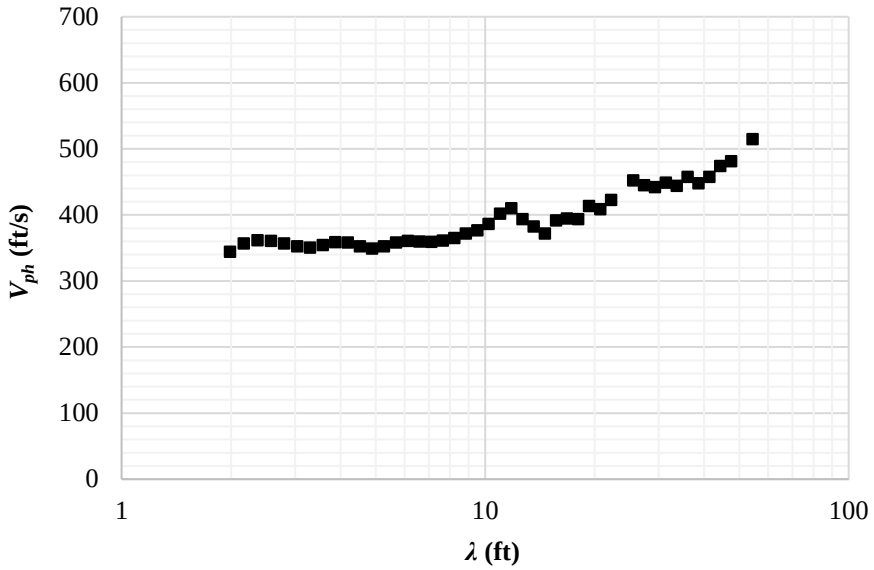

Figure A.17 – Point 30 dispersion curve.

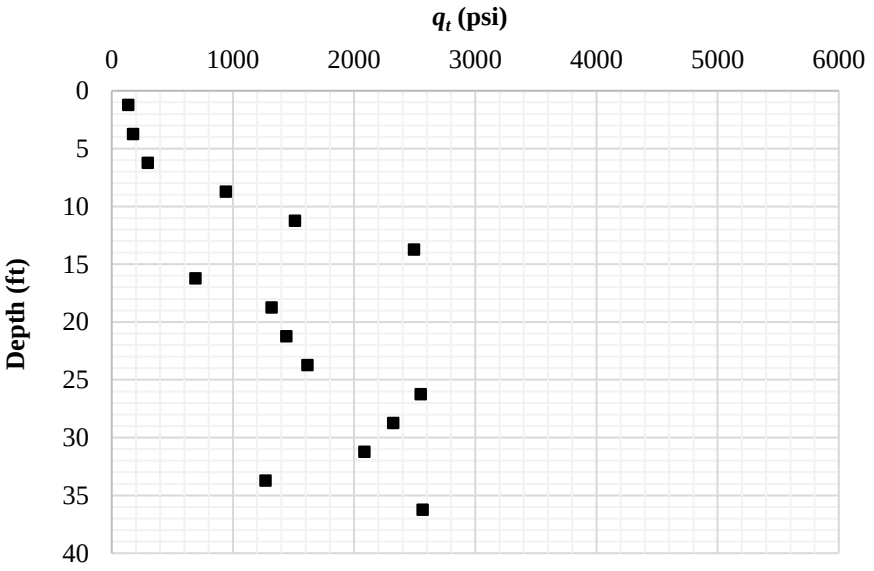

Figure A.18 – Point 30 tip resistance (q_t) vs depth (z).

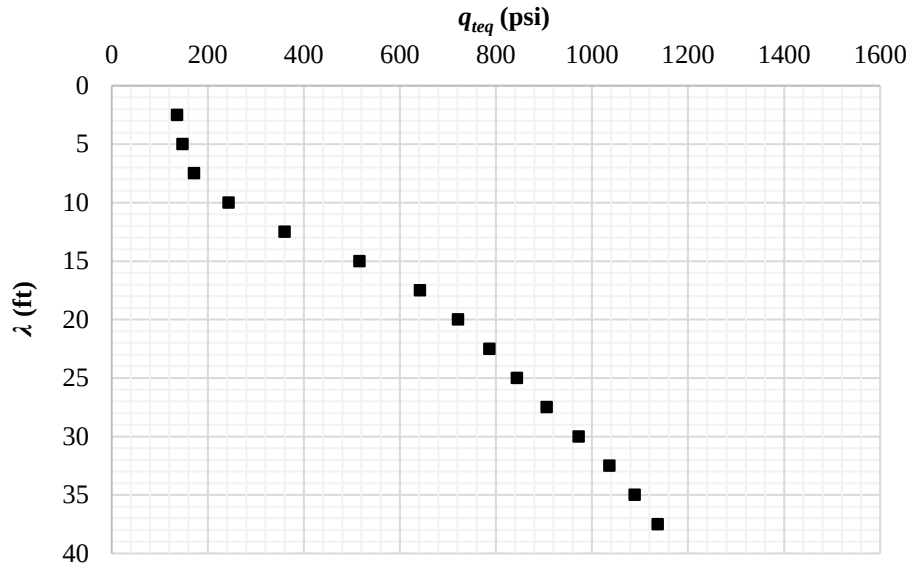

Figure A.19 – Point 30 equivalent tip resistance (q_{teq}) vs wavelength (λ).

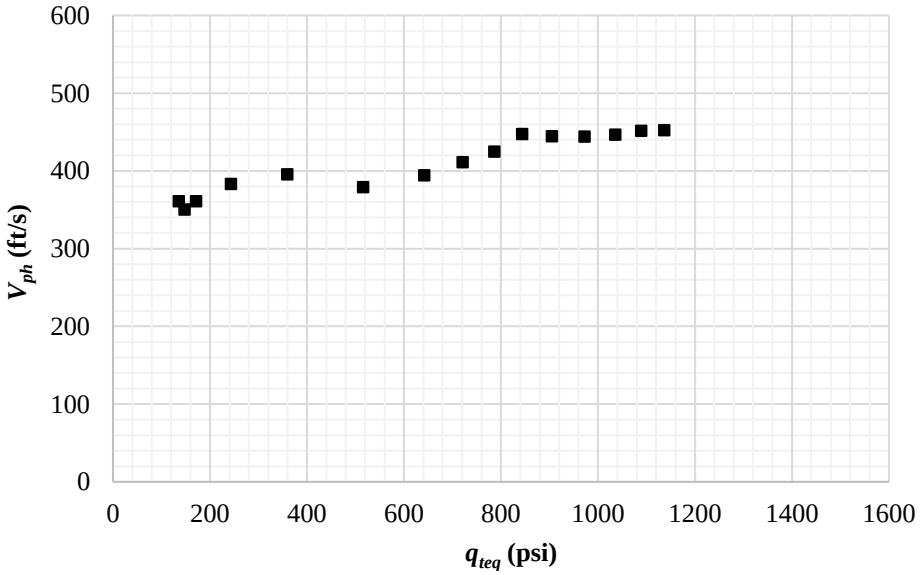

Figure A.20 – Pont 30 equivalent tip resistance (q_{teq}) vs phase velocity (V_{ph}) for the same λ.

Group 80

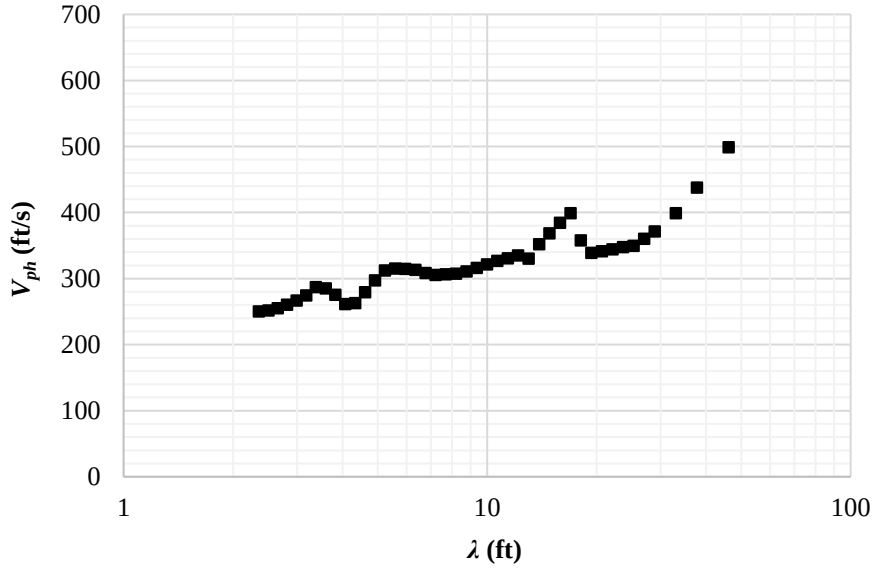

Figure A.21 – Point 64 dispersion curve.

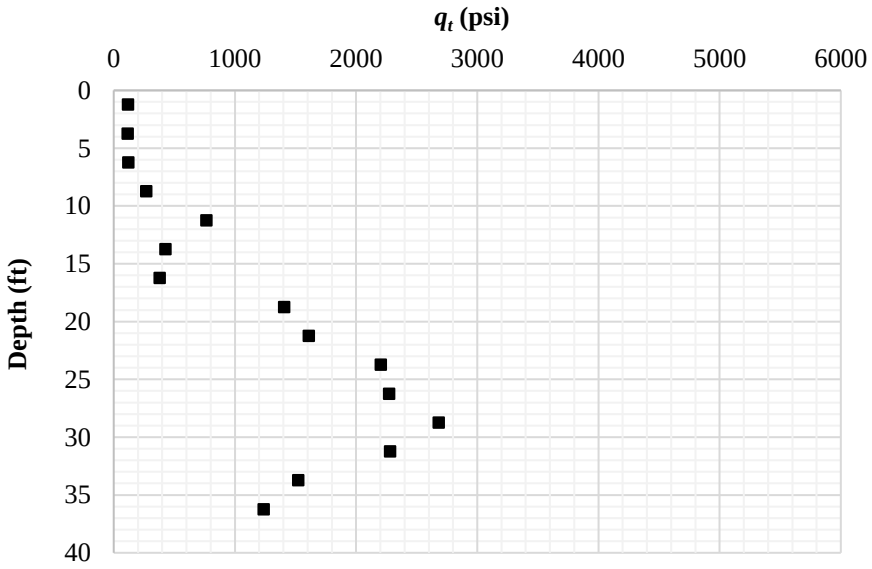

Figure A.22 – Point 64 tip resistance (q_t) vs depth (z).

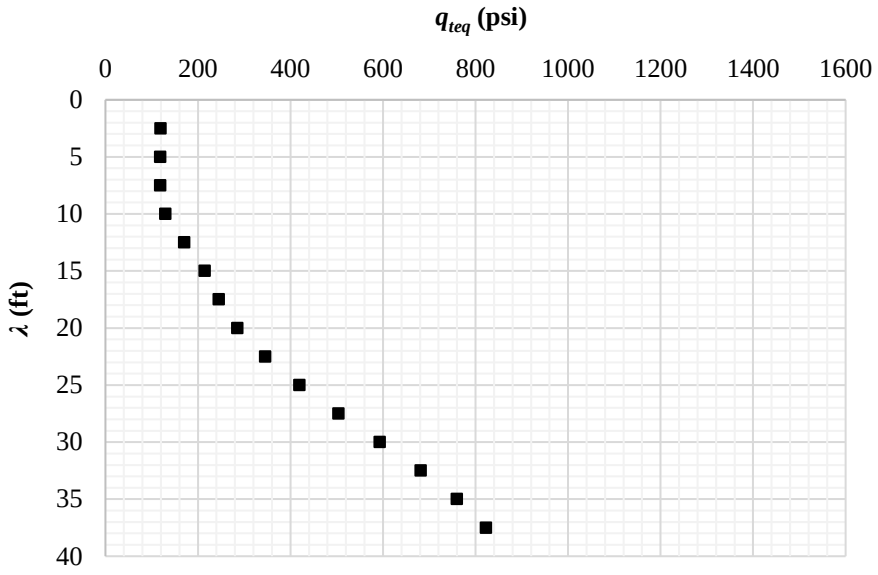

Figure A.23 – Point 64 equivalent tip resistance (q_{teq}) vs wavelength (λ).

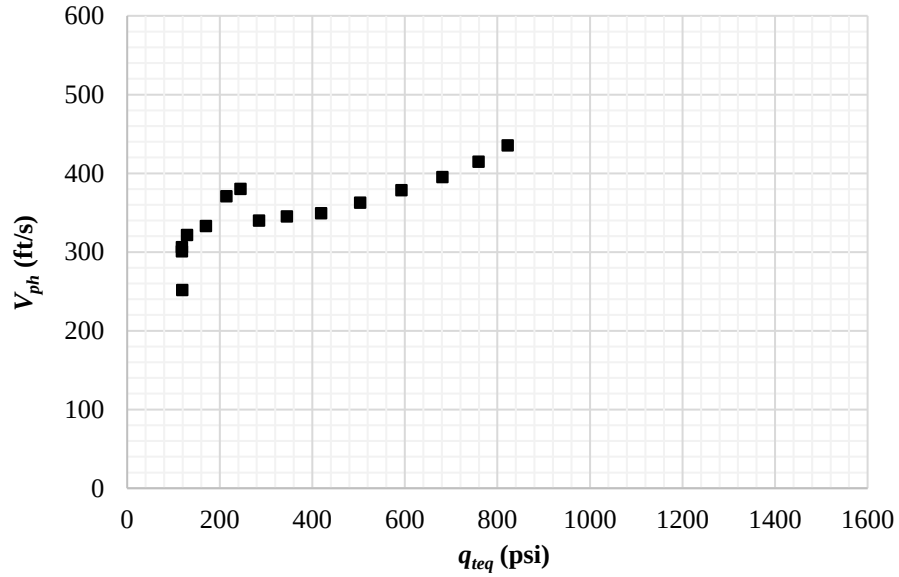

Figure A.24 – Pont 64 equivalent tip resistance (q_{teq}) vs phase velocity (V_{ph}) for the same λ.

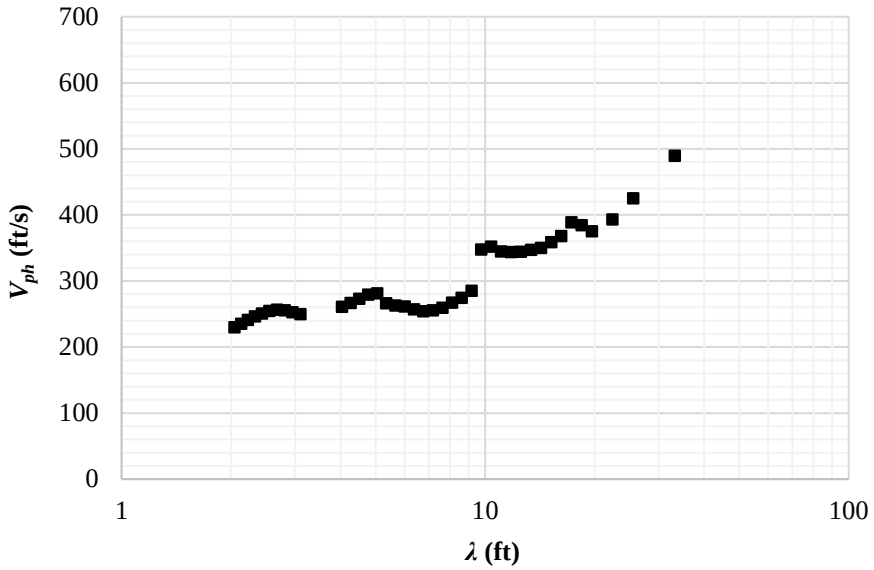

Figure A.25 – Point 66 dispersion curve.

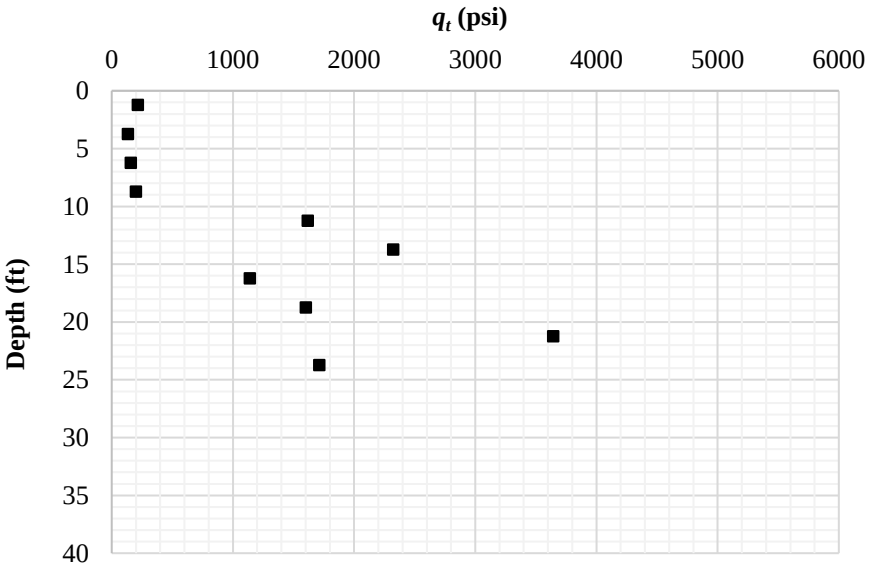

Figure A.26 – Point 66 tip resistance (q_t) vs depth (z).

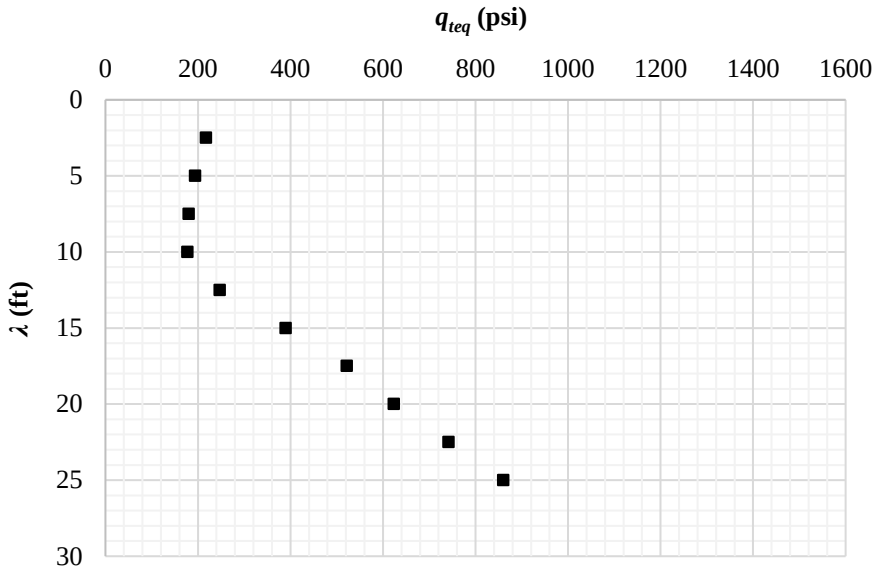

Figure A.27 – Point 66 equivalent tip resistance (q_{teq}) vs wavelength (λ).

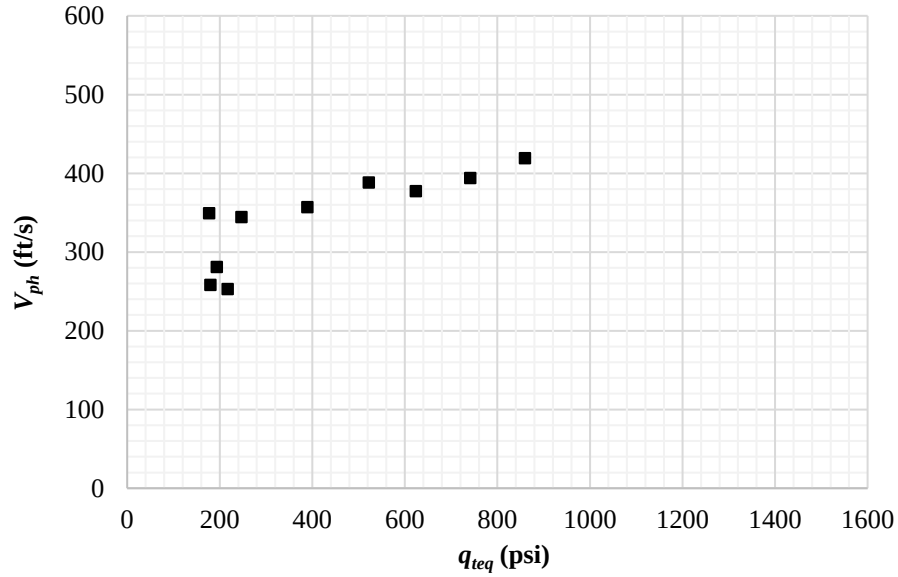

Figure A.28 – Pont 66 equivalent tip resistance (q_{teq}) vs phase velocity (V_{ph}) for the same λ.

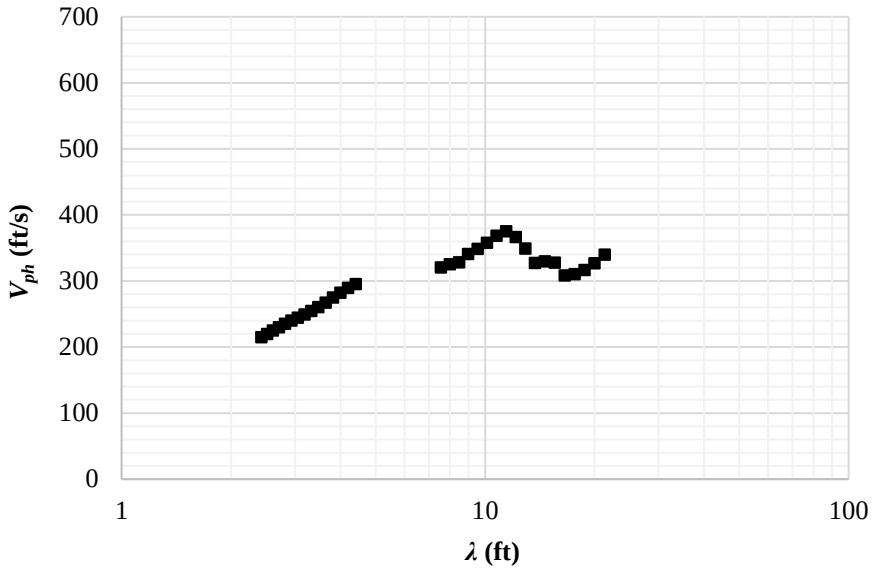

Figure A.29 – Point 80 dispersion curve.

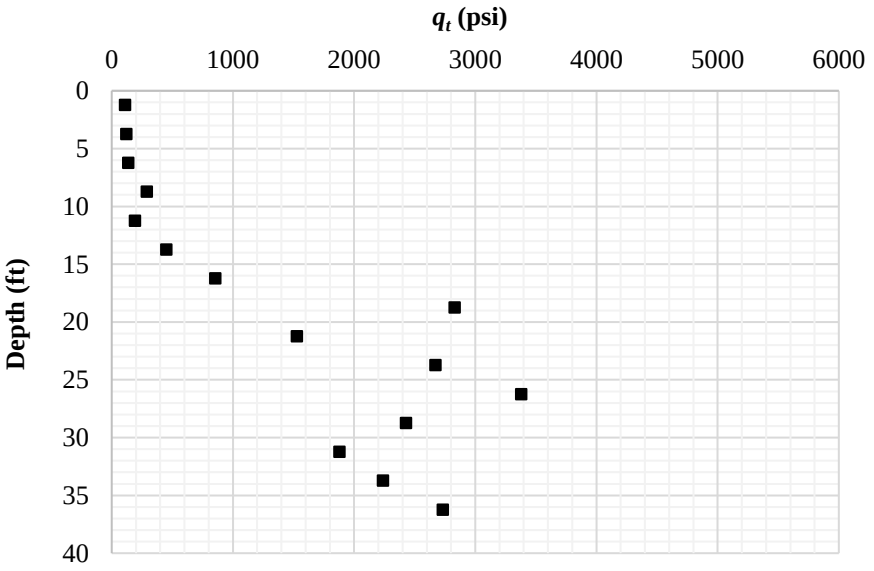

Figure A.30 – Point 80 tip resistance (q_t) vs depth (z).

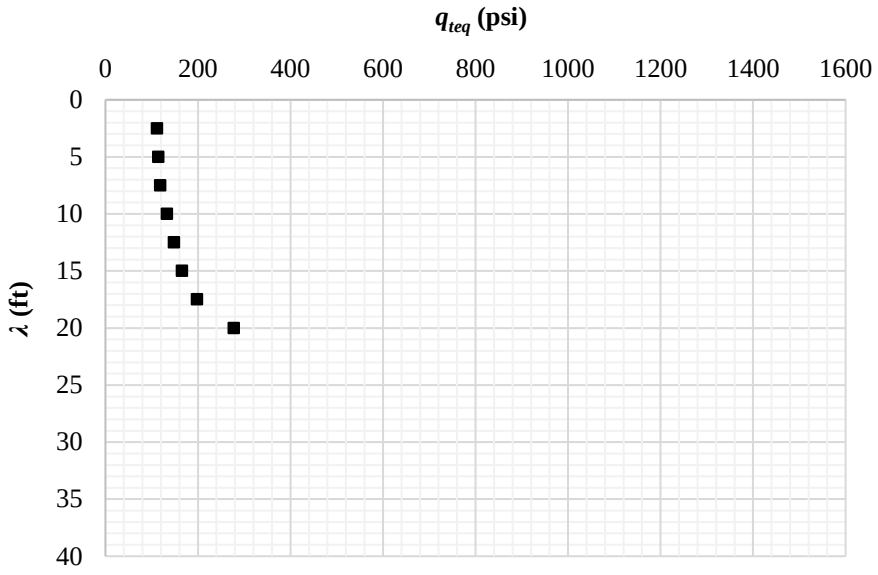

Figure A.31 – Point 80 equivalent tip resistance (q_{teq}) vs wavelength (λ).

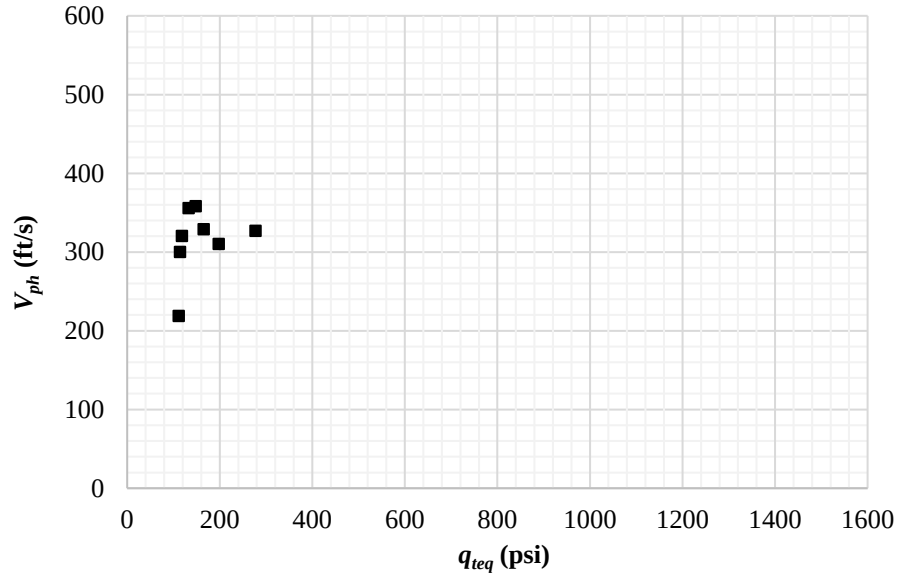

Figure A.32 – Pont 80 equivalent tip resistance (q_{teq}) vs phase velocity (V_{ph}) for the same λ.

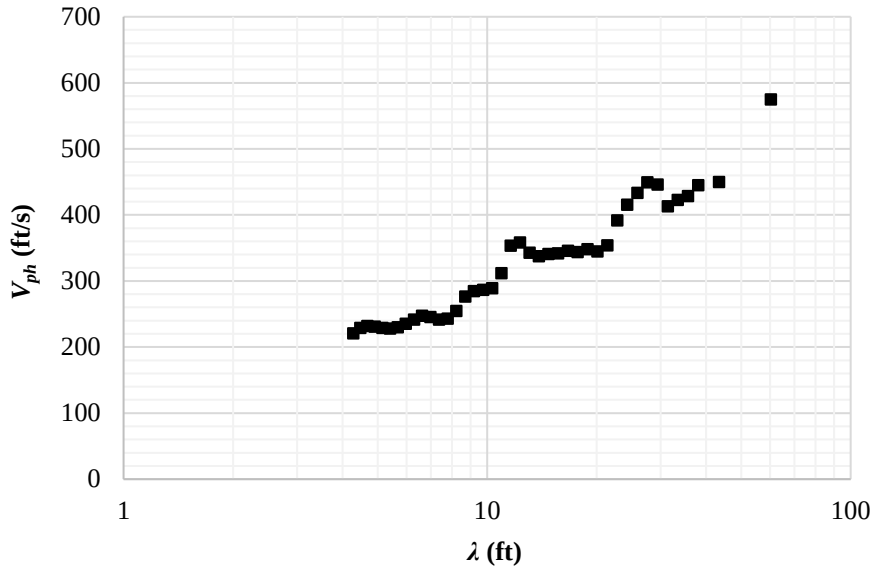

Figure A.33 – Point 94 dispersion curve.

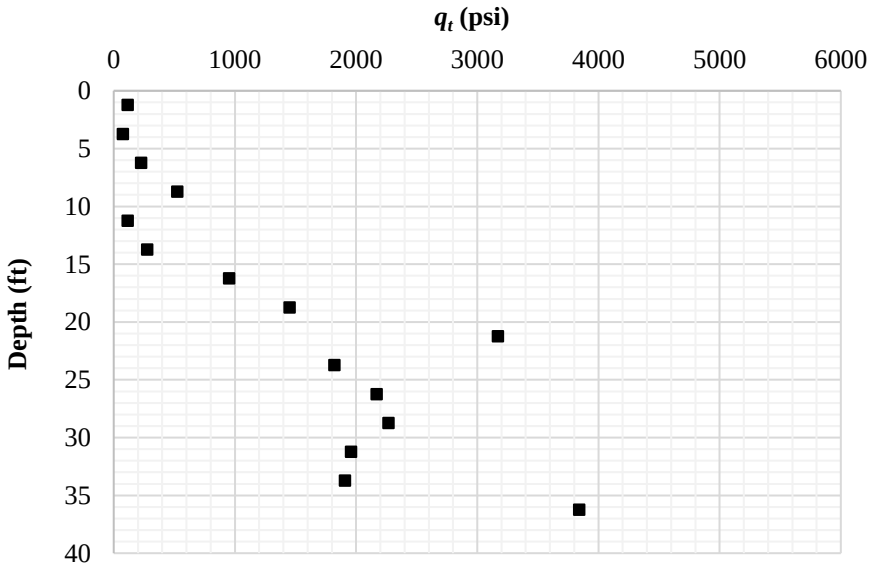

Figure A.34 – Point 94 tip resistance (q_t) vs depth (z).

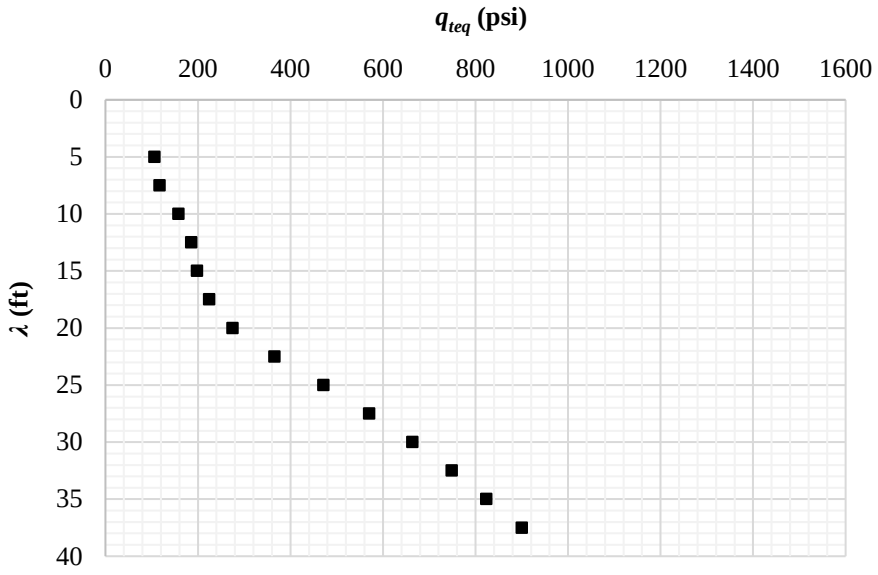

Figure A.35 – Point 94 equivalent tip resistance (q_{teq}) vs wavelength (λ).

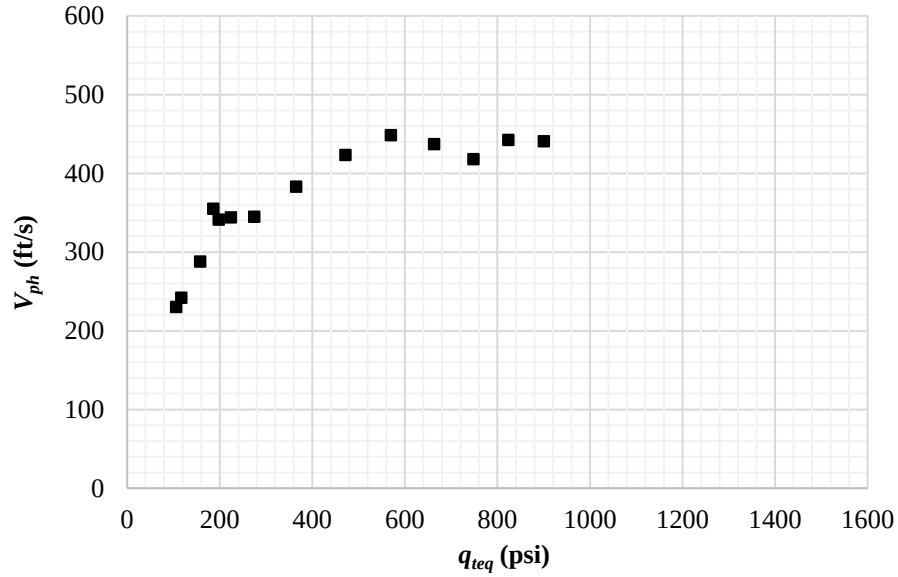

Figure A.36 – Pont 94 equivalent tip resistance (q_{teq}) vs phase velocity (V_{ph}) for the same λ.

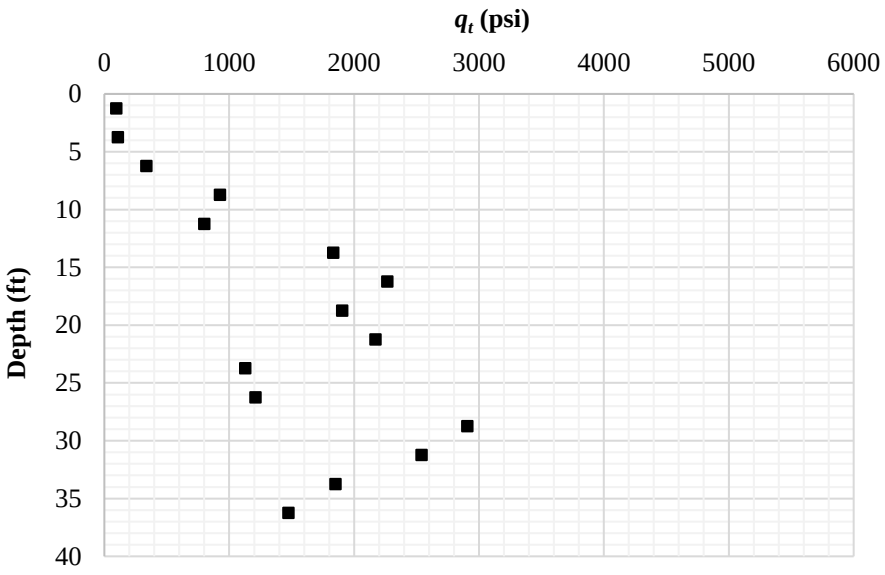

Figure A.37 – Point 68 tip resistance (q_t) vs depth (z).

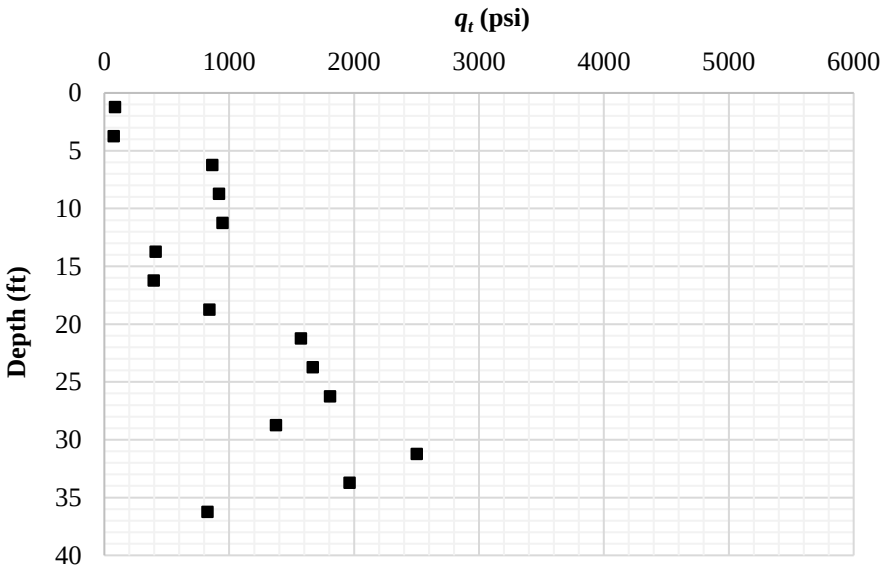

Figure A.38 – Point 70 tip resistance (q_t) vs depth (z).

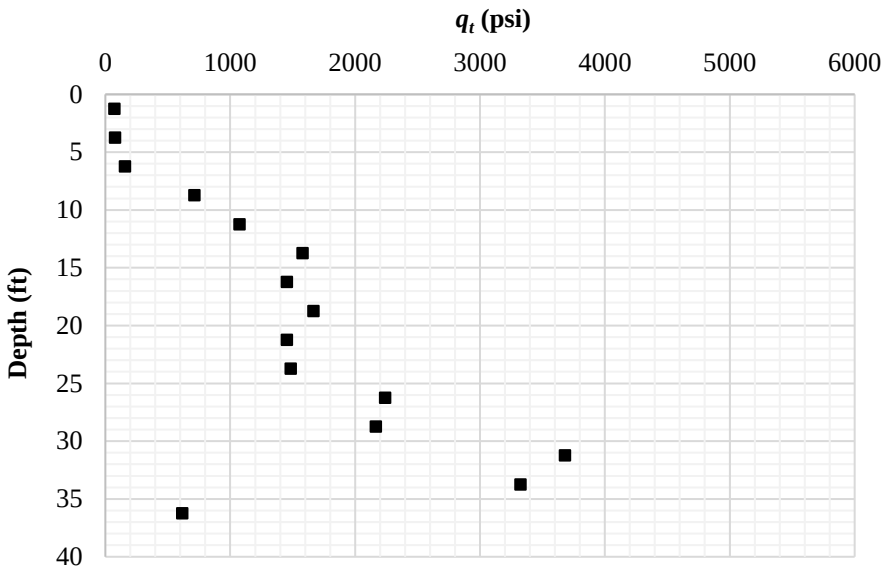

Figure A.39 – Point 84 tip resistance (q_t) vs depth (z).

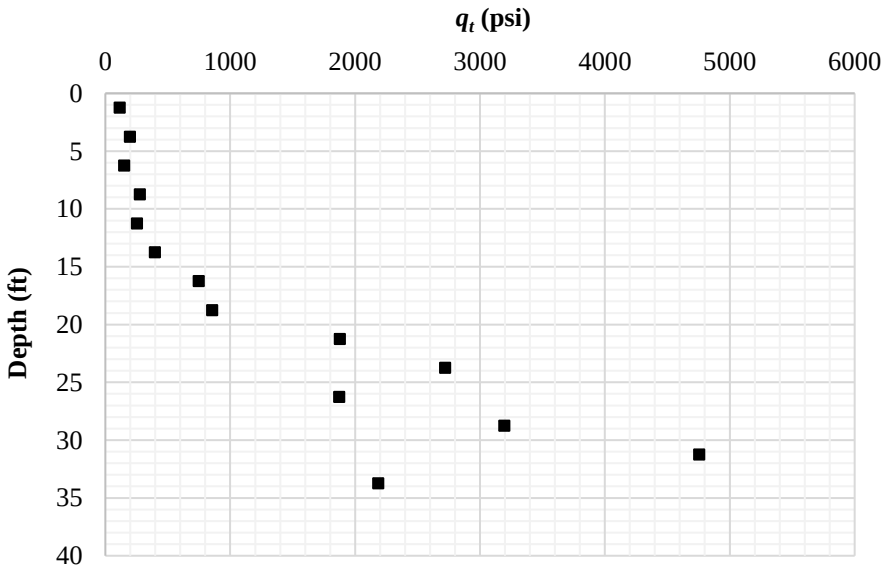

Figure A.40 – Point 96 tip resistance (q_t) vs depth (z).

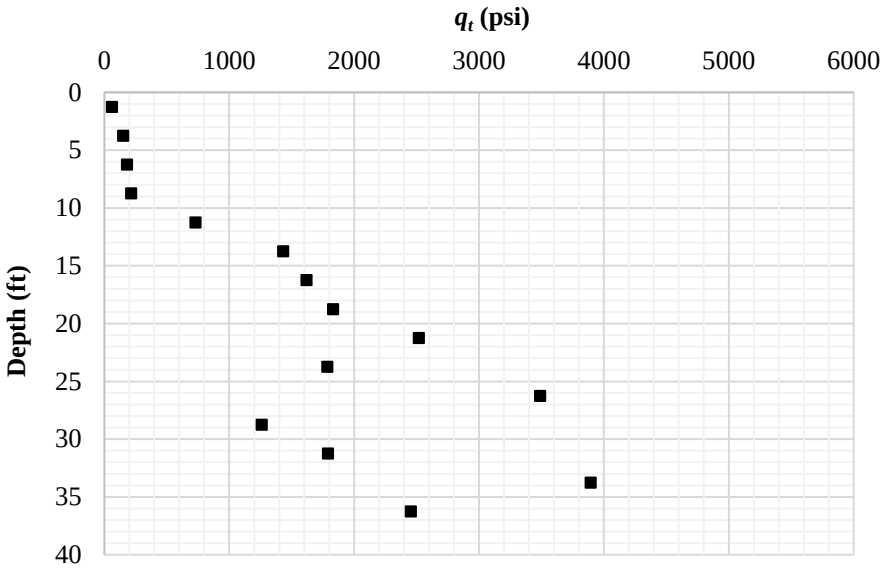

Figure A.41 – Point 98 tip resistance (q_t) vs depth (z).

Group 135

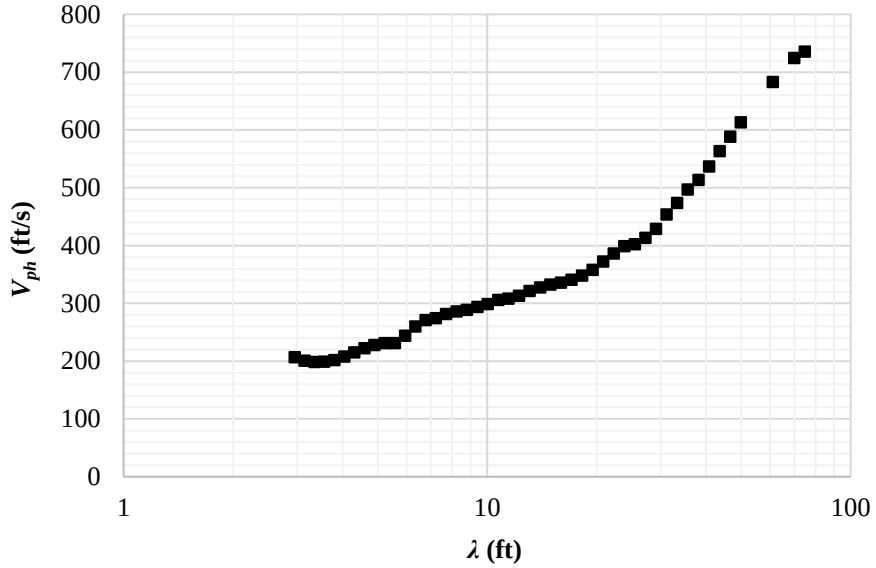

Figure A.42 – Point 121 dispersion curve.

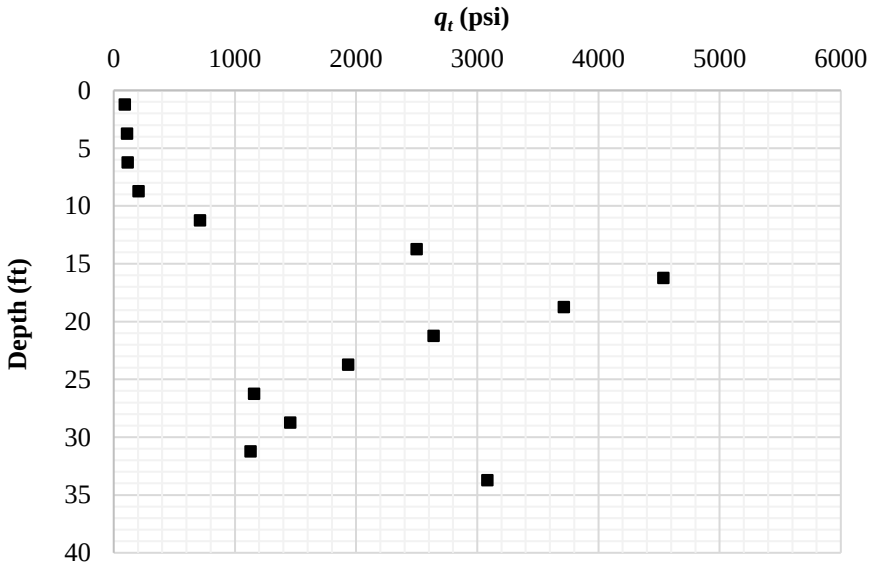

Figure A.43 – Point 121 tip resistance (q_t) vs depth (z).

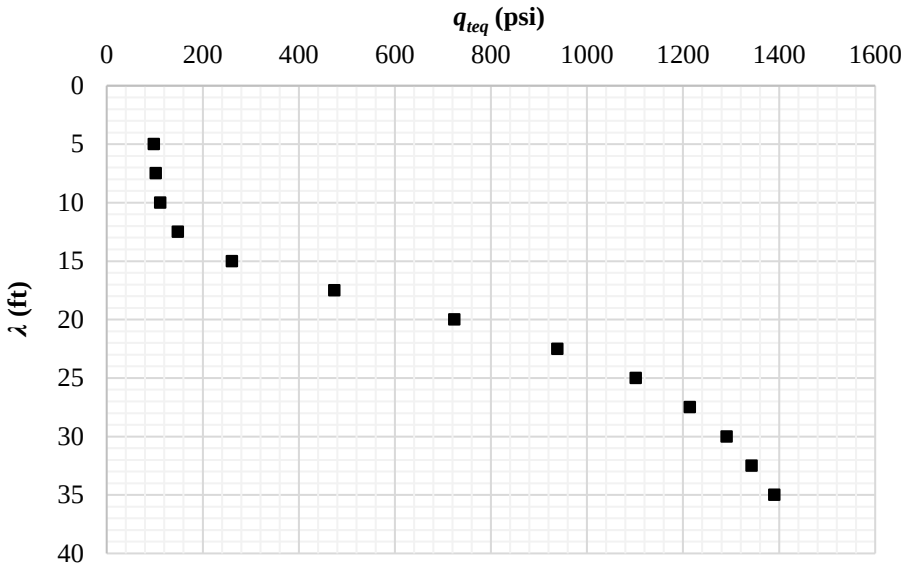

Figure A.44 – Point 121 equivalent tip resistance (q_{teq}) vs wavelength (λ).

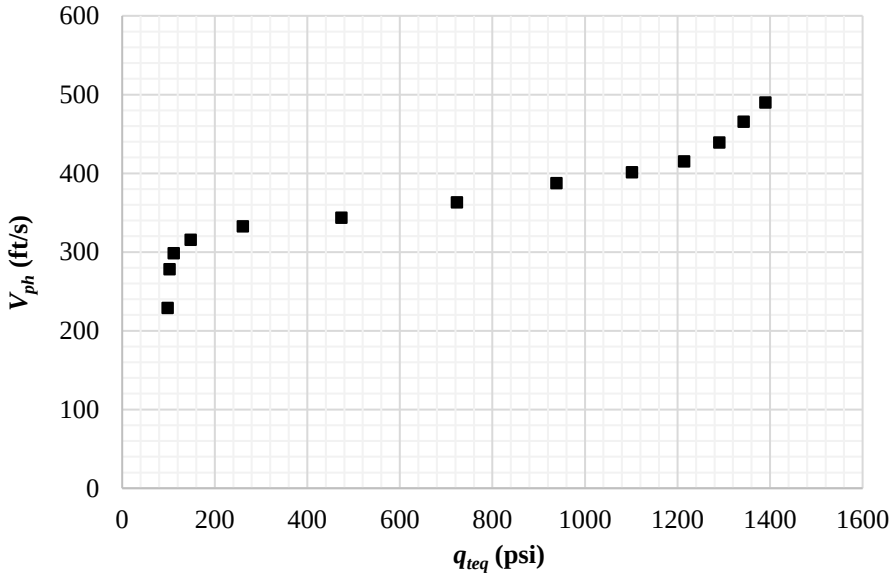

Figure A.45 – Pont 121 equivalent tip resistance (q_{teq}) vs phase velocity (V_{ph}) for the same λ.

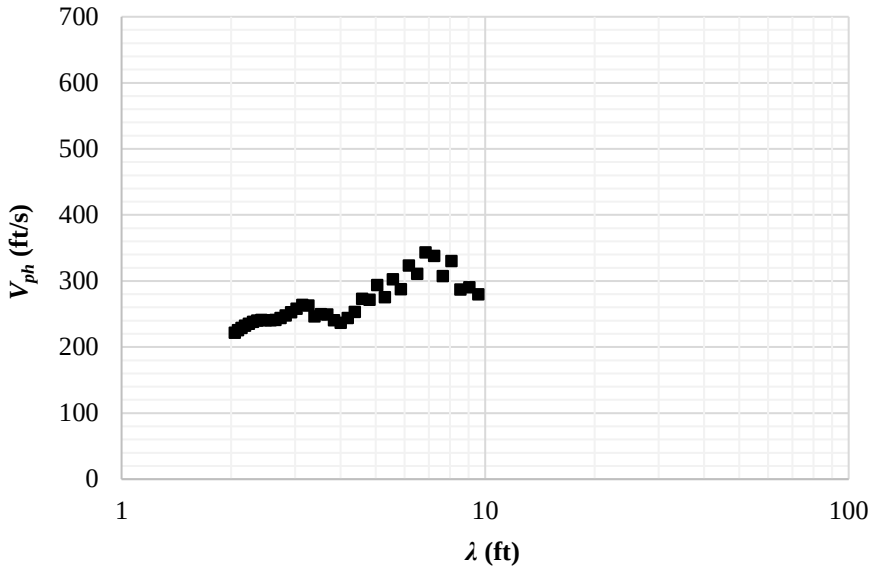

Figure A.46 – Point 123 dispersion curve.

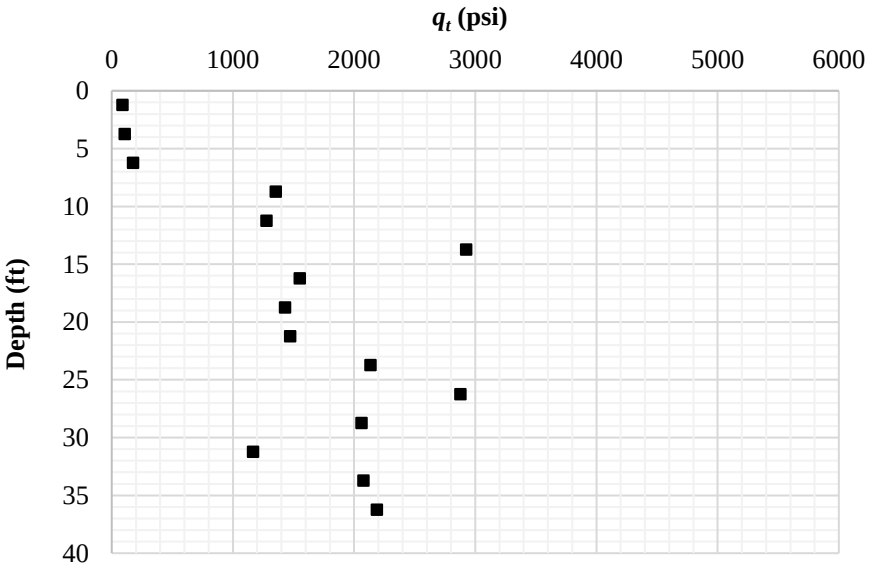

Figure A.47 – Point 123 tip resistance (q_t) vs depth (z).

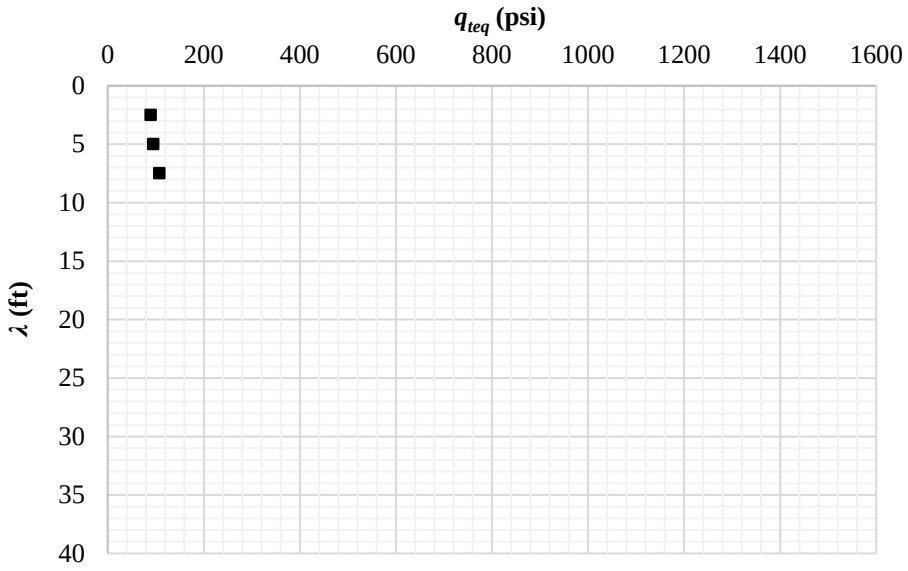

Figure A.48 – Point 123 equivalent tip resistance (q_{teq}) vs wavelength (λ).

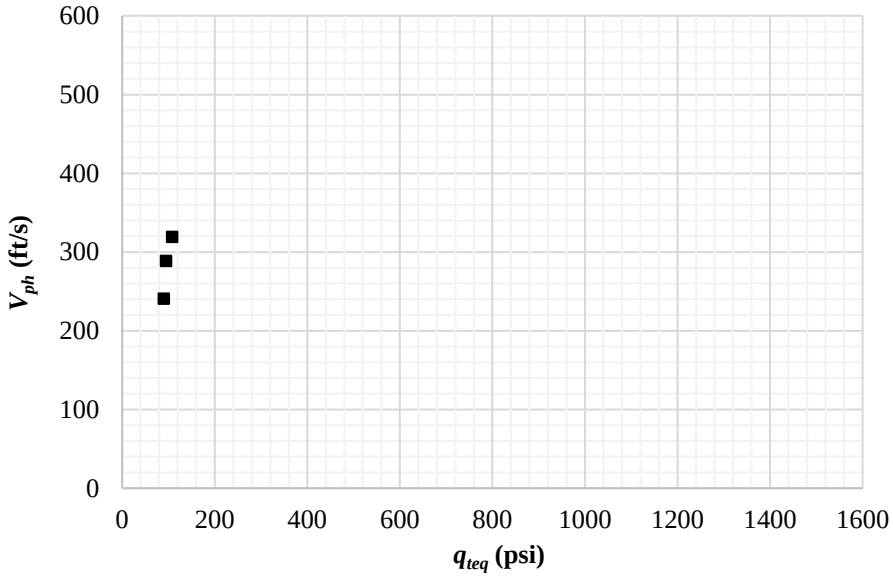

Figure A.49 – Pont 123 equivalent tip resistance (q_{teq}) vs phase velocity (V_{ph}) for the same λ.

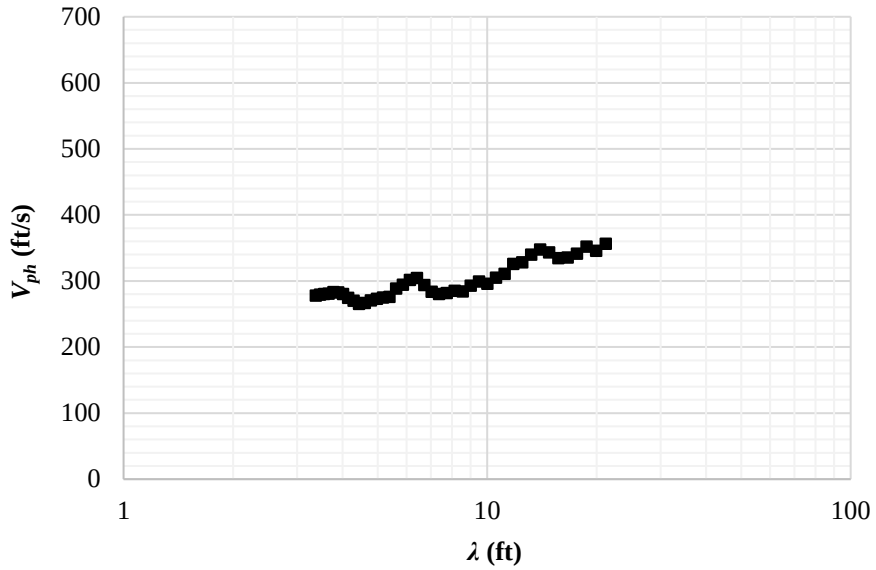

Figure A.50 – Point 135 dispersion curve.

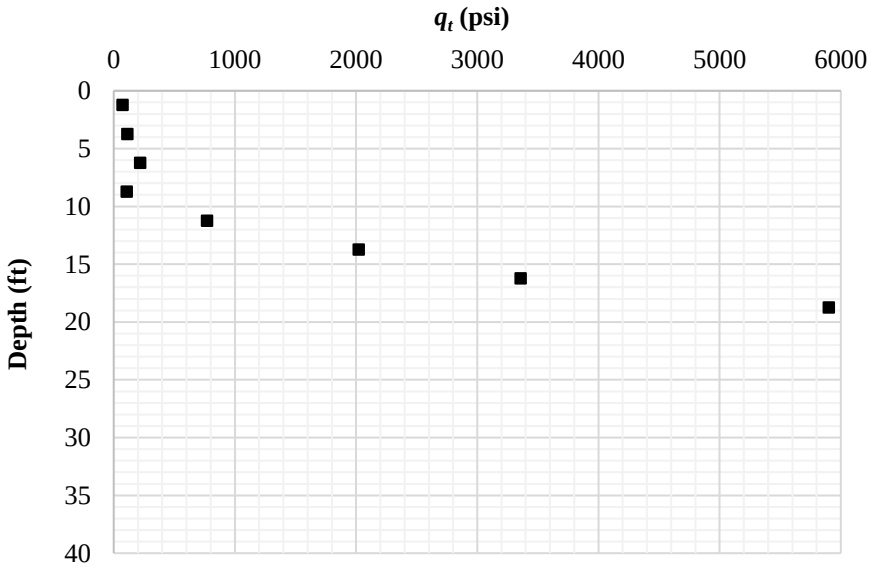

Figure A.51 – Point 135 tip resistance (q_t) vs depth (z).

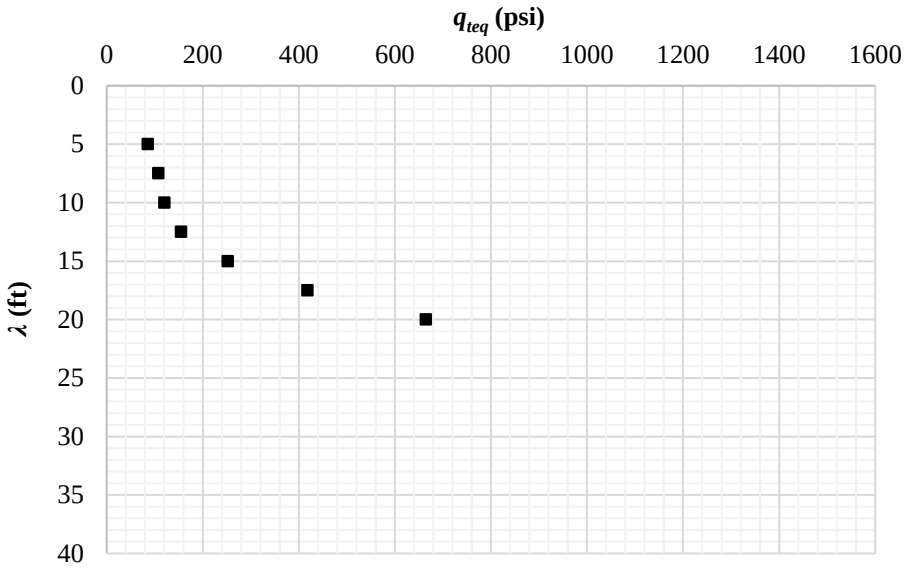

Figure A.52 – Point 135 equivalent tip resistance (q_{teq}) vs wavelength (λ).

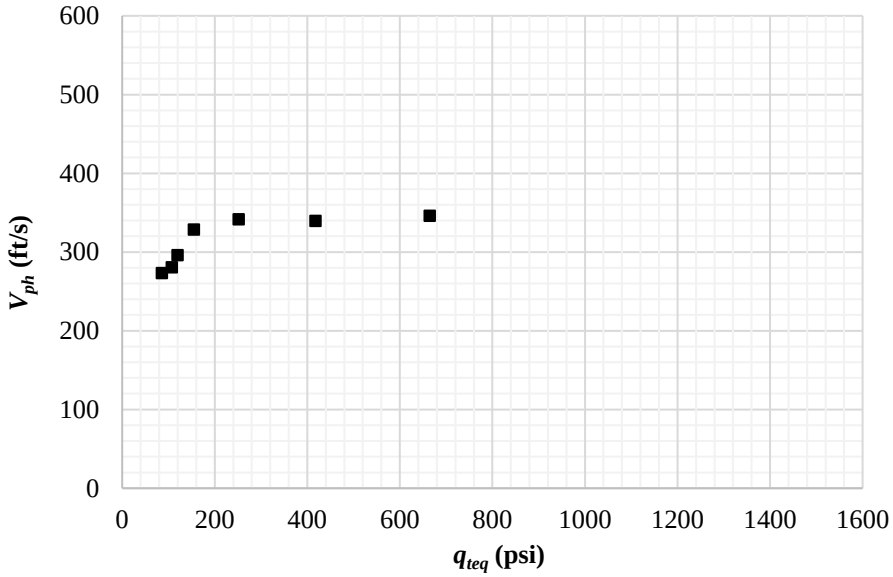

Figure A.53 – Pont 135 equivalent tip resistance (q_{teq}) vs phase velocity (V_{ph}) for the same λ.

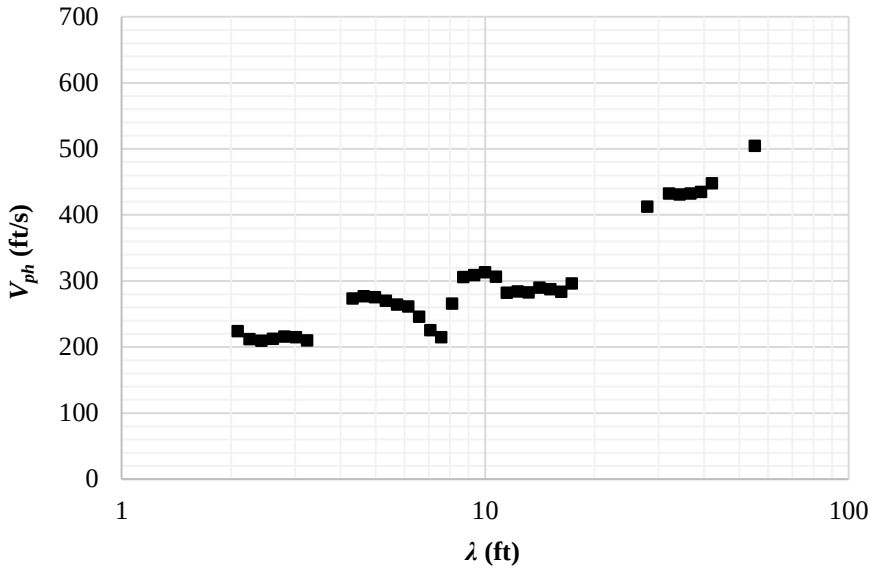

Figure A.54 – Point 147A dispersion curve.

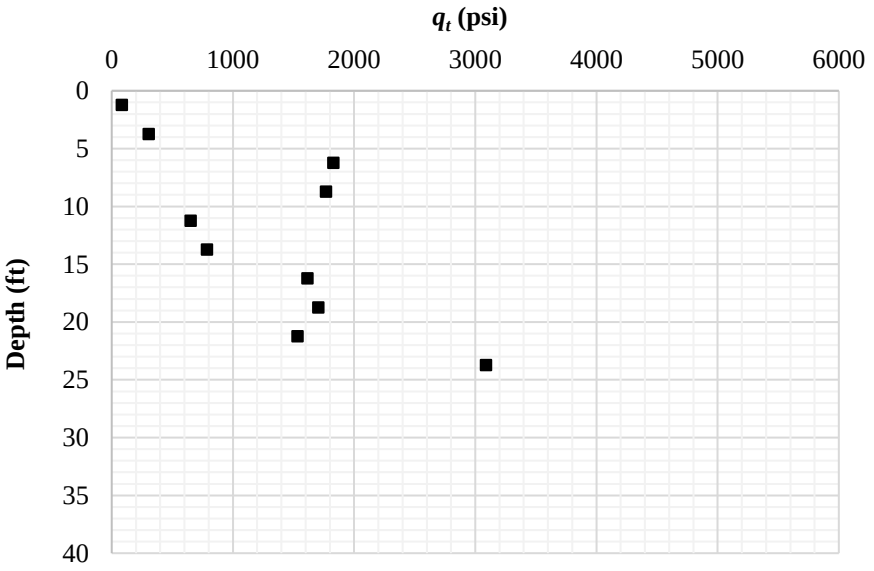

Figure A.55 – Point 147A tip resistance (q_t) vs depth (z).

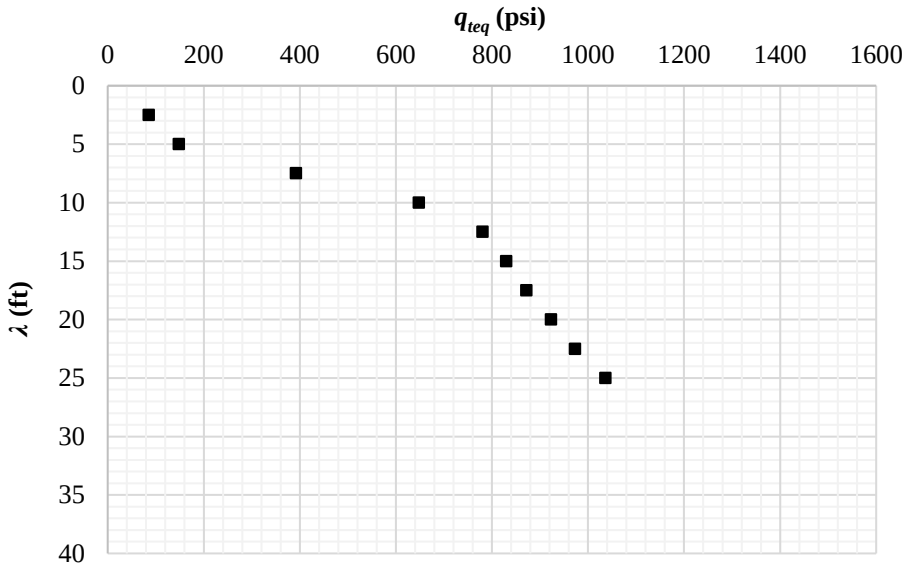

Figure A.56 – Point 147A equivalent tip resistance (q_{teq}) vs wavelength (λ).

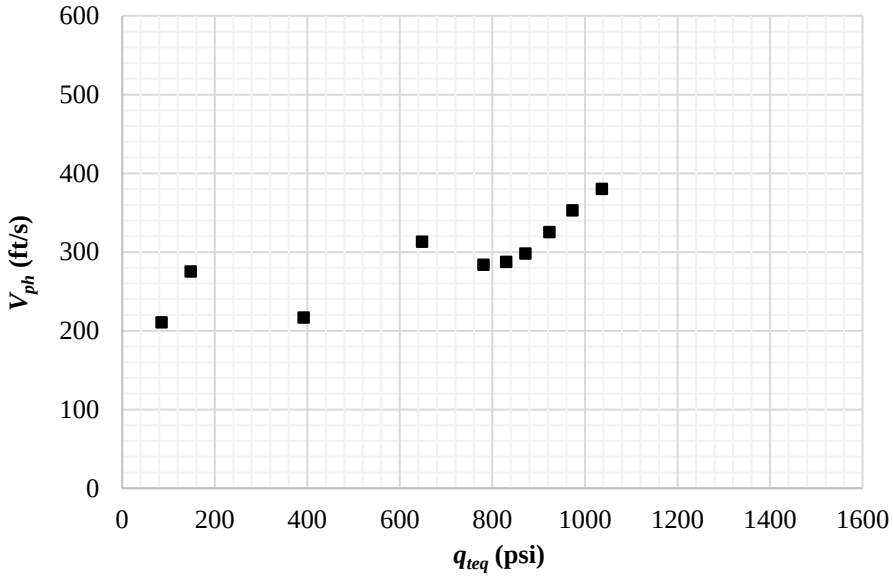

Figure A.57 – Pont 147A equivalent tip resistance (q_{teq}) vs phase velocity (V_{ph}) for the same λ.

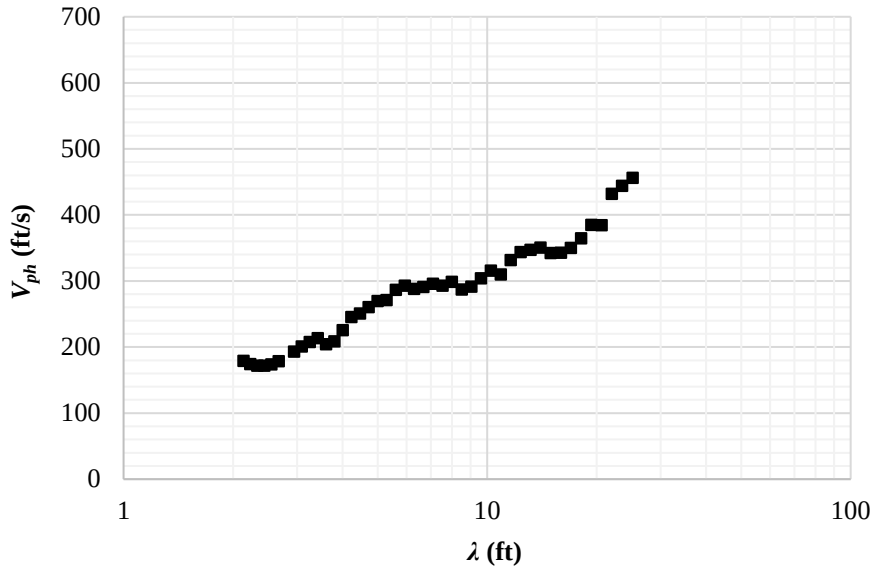

Figure A.58 – Point 149 dispersion curve.

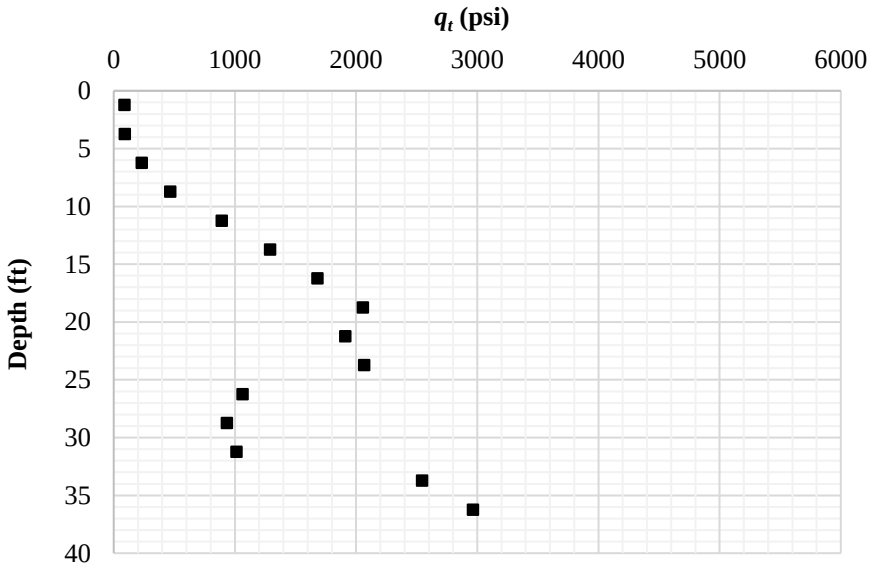

Figure A.59 – Point 149 tip resistance (q_t) vs depth (z).

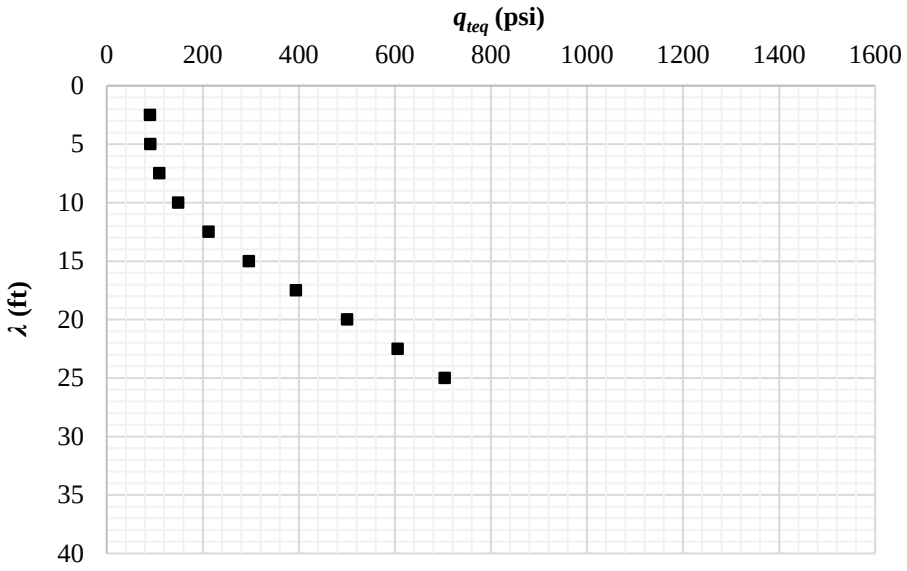

Figure A.60 – Point 149 equivalent tip resistance (q_{teq}) vs wavelength (λ).

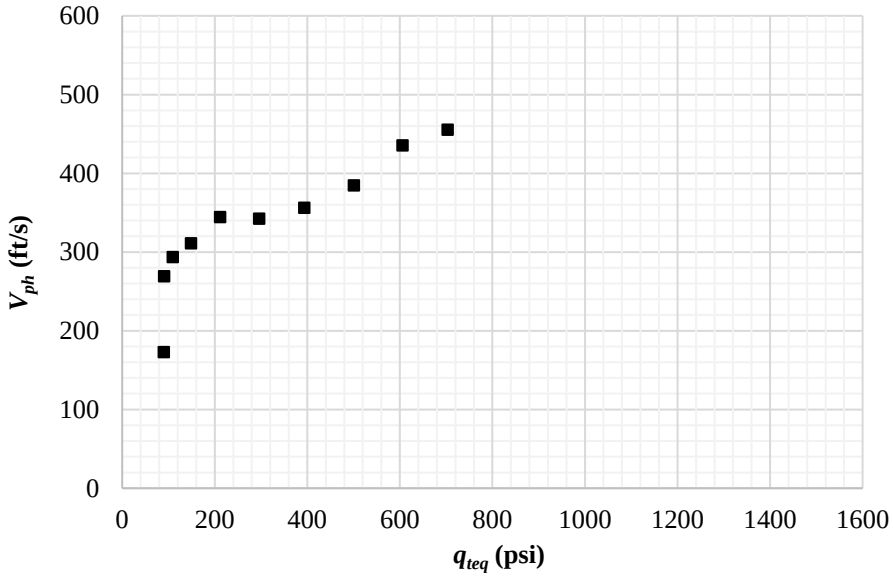

Figure A.61 – Pont 149 equivalent tip resistance (q_{teq}) vs phase velocity (V_{ph}) for the same λ.

Group 180

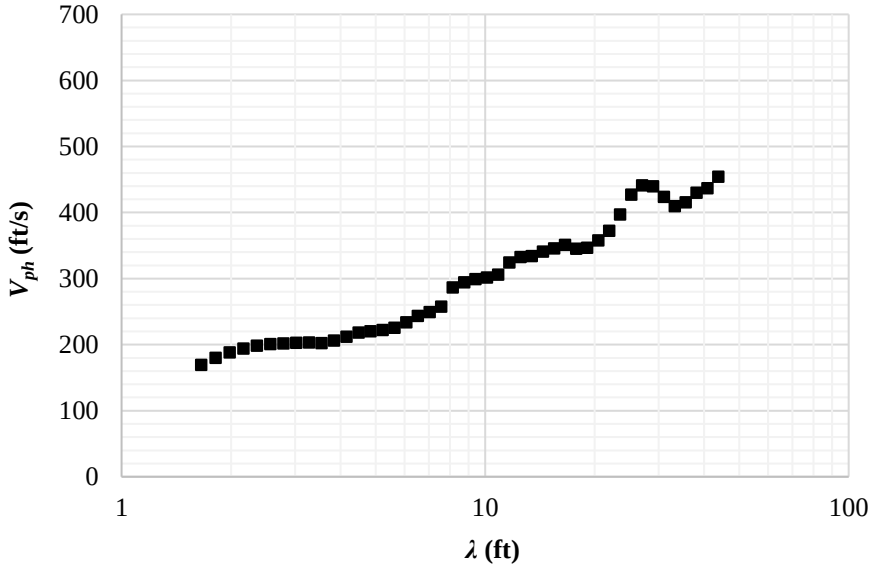

Figure A.62 – Point 168 dispersion curve.

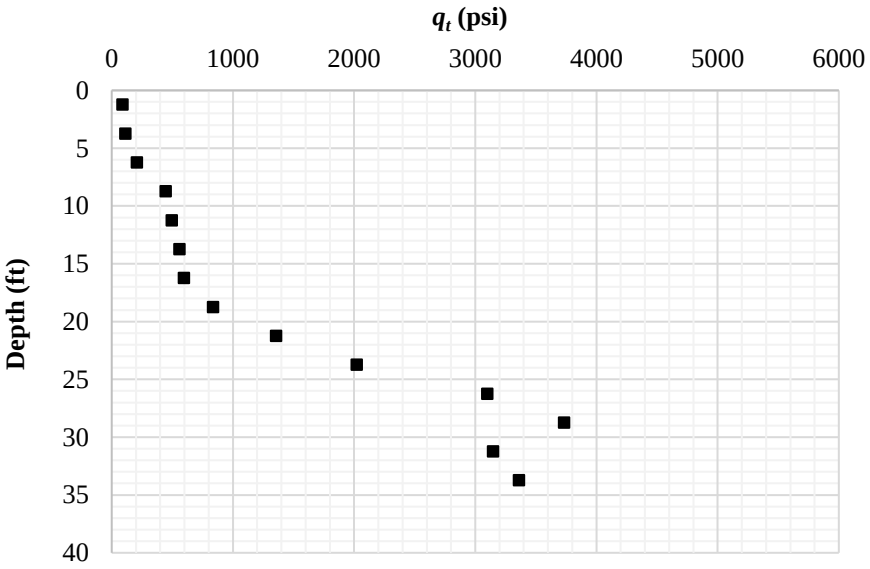

Figure A.63 – Point 168 tip resistance (q_t) vs depth (z).

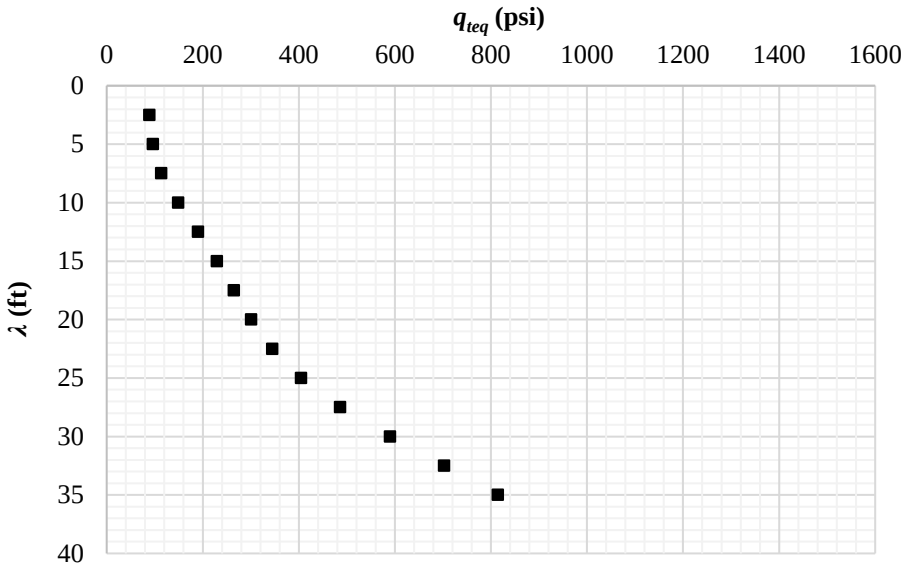

Figure A.64 – Point 168 equivalent tip resistance (q_{teq}) vs wavelength (λ).

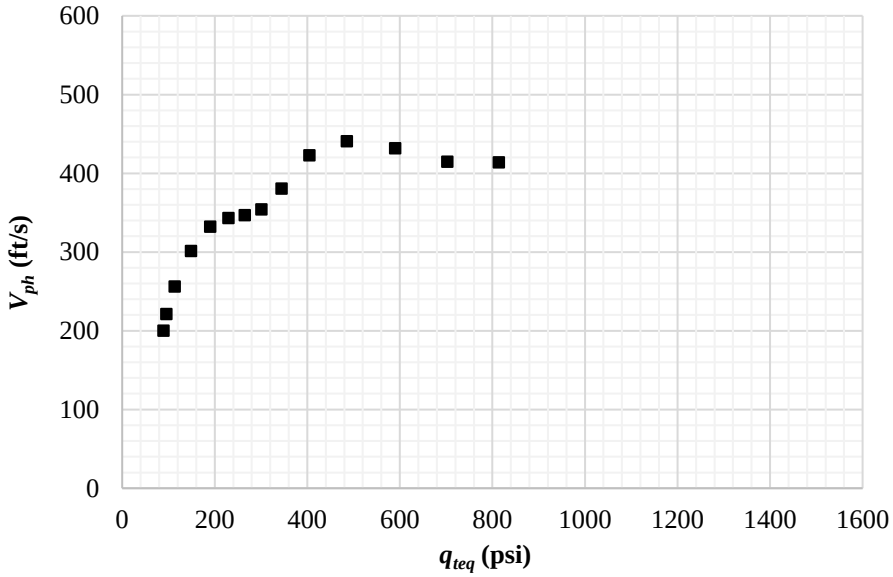

Figure A.65 – Pont 168 equivalent tip resistance (q_{teq}) vs phase velocity (V_{ph}) for the same λ.

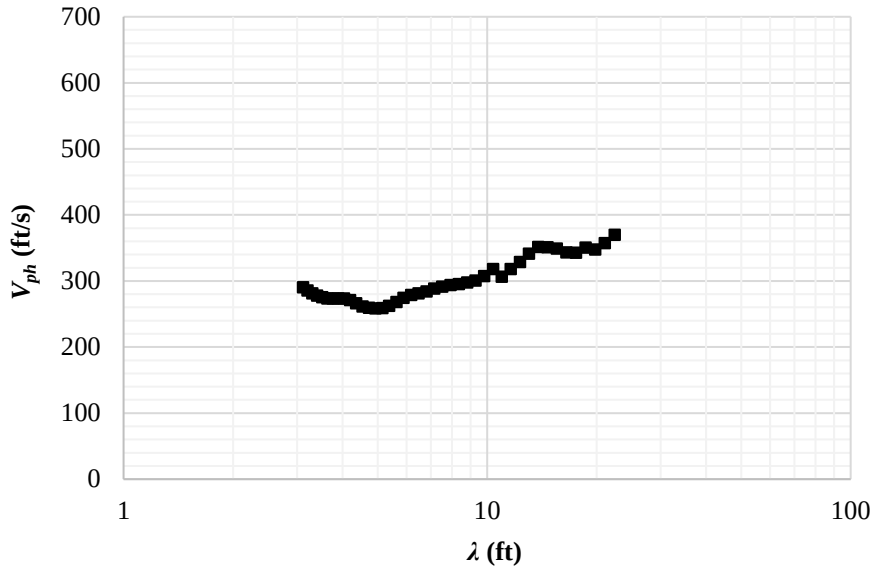

Figure A.66 – Point 170 dispersion curve.

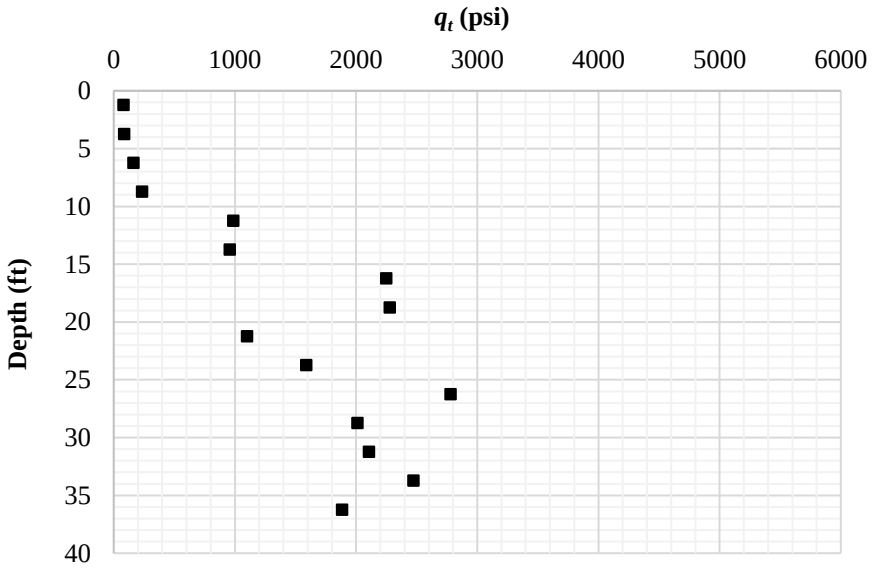

Figure A.67 – Point 170 tip resistance (q_t) vs depth (z).

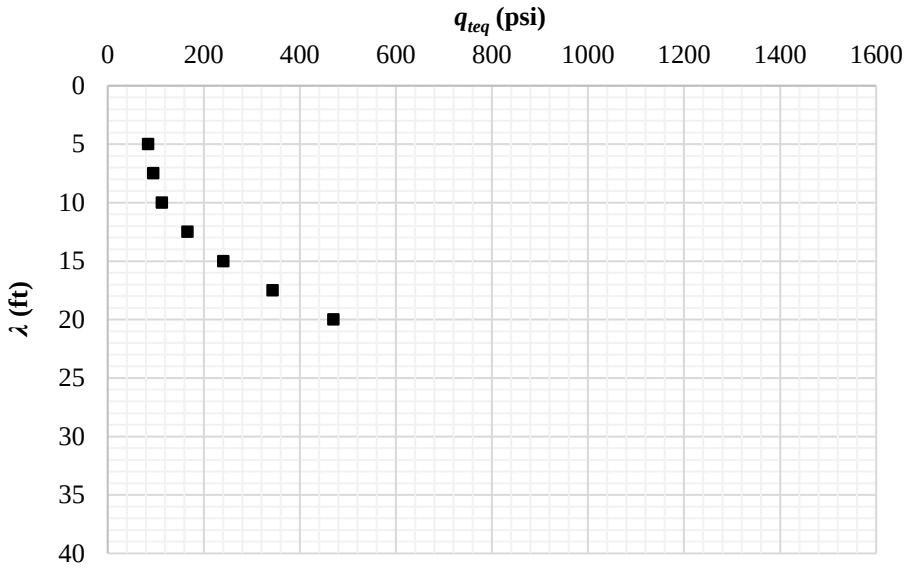

Figure A.68 – Point 170 equivalent tip resistance (q_{teq}) vs wavelength (λ).

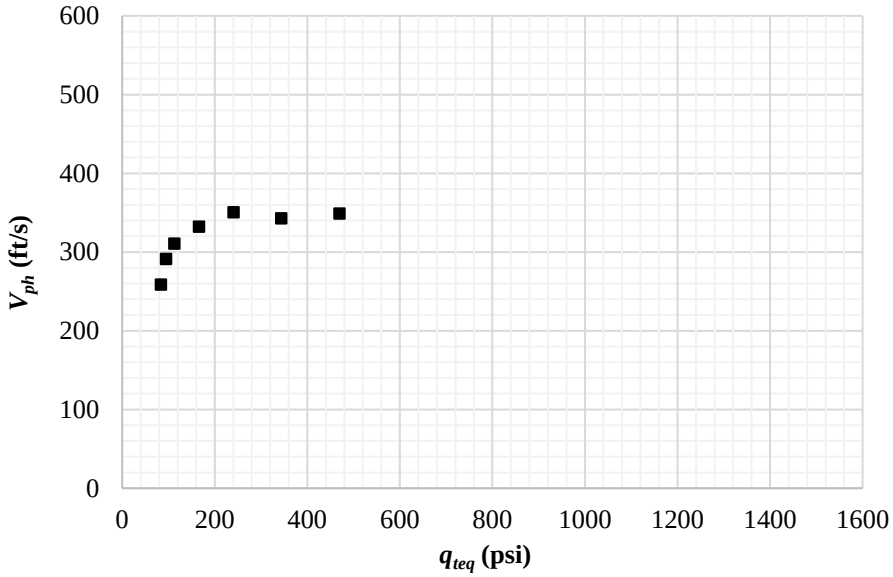

Figure A.69 – Pont 170 equivalent tip resistance (q_{teq}) vs phase velocity (V_{ph}) for the same λ.

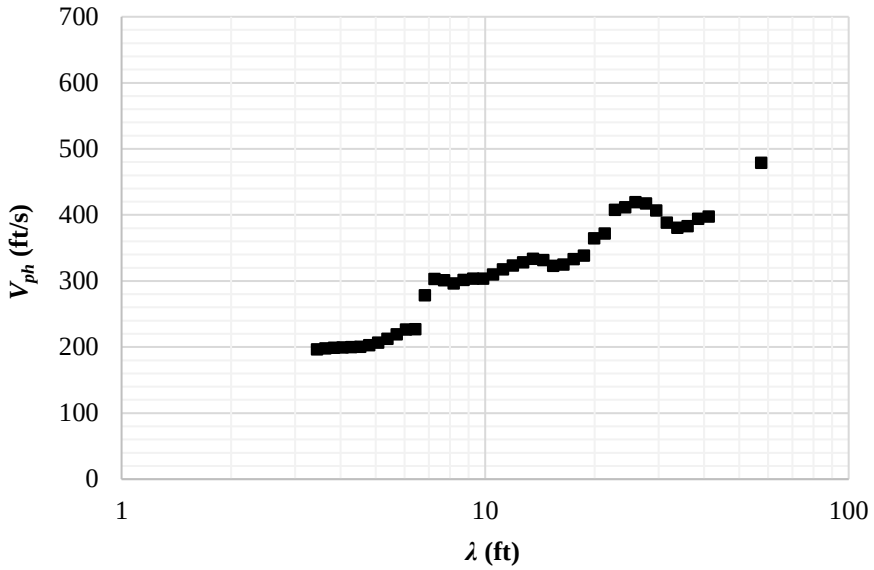

Figure A.70 – Point 180 dispersion curve.

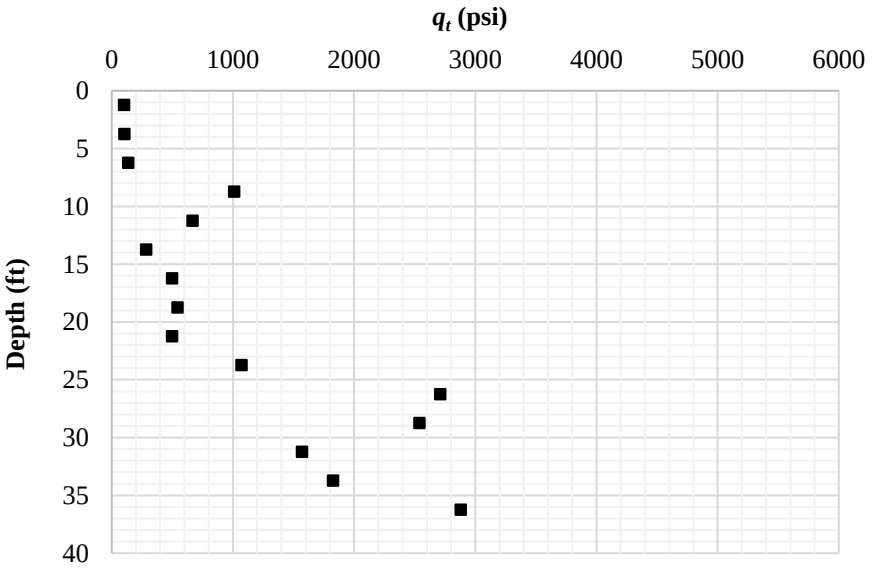

Figure A.71 – Point 180 tip resistance (q_t) vs depth (z).

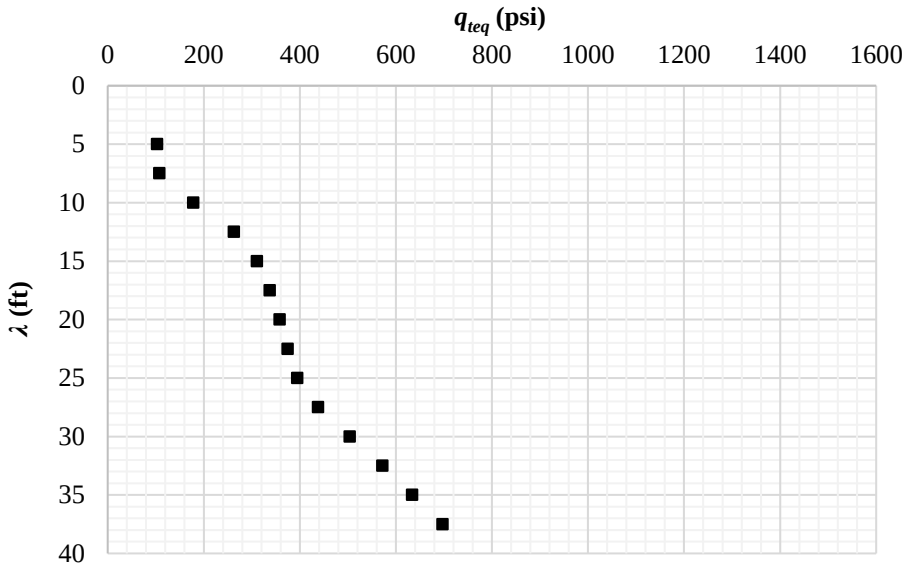

Figure A.72 – Point 180 equivalent tip resistance (q_{teq}) vs wavelength (λ).

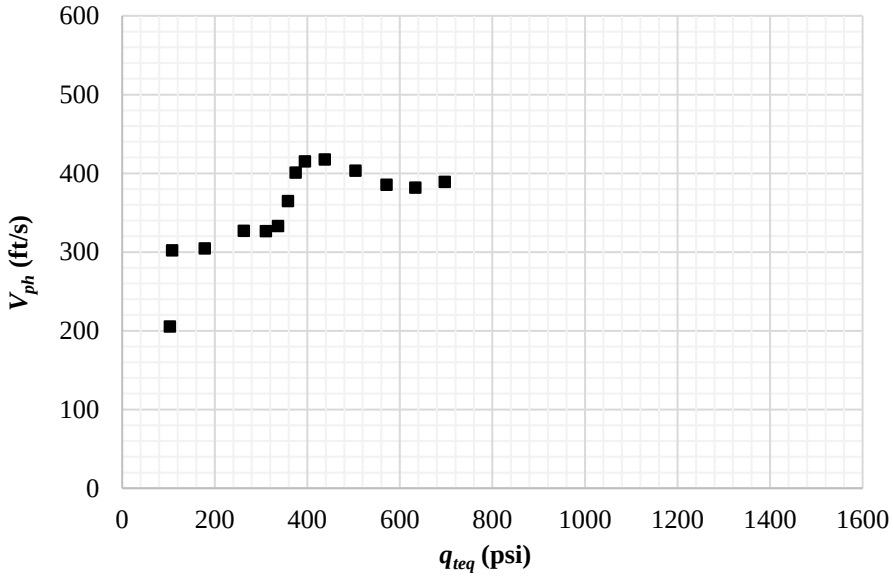

Figure A.73 – Pont 180 equivalent tip resistance (q_{teq}) vs phase velocity (V_{ph}) for the same λ.

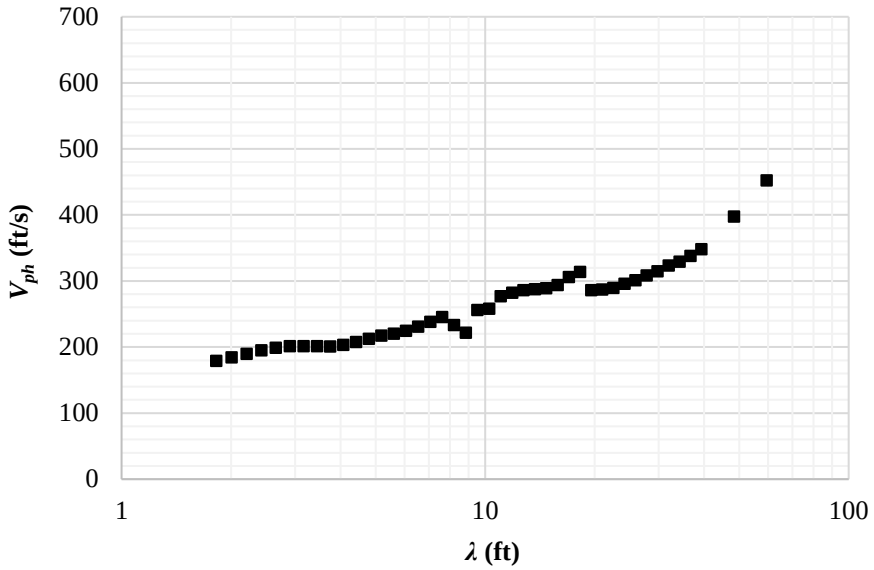

Figure A.74 – Point 190 dispersion curve.

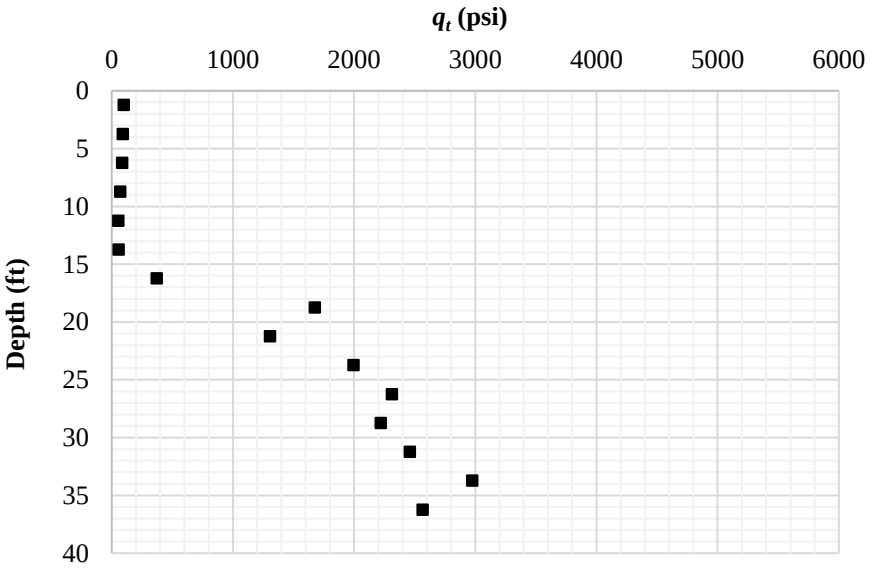

Figure A.75 – Point 190 tip resistance (q_t) vs depth (z).

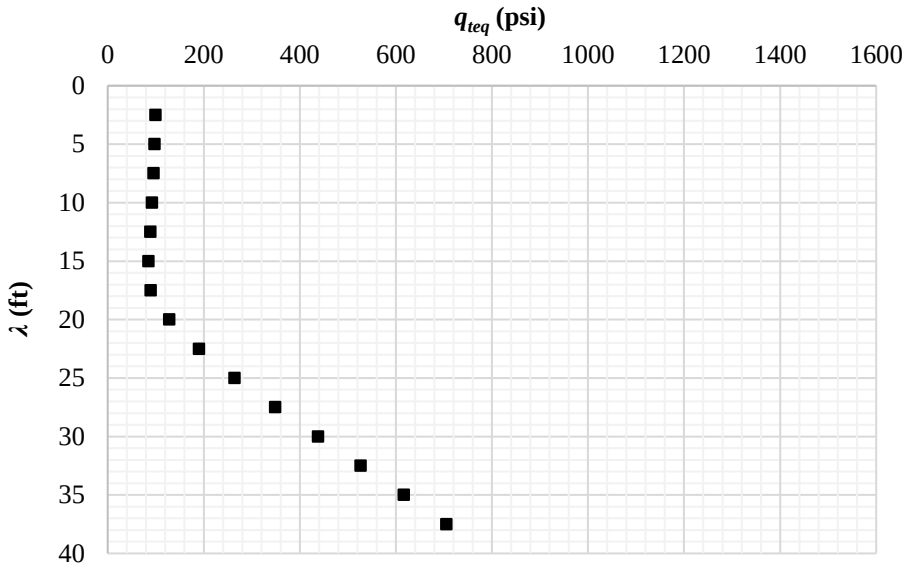

Figure A.76 – Point 190 equivalent tip resistance (q_{teq}) vs wavelength (λ).

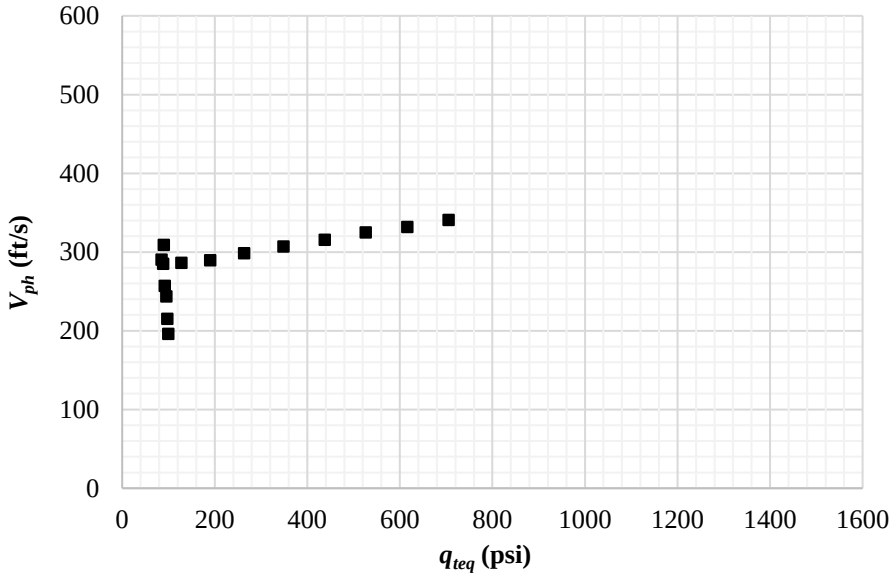

Figure A.77 – Pont 190 equivalent tip resistance (q_{teq}) vs phase velocity (V_{ph}) for the same λ.

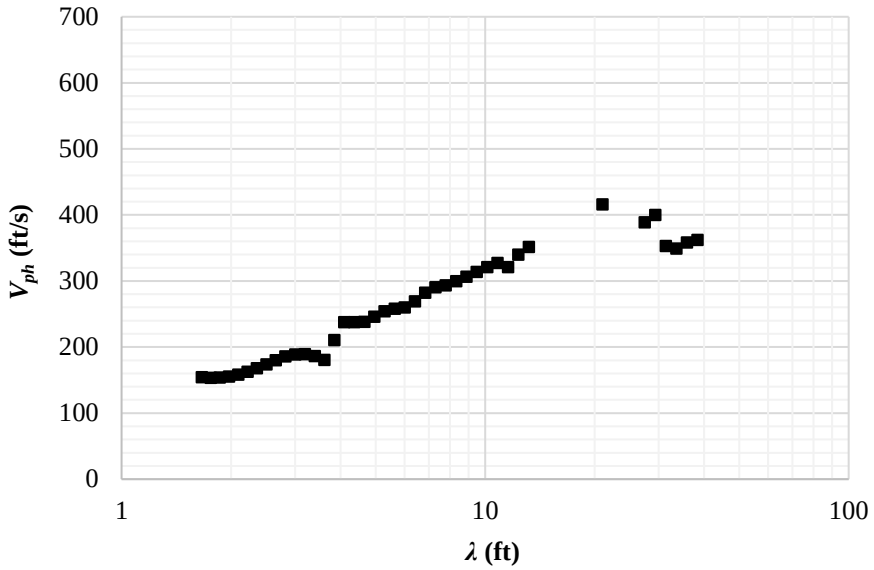

Figure A.78 – Point 192 dispersion curve.

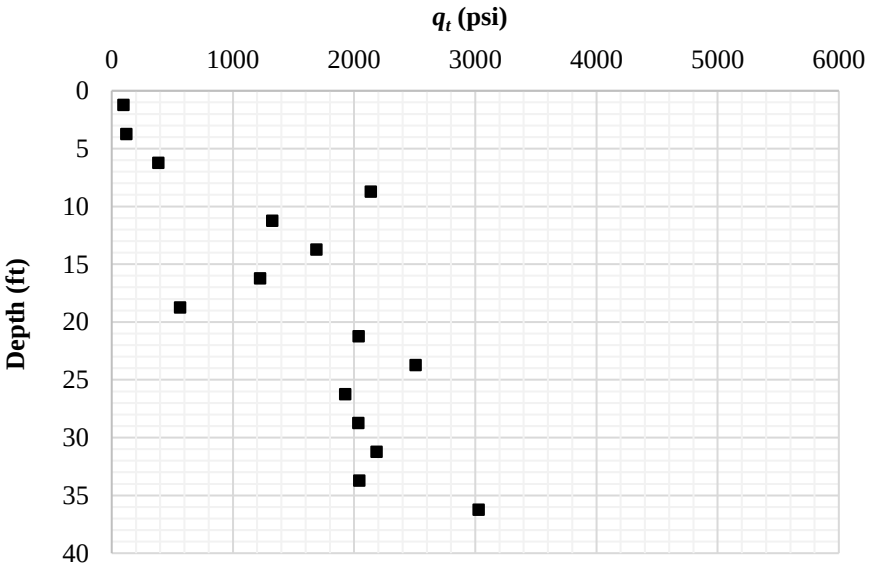

Figure A.79 – Point 192 tip resistance (q_t) vs depth (z).

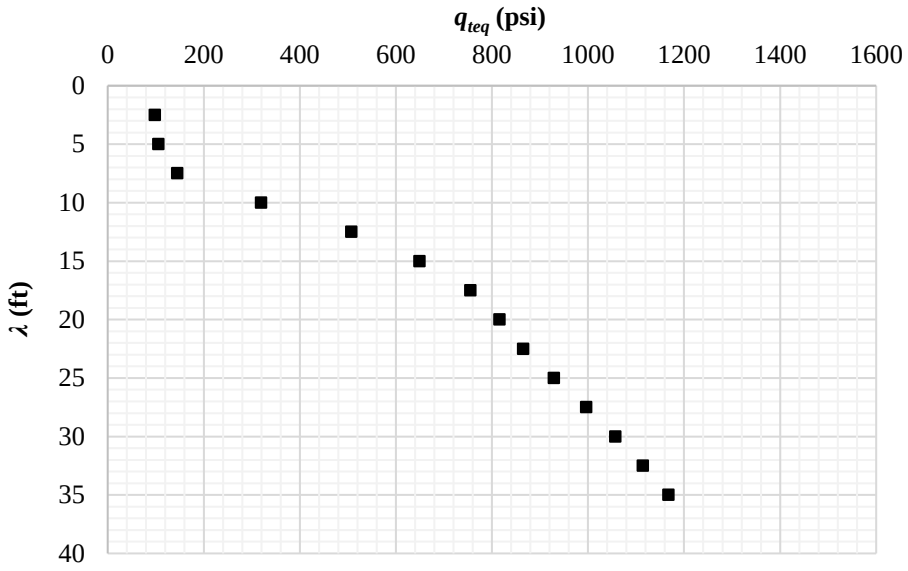

Figure A.80 – Point 192 equivalent tip resistance (q_{teq}) vs wavelength (λ).

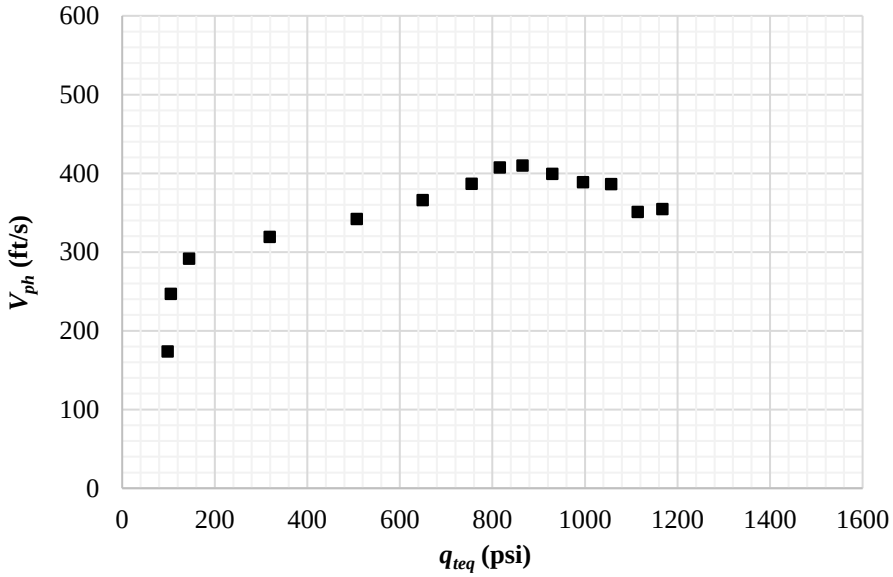

Figure A.81 – Pont 192 equivalent tip resistance (q_{teq}) vs phase velocity (V_{ph}) for the same λ.

Group 184

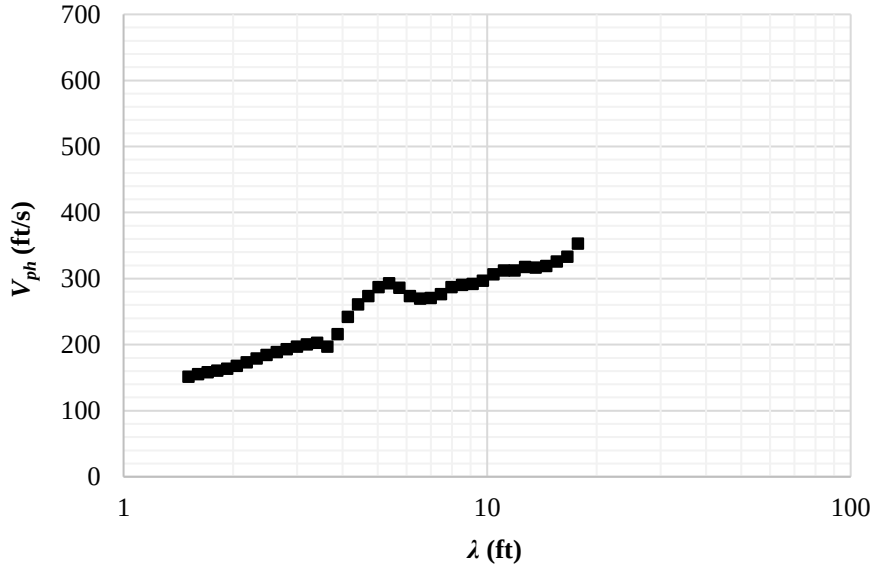

Figure A.82 – Point 172 dispersion curve.

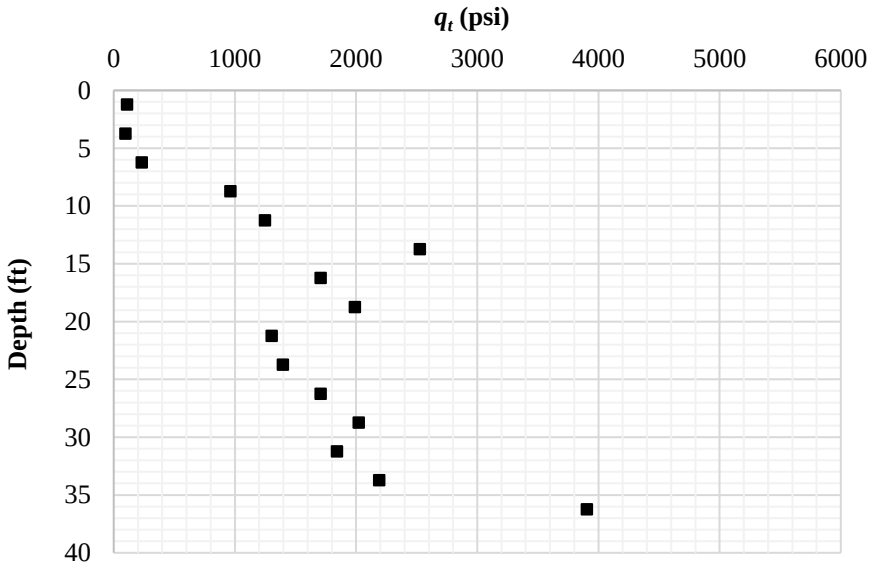

Figure A.83 – Point 172 tip resistance (q_t) vs depth (z).

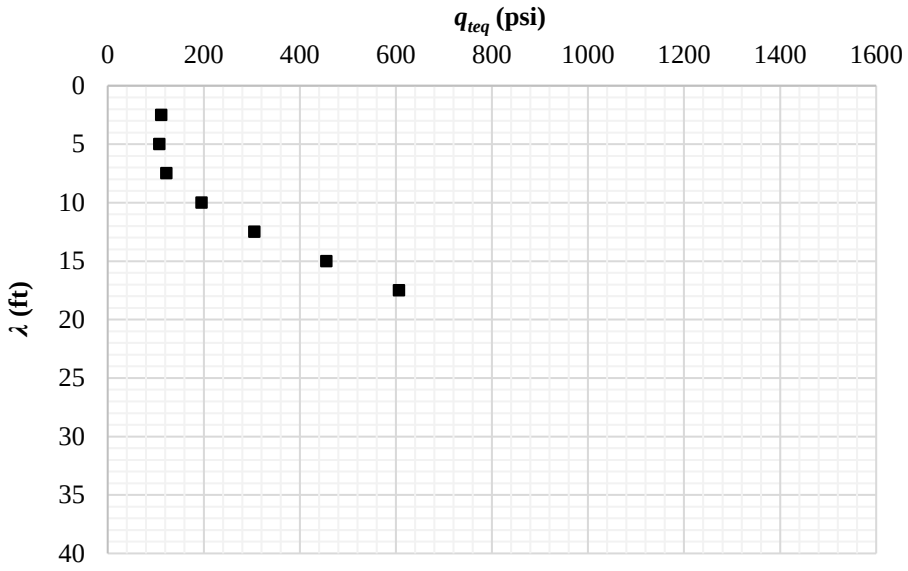

Figure A.84 – Point 172 equivalent tip resistance (q_{teq}) vs wavelength (λ).

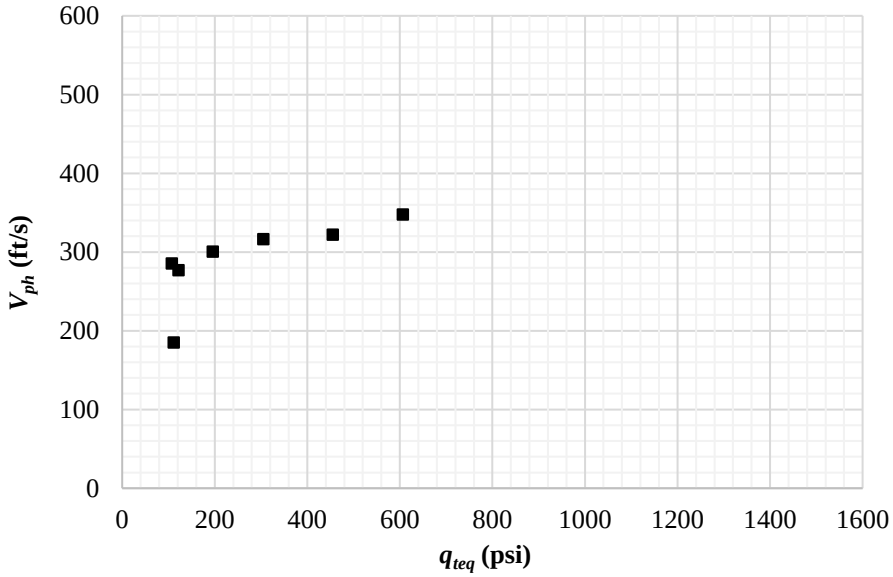

Figure A.85 – Pont 172 equivalent tip resistance (q_{teq}) vs phase velocity (V_{ph}) for the same λ.

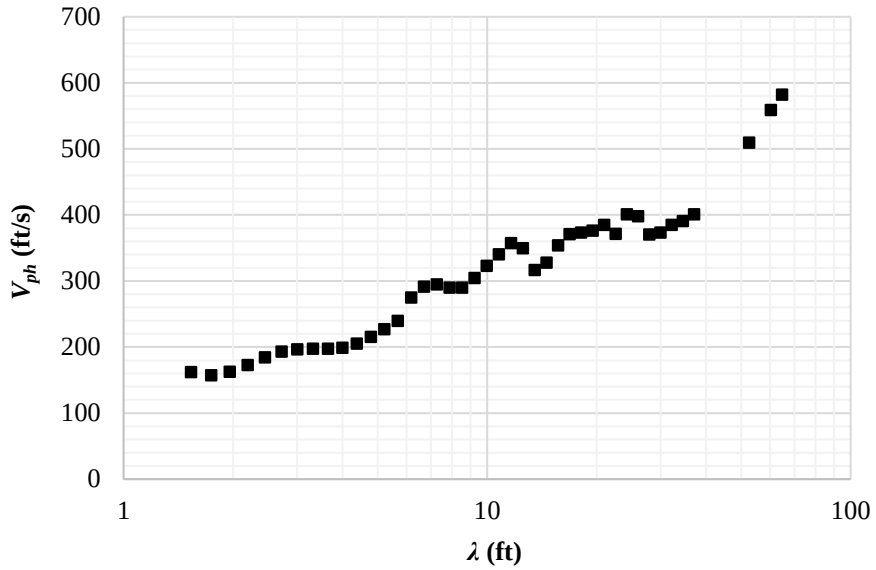

Figure A.86 – Point 174 dispersion curve.

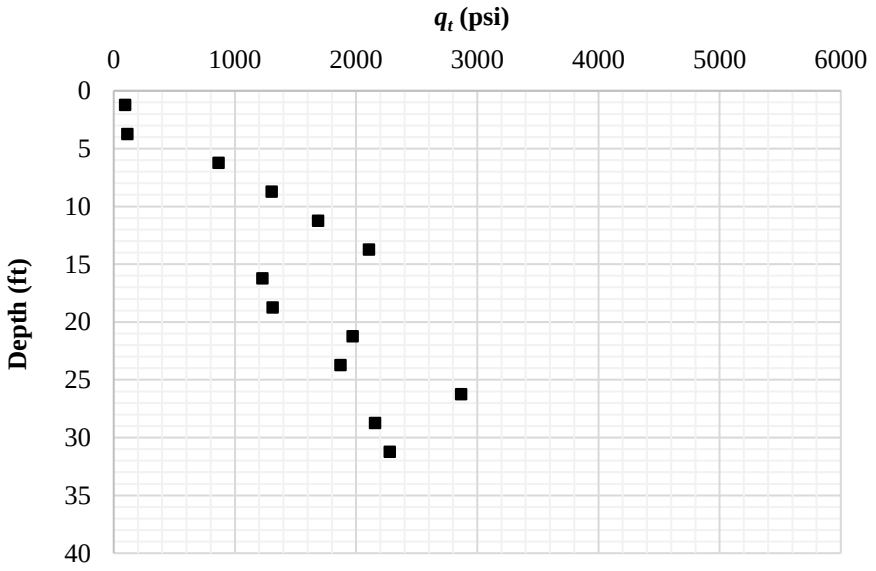

Figure A.87 – Point 174 tip resistance (q_t) vs depth (z).

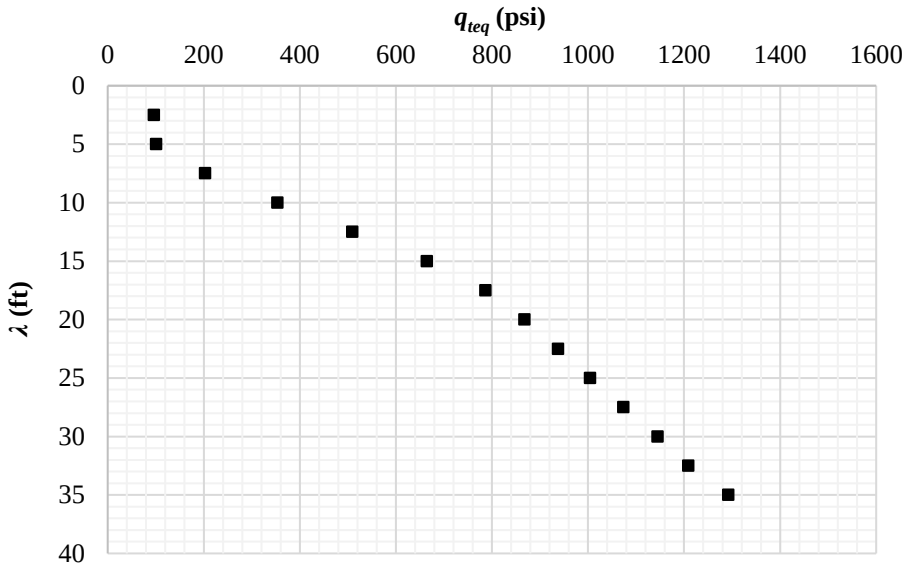

Figure A.88 – Point 174 equivalent tip resistance (q_{teq}) vs wavelength (λ).

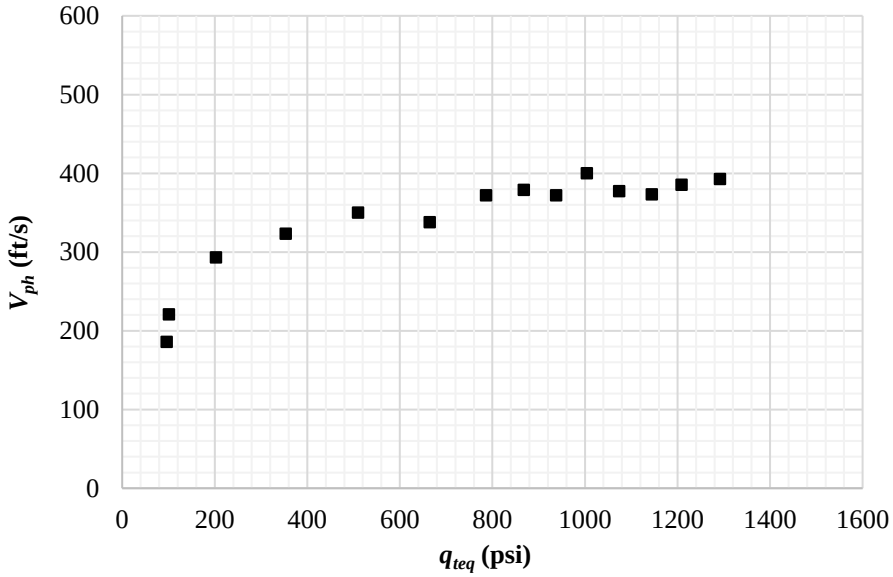

Figure A.89 – Pont 174 equivalent tip resistance (q_{teq}) vs phase velocity (V_{ph}) for the same λ.

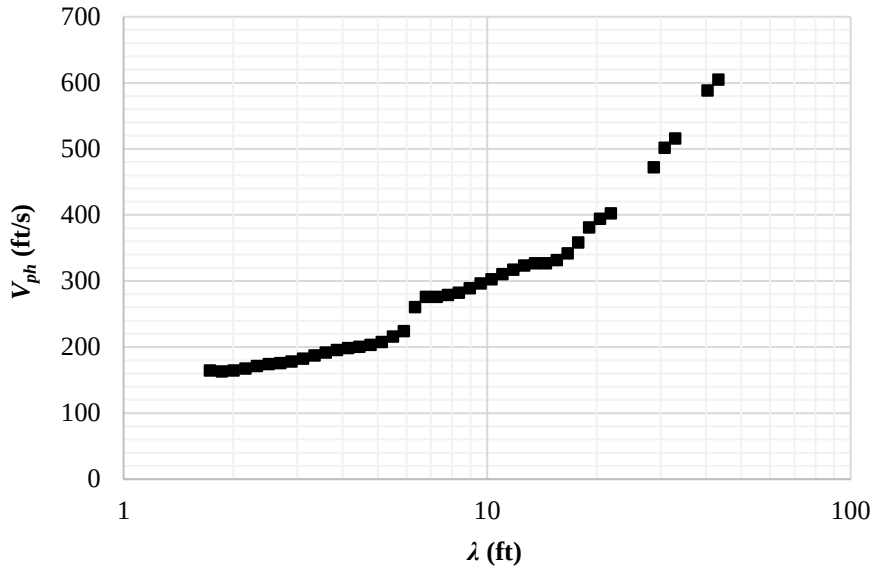

Figure A.90 – Point 184 dispersion curve.

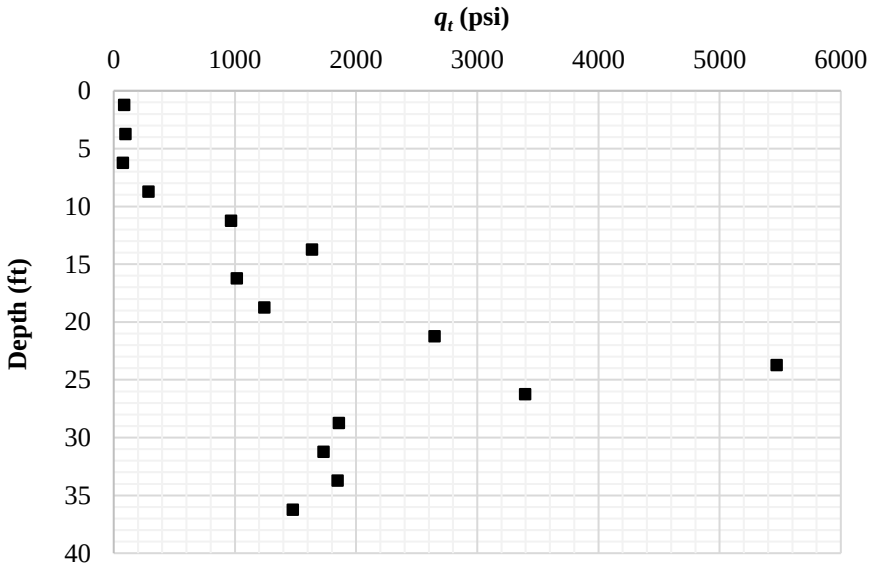

Figure A.91 – Point 184 tip resistance (q_t) vs depth (z).

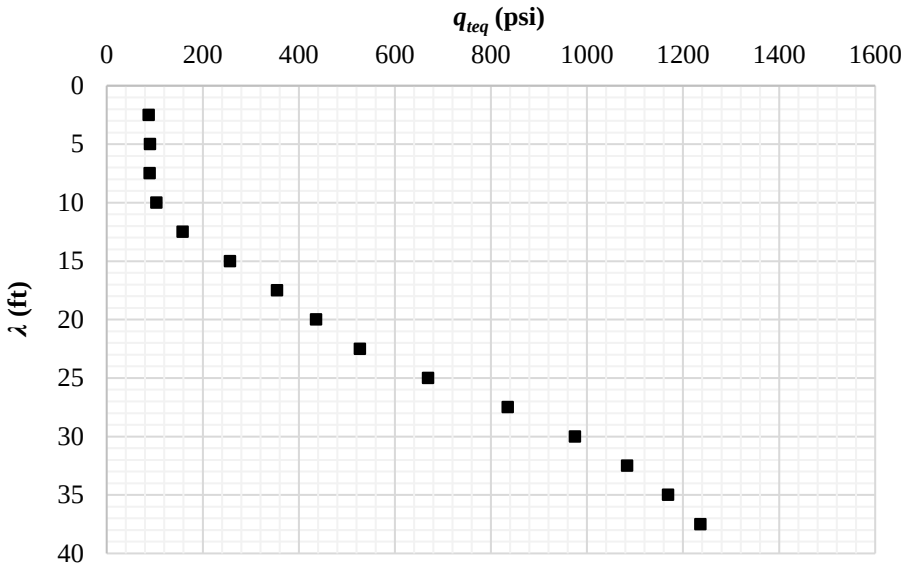

Figure A.92 – Point 184 equivalent tip resistance (q_{teq}) vs wavelength (λ).

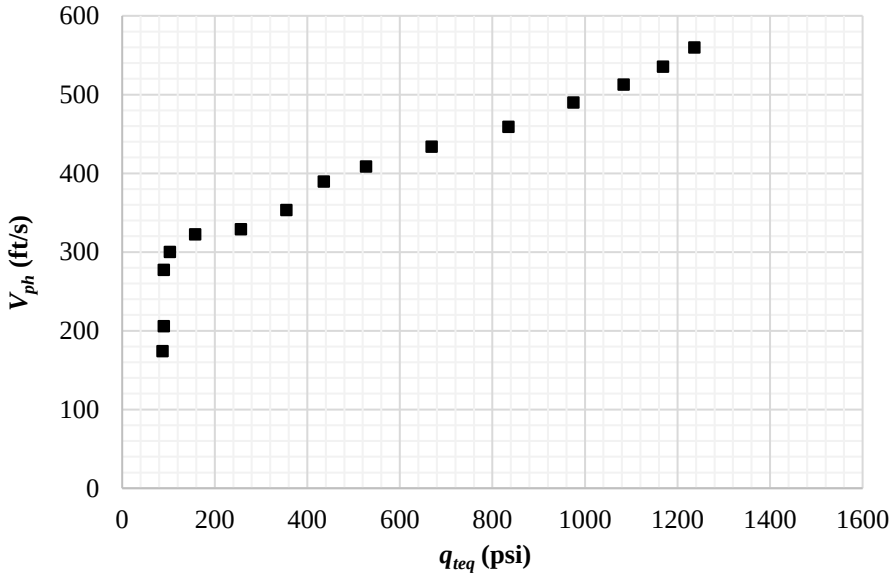

Figure A.93 – Pont 184 equivalent tip resistance (q_{teq}) vs phase velocity (V_{ph}) for the same λ.

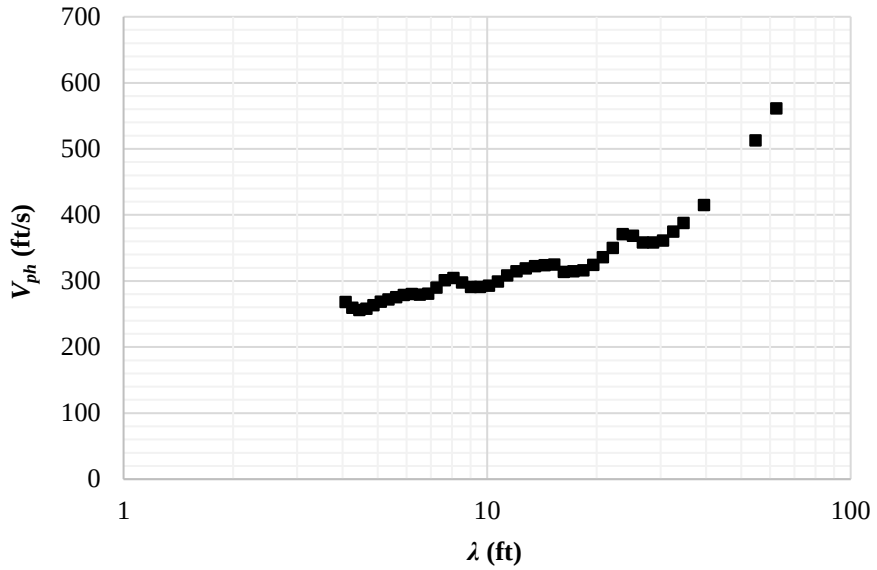

Figure A.94 – Point 194 dispersion curve.

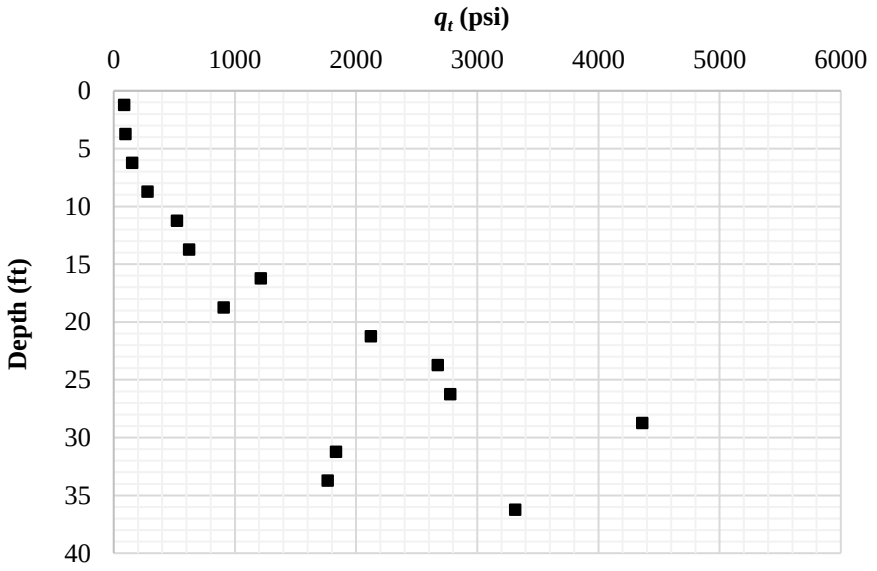

Figure A.95 – Point 194 tip resistance (q_t) vs depth (z).

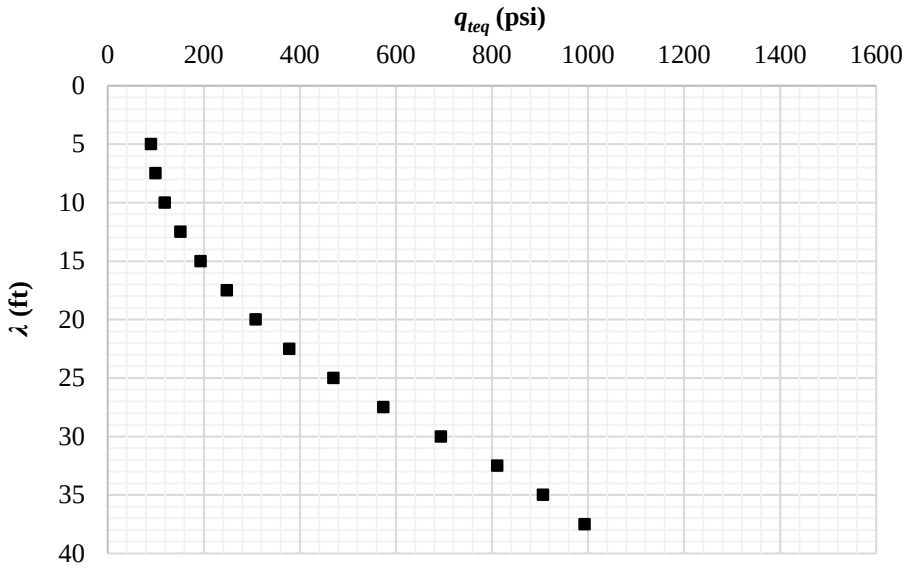

Figure A.96 – Point 194 equivalent tip resistance (q_{teq}) vs wavelength (λ).

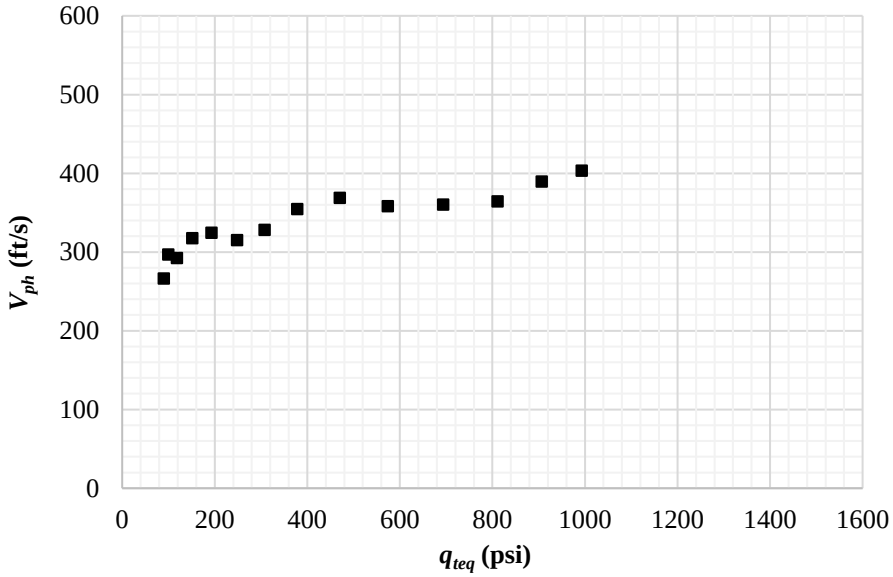

Figure A.97 – Pont 194 equivalent tip resistance (q_{teq}) vs phase velocity (V_{ph}) for the same λ.

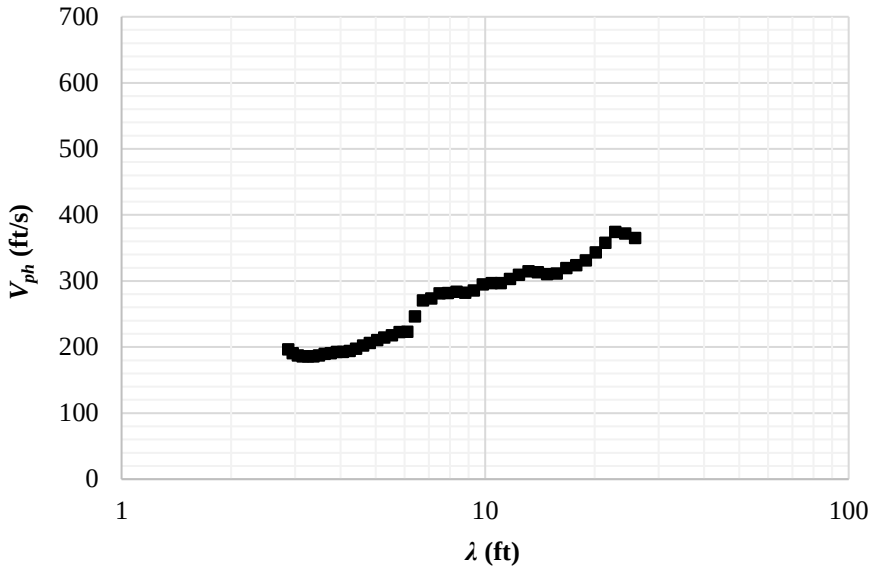

Figure A.98 – Point 196 dispersion curve.

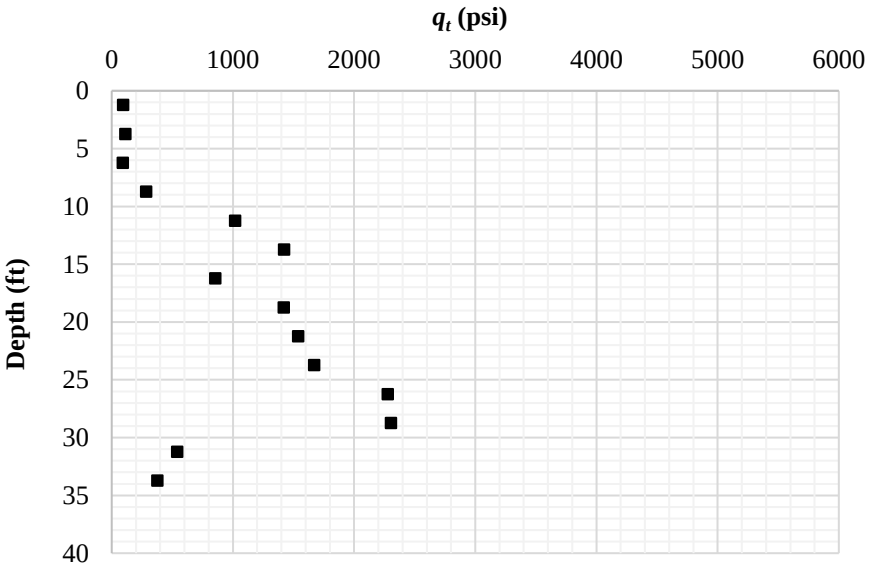

Figure A.99 – Point 196 tip resistance (q_t) vs depth (z).

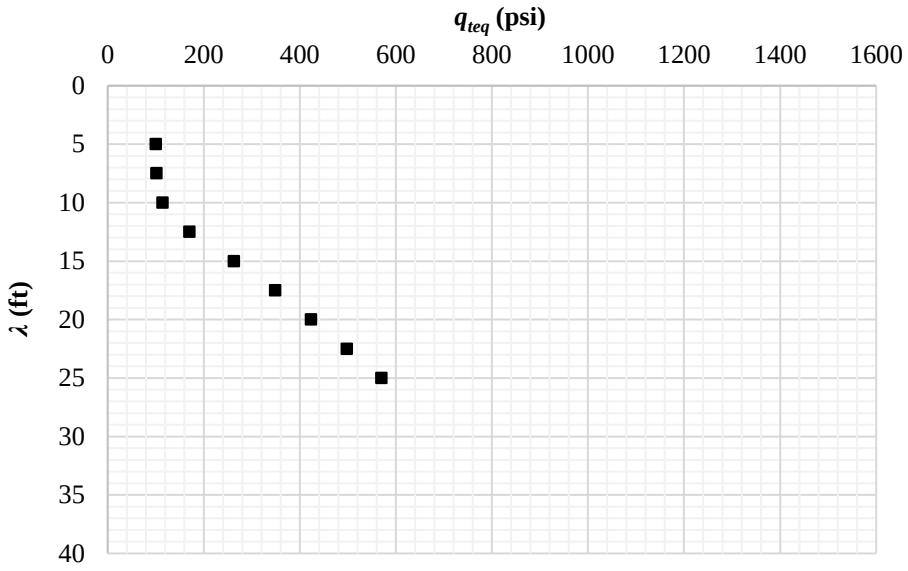

Figure A.100 – Point 196 equivalent tip resistance (q_{teq}) vs wavelength (λ).

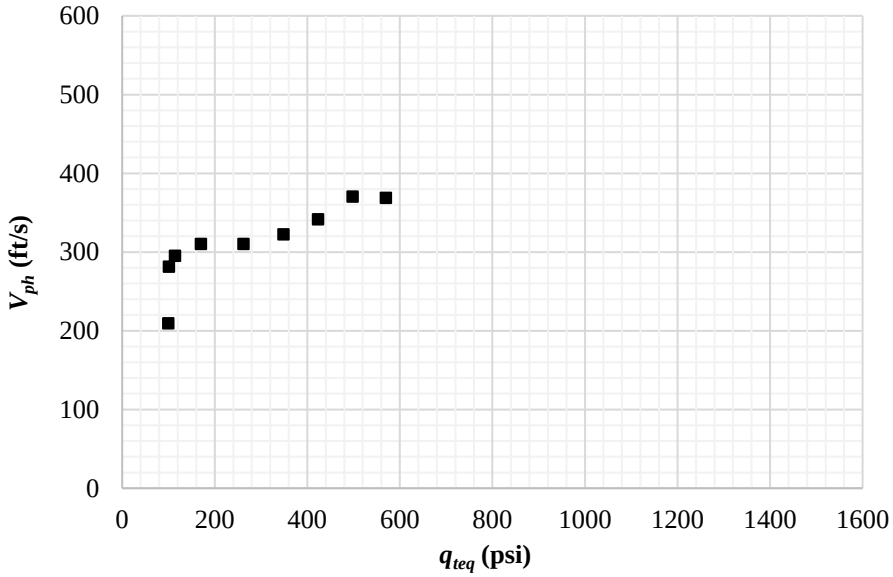

Figure A.101 – Pont 196 equivalent tip resistance (q_{teq}) vs phase velocity (V_{ph}) for the same λ.

Appendix B: Group plots

Group 23

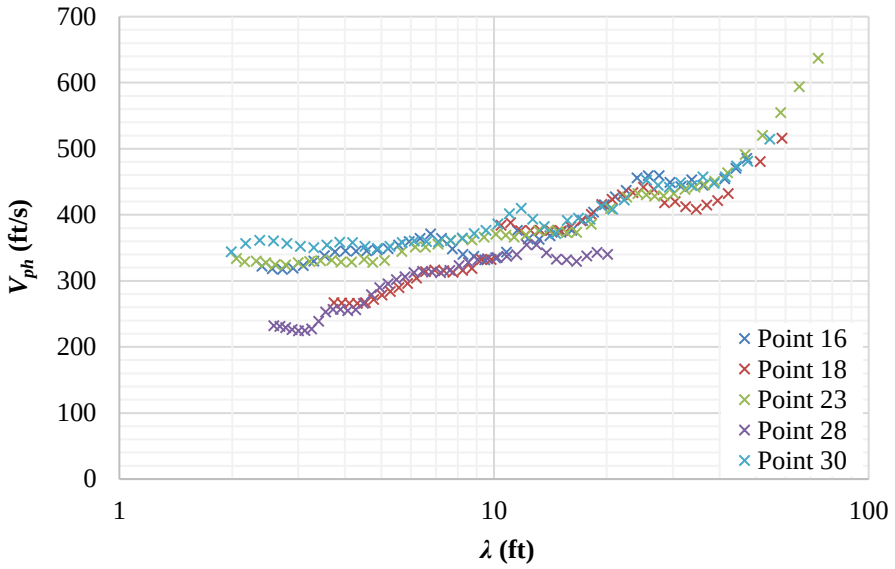

Figure B.1 – Group 23 dispersion curves.

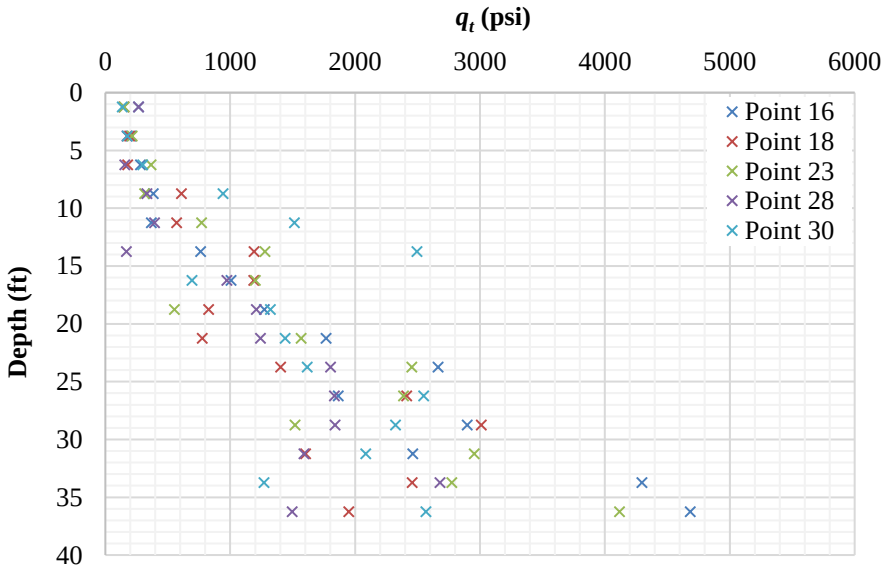

Figure B.2 – Group 23 tip resistance (q_t) vs depth (z).

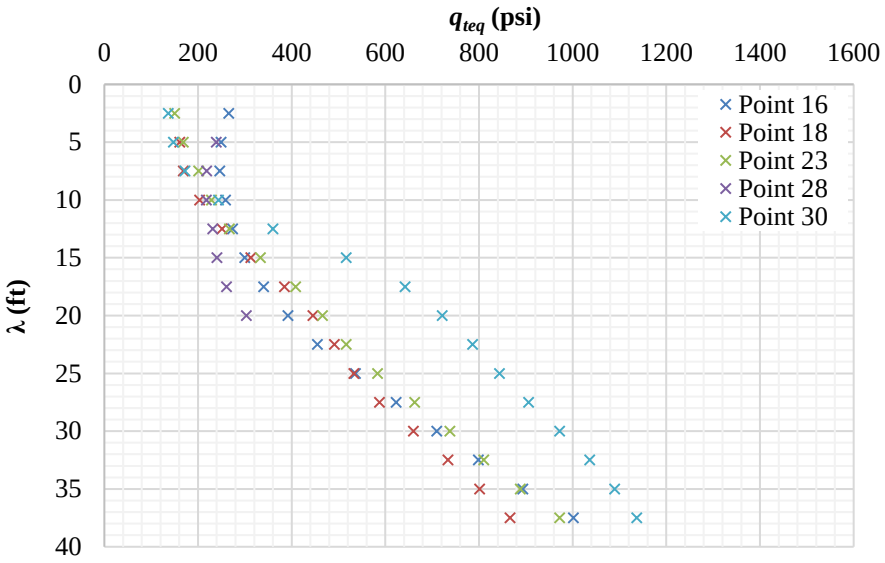

Figure B.3 – Group 23 equivalent tip resistance (q_{teq}) vs wavelength (λ).

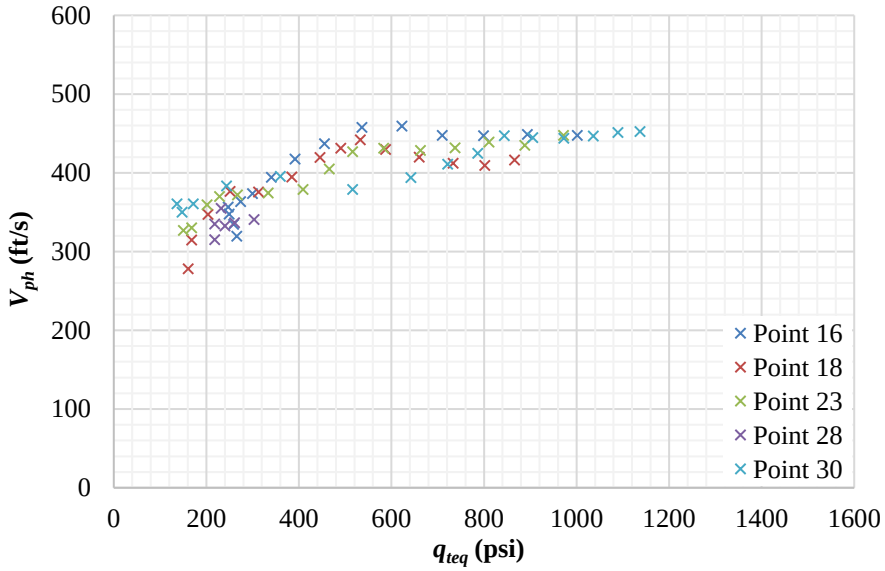

Figure B.4 – Group 23 equivalent tip resistance (q_{teq}) vs phase velocity (V_{ph}) for the same λ.

Group 80

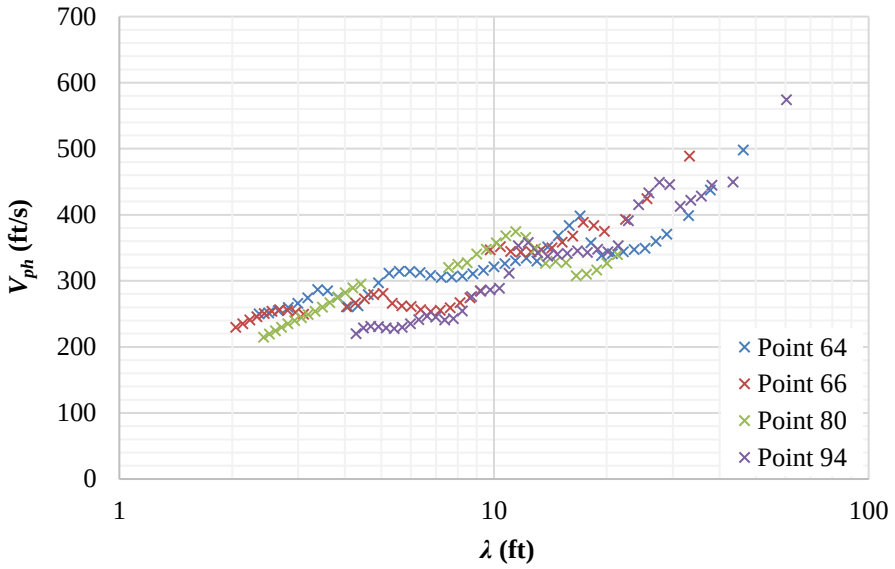

Figure B.5 – Group 80 dispersion curves.

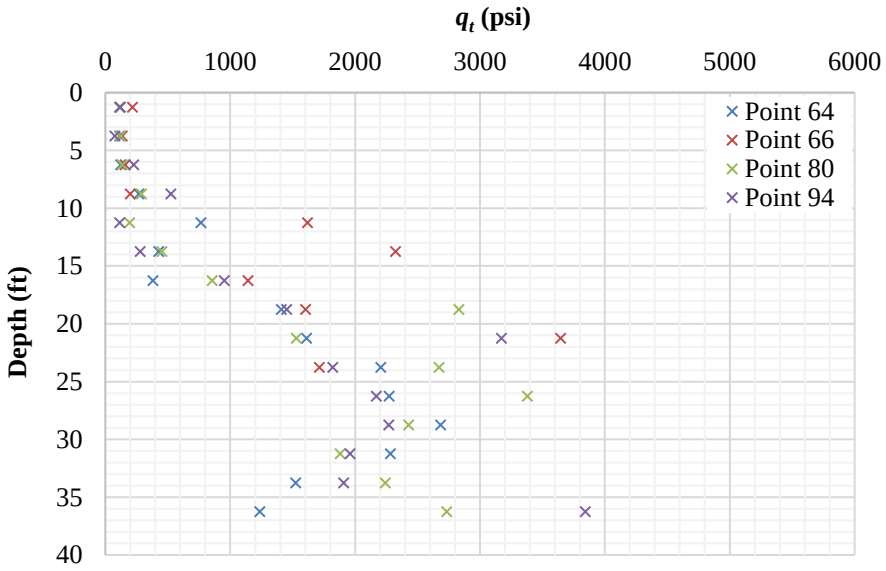

Figure B.6 – Group 80 tip resistance (q_t) vs depth (z).

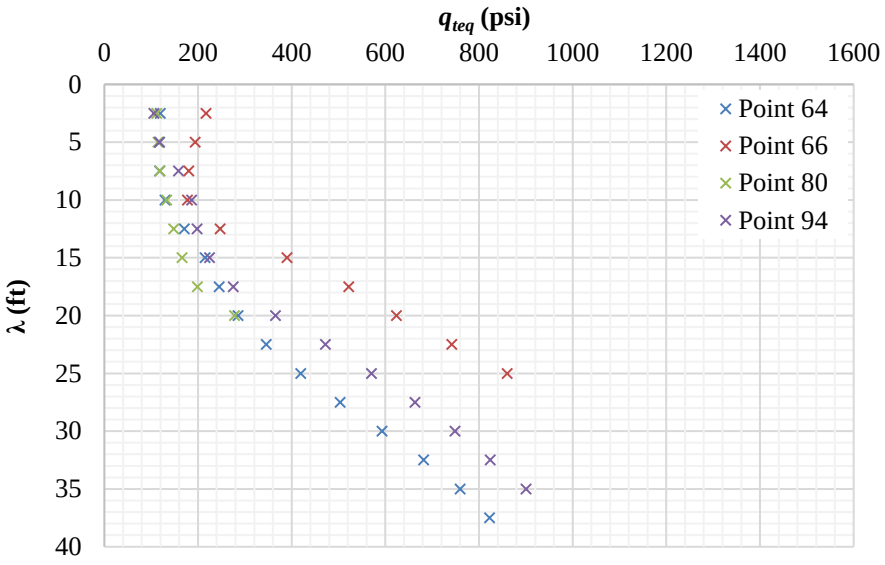

Figure B.7 – Group 80 equivalent tip resistance (q_{teq}) vs wavelength (λ).

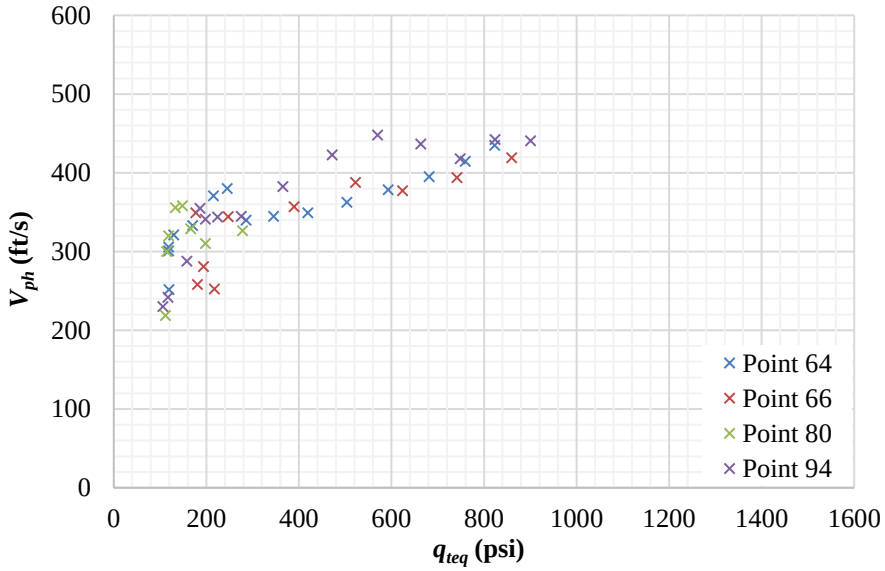

Figure B.8 – Group 80 equivalent tip resistance (q_{teq}) vs phase velocity (V_{ph}) for the same λ.

Group 84

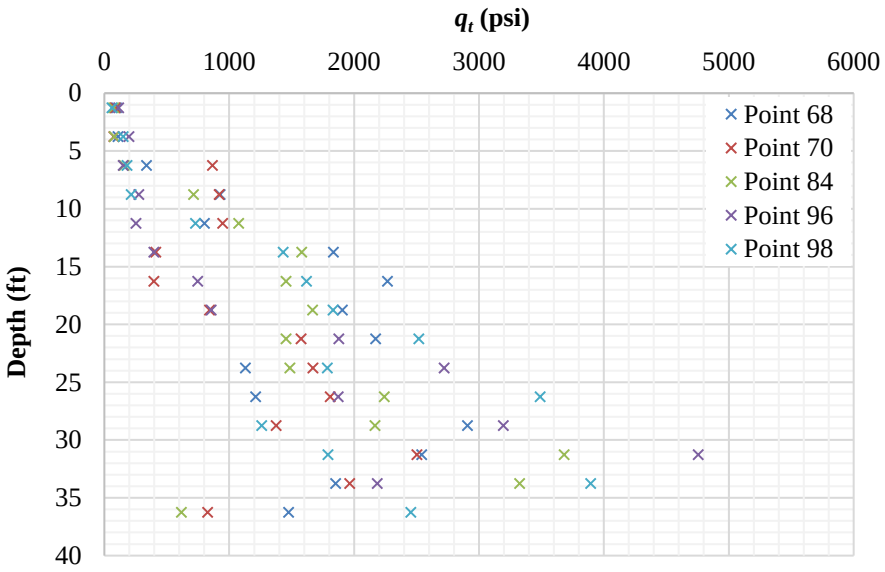

Figure B.9 – Group 84 tip resistance (q_t) vs depth (z).

Group 135

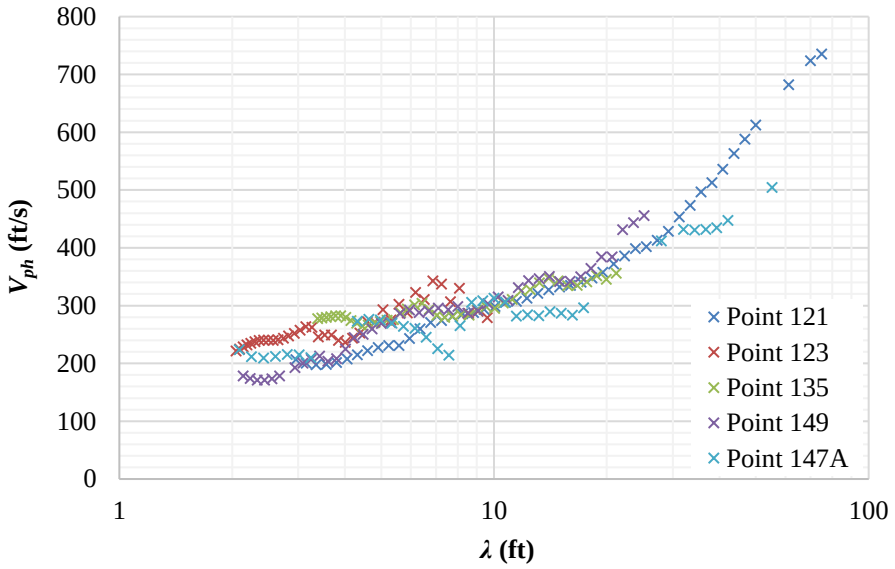

Figure B.10 – Group 135 dispersion curves.

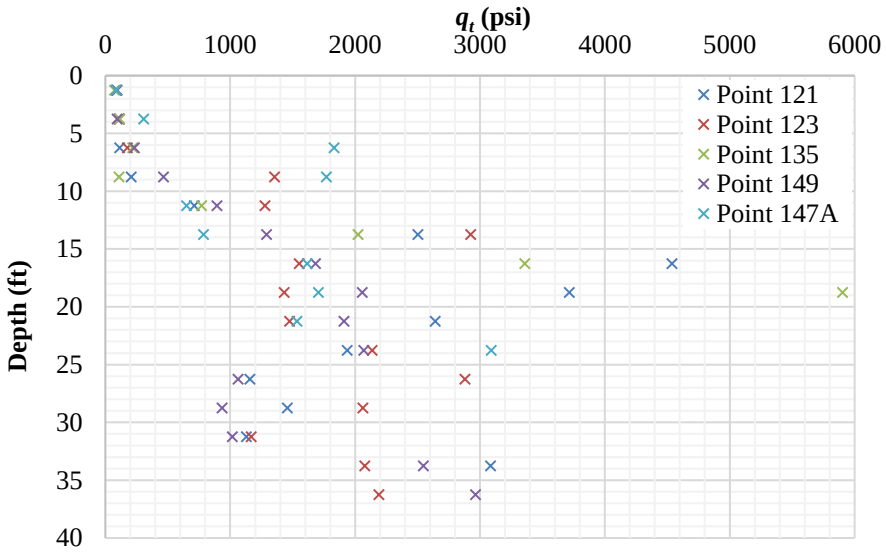

Figure B.11 – Group 135 tip resistance (q_t) vs depth (z).

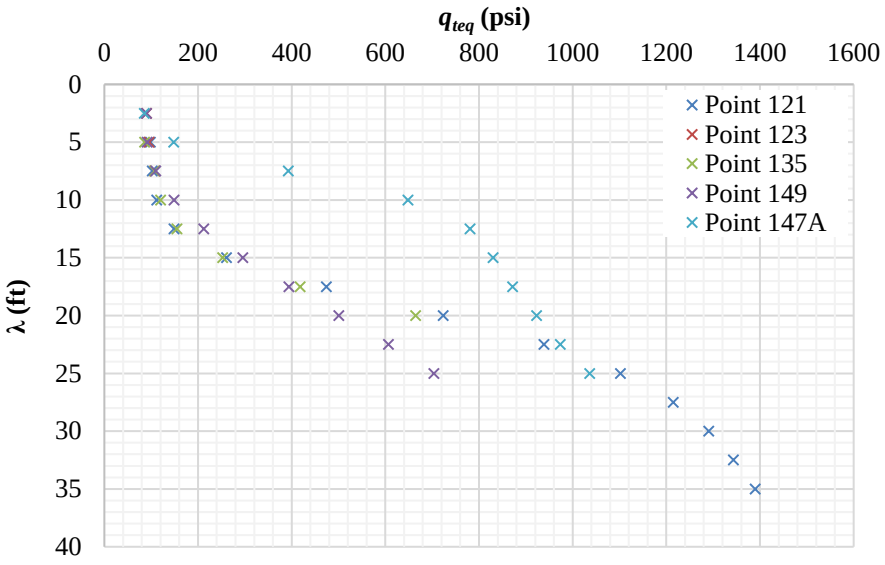

Figure B.12 – Group 135 equivalent tip resistance (q_{teq}) vs wavelength (λ).

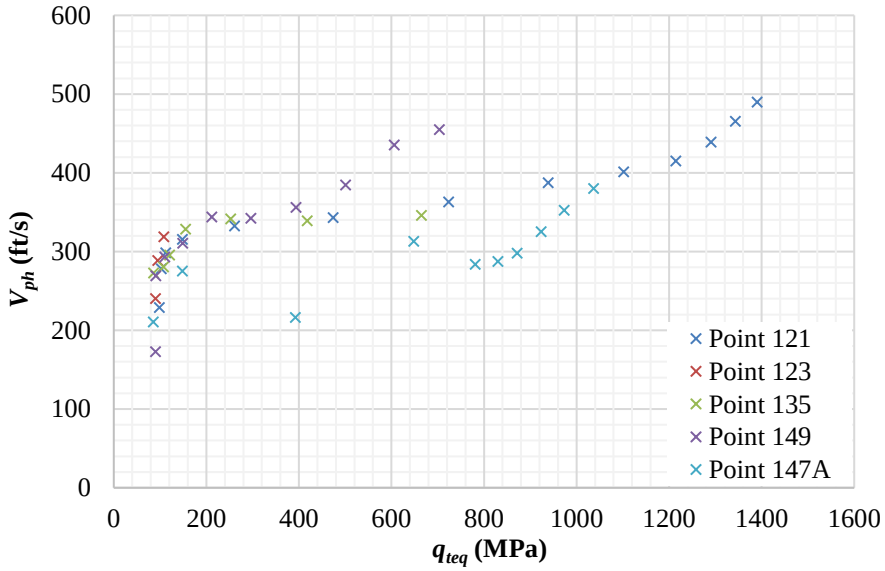

Figure B.13 – Group 135 equivalent tip resistance (q_{teq}) vs phase velocity (V_{ph}) for the same λ.

Group 180

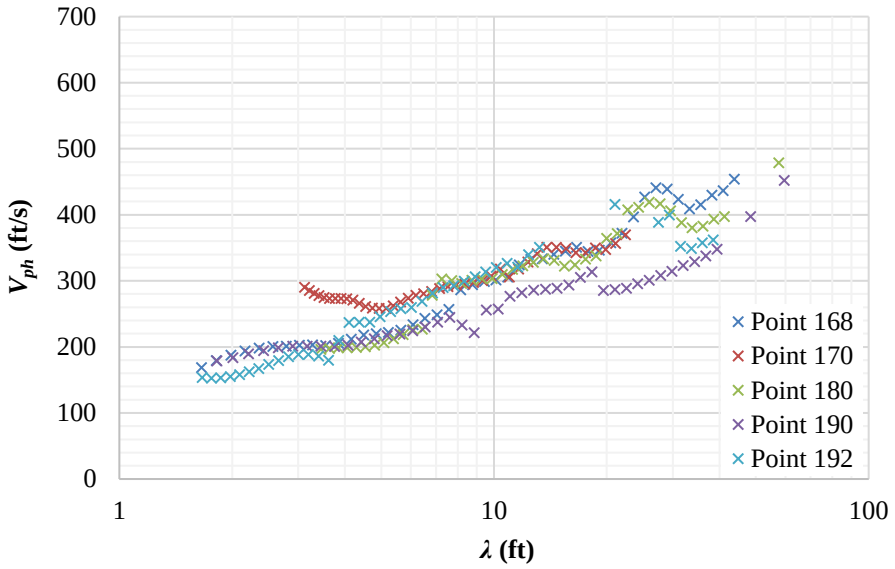

Figure B.14 – Group 180 dispersion curves.

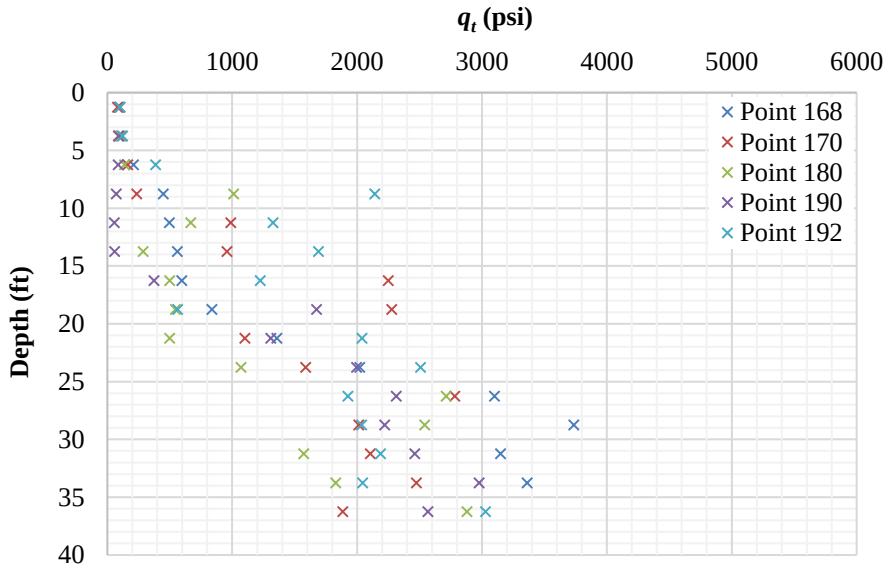

Figure B.15 – Group 180 tip resistance (q_t) vs depth (z).

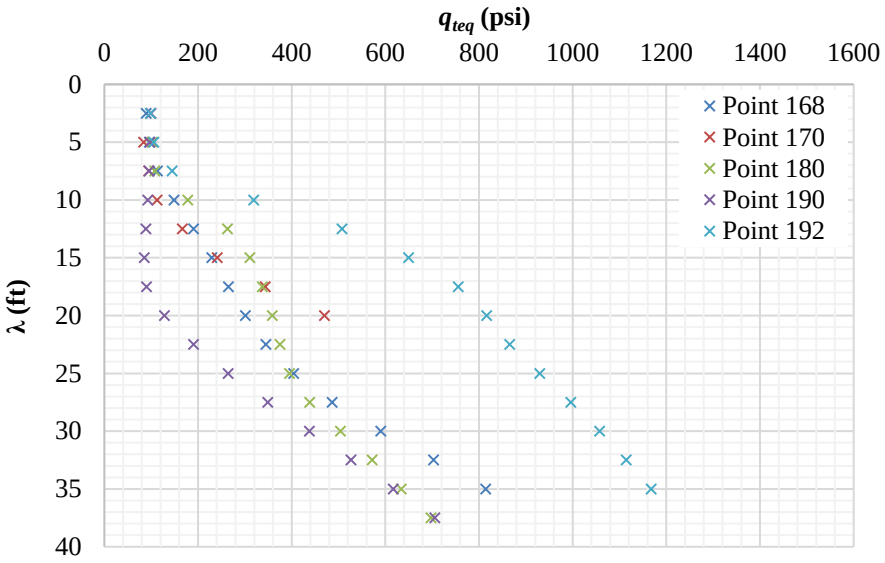

Figure B.16 – Group 180 equivalent tip resistance (q_{teq}) vs wavelength (λ).

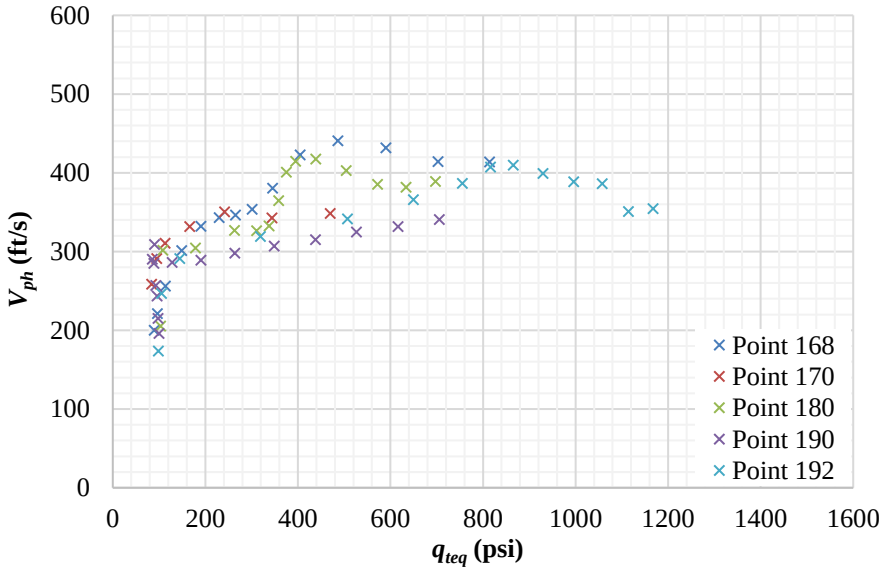

Figure B.17 – Group 180 equivalent tip resistance (q_{teq}) vs phase velocity (V_{ph}) for the same λ.

Group 184

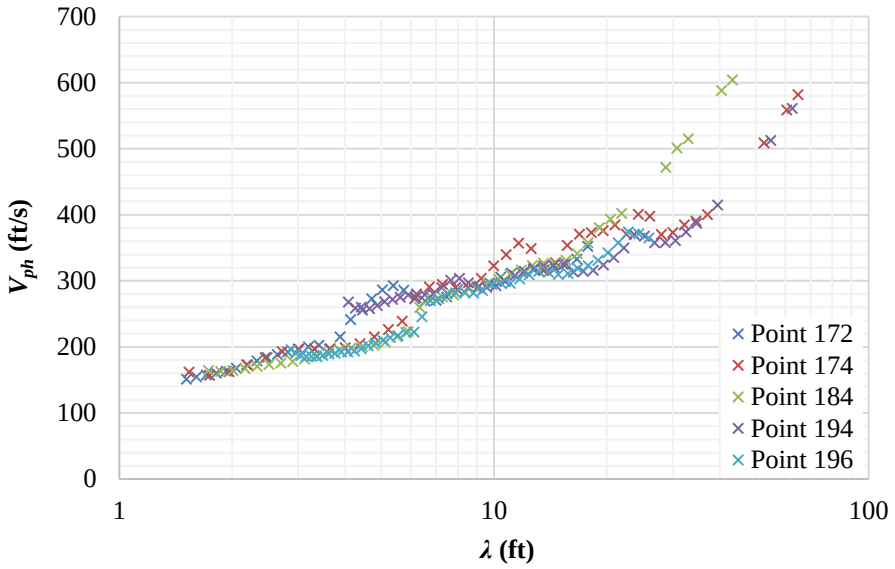

Figure B.18 – Group 184 dispersion curves.

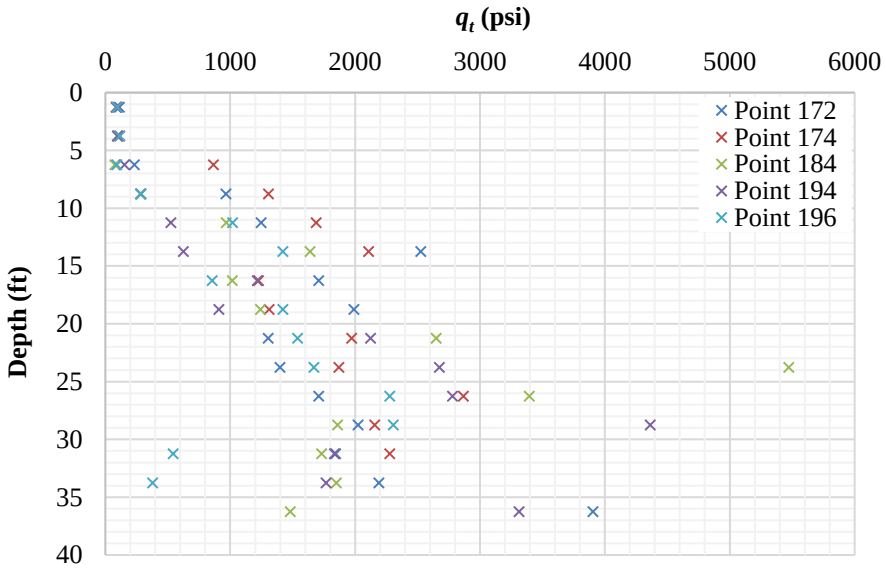

Figure B.19 – Group 184 tip resistance (q_t) vs depth (z).

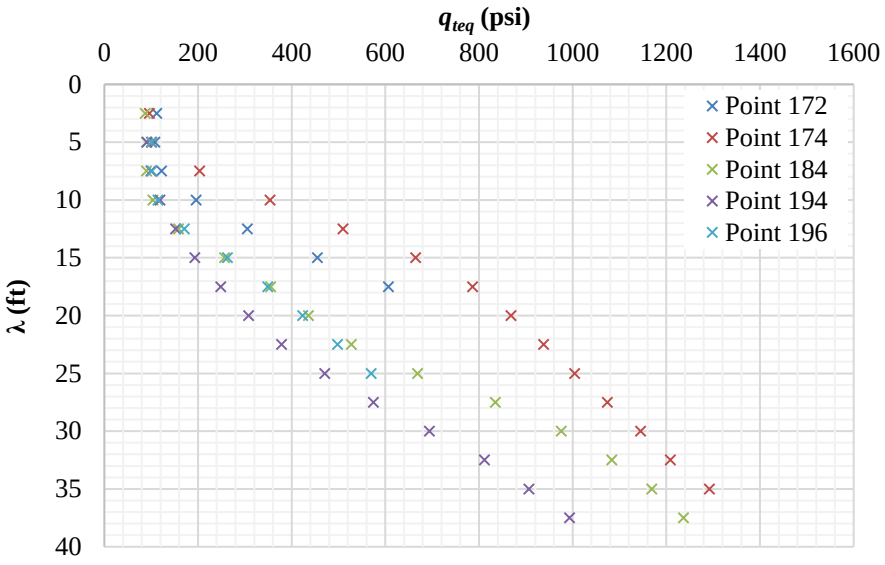

Figure B.20 – Group 184 equivalent tip resistance (q_{teq}) vs wavelength (λ).

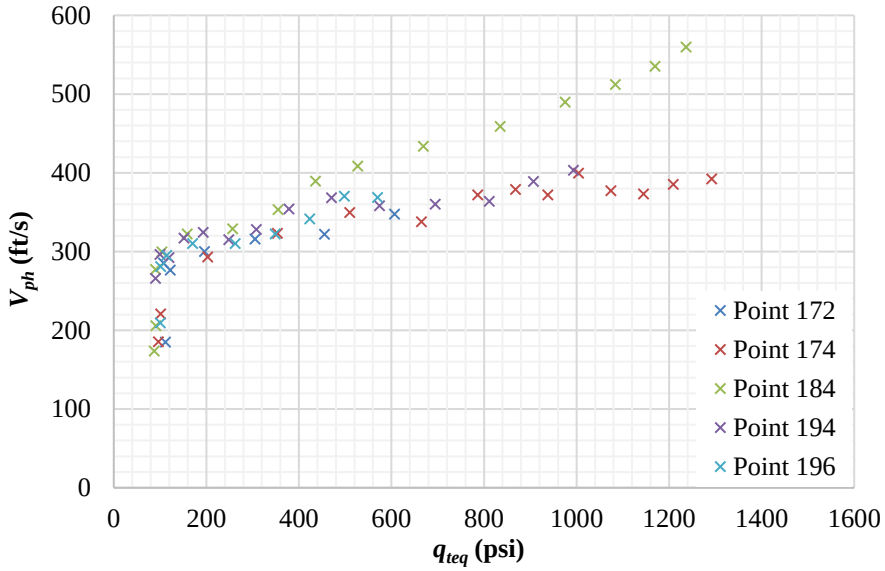

Figure B.21 – Group 184 equivalent tip resistance (q_{teq}) vs phase velocity (V_{ph}) for the same λ.

Appendix C: Measured vs calculated dispersion curves

$$V_{ph}(ft/s) = 101\left(q_{teq}(psi)\right)^{0.212} \quad (6.1)$$

Group 23

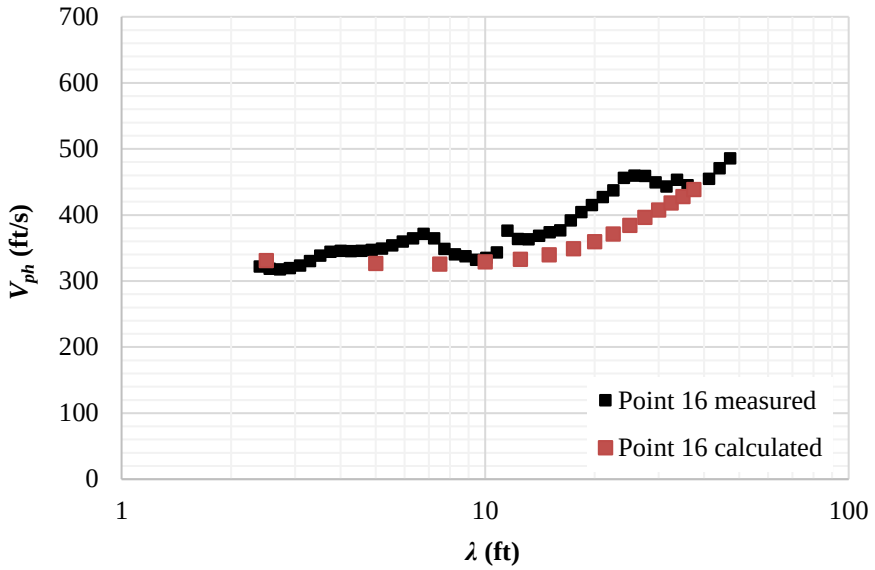

Figure C.1 – Point 16 measured vs calculated dispersion curves.

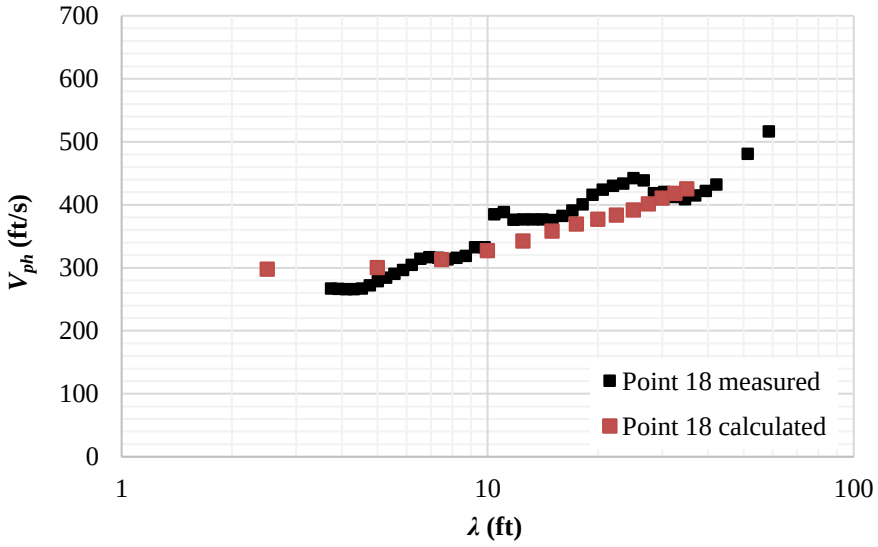

Figure C.2 – Point 18 measured vs calculated dispersion curves.

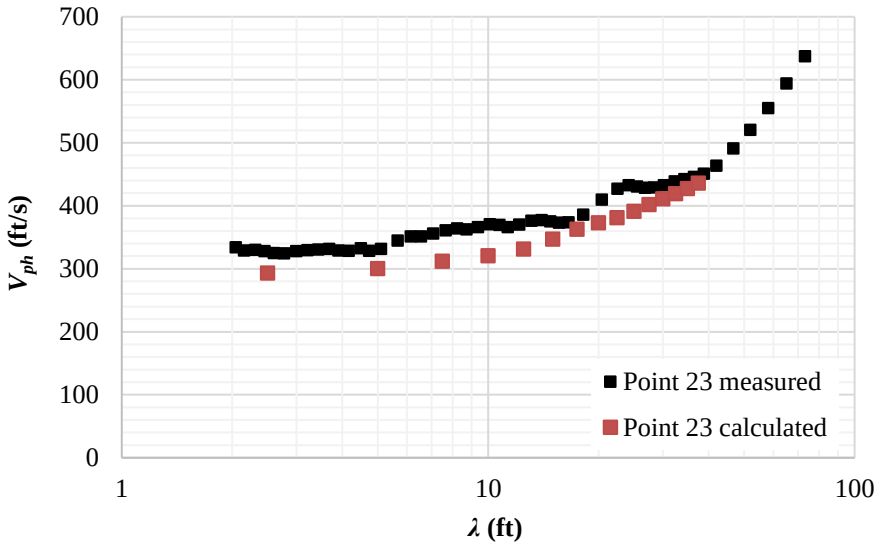

Figure C.3 – Point 23 measured vs calculated dispersion curves.

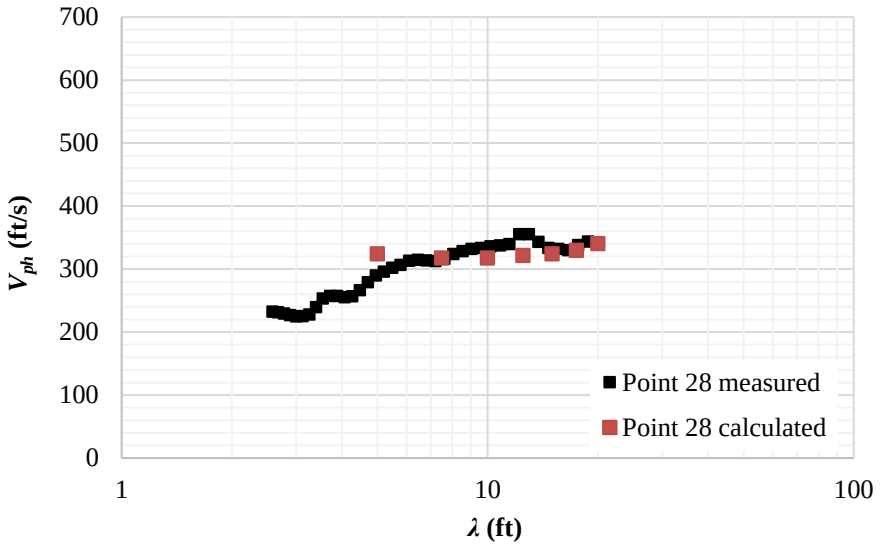

Figure C.4 – Point 28 measured vs calculated dispersion curves.

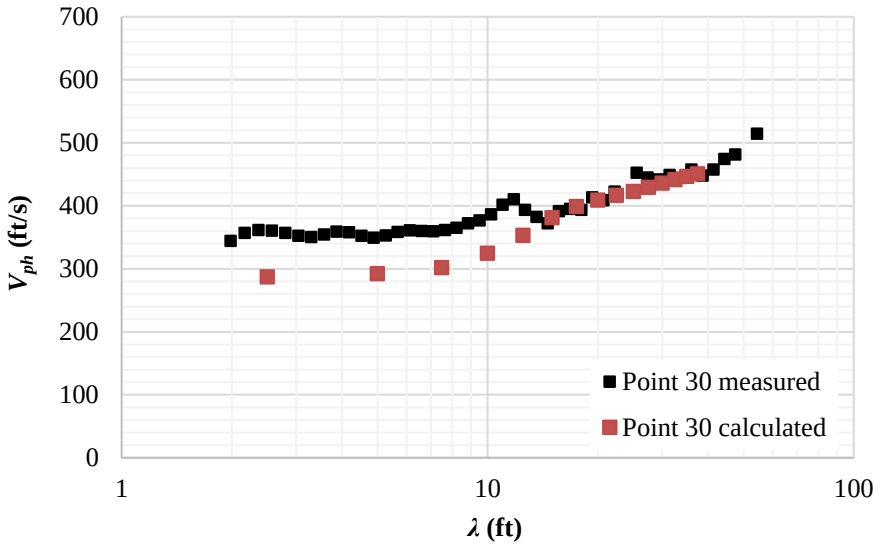

Figure C.5 – Point 30 measured vs calculated dispersion curves.

Group 80

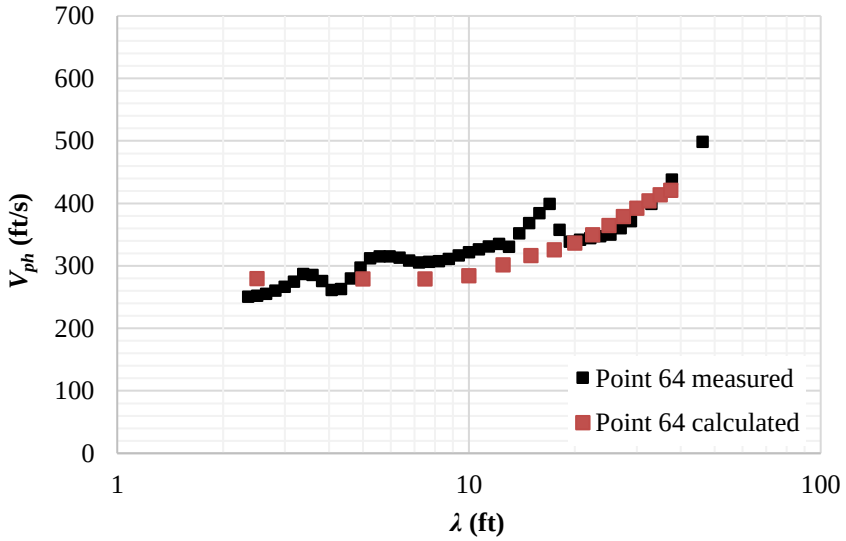

Figure C.6 – Point 64 measured vs calculated dispersion curves.

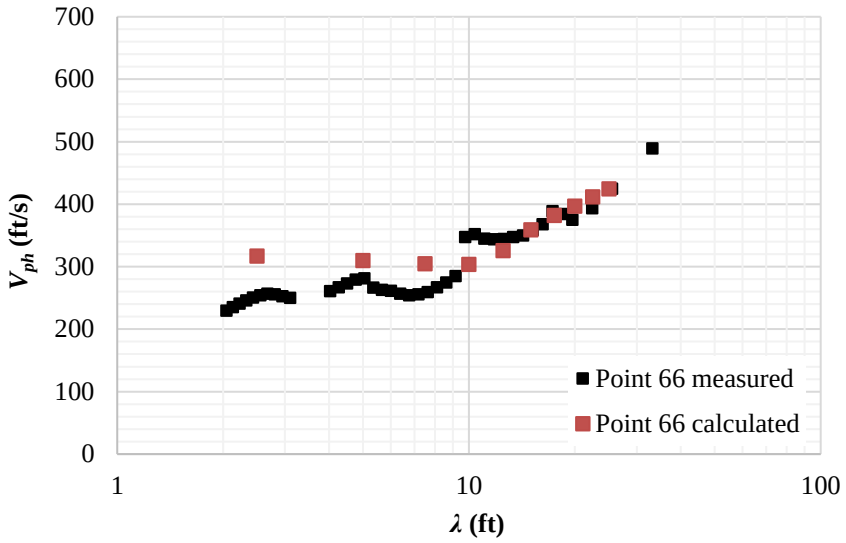

Figure C.7 – Point 66 measured vs calculated dispersion curves.

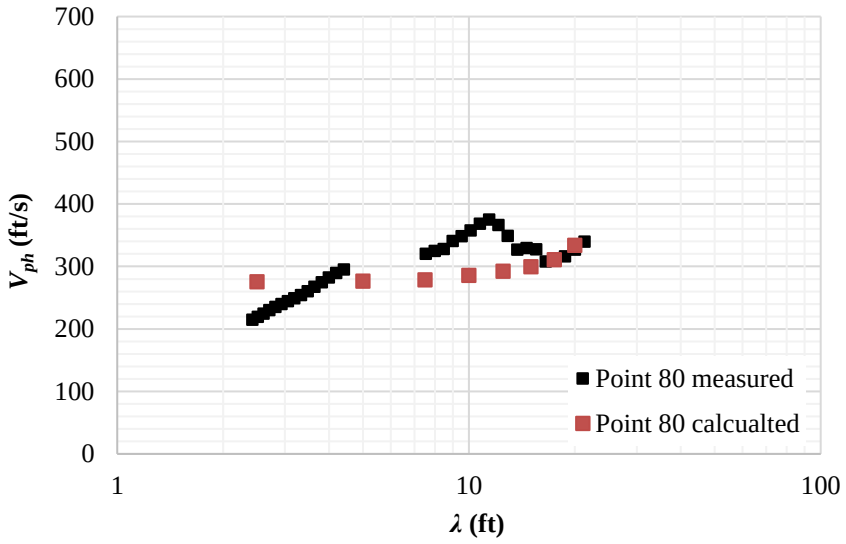

Figure C.8 – Point 80 measured vs calculated dispersion curves.

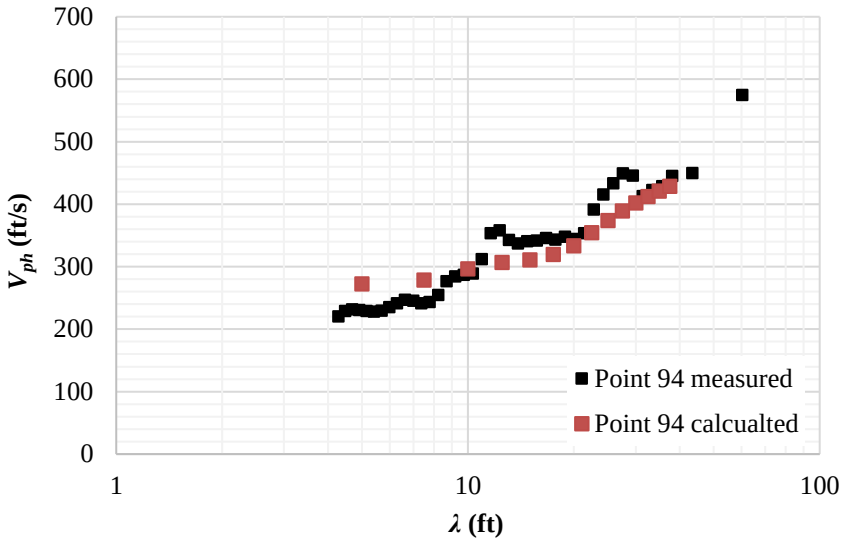

Figure C.9 – Point 94 measured vs calculated dispersion curves.

Group 135

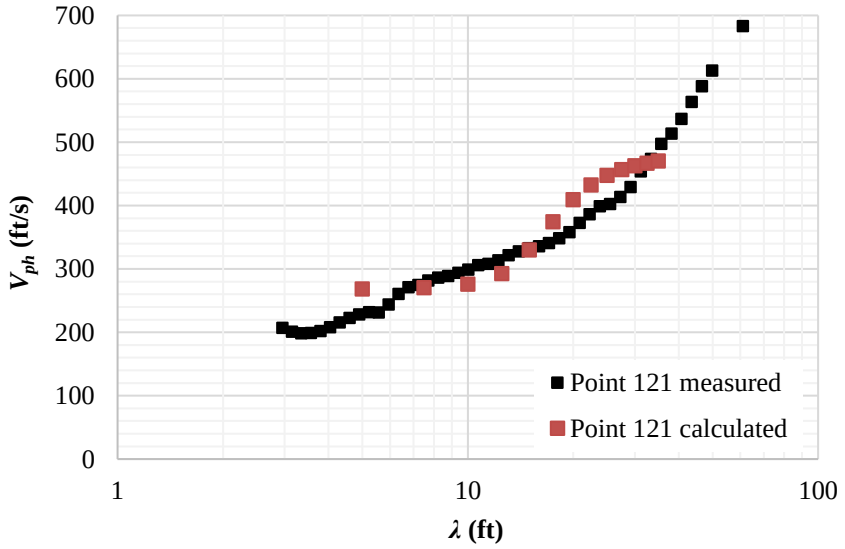

Figure C.10 – Point 121 measured vs calculated dispersion curves.

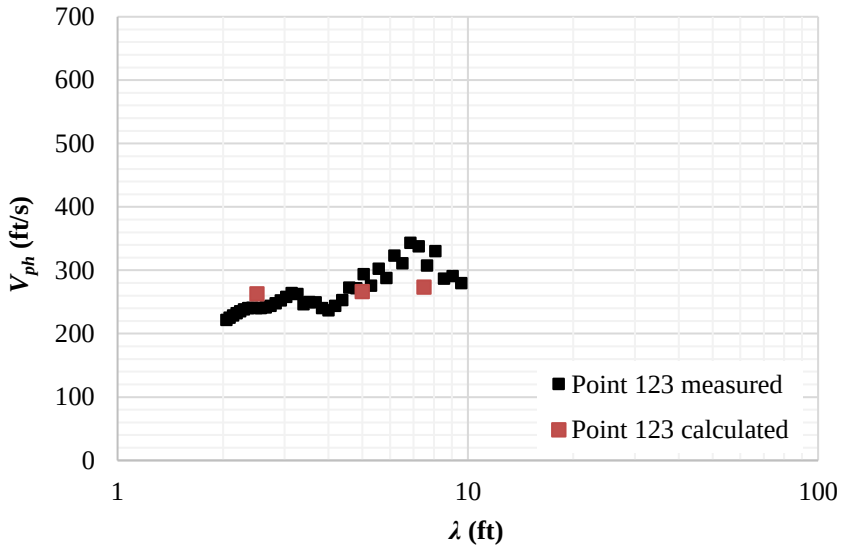

Figure C.11 – Point 123 measured vs calculated dispersion curves.

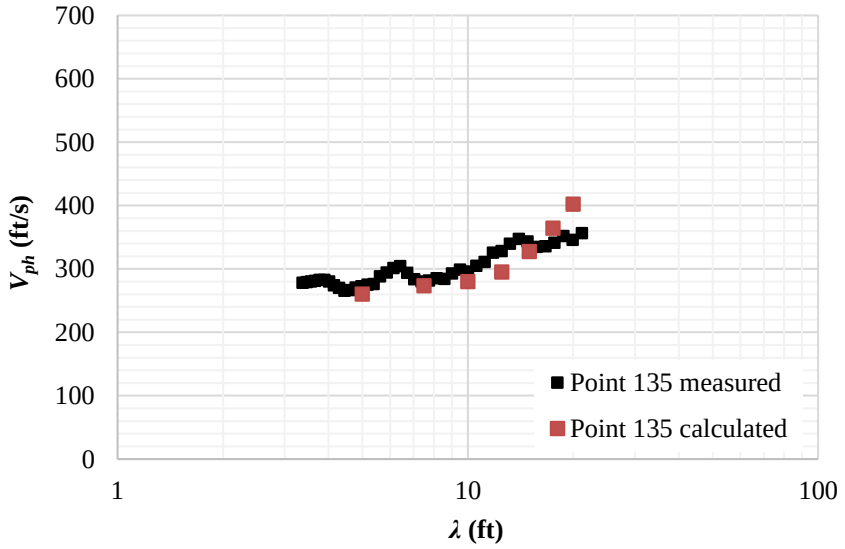

Figure C.12 – Point 135 measured vs calculated dispersion curves.

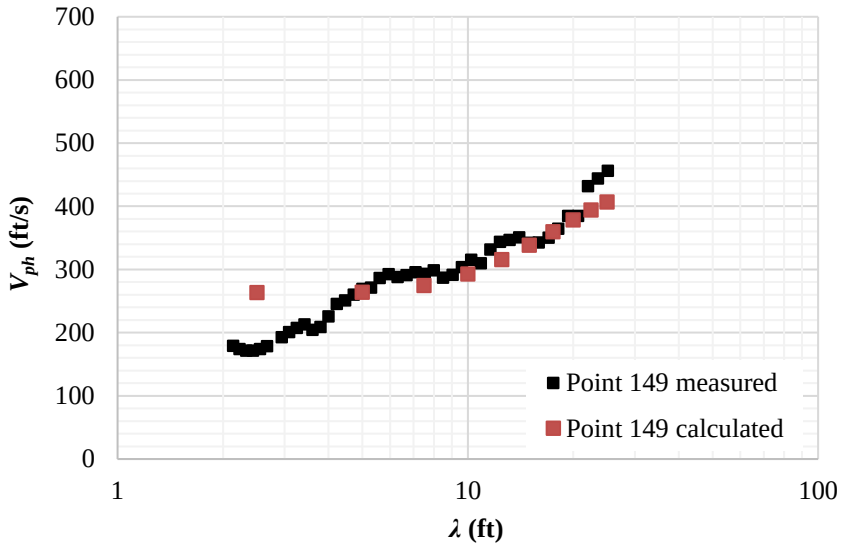

Figure C.13 – Point 149 measured vs calculated dispersion curves.

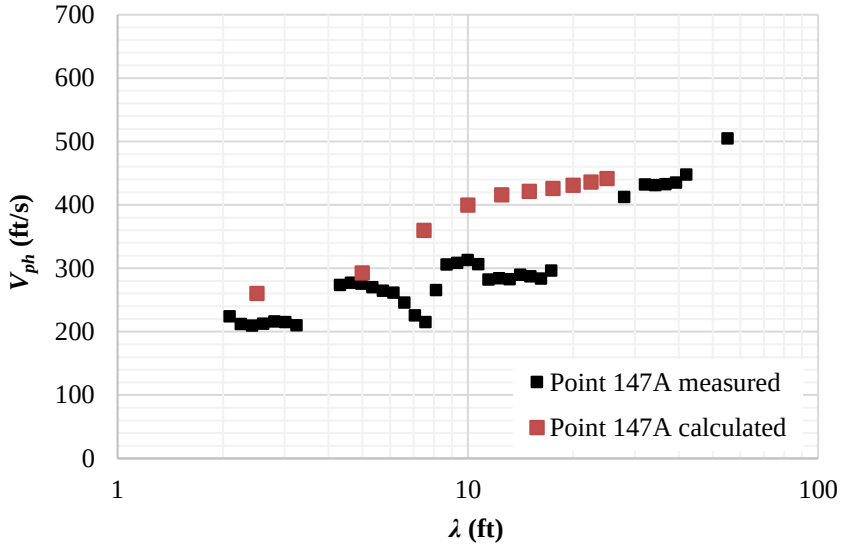

Figure C.14 – Point 147A measured vs calculated dispersion curves.

Group 180

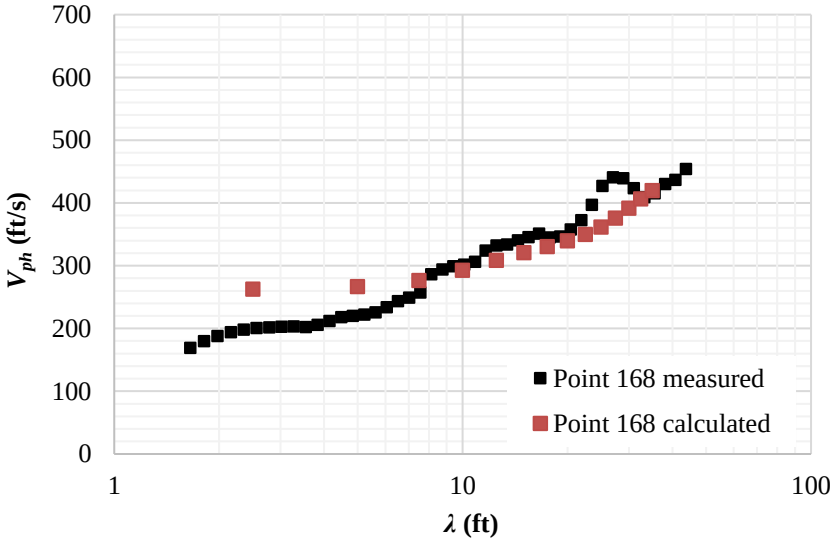

Figure C.15 – Point 168 measured vs calculated dispersion curves.

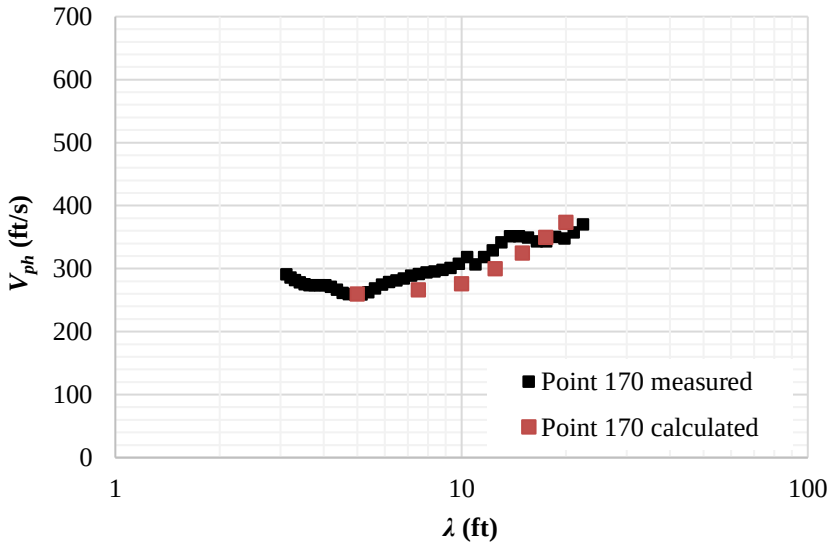

Figure C.16 – Point 170 measured vs calculated dispersion curves.

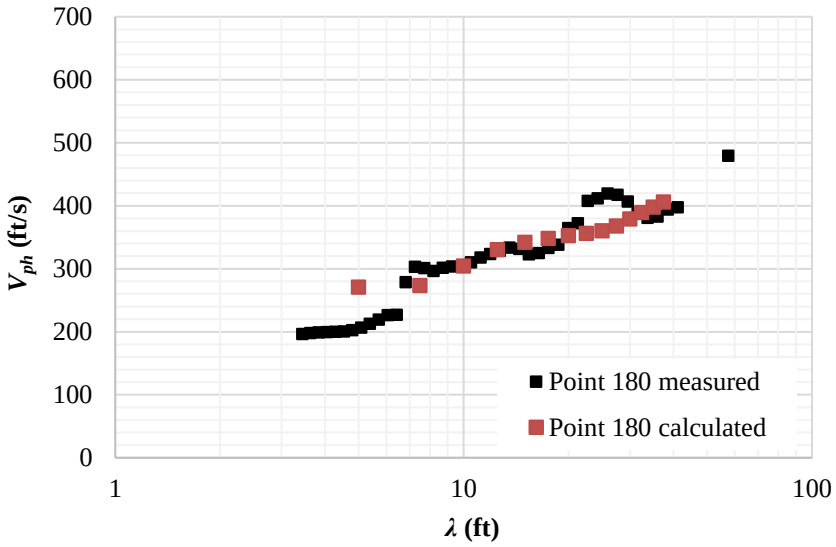

Figure C.17 – Point 180 measured vs calculated dispersion curves.

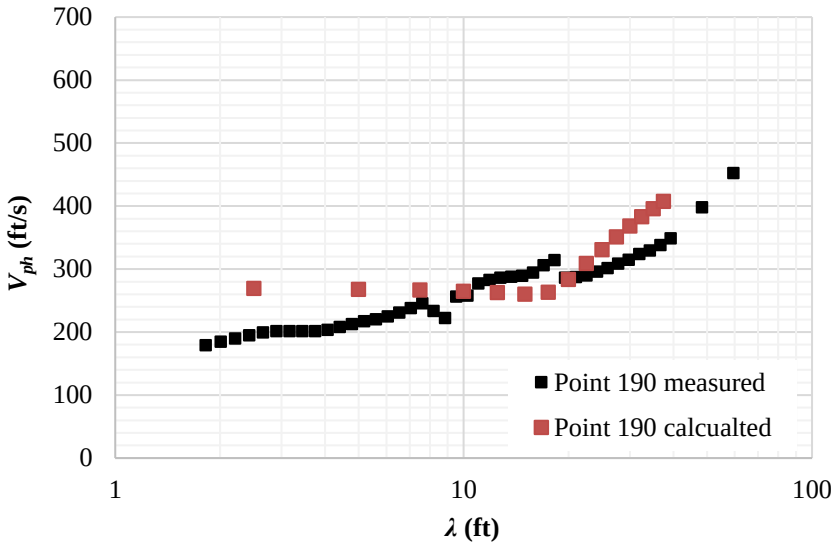

Figure C.18 – Point 190 measured vs calculated dispersion curves.

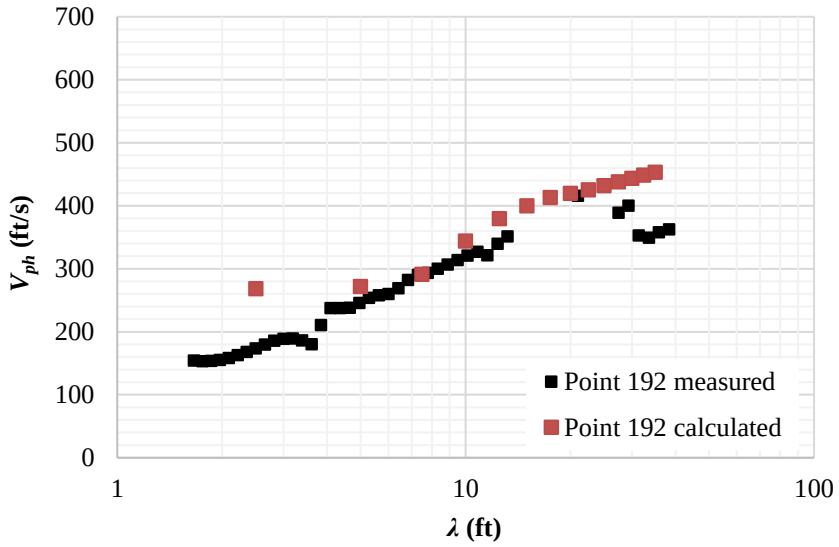

Figure C.19 – Point 192 measured vs calculated dispersion curves.

Group 184

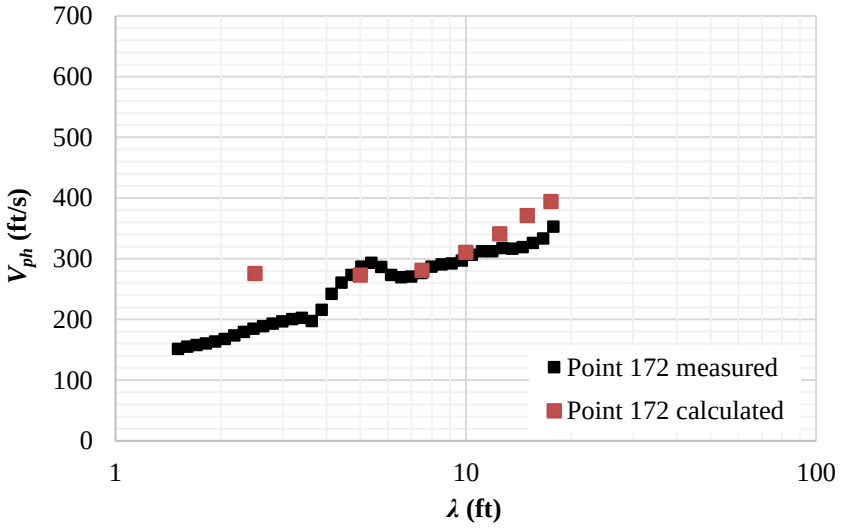

Figure C.20 – Point 172 measured vs calculated dispersion curves.

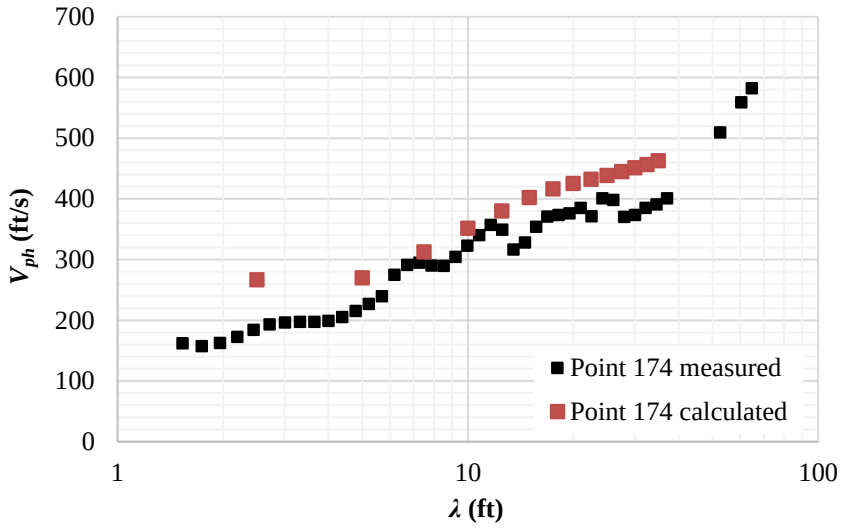

Figure C.21 – Point 174 measured vs calculated dispersion curves.

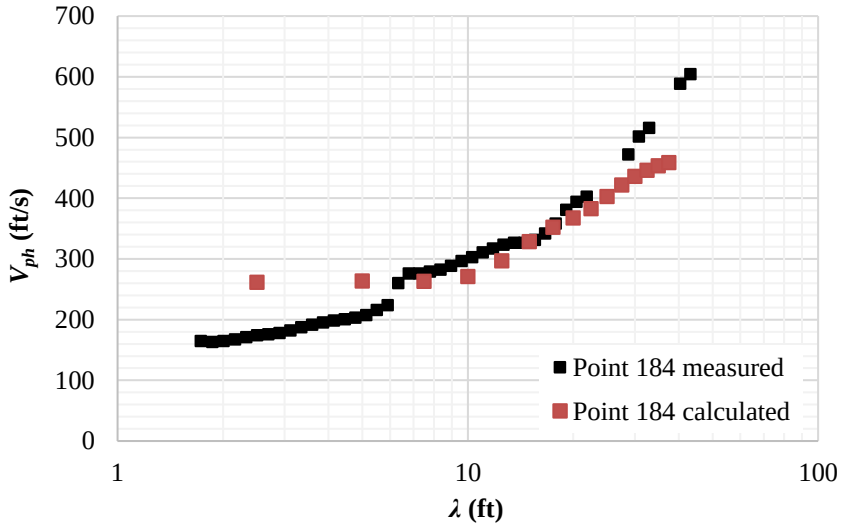

Figure C.22 – Point 184 measured vs calculated dispersion curves.

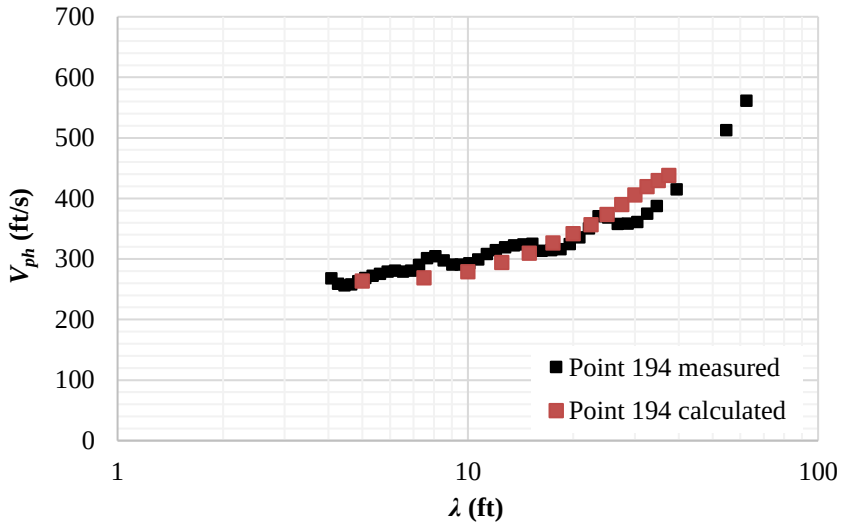

Figure C.23 – Point 194 measured vs calculated dispersion curves.

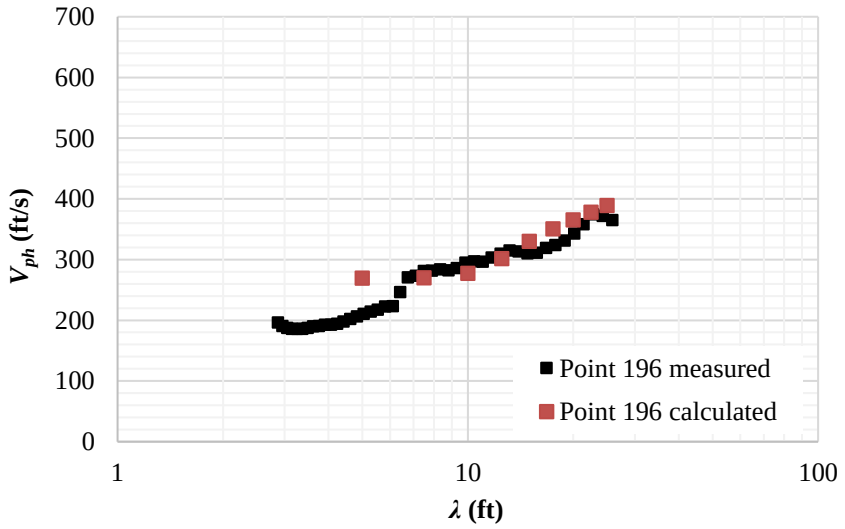

Figure C.24 – Point 196 measured vs calculated dispersion curves.

Appendix D: Sample Labadie UWL borings

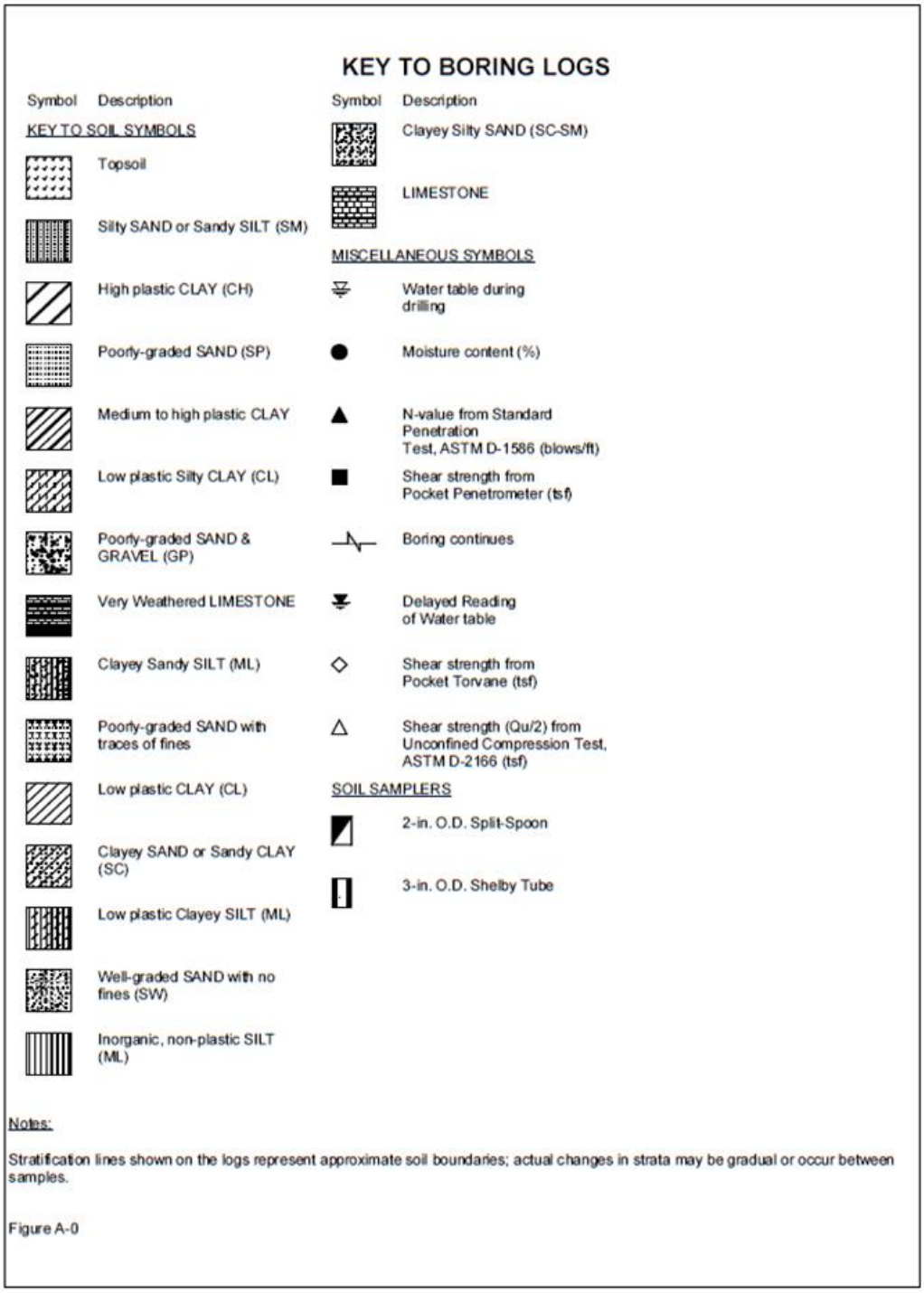

KEY TO BORING LOGS

Symbol	Description
KEY TO SOIL SYMBOLS	
	Topsoil
	Silty SAND or Sandy SILT (SM)
	High plastic CLAY (CH)
	Poorly-graded SAND (SP)
	Medium to high plastic CLAY
	Low plastic Silty CLAY (CL)
	Poorly-graded SAND & GRAVEL (GP)
	Very Weathered LIMESTONE
	Clayey Sandy SILT (ML)
	Poorly-graded SAND with traces of fines
	Low plastic CLAY (CL)
	Clayey SAND or Sandy CLAY (SC)
	Low plastic Clayey SILT (ML)
	Well-graded SAND with no fines (SW)
	Inorganic, non-plastic SILT (ML)

Symbol	Description
	Clayey Silty SAND (SC-SM)
	LIMESTONE
MISCELLANEOUS SYMBOLS	
	Water table during drilling
●	Moisture content (%)
▲	N-value from Standard Penetration Test, ASTM D-1586 (blows/ft)
■	Shear strength from Pocket Penetrometer (tsf)
	Boring continues
	Delayed Reading of Water table
◇	Shear strength from Pocket Torvane (tsf)
△	Shear strength (Qu/2) from Unconfined Compression Test, ASTM D-2166 (tsf)
SOIL SAMPLERS	
	2-in. O.D. Split-Spoon
	3-in. O.D. Shelby Tube

Notes:

Stratification lines shown on the logs represent approximate soil boundaries; actual changes in strata may be gradual or occur between samples.

Figure A-0

Figure D.1 – Boring key from GREDELL Engineering Resources, Inc. and Reitz & Jens, Inc. 2011.

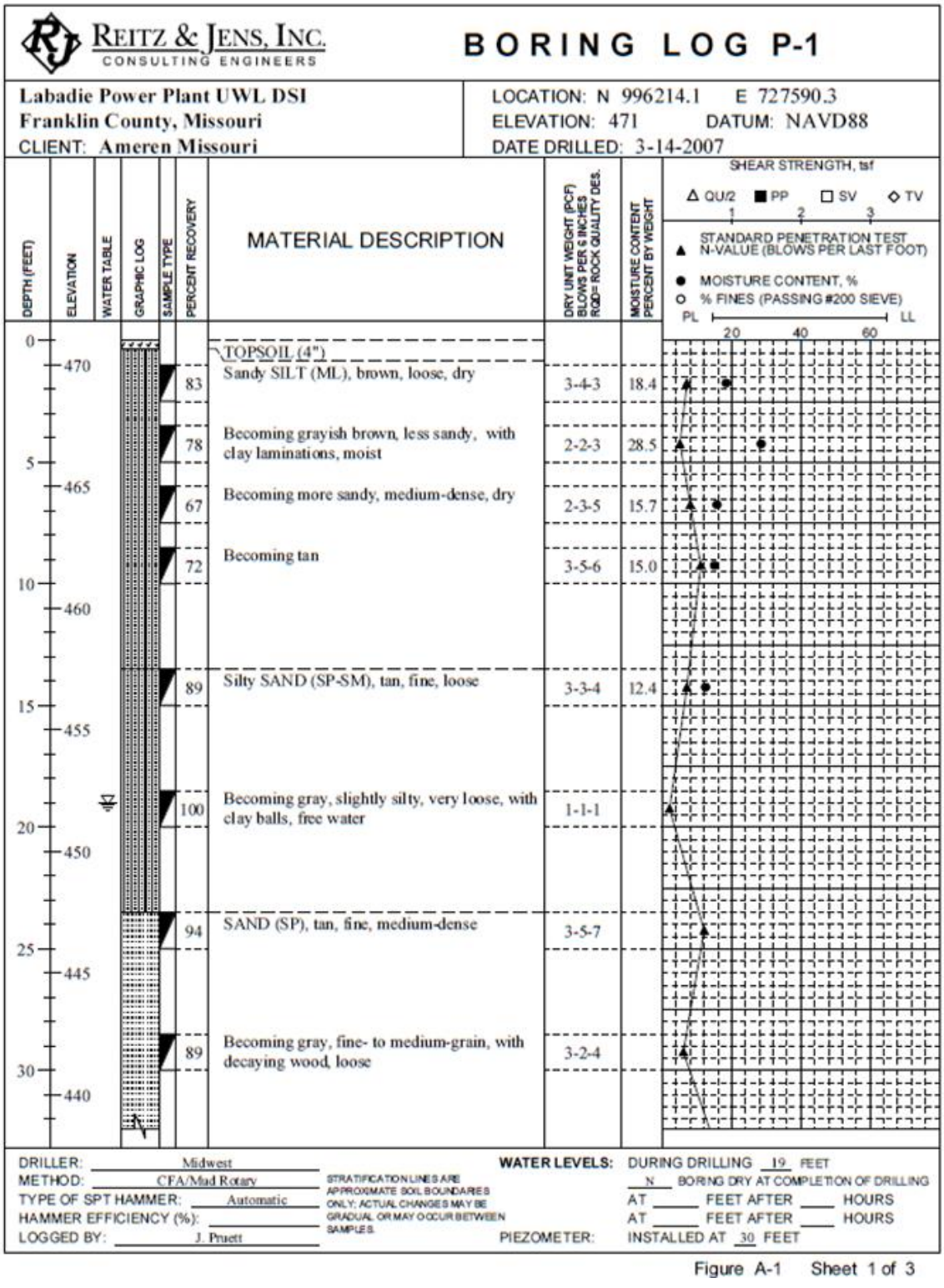

Figure D.2.1 – Boring P1 (approximately 130 yards north of Point 16) from GREDELL Engineering Resources, Inc. and Reitz & Jens, Inc. 2011.

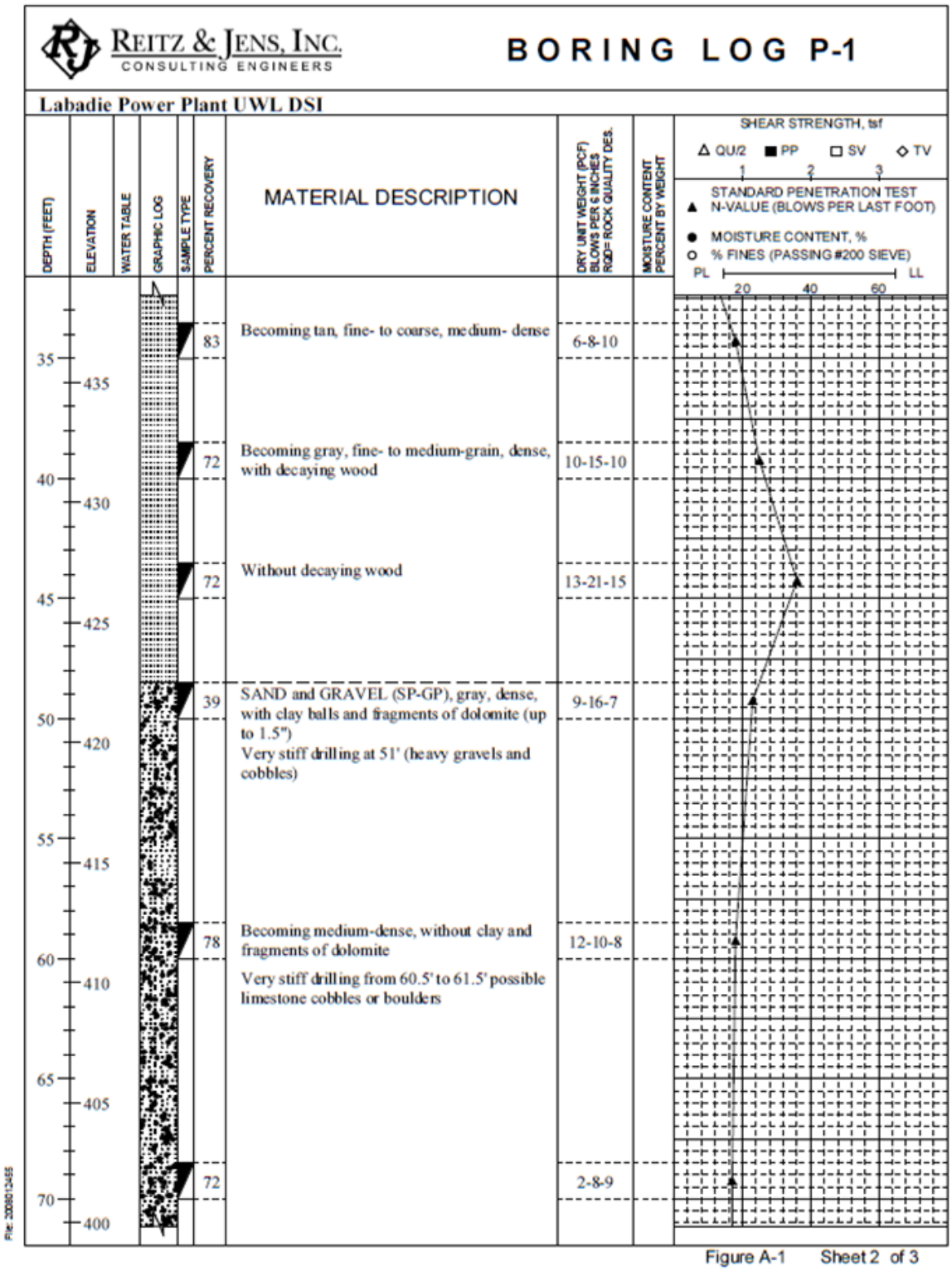

Figure D.2.2 – Boring P1 (approximately 130 yards north of Point 16) from GREDELL Engineering Resources, Inc. and Reitz & Jens, Inc. 2011.

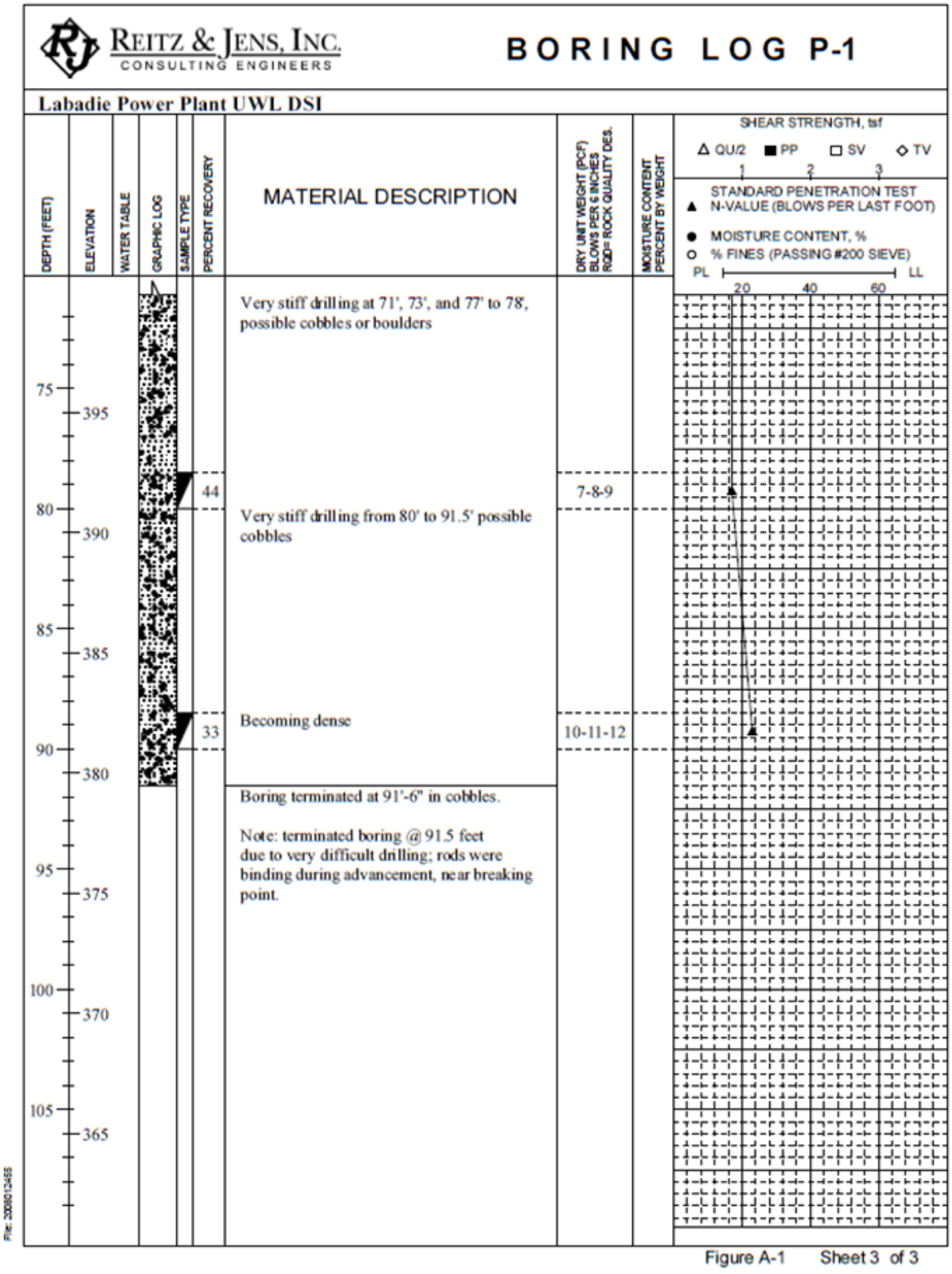

Figure D.2.3 – Boring P1 (approximately 130 yards north of Point 16) from GREDELL Engineering Resources, Inc. and Reitz & Jens, Inc. 2011.

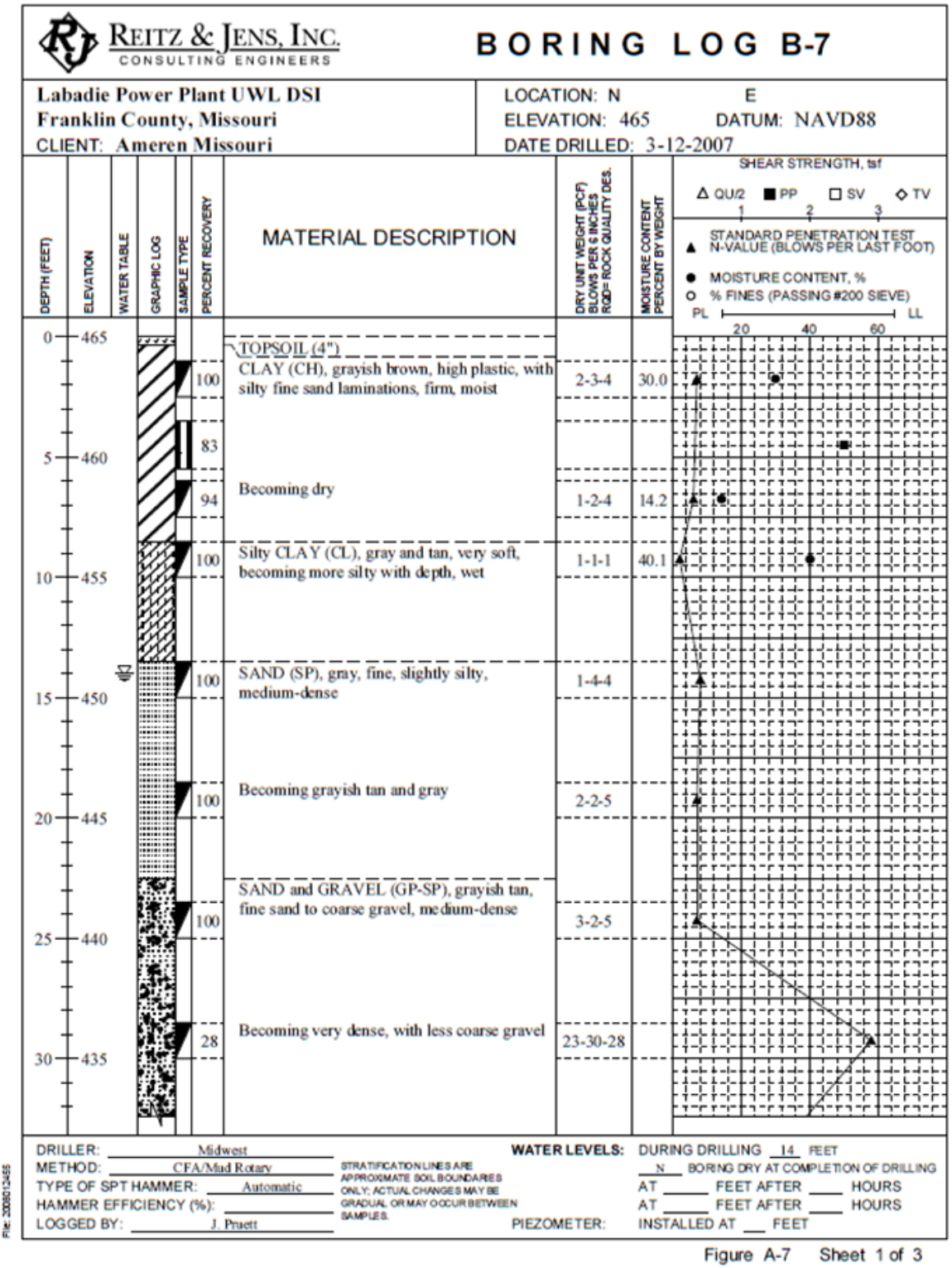

Figure D.3.1 – Boring B7 (approximately 200 yards northwest of Point 168) from GREDELL Engineering Resources, Inc. and Reitz & Jens, Inc. 2011.

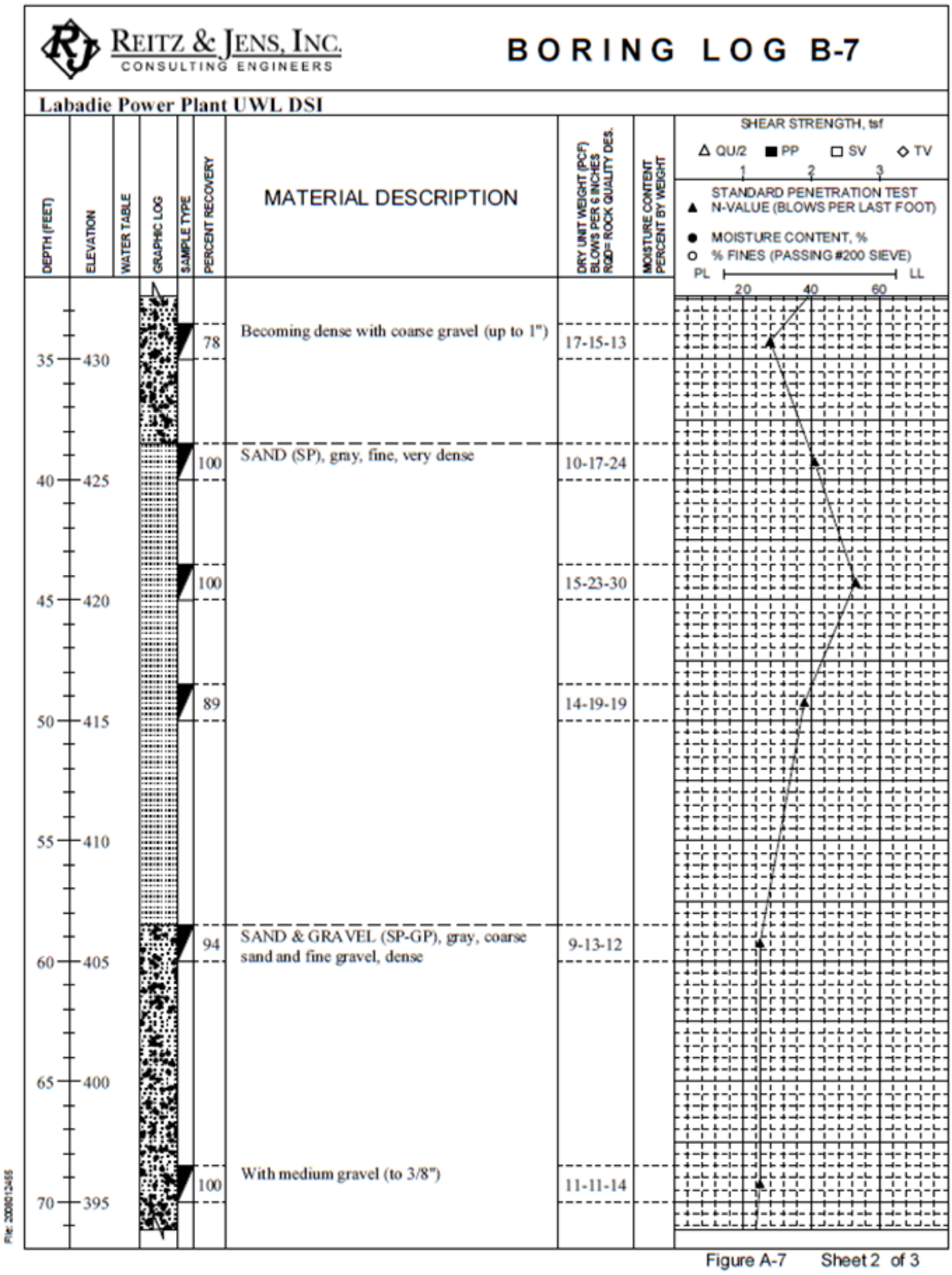

Figure D.3.2 – Boring B7 (approximately 200 yards northwest of Point 168) from GREDELL Engineering Resources, Inc. and Reitz & Jens, Inc. 2011.

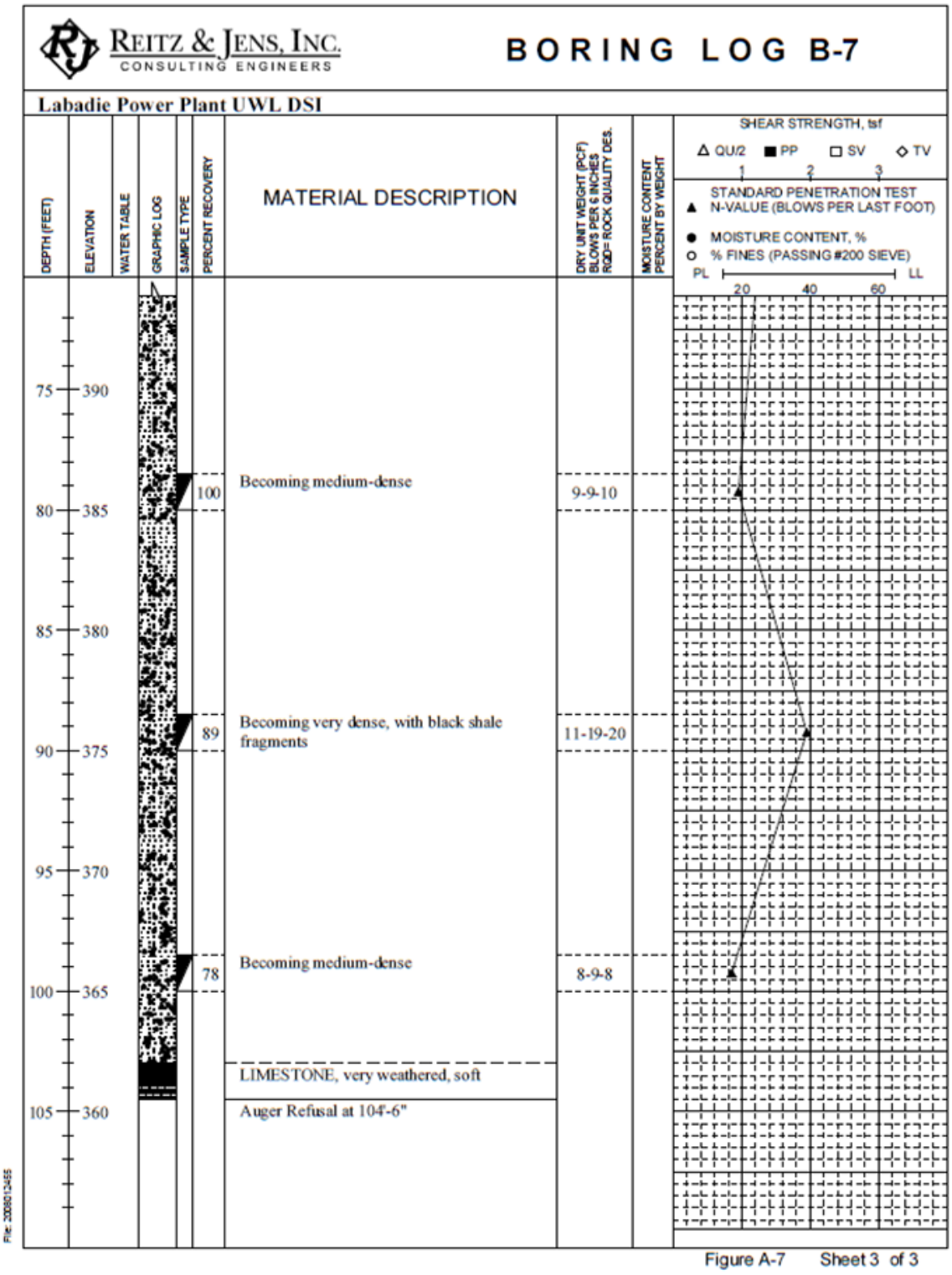

Figure D.3.3 – Boring B7 (approximately 200 yards northwest of Point 168) from GREDELL Engineering Resources, Inc. and Reitz & Jens, Inc. 2011.